DESIGN, SYNTHESES, AND CRYSTAL ENGINEERING OF VERSATILE SUPRAMOLECULAR REAGENTS

by

JOAQUIN FRANCIS URBINA

B.S., Regis University, 2000

AN ABSTRACT OF A DISSERTATION

Submitted in partial fulfillment of the
requirements for the degree

DOCTOR OF PHILOSOPHY

Department of Chemistry
College of Arts and Sciences

KANSAS STATE UNIVERSITY
Manhattan, Kansas

2005

ABSTRACT

Crystal engineering, or non-covalent synthesis in the solid state, requires an understanding of intermolecular forces, and the hydrogen bond has become a reliable non-covalent tool in the construction of supramolecular architectures. In the same way that synthetic chemists refer to a "yield" to quantify a desired product, crystal engineers typically determine the successful formation of a supramolecular product according to the frequency or occurrence of preferred intermolecular interactions between molecules under certain reaction conditions, thus, the *supramolecular yield*. These non-covalent reactions can be effectively carried out using supramolecular reagents (SR's).

A family of ditopic *bis*-imidazol-1-yl/benzimidazol-1-yl compounds were synthesized and used as SR's in combination with a variety of dicarboxylic acids to produce binary solids in 100% yield through the primary acid···imidazol-1-yl/benzimidazol-1-yl synthons even in the presence of potentially disruptive intermolecular interactions. We furthermore noted that secondary C–H···O interactions within and between 1-D chains were of equal structural importance based upon an analysis of the metrics displayed by these interactions. The use of these SR's as ligands with neutrally charged metal complexes was also investigated.

SR's containing benzimidazol-1-yl and carboxamide moieties were synthesized and combined with two different carboxylic acids to make ternary solids through acid···benzimidazol-1-yl and carboxamide···acid hydrogen bonds using a hierarchical approach – the best donor-best acceptor, second best donor-second best acceptor guidelines. These SR's were also employed as ligands for high-yielding syntheses of linear metal complexes where neighboring complexes are linked *via* carboxamide···carboxamide hydrogen bonds.

Asymmetric SR's possessing two different *N*-heterocycles were synthesized and employed in the construction of ternary supermolecules with a high degree of structural selectivity and specificity when introduced to two different carboxylic acids. The stronger acid interacts at the more basic site, while the weaker acid hydrogen-bonds with the less basic nitrogen atom. Finally, an SR containing three different binding sites was designed and synthesized with the aim of producing quaternary co-crystals.

DESIGN, SYNTHESES, AND CRYSTAL ENGINEERING OF VERSATILE SUPRAMOLECULAR REAGENTS

by

JOAQUIN FRANCIS URBINA

B.S., Regis University, 2000

A DISSERTATION

Submitted in partial fulfillment of the
requirements for the degree

DOCTOR OF PHILOSOPHY

Department of Chemistry
College of Arts and Sciences

KANSAS STATE UNIVERSITY
Manhattan, Kansas

2005

Approved by:

Major Professor

Christer Aakeröy

ABSTRACT

Crystal engineering, or non-covalent synthesis in the solid state, requires an understanding of intermolecular forces, and the hydrogen bond has become a reliable non-covalent tool in the construction of supramolecular architectures. In the same way that synthetic chemists refer to a "yield" to quantify a desired product, crystal engineers typically determine the successful formation of a supramolecular product according to the frequency or occurrence of preferred intermolecular interactions between molecules under certain reaction conditions, thus, the *supramolecular yield*. These non-covalent reactions can be effectively carried out using supramolecular reagents (SR's).

A family of ditopic *bis*-imidazol-1-yl/benzimidazol-1-yl compounds were synthesized and used as SR's in combination with a variety of dicarboxylic acids to produce binary solids in 100% yield through the primary acid···imidazol-1-yl/benzimidazol-1-yl synthons even in the presence of potentially disruptive intermolecular interactions. We furthermore noted that secondary C–H···O interactions within and between 1-D chains were of equal structural importance based upon an analysis of the metrics displayed by these interactions. The use of these SR's as ligands with neutrally charged metal complexes was also investigated.

SR's containing benzimidazol-1-yl and carboxamide moieties were synthesized and combined with two different carboxylic acids to make ternary solids through acid···benzimidazol-1-yl and carboxamide···acid hydrogen bonds using a hierarchical approach – the best donor-best acceptor, second best donor-second best acceptor guidelines. These SR's were also employed as ligands for high-yielding syntheses of linear metal complexes where neighboring complexes are linked *via* carboxamide···carboxamide hydrogen bonds.

Asymmetric SR's possessing two different *N*-heterocycles were synthesized and employed in the construction of ternary supermolecules with a high degree of structural selectivity and specificity when introduced to two different carboxylic acids. The stronger acid interacts at the more basic site, while the weaker acid hydrogen-bonds with the less basic nitrogen atom. Finally, an SR containing three different binding sites was designed and synthesized with the aim of producing quaternary co-crystals.

TABLE OF CONTENTS

LIST OF FIGURES

Chapter 1

Chapter 2

Chapter 3

Chapter 6

Chapter 7

Chapter 9

LIST OF SCHEMES

Chapter 2

Chapter 3

Chapter 4

Chapter 5

Chapter 6

Chapter 7

Chapter 8

Chapter 9

LIST OF TABLES

ACKNOWLEDGMENTS

First and foremost, I give thanks to our loving God for giving me the patience and perseverance to endure the challenges in my life.

To my family who has been there for me in every step of the way, and for your love and endless support in all my endeavors.

To Professor Christer Aakeröy, thank you so much for your patience and guidance during my education here at Kansas State University. You have taught me to become a better scientist and a better person.

To the Aakeröy group, both past and present, thanks for all the great times we had together, both inside and outside of lab. I have really enjoyed working with you all.

To the faculty, staff, and graduate students of the Department of Chemistry here at Kansas State University, especially to Dr. John Desper and Dr. Tanya Young, thank you both for your expertise and for taking the time to assist me in various aspects of my research.

To my advisory committee, Professor Eric Maatta, Professor Chris Culbertson, Professor Gary Pierzynski, and Professor Shuting Lei, thank you for all your suggestions and input towards my education.

DEDICATION

I dedicate this dissertation to my family – my mom and dad, Virginia Urbina and Joaquin Urbina, Sr., my brother Adrian, and my sisters, Sheryl and Jacqueline, as well as to my uncle Eusebio Urbina. I also dedicate this to my best friend Angelo Aguilar, his wife Lizette Aguilar, and son, Dimitri Aguilar. Finally, I dedicate this to the most special person in my life, Maria Llinas.

Mom and dad – I would have not been here without your unconditional love and support. Thank you for believing in me and for encouraging me whenever things seemed impossible. I love you both very much.

Adrian, Sher, and Jackie – You have all been a source of inspiration in my life and, despite the fact that we were far away, I always had you all on my mind. I love you all.

Tio Chebo – Without your help I would not have achieved my endeavors. I thank you so much for your support in my education.

Angelo – You have become a very special person in my life, and I will never forget the great times we have spent together. Thanks for being there for me in every way, and for making my stay here a whole lot easier and enjoyable. There is no doubt that you will also achieve your goals in life.

Liz and Dimitri – I have very much enjoyed your company and cherished your kindness. In the near future we will meet again, and we will continue the good times that we have spent together.

Mary – Without you I would not have been where I am today. You have inspired me in every way and have made me realize that everything is possible in life. You have also been with me in good and bad times. I love you very much.

Chapter 1

Introduction to crystal engineering

1.1 Introduction

Crystal engineering can be defined as "…the understanding of intermolecular interactions in the context of crystal packing and in the utilization of such understanding in the design of new solids with desired physical and chemical properties."[1] It is analogous to disciplines such as civil engineering, whereby building blocks are carefully selected by design to construct functional architectures. However, crystal engineering employs *molecular* building blocks, which are assembled *via* intermolecular forces to produce functional solid materials. Crystal engineering stems from *supramolecular chemistry*, which is "chemistry beyond the molecule."[2,3] Inspired by the delicate non-covalent forces that Nature effectively utilizes to hold complex biomolecules together, crystal engineering and supramolecular chemistry seek not only to mimic such natural systems, but also to create new materials possessing specific physical and chemical properties (i.e. non-linear optical, magnetic, porous, catalytic, *etc*.).[4,5,6] To arrive at these materials, *supramolecular*, *intermolecular*, or *non-covalent synthesis*[7] is involved, making use of non-covalent or intermolecular interactions.[8,9]

Contrary to non-covalent synthesis, *covalent synthesis* involves the use of the covalent bond to connect atoms into molecules. The covalent bond is a complex but still a well-studied connector, possessing high directionality, strength over a short distance, as well as versatility in molecular synthesis.[10] In fact, covalent synthesis has been mastered such that even large, biological molecules have been made, for example, Vitamin B_{12}.[2] Therefore, the covalent bond is both predictable and reliable for molecular synthesis.

Can the same level of predictability and reliability be attained from intermolecular interactions? At this point, it is difficult to foresee the assembly of molecules held together by intermolecular forces in the solid state. Since crystal packing depends on a subtle balance of intermolecular interactions, even the smallest change in the structure of the molecular building block can significantly affect the outcome of the extended crystal structure.[11,12] In addition, intermolecular forces are weaker than covalent forces, which

further make crystal structure prediction a formidable task. Despite these challenges, crystal engineering is developing at a rapid pace with the goals of better understanding and studying the nature of intermolecular interactions, the roles these interactions play in the construction of extended crystal structures, and the physical and chemical properties of these ordered structures.

1.2 Historical context of crystal engineering

Light-induced or photochemical reactions of organic molecules in the solid state, such as the photodimerization of cinnamic acids, the reversible photochromy of the anils of salicylaldehyde, fulgides, and tetrachloronaphthoquinone, were well established by the early 20th century.[13] However, the relationship between the photochemistry of organic compounds and the resulting molecular stereochemistry was poorly understood. This problem prompted the use of the term "crystal engineering", which was first introduced by Schmidt and co-workers at the Weizmann Institute in 1964.[1,13] At the time, Schmidt was investigating the interrelationship between the photodimerization reactions of *cis*-[14] and *trans*-[15]cinnamic acid derivatives and their packing motifs in the solid state. *Cis*-cinnamic acid adopts two distinct crystal packing modes, the α- and β-forms. An example of the types of photodimerization reactions of cinnamic acid derivatives in the solid state studied by Schmidt is the [2+2] cycloaddition of the double bonds in two α-*cis*-cinnamic acid molecules to form a cyclobutane dimer, while the same reaction with β-*cis*-cinnamic acid yields the *trans*-isomer, Figure 1.1.[13]

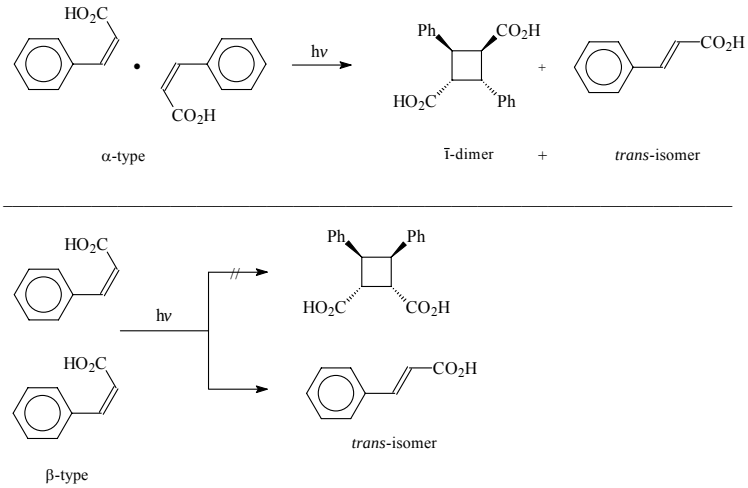

Figure 1.1 Solid-state reactivities of α- and β-*cis*-cinnamic acid.

Contrary to the solid state, photodimerization reactions in solution yield products of different stereochemistries, and if a product possessing a particular stereochemistry is desired, it would be difficult to separate this product from the rest of the mixture. As a result, there is no stereochemical control over these reactions in solution. This disadvantage of photodimerization reactions in solution has prompted extensive studies of the same reactions in the solid state because they occur with minimal atomic or molecular movement (i.e. topochemical reactions).[1] Furthermore, the desired stereoisomer (ī-dimer) can be obtained by employing the *α*-form of *cis*-cinnamic acid in the above example, thus suggesting a high degree of control of the photodimerization reaction in the solid state, and hence the birth of modern crystal engineering.

In the case of cinnamic acid, light of λ = 302 nm is required to induce photodimerization, and the quantum yield was determined to be 0.7. No difference was observed in the photosensitivity of the *α*- and *β*- forms of cinnamic acid. The photodimerization reaction is thought to occur in two steps: 1) formation of an excited monomer molecule from a monomer molecule in the ground state upon irradiation with ultraviolet light, and 2) attack of the excited monomer molecule on a ground state molecule, Equations 1.1 and 1.2.[13]

$$M \xrightarrow{h\nu} M^* \qquad (1.1)$$

$$M^* + M \longrightarrow M_2 \qquad (1.2)$$

These photochemical reactions, Schmidt reasoned, further occurred if the center-to-center distances between the π-electron clouds of C=C double bonds of neighboring molecules were between 3.5 and 4.2 Å, and that the stereochemistry at the nearest-neighbor double bonds were either antiparallel (related by a crystallographic center of symmetry) or parallel (related by a translation axis). If the *p*-orbitals of the π-systems in the two C=C double bonds are misaligned, or if they are too far away for overlap, photodimerization does not occur upon irradiation. These conditions for photodimerization reactions to occur in the solid state upon ultraviolet irradiation became known as the *topochemical rules*.[13]

Schmidt suggested the evolution of solid-state photochemistry to occur in four phases: 1) the phase of the topochemical principle; 2) the phase of the locus of the solid-state reaction; 3) the phase of crystal engineering; and 4) the phase of systematic solid-state photochemistry.[13] According to Schmidt, it is the phase of crystal engineering that is essential towards understanding the roles of intermolecular forces in the crystal structures of organic compounds: "The systematic development of our subject will be difficult if not impossible until we understand the intermolecular forces responsible for the stability of the crystalline lattice of organic compounds…any rational development of the physics and chemistry of the solid state must be based upon a theory of molecular packing; since the molecules studied are complex, the theory will most likely be empirical for some time yet. Rules are now becoming available in what I would regard as phase three, *the phase of crystal engineering*."[13]

Since Schmidt, modern crystal engineering has developed quickly with the advent of modern crystallographic techniques such as the use of four-circle diffractometers and charged-coupled device (CCD) instruments. As a result, modern crystal engineering has expanded to study intermolecular forces in the solid state, as well as structure prediction, control, and analysis. In addition, it incorporates the synthesis of crystalline materials for applications in the pharmaceutical and petrochemical industries, as well as in environmental remediation.[10]

1.3 Intermolecular interactions

Intermolecular forces, particularly hydrogen bonds, are essential for the structural stability and function of biological systems; in fact, without them life would be impossible.[16] Most intermolecular interactions are electrostatic in nature, and can be classified according to strength and directionality for crystal engineering purposes.[10] These intermolecular forces comprise hydrogen bonds and van der Waals forces (dipole-dipole, dipole-induced dipole, induced dipole-induced dipole, π···π interactions).

1.3.1 Hydrogen bonds

1.3.1.1 What constitutes a hydrogen bond?

A hydrogen bond can be defined as D–H···A where D and A are atoms that have electronegativities higher than hydrogen, such as carbon, nitrogen, phosphorus, oxygen, sulfur, selenium, fluorine, chlorine, bromine, and iodine.[17] The hydrogen bond is mainly electrostatic in nature, where the hydrogen atom has a partial positive charge, δ^+, while the more electronegative atoms each have a partial negative charge, δ^-, Figure 1.2.

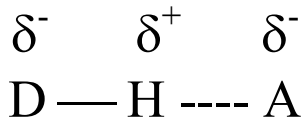

Figure 1.2 Partial positive and negative charges associated with the hydrogen atom (H), the donor atom (D), and the acceptor atom (A) in a hydrogen bond.

The atom that forms a covalent bond with hydrogen is known as the *donor* atom. Meanwhile, the atom that forms a hydrogen bond with hydrogen is the *acceptor* atom. Depending on the electronegativity of the donor and acceptor atoms, hydrogen bonds can be strong, medium, or weak. Two important criteria towards the formation of a hydrogen bond need to be considered: 1) hydrogen-bond geometry involving distance and direction, and 2) the energy associated with the hydrogen bond.[18]

1.3.1.2 Hydrogen-bond geometry

A hydrogen bond can be described as a vector quantity that has both magnitude and direction, Figure 1.3. In order for an interaction to be considered a hydrogen bond, certain geometric criteria need to be met. For instance, the interatomic distances H···A and D···A, and the angle θ are useful to determine whether or not a certain interaction is a hydrogen bond. The H···A–X angle ϕ and the planarity of the DHAX system are also valuable indicators, particularly for strong hydrogen bonds.[4,19]

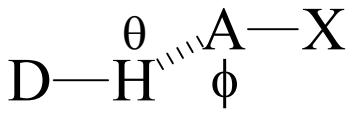

Figure 1.3 Hydrogen bonds have an angular dependence, θ and ϕ.

Typical values for the H···A distance in N–H···O bonds are 1.80 to 2.00 Å and 1.60 to 1.80 Å for O–H···O bonds. Angles θ and ϕ range from about 150-160˚ and about 120-130˚ respectively.[4,19] When considering the distances for H···A and D···A in some hydrogen bonds whose potential energy minima of electrostatic attractive and repulsive forces arise at intermolecular distances greater than the sum of their van der Waals radii, it is necessary to allow for more relaxed values. To illustrate this concept, a typical hydrogen-bond potential energy curve is shown in Figure 1.4.

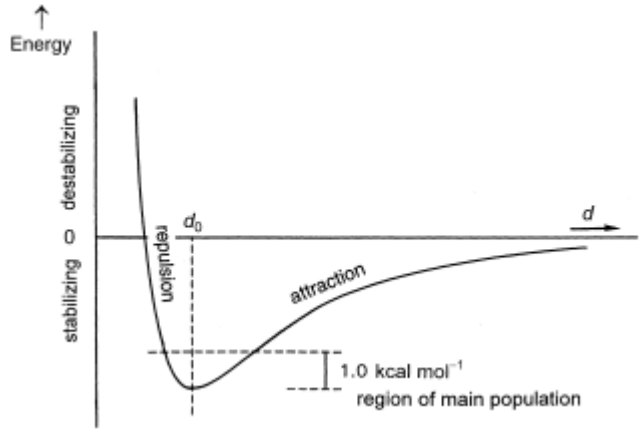

Figure 1.4 Schematic representation of a typical hydrogen-bond potential.[20]

d_0 represents hydrogen-bond distances at the equilibrium distance, or at the distance where the energy is at a minimum. Thus, when the distance d is greater than d_0, an attractive force is observed. Conversely, a repulsive force is observed when d is less than d_0. The total energy of a hydrogen bond (E_{tot}) constitutes electrostatic (E_{el}), polarization (E_{pol}), charge transfer (E_{ct}), dispersion (E_{disp}), and exchange repulsion (E_{er}) forces. Out of all these constituents, E_{el} decreases the least with increasing distance ($-r^{-3}$ for dipole-dipole and $-r^{-2}$ for dipole-monopole interactions). As a result, E_{el} dominates any hydrogen bond potential energy curve, even at long distances. In the case of strong and moderate hydrogen bonds, the hydrogen-bond potential is deep enough (< -20 kJ mol^{-1}) to keep hydrogen-bond distance distributions within the sum of the van der Waals radii of the donor and acceptor atoms. However, for weak hydrogen bonds, the hydrogen-bond

potential is not deep enough (≤ -2 kJ mol^{-1}), thus allowing for a large distribution of hydrogen-bond distances greater than the sum of the van der Waals radii of donor and acceptor atoms, Figure 1.5.

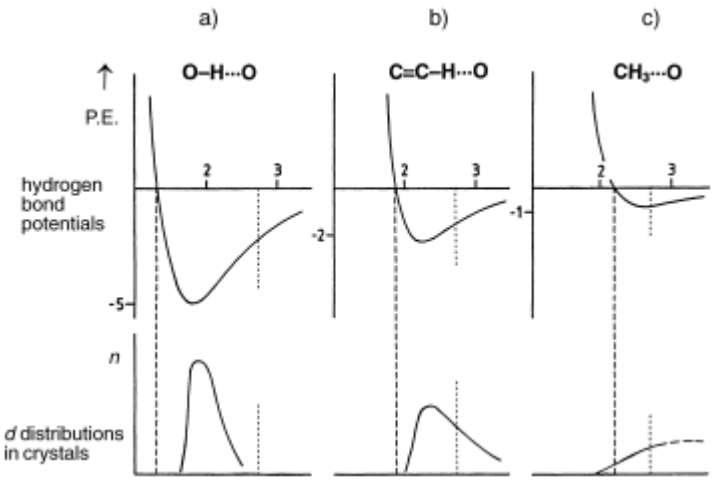

Figure 1.5 Schematic potential energy curves and distance distributions in crystals for moderate hydrogen bonds (a and b) and (c) weak hydrogen bonds.[20]

The relaxed values for weak hydrogen bonds range from 1.40-2.20 Å and 2.50-3.00 Å for H···A and D···A respectively, and the electrostatic attribute of the hydrogen bond is accounted for.[4] Ideally, the values of θ should approach linearity or 180˚; however, this is not usually the case because the number of possible spatial configurations with the D–H···A angle in the range θ to (θ + dθ) is proportional to sin θ. As a result, the average value for θ is about 165˚.[4] The directionality of hydrogen bonds also depends on ϕ. This angle can be identified with the orientation of electron lone pairs of acceptor atoms. For example, oxygen atom lone pair lobes of carbonyl (C=O) groups are in the R_2C=O plane and form angles of about 120˚ with respect to the C=O bond. Another example is provided by thiocarbonyl groups, in which sulfur atom lone pairs form an angle of only 105˚ with the C=S bond.[20] When the acceptor atom is a cyano nitrogen atom, the lone pair forms an angle closer to 180˚ with respect to the C≡N bond.

1.3.1.3 Strength of hydrogen bonds

The strength of hydrogen bonds is primarily governed by the electronegativities of both the donor and acceptor atoms participating in the interaction. For example, the energies for O–H···O and N–H···O hydrogen bonds range from 20 to 40 kJ mol^{-1}.[19] In general, when the donor and acceptor atoms are neutral, hydrogen-bond strength corresponds to energies between 20-65 kJ mol^{-1}.[20] This range is typical of medium-strength hydrogen bonds, while for weaker hydrogen bonds such as C–H···O interactions the energies are between 2-20 kJ mol^{-1}.[19] When the donor and acceptor atoms in a hydrogen bond are ionic (i.e. as a result of proton transfer), hydrogen-bond strength can increase to 40-190 kJ mol^{-1}, and is thus defined as a strong hydrogen bond. Covalent bonds are usually stronger than hydrogen bonds, with energies between 100-400 kJ mol^{-1}, although the strongest of hydrogen bonds can be greater than the weakest of covalent bonds.[20] Hydrogen-bond energies are calculated in the gas phase in which the hydrogen bond is formed between dimers.[20] In addition, hydrogen-bond energies can be determined experimentally by mass spectrometry, in which an equilibrium constant K_c can be obtained from the ratio of hydrogen-bonded dimers to monomers in the gas phase. In particular, bond dissociation energies (ΔH°_D) can be obtained from the temperature dependence of the equilibrium constant for the formation of hydrogen-bonded dimers. Hydrogen-bonded dimers as ions have also been studied by mass spectrometry.[21,22,23]

1.3.1.4 General hydrogen-bond rules

It is convenient to have a set of guidelines at hand when predicting hydrogen-bond patterns in the solid state. A Cambridge Structural Database (CSD) analysis of hydrogen-bond patterns indicates preferred hydrogen-bond motifs and hydrogen-bond selectivity for certain functional groups or for sets of functional groups. From this analysis came about the formulation of three general hydrogen-bond rules.[24] The first rule was developed by Donohue upon observation of only a handful of organic crystal structures: *all acidic hydrogens available in a molecule will be used in hydrogen bonding in the crystal structure of that compound*.[25] This rule is the most useful of all the hydrogen-bond rules. The second and third rules were formulated by Etter based on her work on organic co-crystals: *all good acceptors will be used in hydrogen bonding when there are available hydrogen-bond donors*, and *the best hydrogen-bond donor and the best*

hydrogen-bond acceptor will preferentially form hydrogen bonds to one another.[24,26,27] These rules are based on energetically favorable types of hydrogen bonds and also reflect crystal packing patterns of organic crystal structures. Since the rules were obtained as a result of preparing organic co-crystals, it is necessary to provide a definition for an organic co-crystal.

An organic *co-crystal* is a crystalline compound containing two or more neutral organic components held together by hydrogen bonds.[24] Thus, if an organic crystalline material contains ionic organic components, it is not a co-crystal. The individual components in a co-crystal can have varying numbers of hydrogen-bond donor and acceptor sites, and depending on their donating and accepting abilities a particular hydrogen-bond pattern is formed. In addition, organic co-crystals can be *homomeric* (containing two or more identical hydrogen-bond patterns) or *heteromeric* (containing two or more different hydrogen-bond patterns). Co-crystals are usually prepared by slow evaporation of solutions containing stoichiometric mole ratios of the components. However, they can also be made by grinding the two solid components together, whereby a co-crystal phase is formed from the mixture. As a result, solvent is not necessary in the preparation of co-crystals.[24] Examples of co-crystals are 4-aminobenzoic acid 3,5-dinitrobenzoic acid (1:1), Figure 1.6(a), and 2-amino-4-chloro-6-methylpyrimidine benzoic acid (1:1), Figure 1.6(b).[24]

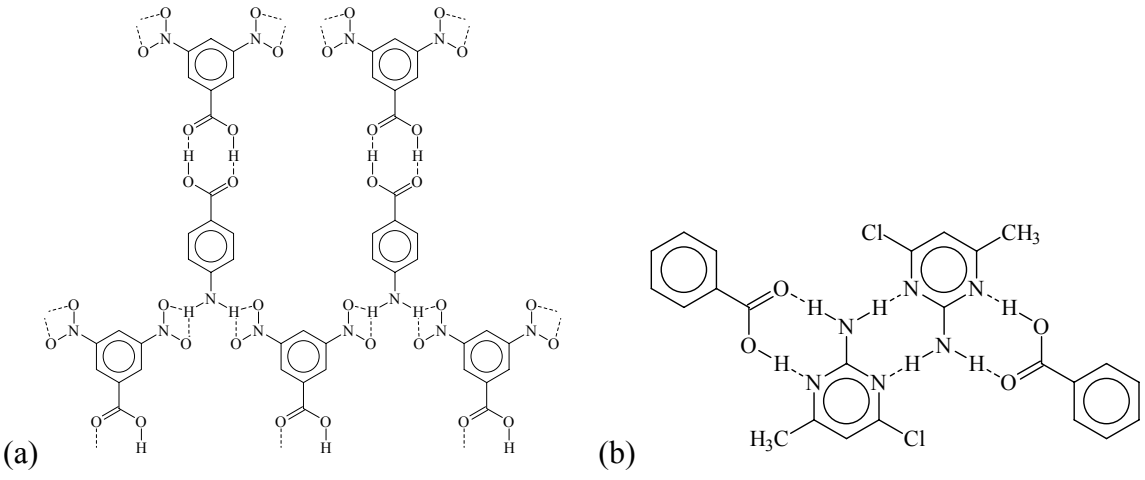

Figure 1.6 Co-crystals of (a) 4-aminobenzoic acid 3,5-dinitrobenzoic acid (1:1) and (b) 2-amino-4-chloro-6-methylpyrimidine benzoic acid (1:1).

1.3.1.5 Graph set notation

Etter formulated a useful method for describing hydrogen-bond patterns in crystal structures based on graph set notation.[24,27] These patterns can be classified according to one of four descriptors: chains (C), rings (R), dimers (D), or intramolecular (S). Following these descriptors, the number of hydrogen-bond acceptors (superscript) and donors (subscript) are designated. The total number of atoms involved in the motif is then provided in parentheses, Figure 1.7.

$$\mathbf{G}_{d}^{a}(n)$$

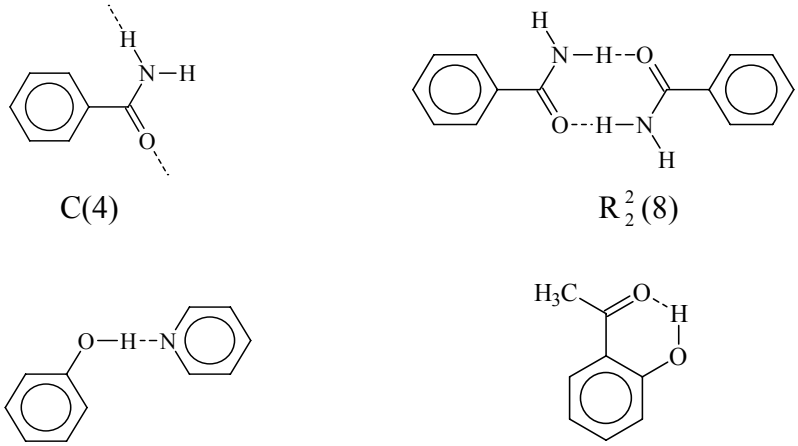

Figure 1.7 Examples of graph set notation in hydrogen-bond patterns.

1.3.2 Van der Waals forces

Van der Waals forces are attractive in nature, and include dipole-dipole interactions, dipole-induced dipole interactions, induced dipole-induced dipole interactions, and π···π interactions.

1.3.2.1 Dipole-dipole interactions

The potential energy of interaction between two polar molecules is a complicated function comprising the dipole moments of the two molecules and the angle, θ, between

them.[28] When the two dipole moments are parallel, Figure 1.8, the potential energy can be described by Equation 1.3.

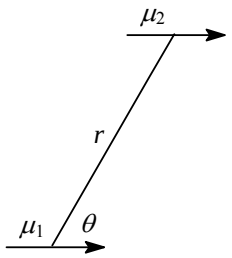

Figure 1.8 Parallel arrangement of two dipoles, separated by distance *r*.

$$V = \frac{\mu_1 \mu_2 f(\theta)}{4\pi\varepsilon_0 r^3} \qquad f(\theta) = 1 - 3\cos^2\theta \qquad (1.3)$$

μ_1 and μ_2 represent the dipole moments of the two molecules, r is the distance between them, θ is the angle between the two dipoles, and ε_0 is the permittivity of a vacuum. Equation 1.3 applies to polar molecules in a fixed, parallel arrangement in a solid.

1.3.2.2 Dipole-induced dipole interactions

A polar molecule with dipole moment μ_1 can also induce a dipole μ_2^* in a neighboring non-polar molecule. The resulting dipoles are attracted together, Figure 1.9.[28]

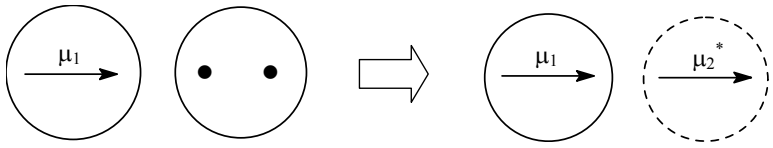

Figure 1.9 Dipole-induced dipole interaction formed when a polar molecule (solid circle) induces a dipole moment on a non-polar molecule (dashed circle).

Consequently, the average interaction energy between the two dipoles can be described by Equation 1.4

$$V = -\frac{C}{r^6} \qquad C = \frac{\mu_1^2 \alpha'_2}{\pi \varepsilon_0} \qquad (1.4)$$

where μ_1 is the permanent dipole moment of the polar molecule, α'_2 is the polarizability volume of the non-polar molecule, r is the distance between the two molecules, and ε_0 is the permittivity of a vacuum.

1.3.2.3 Induced dipole-induced dipole interactions

Non-polar molecules can also induce dipoles on each other, even though neither molecule has a permanent dipole moment. The resulting interaction stems from the transient dipoles that all molecules possess due to changes in the instantaneous positions of electrons. The electrons in one molecule can arrange themselves in such a way as to produce an instantaneous dipole moment μ_1^*. This dipole then produces an electric field that polarizes another molecule to induce an instantaneous dipole moment μ_2^*, Figure 1.10.[28]

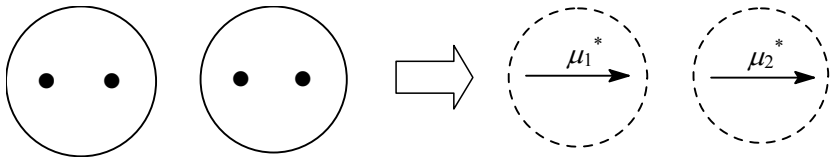

Figure 1.10 Induced dipole-induced dipole interaction formed between two non-polar molecules.

Induced dipole-induced dipole interactions are also called *London dispersion forces*.[28] The potential energy, V, of this interaction is given in Equation 1.5

$$V = -\frac{C}{r^6} \qquad C = \frac{2}{3}\alpha'_1\alpha'_2\frac{I_1 I_2}{I_1+I_2} \qquad (1.5)$$

where α'_1 and α'_2 are the polarizability volumes of the two non-polar molecules, I_1 and I_2 are the ionization energies of the two molecules, and r is the separation between the two molecules.

Dipole-induced dipole and induced dipole-induced dipole interactions decrease more with increasing separation (r^{-6}) than dipole-dipole interactions (r^{-3}) because both the r^{-3} dependence of the magnitude of the induced dipole and the r^{-3} dependence of the potential energy of interaction between the dipoles are accounted for. Dipole-dipole interactions are the most dominant at longer distances of the above van der Waals forces.

1.3.2.4 $\pi\cdots\pi$ interactions

Interactions specific to aromatic π-systems have also been observed. These interactions are essential in Nature, since they stabilize the double helical structure of DNA and are the basis for the tertiary structures of proteins.[29] In the same way that hydrogen bonds meet geometric criteria, π···π interactions are also defined by geometric factors. Perhaps the most reliable geometric parameters for establishing π···π interactions were formulated as a result of experimental studies of porphyrin-porphyrin interactions.[29]

Figure 1.11 illustrates a simple model of two interacting π-systems.

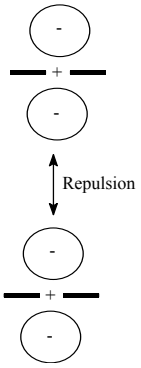

Figure 1.11 Representative model of two π-systems interacting in a face-to-face fashion.[29]

This system consists of a positively charged σ-layer situated between two negatively charged π-electron clouds. If two π-systems stack directly on top of each other, a repulsive interaction is manifested. In order to better represent the electrostatic charge

distribution of a π-system, a set of point charges is employed for each atom involved in the system, Figure 1.12.

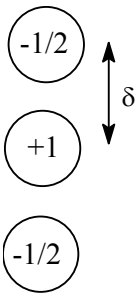

Figure 1.12 Point charges for an atom that contributes one electron to the π-system.[29]

A charge of +1 is given for each carbon atom at its nucleus in a π-system, and two charges of -½ at a distance, δ, above and below the plane of the π-system. This distance was set at 0.47 Å based on the experimental value of the quadrupole moment of benzene.[29] This value for δ can be approximated for other π-systems.

Based on the above representation of π-systems, the preferred geometries of π···π interactions can be considered. When two π-atoms interact at a fixed vertical distance of 3.4 Å,[30] they can be oriented according to Figure 1.13.

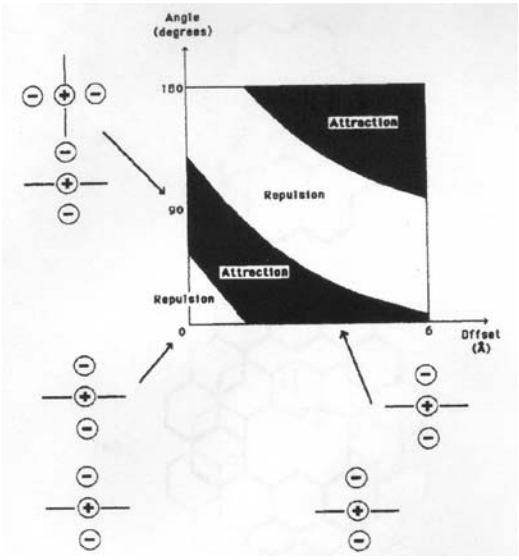

Figure 1.13 Interaction between two π-atoms as a function of their orientation.[29]

When the two π-atoms are oriented in a face-to-face fashion (angle = 0, offset = 0), repulsion is observed; however, when one π-atom is rotated by up to 90˚ with respect to the other, an attractive geometry is formed. Another attractive geometry is formed when

one π-atom is offset laterally with respect to the other. These results for non-polarized π-systems can be summarized with three rules: (1) π···π repulsion dominates in a face-to-face π-stacked geometry; (2) π···σ attraction dominates in an edge-on or T-shaped geometry; and (3) π···σ attraction dominates in an offset π-stacked geometry.[29]

These rules can be validated by experimental evidence from the crystal structures of simple aromatic compounds. Both types of attractive geometries are observed in the crystal structures of kekulene and [18]annulene.[29] The predicted π-stacked geometries for kekulene were also calculated by summing the electrostatic interactions and van der Waals contributions over all the atoms. The calculated kekulene-kekulene interaction energy at the most favorable geometry is -146 kJ mol^{-1}.[29] These results suggest that crystal structures of aromatic compounds are useful for understanding π···π interactions.

In the presence of polarizing groups (i.e. electron donors and acceptors), π···π interactions can adopt six possible orientations, Figure 1.14.

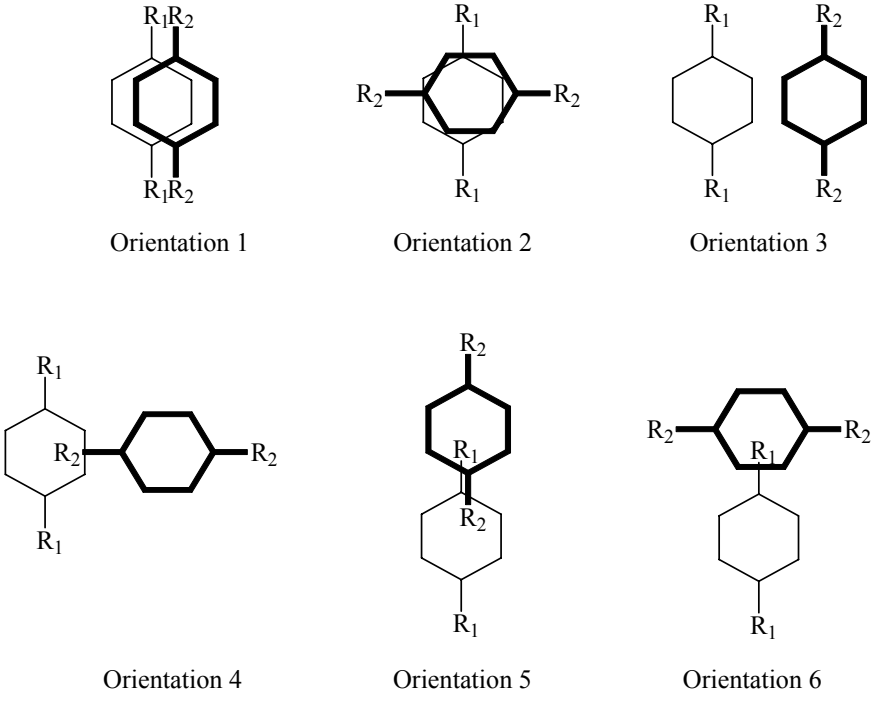

Figure 1.14 Possible orientations for the π···π interactions between polarized π-systems, where R_1 and R_2 are polarizing groups.

Based on the above three rules, offset stacking (orientations 3-6) are attractive, while face-to-face stacking geometries (orientations 1 and 2) are repulsive. However, a fourth

rule can be formulated to predict π···π interactions in the presence of polarizing groups: π-overlap can be favorable in cases where the atoms at the site of contact are π-deficient, and unfavorable when the atoms at the site of contact are π-rich.[29] Thus, the first scenario predicts attractive face-to-face stacking in orientation 2. Experimental evidence of the fourth rule is validated in the crystal structure of tetramethyl-*p*-benzoquinone, Figure 1.15.[29]

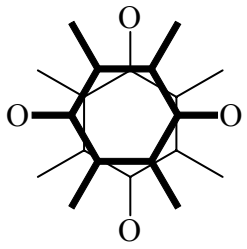

Figure 1.15 Geometry of the face-to-face stacking interaction in the crystal structure of tetramethyl-*p*-benzoquinone.[29]

1.4 Strategies employed in crystal engineering

In the same way that covalent synthesis employs protocols to construct complex organic molecules from simpler building blocks, non-covalent synthesis involves the use of methodologies to construct supramolecular architectures. However, the strategies used in non-covalent synthesis have still not reached the same level of structural predictability. Even though strategies are still being developed to construct predictable assemblies, one important advance in crystal engineering has been the use of *supramolecular synthons* to build various types of extended architectures.[19]

1.4.1 Supramolecular synthons

Supramolecular synthons have been defined as "substructural motifs which incorporate the chemical and geometrical characteristics of intermolecular interactions…They are spatial combinations of intermolecular interactions which can be recognized clearly as design elements for solid-state architecture."[4] These synthons are distinct from intermolecular interactions in that they are derived from designed combinations of interactions and are not the same as the interactions themselves.[19] An

example of a supramolecular synthon is the carboxylic acid dimer, which comprises two centrosymmetrically related C=O···H–O hydrogen bonds, Figure 1.16.

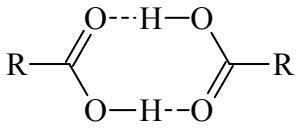

Figure 1.16 The carboxylic acid dimer synthon involving two centrosymmetrically related O–H···O hydrogen bonds.

Despite the strict distinction between supramolecular synthons and intermolecular interactions, there are cases when both the chemical and geometric aspects of intermolecular interactions are intimately linked, thus allowing for interactions such as Cl···Cl or N···Br to be regarded as supramolecular synthons, Figure 1.17.[19]

Figure 1.17 Supramolecular synthons based on Cl···Cl and N···Br intermolecular interactions.

Supramolecular synthons based on intermolecular interactions can either be *homomeric* or *heteromeric* motifs. There are instances when homomeric motifs are formed from two identical centrosymmetrically related hydrogen bonds, such as the carboxylic acid dimer motif. Other synthons that contain self-complementary hydrogen bonds are the carboxamide dimer and oxime dimer motifs, Figure 1.18.

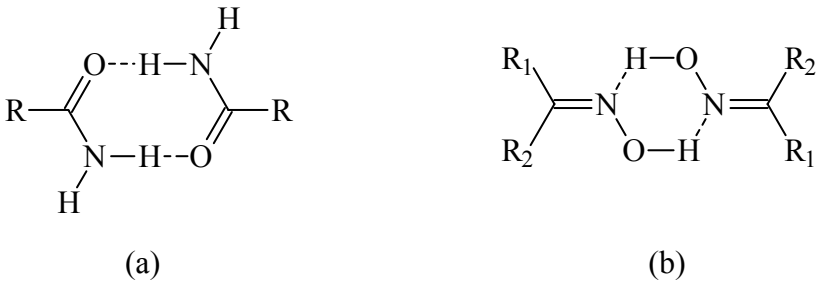

(a) (b)

Figure 1.18 Examples of homomeric synthons containing self-complementary hydrogen bonds in the (a) carboxamide and (b) oxime dimer motifs.

Heteromeric supramolecular synthons constitute intermolecular interactions formed from two different chemical moieties. An example of such a synthon is illustrated in Figure 1.19.

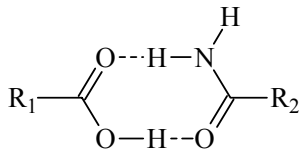

Figure 1.19 Example of a heteromeric supramolecular synthon containing two different types of hydrogen bonds in the carboxylic acid···carboxamide dimer.

Heteromeric motifs are not only limited to strong interactions; they can also arise from a combination of strong and weak interactions. These types of synthons can be formed using heterocycles that contain weakly acidic hydrogens on carbon atoms *ortho*- to the hydrogen-bond acceptor atom. For example, when a carboxylic acid moiety comes in contact with a pyridyl moiety, the carboxylic acid-pyridine supramolecular synthon is formed, Figure 1.20(a).

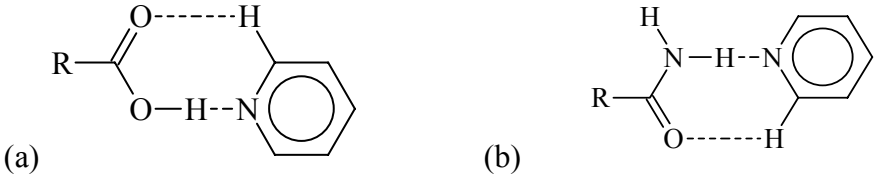

Figure 1.20 (a) The carboxylic acid···pyridine and (b) carboxamide···pyridine supramolecular synthons.

The carboxylic acid-pyridine synthon is formed from a combination of strong O–H···O and weak C–H···O hydrogen bonds. A similar type of synthon can be designed using a carboxamide moiety in place of a carboxylic acid group, Figure 1.20(b).

The above supramolecular synthons are only examples of a library of synthons that can be employed in crystal engineering to construct zero-, one-, two-, and three-dimensional supramolecular architectures.

1.4.2 Zero-dimensional structures

The simplest supramolecular architecture is a zero-dimensional structure, which is a discrete system consisting of molecules held together by supramolecular synthons. An example of a zero-dimensional structure is the benzoic acid dimer, Figure 1.21(a).[19]

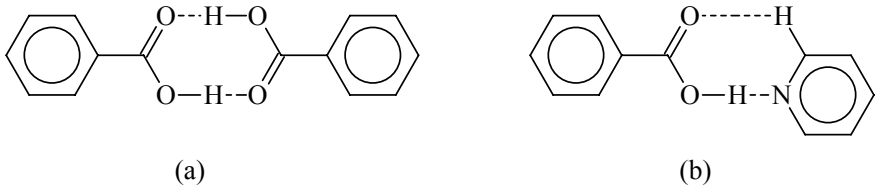

(a) (b)

Figure 1.21 Zero-dimensional structures in the (a) benzoic acid dimer and (b) benzoic acid···pyridine heteromeric system.

Zero dimensional structures can also involve heteromeric synthons such as carboxylic acid···pyridine, which is illustrated in the benzoic acid···pyridine heteromeric system, Figure 1.21(b).

1.4.3 One-dimensional architectures

Zero-dimensional structures can be extended to infinite one-dimensional chains, ribbons, and ladders. This extension is accomplished upon the assembly of molecules possessing at least two recognition sites. The shape of one-dimensional chains depends on the angle between the recognition sites. For instance, terephthalic acid contains two carboxylic acid moieties separated by 180˚ with respect to each other, and upon assembly of these molecules, a linear chain is formed, Figure 1.22.[31]

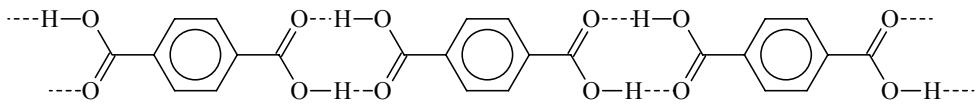

Figure 1.22 An infinite, linear chain formed upon the assembly of terephthalic acid molecules.

Isophthalic acid also forms an infinite one-dimensional chain; however, since the angle between the two carboxylic acid groups is 120˚, the resulting chain adopts a zig-zag pattern, Figure 1.23.[32]

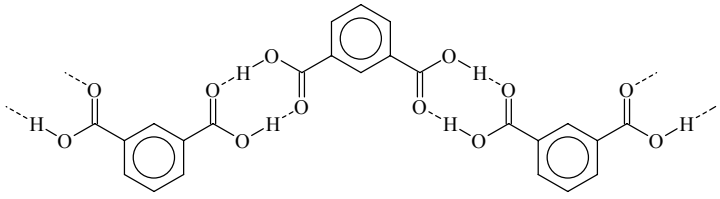

Figure 1.23 An infinite zig-zag chain formed by the assembly of isophthalic acid molecules.

The assembly of one-dimensional architectures is not only limited to hydrogen bonds. Coordination bonds formed from a metal ion with linear coordination geometry and bifunctional organic ligands can also be employed to construct one-dimensional chains. For example, the combination of Ag (I) metal ions and 4,4'-bipyridine affords an infinite, linear chain *via* coordination bonds, Figure 1.24.[33]

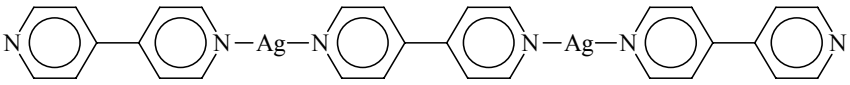

Figure 1.24 Infinite, linear chain formed from Ag (I) and 4,4'-bipyridine using coordination bonds.

It is also possible to generate one-dimensional assemblies through a combination of coordination and hydrogen bonds.[34,35] A ligand containing both a coordination site and a hydrogen-bond moiety can be used in conjunction with a metal ion possessing a linear coordination geometry whereby the coordination site on the ligand forms a coordination bond to the metal ion and the hydrogen-bond moiety interacts with another ligand *via* hydrogen bonds. An example of an infinite, one-dimensional chain that employs such a strategy is constructed from Ag (I) and 3-aldoximepyridine, Figure 1.25.[35]

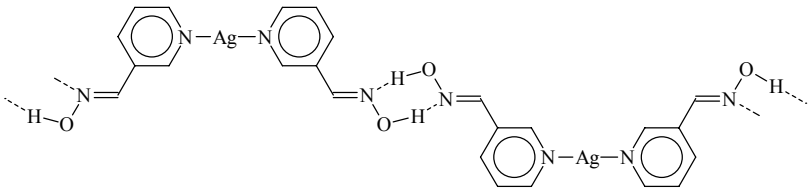

Figure 1.25 Infinite one-dimensional chain formed from Ag (I) ions and 3-aldoximepyridine ligands through coordination and hydrogen bonds.

1.4.4 Two-dimensional sheets

Two-dimensional architectures arise when molecules possess at least one more recognition site, thus further expanding a one-dimensional system.[36] In the case of trimesic acid, which contains one more carboxylic acid moiety than isophthalic acid, the cross-linking of chains formed by isophthalic acid fragments yields an infinite two-dimensional honeycomb sheet, Figure 1.26.[37]

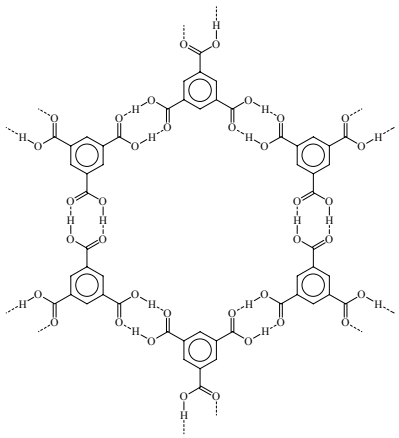

Figure 1.26 An infinite two-dimensional honeycomb sheet formed from the assembly of trimesic acid molecules.

Two-dimensional supramolecular architectures have also been constructed using coordination bonds. In particular, two-dimensional square grids have been assembled employing metal ions with square planar or octahedral coordination geometries and bifunctional organic ligands. In the case of Ni(II) ions and 4,4'-bipyridine ligands, a two-dimensional square grid is formed upon coordination at the equatorial sites of the metal ions, Figure 1.27.[38]

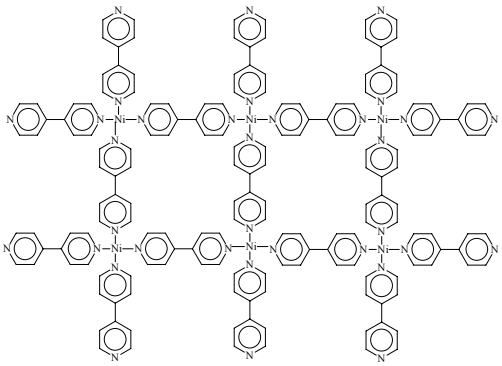

Figure 1.27 A two-dimensional square grid formed by Ni(II) ions and 4,4'-bipyridine ligands.

Two-dimensional architectures have also been synthesized through a combination of coordination and hydrogen bonds.[39,40] For example, inorganic-organic hybrid sheets have been prepared using Ni(II) ions and 4-oximepyridine, whereby the pyridine nitrogen on each ligand is coordinated to the equatorial sites of the metal ion while the oxime moiety forms O–H···O hydrogen bonds, Figure 1.28.[40]

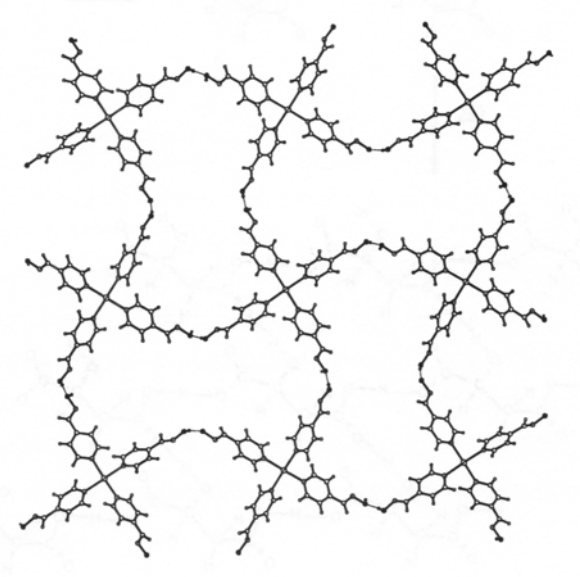

Figure 1.28 A two-dimensional inorganic-organic hybrid sheet formed from Ni(II) ions and 4-oximepyridine *via* coordination and hydrogen bonds.[40]

1.4.5 Three-dimensional architectures

Three-dimensional architectures are the most sophisticated of supramolecular systems in crystal engineering because they require extensions of building blocks in all three

spatial coordinates. Simultaneously, they also find the most application in porous and catalytic materials due to the pores or cavities created in these materials. These three-dimensional systems can be constructed into *discrete* or *infinite* architectures. Discrete architectures usually adopt polyhedral or high-symmetry forms, and can be built from a combination of metal ions and organic ligands, both possessing specific geometries, through coordination bonds, Figure 1.29.[41]

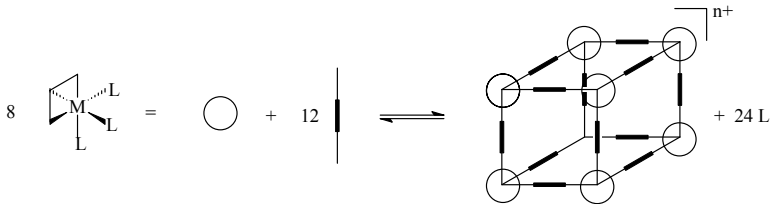

Figure 1.29 Discrete three-dimensional architecture based on metal ions and organic ligands.

Infinite architectures can be built from metal ions and organic ligands *via* coordination bonds, which in many cases can also be structurally robust and highly porous.[42] For example, the combination of a copper paddle-wheel cluster with adamantane-1,3,5,7-tetracarboxylic acid affords a porous, three-dimensional framework, Figure 1.30.[43]

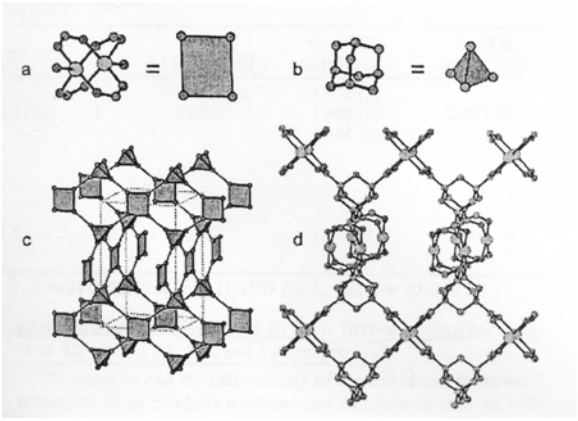

Figure 1.30 Construction of a porous, three-dimensional framework using a copper paddle-wheel cluster and 1,3,5,7-adamantane tetracarboxylic acid *via* coordination bonds.[43]

Infinite three-dimensional architectures can also be constructed from organic building blocks *via* hydrogen bonding.[19,44,45] In the crystal structure of adamantane-1,3,5,7-tetracarboxylic acid, a three-dimensional diamondoid structure is formed, in which the

carboxylic acid moieties are arranged tetrahedrally about the adamantyl center, Figure 1.31.[46]

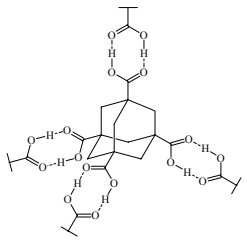

Figure 1.31 Three-dimensional diamondoid framework formed from adamantane-1,3,5,7-tetracarboxylic acid molecules connected by the carboxylic acid synthon.

There are also cases when three-dimensional architectures are constructed from a combination of coordination and hydrogen bonds, although they are rare.[6,47,48,49] An example of such architectures involves the use of Ag(I) ions and *iso*nicotinamide ligands, in which Ag(I) ions adopt a trigonal geometry and each Ag(I) complex is connected by self-complementary amide···amide hydrogen bonds, Figure 1.32.[49]

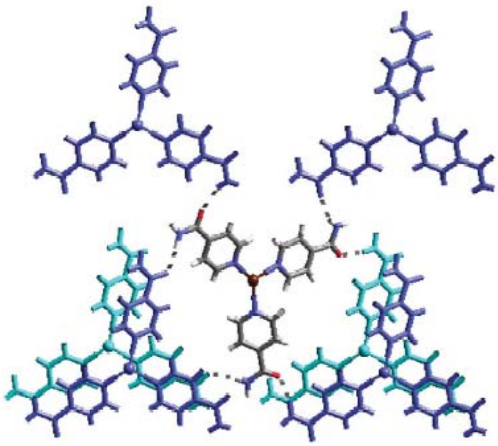

Figure 1.32 Three-dimensional architecture formed from trigonal Ag(I) ions and *iso*nicotinamide ligands through coordination and hydrogen bonds.

1.5 Goals

Bearing the principles of crystal engineering in mind, the subsequent chapters will focus on the fundamental aspects of the discipline. These goals include the: 1) study of reliabilities of intermolecular interactions, 2) construction of inorganic-organic supramolecular architectures, and 3) systematic study of the hierarchy of supramolecular synthons using supramolecular reagents (SR's).

1.5.1 Study of reliabilities of intermolecular interactions

The reliability of an intermolecular interaction is typically reflected by its frequency or occurrence in a given number of crystal structures. In the same way that organic chemists determine molecular yields through a ratio of product to starting material, suparmolecular yields can be determined from the ratio of the frequency of that interaction to the total number of crystal structures. In particular, the reliability of heteromeric synthons containing O–H···N and C–H···O hydrogen bonds will be studied in organic co-crystals (Chapters 2 and 3). As a result, we can conclude whether they can be employed as tools for the construction of more elaborate supramolecular architectures.

Another critical aspect of this study is to establish whether the C–H···O interactions arise from the most acidic hydrogen on C–H moieties. One of the Etter rules states that the most acidic hydrogen will form a hydrogen bond to the best hydrogen-bond acceptor, the second most acidic hydrogen will form a hydrogen bond to the second best hydrogen-bond acceptor, and so on. A systematic study of organic co-crystals in Chapter 3 will enable us to determine if this rule is consistent.

1.5.2 Construction of inorganic-organic supramolecular architectures

Inorganic-organic supramolecular architectures will also be built from a combination of metal ions and organic ligands through coordination and hydrogen bonds (Chapters 5 and 6). While taking advantage of the versatility of hydrogen bonds in coordination chemistry, we will also focus on longer and more structurally flexible ligands. We will attempt to construct one-dimensional supramolecular architectures by employing these ligands and metal ions with inherent linear coordination geometries.

1.5.3 Systematic study of the hierarchy of supramolecular synthons

The Etter rules will be used as guidelines in the systematic study of the hierarchy of supramolecular synthons. The primary rule states that the best hydrogen-bond donor will form a hydrogen bond with the best hydrogen-bond acceptor, the second best hydrogen-bond donor will form a hydrogen bond with the second best hydrogen-bond acceptor, and so on. In order to realize this study, organic co-crystals of two or more molecules and an SR, containing different hydrogen-bond moieties, will be analyzed to determine which

synthons are preferred over others under certain reaction conditions (Chapters 4, 7, 8, and 9). In other words, the hydrogen-bond moieties compete to form preferred supramolecular synthons. Based on a balance between, and awareness of these interactions in ternary, quaternary, and higher-order co-crystals, we can begin to establish a hierarchy of supramolecular synthons using a systematic, modular, and transferable non-covalent synthetic protocol.

References

[1] Desiraju, G. R. *Crystal Engineering: The Design of Organic Solids*; Elsevier Science Publishers B.V.: Amsterdam, 1989.

[2] Lehn, J.-M. *Supramolecular Chemistry: Concepts and Perspectives*; VCH: Weinheim, 1995.

[3] Lehn, J.-M. *Angew. Chem. Int. Ed. Engl.* **1988**, *27*, 89.

[4] Desiraju, G. R. *The Crystal as a Supramolecular Entity*; John Wiley & Sons, Ltd., 1996.

[5] Reinhoudt, D. N.; C.-Calama, M. *Science* **2002**, *295*, 2403.

[6] Aakeröy, C. B.; Beatty, A. M. *Aust. J. Chem.* **2001**, *54*, 409.

[7] These terms are used interchangeably by different authors to connote the syntheses of new materials using intermolecular interactions.

[8] Fyfe, M. C. T.; Stoddart, J. F. *Acc. Chem. Res.* **1997**, *30*, 393.

[9] Whitesides, G. M.; Simanek, E. E.; Mathias, J. P.; Seto, C. T.; Chin, D. N.; Mammen, M.; Gordon, D. M. *Acc. Chem. Res.* **1995**, *28*, 37.

[10] Steed, J. W.; Atwood, J. L. *Supramolecular Chemistry*; John Wiley & Sons, Ltd.: Chichester, 2000**.**

[11] Aakeröy, C. B. *Acta Crystallogr.* **1997**, *B53*, 569.

[12] Sarma, J. A. R. P.; Desiraju, G. R. *Cryst. Growth Des.* **2002**, *2*, 93.

[13] Schmidt, G. M. J. *Pure Appl. Chem.* **1971**, *27*, 647.

[14] Bregman, J.; Osaki, K.; Schmidt, G. M. J.; Sonntag, F. I. *J. Chem. Soc.* **1964**, 2021.

[15] Schmidt, G. M. J. *J. Chem. Soc.* **1964**, 2014.

[16] Jeffrey, G. A.; Saenger, W. *Hydrogen Bonding in Biological Structures*; Springer-Verlag Berlin Heidelberg, 1991.

[17] Joesten, M. D.; Schaad, L. J. *Hydrogen Bonding*; Marcel Dekker, Inc.: New York, 1974.

[18] Hamilton, W. C.; Ibers, J. A. *Hydrogen Bonding in Solids*; W. A. Benjamin, Inc.: New York, 1968**.**

[19] Desiraju, G. R. *Angew. Chem. Int. Ed. Engl.* **1995**, *34*, 2311.

[20] Steiner, T. *Angew. Chem. Int. Ed. Engl.* **2002**, *41*, 48.

[21] Meot-Ner, M. *J. Am Chem. Soc.* **1984**, *106*, 1257.

[22] Meot-Ner, M.; Deakyne, C. A. *J. Am. Chem. Soc.* **1985**, *107*, 469.

[23] Deakyne, C. A.; Meot-Ner, M. *J. Am. Chem. Soc.* **1985**, *107*, 474.

[24] Etter, M. C. *J. Phys. Chem.* **1991**, *95*, 4601.

[25] Donohue, J. *J. Phys. Chem.* **1952**, *56*, 502.

[26] Etter, M. C. *J. Am. Chem. Soc.* **1982**, *104*, 1095.

[27] Etter, M. C. *Acc. Chem. Res.* **1990**, *23*, 120.

[28] Atkins, P. W. *Physical Chemistry 6th Ed.*; Oxford University Press, 1998.

[29] Hunter, C. A.; Sanders, J. K. M. *J. Am. Chem. Soc.* **1990**, *112*, 5525.

[30] This distance was determined from solution and solid-state studies of π-stacked porphyrins, with interplanar separations ranging from 3.4 – 3.6 Å.

[31] Bailey, M.; Brown, C. J. *Acta Crystallogr.* **1967**, *22*, 387.

[32] Alcala, R.; Martinez-Carrera, S. *Acta Crystallogr.* **1972**, *B28*, 1671.

[33] Blake, A. J.; Champness, N. R.; Crew, M.; Larsons, S. *New J. Chem.* **1999**, *23*, 13.

[34] Aakeröy, C. B.; Beatty, A. M. *Chem. Commun.* **1998**, 1067.

[35] Aakeröy, C. B.; Beatty, A. M.; Leinen, D. S. *J. Am. Chem. Soc.* **1998**, *120*, 7383.

[36] (a) Barnett, S. A.; Blake, A. J.; Champness, N. R. *CrystEngComm* **2003**, *5*, 134. (b) Ma, B.; Coppens, P. *Chem. Commun.* **2003**, 2290. (c) Arora, K. K.; Pedireddi, V. R. *J. Org. Chem.* **2003**, *68*, 9177. (d) Sharma, C. V. K.; Zaworotko, M. J. *Chem. Commun.* **1996**, 2655.

[37] Duchamp, D. J.; Marsh, R. E. *Acta Crystallogr.* **1969**, *B25*, 5.

[38] Biradha, K.; Zaworotko, M. J. *Chem. Commun.* **1999**, 1327.

[39] Aakeröy, C. B.; Beatty, A. M.; Lorimer, K. R. *J. Chem. Soc., Dalton Trans.* **2000**, 3869.

[40] Aakeröy, C. B.; Beatty, A. M.; Leinen, D. S. *Angew. Chem. Int. Ed.* **1999**, *38*, 1815.

[41] (a) Klaussmeyer, K. K.; Wilson, S. R.; Rauchfuss, T. B. *J. Am. Chem. Soc.* **1999**, *121*, 2705. (b) Klaussmeyer, K. K.; Rauchfuss, T. B.; Wilson, S. R. *Angew. Chem. Int. Ed.* **1998**, *37*, 1694. (c) Roche, S.; Hasalm, C.; Adams, H.; Heath, S. L.; Thomas, J. A. *J. Chem. Soc., Chem. Commun.* **1998**, 1681. (d) Caulder, D. L.; Raymond, K. N. *Acc. Chem. Res.* **1999**, *32*, 975.

[42] (a) Eddaoudi, M.; Moler, D. B.; Li, H.; Chen, B.; Reineke, T. M.; O'Keeffe, M.; Yaghi, O. M. *Acc. Chem. Res.* **2001**, *34*, 319. (b) Plévert, J.; Gentz, T. M.; Laine, A.; Li, H.; Young, V. G.; Yaghi, O. M.; O'Keeffe, M. *J. Am. Chem. Soc.* **2001**, *123*, 12706. (c) Chae, H. K.; Eddaoudi, M.; Kim, J.; Hauck, S. I.; Hartwig, J. F.; O'Keeffe, M.; Yaghi, O. M. *J. Am. Chem. Soc.* **2001**, *123*, 11482. (d) Eddaoudi, M.; Li, H.;

Yaghi, O. M. *J. Am. Chem. Soc.* **2000**, *122*, 1391. (e) Yaghi, O. M.; Li, H.; Davis, C.; Richardson, D.; Groy, T. L. *Acc. Chem. Res.* **1998**, *31*, 474. (f) Yaghi, O. M.; Li, H.; Groy, T. L. *J. Am. Chem. Soc.* **1996**, *118*, 9096.

[43] Chen, B.; Eddaoudi, M.; Reineke, T. M.; Kampf, J. W.; O'Keeffe, M.; Yaghi, O. M. *J. Am. Chem. Soc.* **2000**, *122*, 11559.

[44] Aakeröy, C. B.; Nieuwenhuyzen, M. *J. Am. Chem. Soc.* **1994**, *116*, 10983.

[45] MacGillivray, L. R.; Papaefstathiou, G. S.; Reid, J. L.; Ripmeester, J. A. *Cryst. Growth Des.* **2001**, *1*, 373.

[46] Ermer, O. *J. Am. Chem. Soc.* **1988**, *110*, 3747.

[47] Beatty, A. M. *CrystEngComm.* **2001**, *51*, 1.

[48] Munakata, M.; Wu, L. P.; Yamamoto, M.; Kuroda-Sowa, T.; Maekawa, M. *J. Am. Chem. Soc.* **1996**, *118*, 3117.

[49] Aakeröy, C. B.; Beatty, A. M.; Helfrich, B. A. *J. Chem. Soc.*, *Dalton Trans.* **1998**, 1943.

Chapter 2

Is conformational flexibility in a supramolecular reagent advantageous for high-yielding co-crystallization reactions?

2.1 Introduction

An integral part of organic supramolecular chemistry is the design of discrete building blocks with intermolecular preferences that can be utilized for the directed assembly of homomeric[1] or heteromeric[2] solid-state architectures with predictable and desirable connectivities. These building blocks, or supramolecular reagents (SR's), frequently operate with hydrogen-bond based supramolecular synthons as their organizational tools.[1a,3] The carboxylic acid···pyridine heteromeric synthon, Scheme 2.1, has been used extensively as a synthetic tool for the construction of co-crystals not only because of its strength and directionality, but also because it is relatively tolerant of the presence of other potentially competing or disruptive hydrogen-bonding moieties.[4]

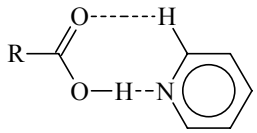

Scheme 2.1 The carboxylic acid···pyridine synthon.

An important attribute of every SR is its latent supramolecular dimensionality, *i.e.* a molecule with a single hydrogen-bond acceptor site can only act as a terminating or capping reagent in a hydrogen-bonded network, whereas a molecule with two self-complementary sites is designed to produce extended 1-D motifs. Suitable combinations of relatively simple molecular building blocks can then lead to 3-D architectures of considerable complexity. For example, in the 1:1 co-crystal of 1,4-naphthalenedicarboxylic acid and 4,4'-bipyridine (bipy),[5] neighboring components interact through heteromeric O–H···N hydrogen bonds resulting in an infinite 1-D chain. The primary extended structural element in this co-crystal is readily predictable since both components are inherently supramolecularly linear. Infinite one-dimensional chains can also be generated from more structurally flexible dicarboxylic acid-based SR's and

bipy and its homologues, which illustrates the generality of reliable non-covalent synthesis.[6]

If, instead, 1,3,5-tricarboxylic acid benzene (trimesic acid, a 2-D builder) is allowed to react with bipy, an elegant two-dimensional "chicken-wire" framework is afforded *via* heteromeric O–H···N interactions,[7] Scheme 2.2.

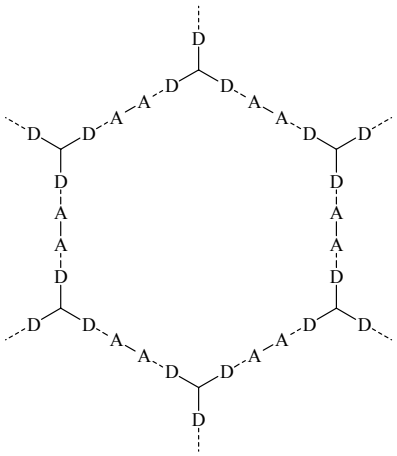

Scheme 2.2 Representation of a two-dimensional hexagonal motif formed from a three-fold symmetric SR and a ditopic base through hydrogen bonds. D = hydrogen-bond donor, A = hydrogen-bond acceptor.

In this case, trimesic acid is a suitable SR for two-dimensional architectures since it contains three carboxyl groups that are "locked" into a conformation with three-fold symmetry. The highly symmetric nature of trimesic acid has thus become a source of inspiration for deliberate strategies and subsequent formulation of aesthetically pleasing host-guest complexes[8] and co-crystals.[8a,9] At the same time, however, researchers have been compelled to employ relatively unconventional and/or harsher crystal growing techniques such as hydrothermal synthesis,[8a] CS_2 as a solvent system,[8b] as well as vapor condensation on cold surfaces[8d] in order to obtain these architectures. Although the structural rigidity in trimesic acid is advantageous for preparing the intended supramolecular frameworks, the poor solubility that accompanies this highly symmetric molecule is a distinct drawback. This is arguably the reason for why there is not an abundance of molecular co-crystals in the Cambridge Structural Database (CSD)[10]

involving trimesic acid; instead, only a relatively small collection of solvates,[11] co-crystals,[9] and organic salts[12] with trimesic acid have been crystallographically characterized.

To compensate for poor solubility, the structural rigidity of a three-fold symmetric SR can be tempered by introducing a more flexible backbone. For example, 1,3,5-cyclohexanetricarboxylic acid (CTA) contains a cyclohexane framework, which organizes the C–C bonds involving the carboxyl groups in a non-planar manner whereas those of trimesic acid are co-planar with the phenyl ring. In co-crystals of CTA and bipy[13] and its ditopic homologues,[14] it is clear that this SR at times is capable of directing the formation of two-dimensional hexagonal frameworks through O–H···N hydrogen bonds.[5,15]

What would happen then if even more conformational flexibility was added to a supramolecular reagent with, in principle, three-fold symmetry? Would such a SR be able to yield predictable two-dimensional hexagonal motifs in combination with bipy and its homologues as is the case with trimesic acid? Will improved solubility facilitate the formation of co-crystals? To try to answer these questions we have carried out a structural study of some co-crystals based around 2,4,6-*tris*-(4-carboxyphenoxy)-1,3,5-triazine (TCPT), Scheme 2.3.

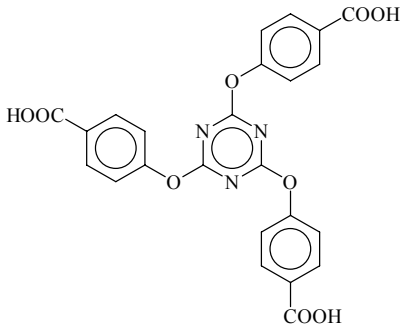

Scheme 2.3 2,4,6-*tris*-(4-carboxyphenoxy)-1,3,5-triazine (TCPT).

TCPT possesses three carboxyl groups that can rotate about the C–C bonds and are also located at the end of molecular "arms" that can rotate about the ether C–O–C bonds. This degree of conformational flexibility is not present in trimesic acid and, as a result, TCPT would be expected to be soluble in a wider range of solvents.

In this chapter, we present six crystal structures involving TCPT with bipy and some of its homologues in order to examine the balance between conformational flexibility and supramolecular efficiency. The latter will be assessed based upon the reproducibility of the desired intermolecular motif as well as the ease with which co-crystals can be prepared. The following crystal structures are reported; TCPT $bipy_{1.5}$, **1**; TCPT $bipy_{1.5}(H_2O)_{0.3}$, **2**; TCPT *trans*-1,2-*bis*-(4-pyridyl)-ethylene $(bipye)_{1.5}$, **3**; TCPT *bis*-(4-pyridyl)-ethane $(bipya)_{1.5}$, **4**; $TCPT^-$ 4,4'-trimethylenedipyridinium ($tmdipyH^+$), **5**; and TCPT $bipya_{0.5}$ DMF, **6**.

2.2 Experimental

2.2.1 Synthesis

All starting materials were purchased from Aldrich and used without further purification. Melting points were determined on a Fisher-Johns melting point apparatus and are uncorrected.

2.2.1.1 Synthesis of 2,4,6-*tris*-4-(bromophenoxy)-1,3,5-triazine[16]

4-Bromophenol (6.06 g, 35.0 mmol) and cyanuric chloride (1.84 g, 10.0 mmol) were added to a 50-mL round-bottomed flask. A reflux condenser was attached, and the two solids were heated and stirred under reflux in a sand bath at 210˚C for 8 h. Once the brown-white solid crude product was formed at the bottom of the flask, the reaction was stopped and set to cool. The solid was then washed with 30 mL of hot ethanol by heating and stirring the mixture under reflux for 30 min. An off-white solid was obtained after filtration of the ethanolic mixture and then recrystallized from 300 mL of chloroform by heating and stirring the solution under reflux for 30 min., which upon cooling gave white needles. The pure product was obtained *via* vacuum filtration and collected. Yield 4.85 g (82.0 %); m.p. 235-238˚C; IR (KBr) ν 1567, 1095, 1067 cm^{-1}; ^1H NMR ($CDCl_3$, 400 MHz) δ 6.98 (d, 6H, J = 8 Hz), 7.45 (d, 6H, J = 8 Hz); MS (MALDI) *m/e* = 591.851 $(M + H)^+$.

2.2.1.2 Synthesis of 2,4,6-*tris*-(4-carboxyphenoxy)-1,3,5-triazine (TCPT)[17]

2,4,6-*tris*-4-(bromophenoxy)-1,3,5-triazine (4.00 g, 6.77 mmol) was dissolved in 400 mL of dry THF with stirring. The reaction mixture was cooled to -110˚C with liquid nitrogen/ethanol slush. 20 mL of 1.6*M* butyllithium cooled to -110˚C was added to the stirring solution under nitrogen, and the mixture was stirred for 10 min. at that temperature. The pale yellow solution was poured onto solid carbon dioxide covered with diethyl ether. The mixture was then allowed to warm to room temperature. 30 mL of water was added to the mixture, and the ether phase was extracted 7 times with 30 mL portions of water and then with 20 mL of 1*M* NaOH. 6*M* HCl was added to the combined aqueous solutions until a white flaky precipitate came out and the pH of 2-3 was attained. The crude product was obtained *via* vacuum filtration and then recrystallized from 500 mL THF to give the pure product. Yield 2.22 g (67.0 %); m.p. >300˚C; IR (KBr) ν 3430, 1696, 1572, 1127, 1087 cm^{-1}; ^1H NMR (DMSO-d_6, 400 MHz) δ 7.37 (d, 6H, J = 7.4 Hz), 7.99 (d, 6H, J = 6.6 Hz), 13.00 (s, 3H, broad); MS (MALDI) *m/e* = 490 $(M + H)^+$.

2.2.2 Syntheses of co-crystals and salts

2.2.2.1 Synthesis of 2,4,6-*tris*-(4-carboxyphenoxy)-1,3,5-triazine 4,4'-bipyridine$_{1.5}$, **1**

TCPT (0.05 g, 0.10 mmol) was dissolved in 25 mL of THF. To this solution was added a solution of bipy (0.03 g, 0.20 mmol) in 5 mL of absolute ethanol. Yellow plates were obtained after a few days upon slow evaporation of the solvent. M.p. >300˚C.

2.2.2.2 Synthesis of 2,4,6-*tris*-(4-carboxyphenoxy)-1,3,5-triazine 4,4'-bipyridine$_{1.5}$ $(H_2O)_{0.3}$, **2**

To a solution of TCPT (0.05 g, 0.10 mmol) in THF (25 mL) was added a solution of bipy (0.02 g, 0.15 mmol) in absolute ethanol (5 mL). The resulting clear solution was left to evaporate slowly in ambient air. Colorless plates crystallized after a few days. M.p. >300˚C.

2.2.2.3 Synthesis of 2,4,6-*tris*-(4-carboxyphenoxy)-1,3,5-triazine *trans*-1,2-bis-(4-pyridyl)-ethylene$_{1.5}$, **3**

To a solution of TCPT (0.05 g, 0.10 mmol) in THF (25 mL) was added a solution of bipye (0.03 g, 0.15 mmol) in absolute ethanol (5 mL). The resulting clear solution was allowed to evaporate slowly in ambient air. Colorless prisms were obtained after a few days. M.p. 228-230˚C (decomp.).

2.2.2.4 Synthesis of 2,4,6-*tris*-(4-carboxyphenoxy)-1,3,5-triazine *bis*-(4-pyridyl)-ethane$_{1.5}$, **4**

To a solution of TCPT (0.05 g, 0.10 mmol) in DMF (5 mL) was added a solution of bipya (0.03 g, 0.15 mmol) in DMF (5 mL). The resulting yellow solution was allowed to evaporate slowly in ambient air. Colorless plates were obtained after two days. M.p. >300˚C (decomp.).

2.2.2.5 Synthesis of 4,4'-trimethylenedipyridinium 2,4-*bis*-(4-carboxyphenoxy)-6-(4-carboxylatephenoxy)-1,3,5-triazine, **5**

To a solution of TCPT (0.05 g, 0.10 mmol) in 5 mL of DMF was added a DMF solution (5 mL) containing 4,4'-trimethylenedipyridine (tmdipy) (0.03 g, 0.15 mmol). Slow evaporation of the solvent produced colorless prisms after two days. M.p. 218-221˚C (decomp.).

2.2.2.6 Synthesis of 2,4,6-*tris*-(4-carboxyphenoxy)-1,3,5-triazine *bis*-(4-pyridyl)-ethane$_{0.5}$ DMF, **6**

TCPT (0.05 g, 0.10 mmol) was dissolved in 5 mL of DMF. To this solution was added a DMF solution (5 mL) containing bipya (0.02 g, 0.10 mmol). Slow evaporation of the solvent yielded yellow prisms after two weeks. M.p. 190-195˚C (decomp.).

2.2.3 X-ray crystallography

X-ray data were collected on a Bruker SMART 1000 four-circle CCD diffractometer using a fine-focus molybdenum Kα tube. Data were collected using SMART.[18] Initial cell constants were found by small widely separated "matrix" runs. Preliminary Laué symmetry was determined from axial images. Generally, an entire hemisphere of reciprocal space was collected regardless of Laué symmetry. Scan speed and scan width were chosen based on scattering power and peak rocking curves. Unless otherwise noted,

0.3 ° scans were used. Unit cell constants and orientation matrix were improved by least-squares refinement of reflections "thresholded" from the entire dataset. Integration was performed with SAINT,[19] using this improved unit cell as a starting point. Precise unit cell constants were calculated in SAINT from the final merged dataset. Lorenz and polarization corrections were applied, but data were not corrected for absorption. Laué symmetry, space group, and unit cell contents were found with XPREP. Data were reduced with SHELXTL.[20] The structures were solved in all cases by direct methods without incident. In general, hydrogen atoms were assigned to idealized positions and were allowed to ride. Unless otherwise noted, the coordinates of hydrogen-bonding hydrogen atoms were allowed to refine.

2.2.4 Powder X-ray diffraction

Powder XRD data were collected on a Bruker/Nonius D8 ADVANCE diffractometer with Bragg-Brentano geometry. For a sample containing a 1:1 ratio between TCPT and bipya, a step size of 0.04˚ and a step time of 45.7 sec per step were used. A step size of 0.04˚ and a step time of 24 sec per step were used for a sample containing a 1:2 ratio between TCPT and bipya. Data for **6** were obtained over a 5-50˚ 2-θ range in both cases. Data were then processed using EVA v8.0.[21]

2.3 Results

Crystallographic data are given in Tables A1-A6. Hydrogen-bond geometries for **1-6** are provided in Table 2.1. Thermal ellipsoid plots showing numbering schemes and molecular geometries are displayed in Figure 2.1.

Table 2.1 Hydrogen-bond geometries for **1-6**.

Compound	D-H A	D-H/Å	H…A/Å	D…A/Å	<(DHA)/°	generator for A
1	O27 H27 N51	0.85(3)	1.86(3)	2.714(2)	175(3)	-1+x, y, z
	O37 H37 N71	1.04(3)	1.55(3)	2.578(2)	172(2)	1+x, y, z
	O47 H47 N61	1.08(2)	1.54(3)	2.602(2)	168(2)	-1-x, 1-y, 1-z
2	O29 H29 N71	0.92(3)	1.80(3)	2.717(2)	178(2)	1+x, y, z
	O39 H39 N51	0.98(3)	1.61(3)	2.589(2)	172(2)	-1+x, y, z
	O49 H49 N61	1.10(3)	1.52(3)	2.617(2)	170(2)	2-x, 1-y, -z
3	O27 H27 N51	1.09(4)	1.49(4)	2.575(3)	172(3)	2-x, 1-y, 1-z
	O37 H37 N71	1.04(4)	1.63(4)	2.654(4)	167(4)	x, y, -1+z
	O47 H47 N61	0.85(5)	1.88(5)	2.657(4)	151(5)	1+x, -1+y, z
4	O27 H27 N61	1.07(3)	1.51(3)	2.573(3)	175(3)	1+x, y, 1+z
	O37 H37 N51	0.98(4)	1.66(4)	2.623(3)	166(3)	2-x, 1-y, 1-z
	O47 H47 N71	1.09(4)	1.59(4)	2.663(3)	167(3)	-x, 1-y, 1-z
5	N51 H51 O27	1.12(4)	1.52(4)	2.625(5)	170(4)	-1+x, y, z
	O37 H37 O28	1.10(5)	1.46(5)	2.538(4)	165(4)	2-x, 1-y, 1-z
	O47 H47 N61	1.00(5)	1.66(5)	2.654(5)	171(5)	-1+x, 1+y, 1+z
6	O27 H27 O1S	1.01(2)	1.58(2)	2.5963(15)	176(2)	-1+x, 1-y, z
	O37 H37 N51	1.04(2)	1.55(2)	2.5778(17)	169(2)	1+x, y, z
	O47 H47 O48	0.926(18)	1.686(19)	2.6061(13)	172.3(19)	2-x, -y, -z

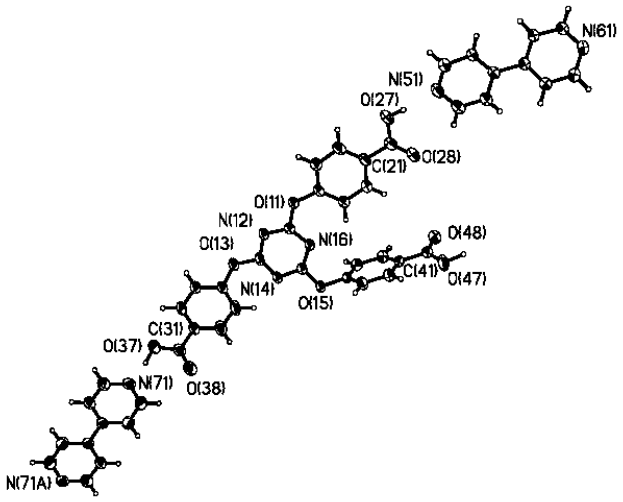

(a)

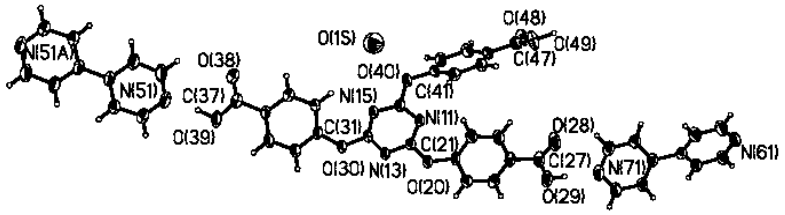

(b)

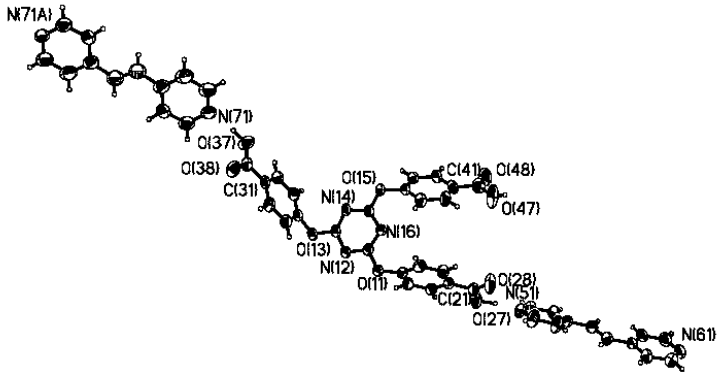
N(71A)
N(71)
O(37)
O(38)
C(31)
O(15)
C(41)
O(48)
N(14)
O(47)
N(16)
O(13)
N(12)
O(11)
C(21)
O(28)
N(51)
O(27)
N(61)

(c)

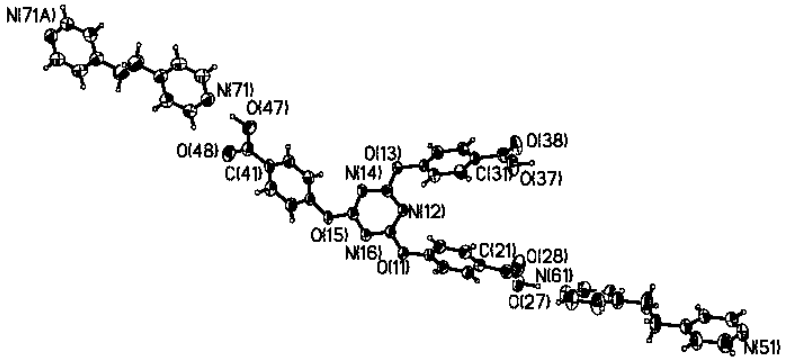
N(71A)
N(71)
O(47)
O(48)
C(41)
O(13)
N(14)
O(38)
C(31)
O(37)
N(12)
O(15)
N(16)
C(21)
O(28)
O(11)
N(61)
O(27)
N(51)

(d)

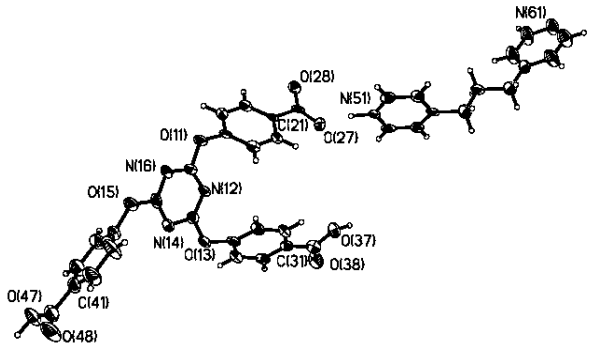
N(61)
O(28)
N(51)
C(21)
O(27)
O(11)
N(16)
O(15)
N(12)
N(14)
O(37)
O(13)
C(31)
O(38)
O(47)
C(41)
O(48)

(e)

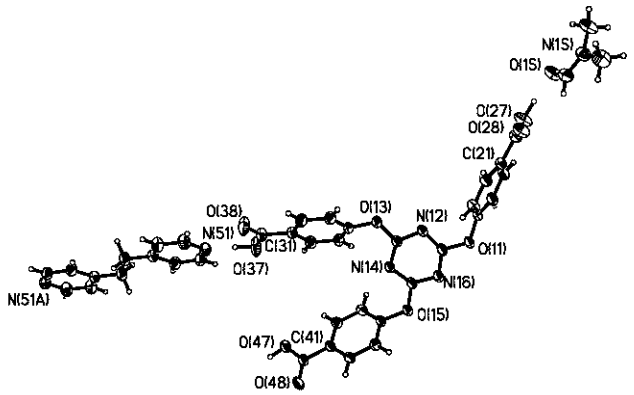

(f)

Figure 2.1a-f Thermal ellipsoid plots (50% probabilities) and labeling schemes for **1**-**6**.

*2.3.1 Crystal structure of 2,4,6-*tris*-(4-carboxyphenoxy)-1,3,5-triazine 4,4'-bipyridine$_{1.5}$,* **1**

The crystal structure of **1** consists of one molecule of TCPT and one and a half molecules of bipy in the asymmetric unit, Figure 2.1a. These molecules interact through three crystallographically unique O–H···N hydrogen bonds involving the O–H protons on the carboxylic acid moieties in TCPT and the pyridine nitrogen atoms on bipy (O27···N51, 2.714(2) Å; O37···N71, 2.578(2) Å; O47···N61, 2.602(2) Å). Two of the "arms" in TCPT are oriented in one direction while the third "arm" is situated in another direction together to adopt a φ- conformation, Scheme 2.4.

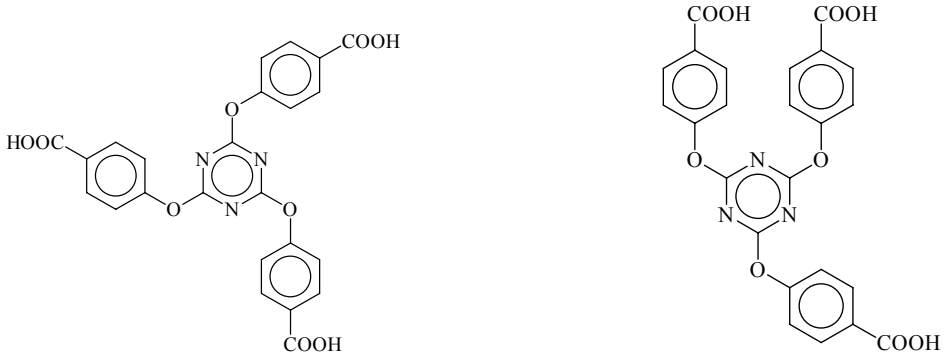

a **b**

Scheme 2.4 Two different possible conformations of TCPT: (a) the high-symmetry Δ-conformation and (b) the low-symmetry φ-conformation.

One of the three carboxyphenoxy moieties is oriented almost perpendicular to the plane of the triazine core (C15-O15-C44-C43, -98.7(2)˚). The three intermolecular O–H···N interactions produce an infinite 1-D assembly, Figure 2.2.

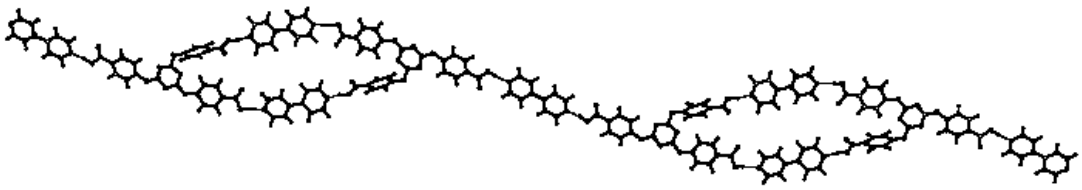

Figure 2.2 Infinite one-dimensional motif in **1**.

Two C–H···O bonds are also observed in the crystal structure of **1** between *ortho*- C–H moieties on bipy and carbonyl oxygen atoms on the carboxy groups in TCPT (C56–H56···O28, 3.14 Å; C72–H72···O38, 3.34 Å). These interactions augment two of the three primary carboxylic acid···pyridine hydrogen bonds.

*2.3.2 Crystal structure of 2,4,6-*tris*-(4-carboxyphenoxy)-1,3,5-triazine 4,4'-bipyridine$_{1.5}$ (H_2O)$_{0.3}$,* **2**

The asymmetric unit of **2** contains one molecule of TCPT, one and a half molecules of bipy, and one molecule of water of 30 % occupancy, Figure 2.1b. Three crystallographically distinct O–H···N hydrogen bonds occur between the O–H groups on the carboxylic acid moieties in TCPT and the pyridine nitrogen atoms on bipy (O29···N71, 2.717(2) Å; O39···N51, 2.589(2) Å; O49···N61, 2.617(2) Å). The TCPT molecule displays a φ-conformation similar to the one observed for TCPT in the crystal structure of **1**. One of the three carboxyphenoxy moieties is almost perpendicular to the plane of the triazine core (C16-O40-C41-C46, -98.4(2)˚). A water molecule is located between the two arms on the acid that are pointing in the same direction; however, since the hydrogen atoms could not be located, no hydrogen bonds were assigned within this structural unit. The asymmetric unit is propagated through an inversion center into an infinite one-dimensional chain, Figure 2.3, where two water molecules are located in each loop of the chain.

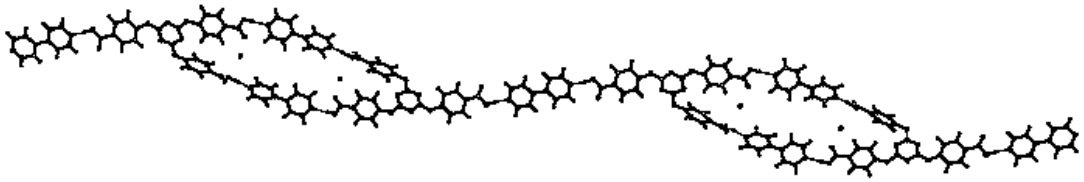

Figure 2.3 Extended one-dimensional chain in **2** showing water molecules inside the loops.

Two C–H···O hydrogen bonds are present in the crystal structure of **2** between the *ortho*-C–H moieties on bipy and the carbonyl oxygen atoms on carboxyl groups in TCPT (C52–H52···O38, 3.35 Å; C76–H76···O28, 3.14 Å). There are no significant interchain interactions in this crystal structure.

2.3.3 Crystal structure of 2,4,6-tris-*(4-carboxyphenoxy)-1,3,5-triazine* trans-*1,2*-bis-*(4-pyridyl)-ethylene*$_{1.5}$, **3**

The asymmetric unit of **3** consists of one molecule of TCPT and one and a half molecules of bipye, Figure 2.1c. These molecules interact through three crystallographically inequivalent O–H···N hydrogen bonds formed by the O–H groups on the carboxyl moieties in TCPT and the pyridine nitrogen atoms on bipye (O27···N51, 2.574(3) Å; O37···N71, 2.654(4) Å; O47···N61, 2.654(4) Å). Two of the carboxyphenoxy groups in TCPT are located in one direction while the third carboxyphenoxy moiety is oriented in the opposite direction with respect to the first two groups resulting in a φ-conformation. The intermolecular O–H···N hydrogen bonds organize TCPT and the ditopic hydrogen-bond acceptors into an extended one-dimensional chain, Figure 2.4.

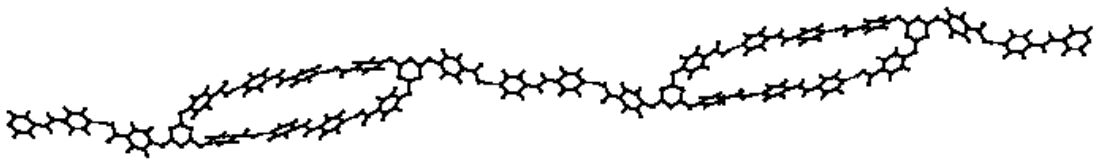

Figure 2.4 Infinite one-dimensional chain in the crystal structure of **3**.

The bipye molecules that form part of a loop are aligned in a parallel manner with respect to each other separated by *ca*. 7 Å. No C–H···O interactions are present in the crystal structure, as the *ortho*- C–H moieties on bipye and the carbonyl oxygen atoms on the carboxyl groups in TCPT are not co-planar. There are no significant directional interactions exist between neighboring chains.

*2.3.4 Crystal structure of 2,4,6-*tris*-(4-carboxyphenoxy)-1,3,5-triazine* bis*-(4-pyridyl)-ethane$_{1.5}$,* **4**

The asymmetric unit in **4** contains one molecule of TCPT and one and a half molecules of bipya, Figure 2.1d. These molecules are interconnected through three crystallographically unique O–H···N hydrogen bonds involving the O–H groups of carboxyl groups in TCPT and pyridine nitrogen atoms in bipya (O27···N61, 2.571(3) Å; O37···N51, 2.621(3) Å; O47···N71, 2.661(3) Å). Two of the carboxyphenoxy moieties are pointing in one vector whereas the third carboxyphenoxy group is located in the opposite direction to generate a φ-conformation. The asymmetric units are assembled into infinite one-dimensional hydrogen-bonded chains, Figure 2.5.

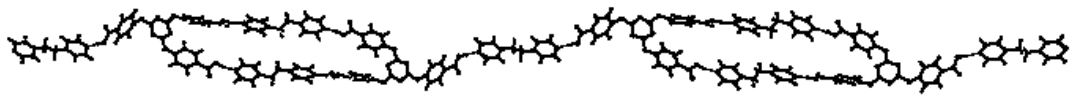

Figure 2.5 Infinite one-dimensional hydrogen-bonded chain in the crystal structure of **4**.

The two bipya molecules in each loop of the chain are aligned in a parallel fashion with respect to each other, separated by approximately 7 Å. There are no short C–H···O contacts present in the crystal structure, as the *ortho*- C–H protons on bipya and carbonyl oxygen atoms on carboxyl groups in TCPT are not co-planar. There are no readily identifiable directional interactions between adjacent chains.

*2.3.5 Crystal structure of 4,4'-trimethylenedipyridinium 2,4-*bis*-(4-carboxyphenoxy)-6-(4-carboxylatephenoxy)-1,3,5-triazine,* **5**

The crystal structure of **5** consists of one anion of $TCPT^-$ and one cation of $tmdipyH^+$ in the asymmetric unit, Figure 2.1e. A charge-assisted N–H···O interaction forms as a consequence of proton transfer between one of the carboxyl moieties in TCPT and a pyridine nitrogen atom in tmdipy (N51···O27, 2.625(5) Å). The anion in the crystal structure of **5** displays the φ-conformation which is similar to that presented by TCPT in **1-4**. One of the carboxyphenoxy groups and the carboxylatephenoxy moiety in $TCPT^-$ are oriented in one direction while the other carboxyphenoxy group is pointing in the opposite direction. The asymmetric units are in turn connected into an infinite undulating 1-D ladder, Figure 2.6, by O–H···N hydrogen bonds between the O–H groups on carboxyl moieties in $TCPT^-$ and the pyridine nitrogen atoms in $tmdipyH^+$ (O47···N61, 2.654(5) Å) as well as O–H···O hydrogen bonds between carboxylate units in $TCPT^-$ and neighboring $TCPT^-$ carboxyl groups (O37···O28, 2.538(4) Å).

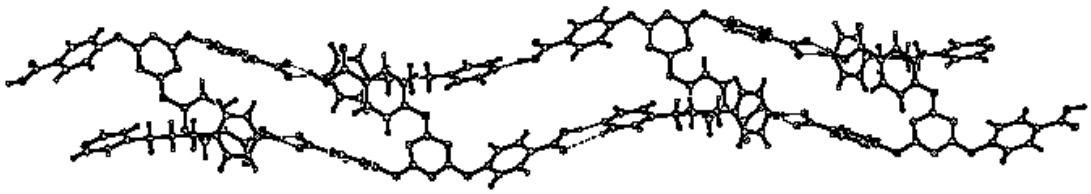

Figure 2.6 Infinite one-dimensional ladder motif in **5**.

The O–H···N hydrogen bonds are accompanied by C–H···O interactions formed between the *ortho*- C–H pmoieties on $tmdipyH^+$ and carbonyl oxygen atoms of carboxyl groups on $TCPT^-$ (C66–H66···O48, 3.19 Å). No significant directional interactions occur between adjacent ladders in **5**.

*2.3.6 Crystal structure of 2,4,6-*tris*-(4-carboxyphenoxy)-1,3,5-triazine* bis*-(4-pyridyl)-ethane$_{0.5}$ DMF,* **6**

The crystal structure of **6** contains one molecule of TCPT, half a molecule of bipya, and one molecule of DMF in the asymmetric unit, Figure 2.1f. These components interact through an O–H···N hydrogen bond between a carboxyl O–H group on TCPT and a pyridine nitrogen atom in bipya (O37···N51, 2.5780(17) Å) and an O–H···O

hydrogen bond between another carboxyl O–H moiety on TCPT and the oxygen atom in DMF (O27···O1S, 2.5972(14) Å). Once again, two of the carboxyphenoxy moieties in TCPT are located in one direction while the third carboxyphenoxy group is oriented in the opposite direction, resulting in a φ-conformation. The primary supramolecular motif is an undulating one-dimensional chain assembled by means of additional O–H···O hydrogen bonds between carboxyl groups in adjacent TCPT molecules (O47···O48, 2.6061(13) Å), Figure 2.7.

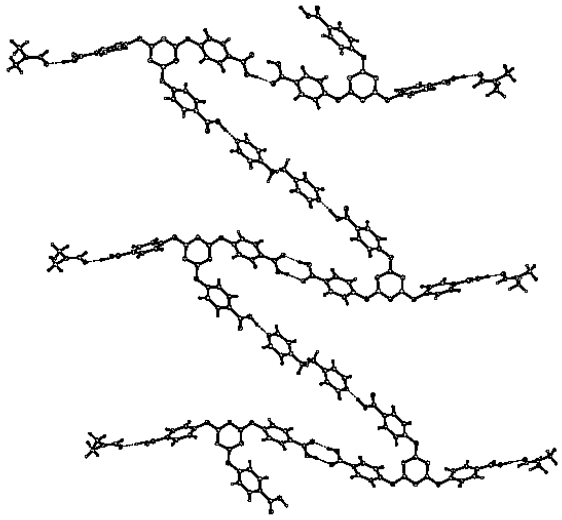

Figure 2.7 Infinite undulating 1-D motif in the crystal structure of **6** obtained through capping of outer carboxyphenoxy moieties with DMF molecules.

C–H···O interactions between *ortho*- C–H moieties of bipya and carbonyl oxygen atoms of carboxyl units in TCPT accompany the primary O–H···N hydrogen bonds (C52–H52···O38, 3.47 Å). No other noteworthy interactions occur in the crystal structure of **6**.

2.4 Discussion

Compounds **1**-**6** were all obtained upon crystallization of TCPT with bipy or its homologues in polar solvents. In each case, the solubility of TCPT was compatible with that of the ditopic base, which assisted the formation of binary co-crystals. The improved solubility of TCPT, compared with that of trimesic acid, has allowed for the facile

preparation of co-crystals, all of which contain the expected heteromeric O–H···N interaction. To date, there are only two crystallographically characterized molecular co-crystals of trimesic acid with bipy and its homologues[7] which, undoubtedly, is largely due to its poor solubility compared to that of the bipy counterparts. Consequently, simply in terms of generating a larger number of co-crystals, the SR examined herein possesses an advantage over trimesic acid. At the same time however, crystal structures **1**-**6** do not display the intended two-dimensional hexagonal frameworks as shown in Figure 2.2; instead, they all yield infinite one-dimensional architectures.

Structures **1**-**4** contain identical primary supramolecular chain-like motifs where interconnected loops are obtained as a result of O–H···N hydrogen bonding between the carboxyphenoxy moieties (in a φ-conformation) and the bipyridine homologues. The graph–set notations[22] for the loops are $R_4^4(54)$ (for **1** and **2**), and $R_4^4(58)$ (for **3** and **4**), which reflects the fact that a slightly longer ditopic hydrogen-bond acceptor is used for the latter structures; the number of hydrogen-bonds, however, stays the same. No proton transfer from acid to base takes place in any of these four structures. Furthermore, water molecules have been incorporated into the crystal structure of **2**, and the solvent molecules are located within the loops of the extended chains without disrupting the primary O–H···N hydrogen-bonded motif. The parallel alignment of the double bonds of bipye molecules in **3** resembles that obtained from resorcinol-directed assembly of bipye molecules;[2c] however, the distance between adjacent double bonds in **3** is too great (*ca*. 7 Å), to make it a suitable candidate for successful photoinduced 2+2 cycloaddition.

The crystal structure of **5** reveals a different connectivity than **1**-**4** since an ionic compound had formed as a consequence of proton transfer between one of the carboxyphenoxy moieties in TCPT and one of the pyridine nitrogen atoms in tmdipy. In addition to this primary $N–H^+···O^-$ interaction, complementary carboxylic acid···carboxylate hydrogen bonds occur between adjacent TCPT units. Thus, only one of the carboxyphenoxy groups interacts with a pyridine nitrogen atom in tmdipy to form a neutral O–H···N hydrogen bond. The same structural conformation of TCPT in **1**-**4** was also observed in **5**.

The crystal structure of **6** contains DMF solvent molecules, which is not observed in **4**. In **4**, the supramolecular reaction was set up in a 1:1.5 ratio whereas in **6** the reaction

was carried out in a 1:1 stoichiometry. The solvated structure, **6**, was also obtained from a reaction between TCPT and bipya in a 1:2 molar ratio. The central SR once again adopts the φ-conformation.

The structural homogeneities of bulk samples of co-crystals consisting of TCPT and bipya in both 1:1 and 1:2 molar ratios were examined using powder XRD. When TCPT and bipya were set up in a 1:1 stoichiometry, the DMF-solvated structure was obtained (**6**) but the experimental powder pattern of the bulk, Figure 2.8b, also contain peaks that originate from the crystal structure of **4**, as demonstrated by the simulated powder pattern for this structure, Figure 2.8a. Consequently, the supramolecular reaction yielded a mixture of the two products. When the reaction between TCPT and bipya was carried out in a 1:2 molar ratio, diffraction peaks derived from both crystalline compounds **4** and **6** were observed, Figure 2.8c. The powder diffraction work indicates that the structural outcome cannot be fully controlled by controlling stoichiometries of the two reactants, and the reactions do not proceed completely to a single new crystalline phase under the different conditions that we have examined.

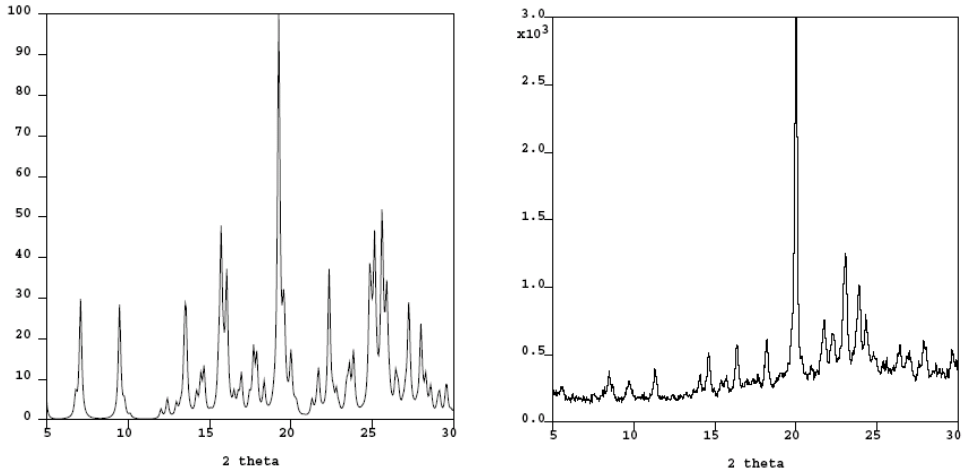

(a) (b)

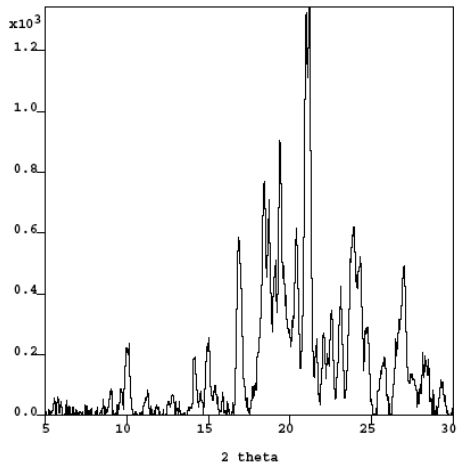

(c)

Figure 2.8 Powder XRD patterns for (a) **4** (simulated); (b) TCPT:bipya 1:1 (experimental); and (c) TCPT:bipya 1:2 (experimental).

There are two different possible conformations for TCPT, Δ and φ, Scheme 2.4. In every structure, **1**-**6**, TCPT appears in the low-symmetry φ-conformation. For each possible conformation, the primary robust O–H···N hydrogen bonds in co-crystals of TCPT and ditopic bases could, in principle, be the same. The energetically more "stable" high-symmetry conformation is, however, abandoned each time in favor of the φ-conformation. This is probably because the low-symmetry φ-conformation results in a supramolecular motif (an infinite chain) that can produce a closer packed structure compared to the much more open hexagonal extended framework that would result if TCPT had adopted the Δ-conformation. In **1**-**6**, the carboxyphenoxy groups in the φ-conformation of TCPT are frequently coplanar with the triazine ring. Such a conformation is similar to that observed in other structurally flexible tritopic SR's containing bridging methylene groups in the "arms" such as 1,3,5-*tris*-(imidazol-1-ylmethyl)-2,4,6-trimethylbenzene;[23] in this SR, however, the imidazol-1-ylmethyl moieties are not coplanar with respect to the benzene core.

We furthermore noted in the CSD that in the absence of any hydrogen-bond functionalities, similar 2,4,6-*tris*-phenoxy-1,3,5-triazine compounds adopt the Δ-conformation and are mainly stabilized by weaker intermolecular interactions.[16a,24]

In an attempt to induce three-fold symmetry in our SR (in order to construct infinite 2-D networks) we proceeded to set up co-crystallizations employing highly symmetric

guests and/or co-solvents such as hexachlorobenzene, hexamethylbenzene, and tribromobenzene that can act as templates for a three-fold symmetric framework.[25] However, even in the presence of a variety of rigid tritopic guests or co-solvents we were unable to produce co-crystals that contained TCPT in the high-symmetry Δ-conformation.

2.5 Conclusions

The structurally flexible TCPT does provide an advantage over the rigid trimesic acid in that it is more soluble and thus creates more opportunity for co-crystal formation. At the same time, however, such flexibility also changes the supramolecular product to a 1-D motif, instead of the desired 2-D hexagonal network. On one hand, if the goal is to maintain high symmetry, then a more structurally rigid SR such as trimesic acid can be employed as long as the inherent problems with solvent compatibility between the two or more reactants can be overcome. One the other hand, if the goal is to facilitate co-crystallization formation with heterocyclic hydrogen-bond acceptors then a more structurally flexible SR such as TCPT is a better choice for a co-crystallizing agent. The latter option is often desired in the pharmaceutical industry, since co-crystal formation may provide improvement in the physical properties of a pharmaceutical product, thereby acquiring a higher priority than supramolecular predictability.[26,27]

References

[1] (a) Desiraju, G. R. *Angew. Chem. Int. Ed. Engl.* **1995**, *34*, 2311. (b) Bailey, M.; Brown, C. J. *Acta Crystallogr.* **1967**, *22*, 387. (c) Alcala, R.; Martinez-Carrera, S. *Acta Crystallogr.* **1972**, *B28*, 1671; (d) Duchamp, D. J.; Marsh, R. E. *Acta Crystallogr.* **1969**, *B25*, 5. (e) Etter, M. C. *J. Phys. Chem.* **1991**, *95*, 4601. (f) Vishweshwar, P.; Nangia, A.; Lynch, V. M. *J. Org. Chem.* **2002**, *67*, 556.

[2] (a) Whitesides, G. M.; Simanek, E. E.; Mathias, J. P.; Seto, C. T.; Chin, D. N.; Mammen, M.; Gordon, D. M. *Acc. Chem. Res.* **1995**, *28*, 37. (b) Batchelor, E.; Klinowski, J.; Jones, W. *J. Mater. Chem.* **2000**, *10*, 839. (c) MacGillivray, L. R.; Reid, J. L.; Ripmeester, J. A. *J. Am. Chem. Soc.* **2000**, *122*, 7817. (d) MacGillivray, L. R.; Papaefstathiou, G. S.; Reid, J. L.; Ripmeester, J. A. *Cryst. Growth Des.* **2001**, *1*, 373. (e) Zaman, M. B.; Tomura, M.; Yamashita, Y. *J. Org. Chem.* **2001**, *66*, 5987. (f) Pedireddi, V. R. *CrystEngComm* **2002**, *4*, 315. (g) Shan, N.; Batchelor, E.; Jones, W. *Tetrahedron Lett.* **2002**, *43*, 8721. (h) Kumar, V. S. S.; Nangia, A.; Katz, A. K.; Carrell, H. L. *Cryst. Growth Des.* **2002**, *2*, 313. (i) Barnett, S. A.; Blake, A. J.; Champness, N. R. *CrystEngComm* **2003**, *5*, 134. (j) Arora, K. K.; Pedireddi, V. R. *J. Org. Chem.* **2003**, *68*, 9177. (k) Bowers, J. R.; Hopkins, G. W.; Yap, G. P. A.; Wheeler, K. A. *Cryst. Growth Des.* **2005**, *5*, 727. (l) Aakeröy, C. B.; Desper, J.; Leonard, B.; Urbina, J. F. *Cryst. Growth Des.*, **2005**, DOI: 10.1021/cg049682i.

[3] Desiraju, G. R.; Sharma, C. V. K. *The Crystal as a Supramolecular Entity*; John Wiley & Sons, Ltd., 1996.

[4] (a) Aakeröy, C. B.; Beatty, A. M.; Helfrich, B. A. *Angew. Chem. Int. Ed. Engl.* **2001**, *40*, 3240. (b) Aakeröy, C. B.; Beatty, A. M.; Helfrich, B. A. *J. Am. Chem. Soc.* **2002**, *124*, 14425.

[5] Shan, N.; Bond, A. D.; Jones, W. *Cryst. Eng.* **2002**, *5*, 9.

[6] Liu, R.; Valiyaveettil, S.; Mok, K.-F.; Vittal, J. J.; Hoong, A. K. M. *CrystEngComm* **2002**, *4*, 574.

[7] Sharma, C. V. K.; Zaworotko, M. J. *Chem. Commun.* **1996**, 2655.

[8] (a) Ma, B.-Q.; Coppens, P. *Chem. Commun.* **2003**, 2290. (b) Ermer, O.; Neudörfl, J. *Helv. Chim. Acta* **2001**, *84*, 1268. (c) Herbstein, F. H.; Kapon, M.; Shteiman, V. *Acta Crystallogr.* **2001**, *B57*, 692. (d) Kolotuchin, S. V.; Fenlon, E. E.; Wilson, S. R.; Loweth, C. J.; Zimmerman, S. C. *Angew. Chem. Int. Ed. Engl.* **1995**, *34*, 2654. (e) Herbstein, F. H.; Kapon, M.; Reisner, G. M. *J. Inclusion Phenom. Macrocyclic Chem.* **1987**, *5*, 211. (f) Herbstein, F. H.; Kapon, M.; Reisner, G. M. *Acta Crystallogr.* **1985**, *B41*, 348. (g) Herbstein, F. H.; Marsh, R. E. *Acta Crystallogr.* **1977**, *B33*, 2358.

[9] (a) Liu, R.; Mok, K.-F.; Valiyaveettil, S. *New J. Chem.* **2001**, *25*, 890. (b) Ermer, O.; Neudörfl, J. *Chem. Eur. J.* **2001**, *7*, 4961. (c) Videnova-Adrabinska, V. *J. Mol. Struct.* **1996**, *374*, 199. (c) Lynch, D. E.; Smith, G.; Byriel, K. A.; Kennard, C. H. L. *Aust. J. Chem.* **1992**, *45*, 835.

[10] Allen, F. A. *Acta Crystallogr., Sect. B.* **2002**, *58*, 380.

[11] (a) Chatterjee, S.; Pedireddi, V. R.; Ranganathan, A.; Rao, C. N. R. *J. Mol. Struct.* **2000**, *520*, 107. (a) Barrio, C.; García-Granda, S.; Gómez-Beltrán, F. *Acta Crystallogr.* **1993**, *C49*, 253. (b) Herbstein, F. H.; Kapon, M.; Maor, I.; Reisner, G. M. *Acta Crystallogr.* **1981**, *B37*, 136. (c) Herbstein, F. H.; Kapon, M.; Wasserman, S. *Acta Crystallogr.* **1978**, *B34*, 1613. (d) Herbstein, F. H.; Kapon, M. *Acta Crystallogr.* **1978**, *B34*, 1608.

[12] (a) Almeida Paz, F. A.; Klinowski, J. *CrystEngComm* **2003**, *5*, 238. (b) Meléndez, R. E.; Sharma, C. V. K.; Zaworotko, M. J.; Bauer, C.; Rogers, R. D. *Angew. Chem. Int. Ed. Engl.* **1996**, *35*, 2213.

[13] Bhogala, B. R.; Vishweshwar, P.; Nangia, A. *Cryst. Growth Des.* **2002**, *2*, 325.

[14] Bhogala, B. R.; Nangia, A. *Cryst. Growth Des.* **2003**, *3*, 547.

[15] Even though two-dimensional hexagonal systems exist between CTA and ditopic bases, there are also examples of one-dimensional tapes and two-dimensional sheets: Shan, N.; Bond, A. D.; Jones, W. *New J. Chem.* **2003**, *27*, 365.

[16] (a) Thalladi, V. R.; Brasselet, S.; Weiss, H.-C.; Bläser, D.; Katz, A. K.; Carrell, H. L.; Boese, R.; Zyss, J.; Nangia, A.; Desiraju, G. R. *J. Am. Chem. Soc.* **1998**, *120*, 2563. (b) Jetti, R. K. R.; Thallapally, P. K.; Xue, F.; Mak, T. C. W.; Nangia, A. *Tetrahedron*, **2000**, *56*, 6707.

[17] Gronowitz, S.; Röe, J. *Acta Chem. Scand.* **1965**, *19*, 1741.

[18] SMART v5.060; Bruker Analytical X-ray Systems: Madison, WI, 1997-1999.

[19] SAINT v6.02; Bruker Analytical X-ray Systems: Madison, WI, 1997-1999.

[20] SHELXTL v5.10; Bruker Analytical X-ray Systems: Madison, WI, 1997.

[21] EVA v8.0; Bruker AXS Gmbh: Karlsruhe, West Germany, 1997-2002.

[22] (a) Etter, M. C.; MacDonald, J. C.; Bernstein, J. *Acta Cryst.* **1990**, *B46*, 256. (b) Bernstein, J.; Davis, R. E.; Shimoni, L.; Chang, N. -L. *Angew. Chem. Int. Ed. Engl.* **1995**, *34*, 1555.

[23](a) Liu, H. K.; Sun, W. Y.; Tang, W. X.; Yamamoto, T.; Ueyama, N. *Inorg. Chem.* **1999**, *38*, 6313. (b) Cai, Y. P.; Kang, B. S.; Su, C. Y.; Zhang, H. X.; Yang, X. P.; Deng, L. R.; Xu, A. W.; Zhou, Z. Y.; Chan, A. S. C. *Chinese J. Struct. Chem.* **2001**, *20*, 262.

[24] (a) Boese, R.; Desiraju, G. R.; Jetti, R. K. R.; Kirchner, M. T.; Ledoux, I.; Thalladi, V. R.; Zyss, J. *Struct. Chem.*, **2002**, *13*, 321. (b) Thalladi, R.; Boese, R.; Brasselet, S.; Ledoux, I.; Zyss, J.; Jetti, R. K. R.; Desiraju, G. R. *Chem. Commun.* **1999**, 1639. (c) Anthony, A.; Desiraju, G. R.; Jetti, R. K. R.; Kuduva, S. S.; Madhavi, N. N. L.; Nangia, A.; Thaimattam, R.; Thalladi, V. R. *Cryst. Eng.* **1998**, *1*, 1. (d) Jessiman, A. S.; MacNicol, D. D.; Malinson, P. R.; Vallance, I. *Chem. Commun.* **1990**, 1619.

[25] (a) Jetti, R. K. R.; Nangia, A.; Xue, F.; Mak, T. C. W. *Chem. Commun.* **2001**, 919. (b) Jetti, R. K. R.; Thallapally, P. K.; Nangia, A.; Lam, C.-K.; Mak, T. C. W. *Chem. Commun.* **2002**, 952.

[26] Aakeröy, C. B.; Beatty, A. M.; Helfrich, B. A.; Nieuwenhuyzen, M. *Cryst. Growth Des.* **2003**, *3*, 159.

[27] Almarsson, Ö.; Zawarotko, M. J. *Chem. Commun*, **2004**, 1889.

Chapter 3

Directed assembly of ditopic imidazoles/benzimidazoles and dicarboxylic acids into co-crystals *via* selective O–H···N hydrogen bonds

3.1 Introduction

Understanding the nature of intermolecular interactions is a crucial aspect of crystal engineering,[1,2,3] and the hydrogen bond has been established as the most effective tool for constructing sophisticated assemblies from discrete ionic or molecular building blocks due to its strength and directionality.[1,3] A key requirement in the development of strategies for non-covalent synthesis is the availability of reliable supramolecular synthons.[4,5] The usefulness of supramolecular synthons is related to the frequency of occurrence of desired intermolecular interactions between molecules under certain reaction conditions. Such reliability can be paralleled to named reactions in organic chemistry where molecular transformations or specific bond-making/breaking events take place under particular reaction conditions with high degrees of certainty. Typically, reliable supramolecular synthons need to be insensitive to subtle changes in molecular shape, substituent groups, as well as to competition from other intermolecular interactions such as π···π interactions and interactions with solvent molecules.

In Chapter 2 we examined a supramolecular synthon that has been employed frequently in the construction of extended architectures in the solid state – the carboxylic acid···pyridine (COOH···Py) synthon, Scheme 3.1.

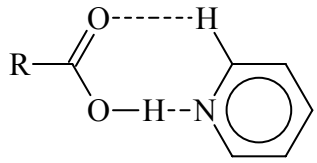

Scheme 3.1 The carboxylic acid···pyridine synthon.

The COOH···Py synthon consists of the primary O–H···N hydrogen bond and the auxiliary C–H···O interaction (although the latter may not always be present). It has been instrumental in the design of one- and two-dimensional supramolecular architectures,

such as infinite chains,[6] honeycomb layers,[7] and sheets,[8] utilizing 4,4'-bipyridine and its derivatives as the hydrogen-bond acceptor.

Since crystal engineering also seeks to mimic sophisticated and delicate systems observed in Nature, it is necessary to identify synthons built upon chemical moieties compatible with or encountered in biology and biochemistry. As a result, we will focus on the carboxylic acid···imidazole (COOH···Im) and carboxylic acid···benzimidazole (COOH···Bzim) interactions, which have more biological relevance than the COOH···Py synthon.

Imidazole (Im), benzimidazole (Bzim), and their derivatives are ubiquitous in biological and biochemical structure and function, such as the roles of histidine as a metal ion binding site in metalloenzymes[9] and in the catalytic mechanisms of ribonucleases and other phosphoesterases.[10] Histidine also plays a part in cytochrome *c* peroxidase[11] as well as in copper transport in humans.[12] Im and Bzim derivatives have also found applications in drug design in the forms of antitumor[13] and anticancer[14] agents. In fact, these derivatives are known to treat a variety of physiological disorders.[15] Consequently, the importance of imidazoles and benzimidazoles in biology and biochemistry cannot be overstated.

We are interested in exploring the reliability of the COOH···Im and COOH···Bzim synthons in the presence of potentially disruptive intermolecular interactions such as π···π interactions and interactions with solvent molecules. In addition, we will study the effect of molecular shape, molecular isomerism, and substituent groups on these synthons by altering the geometry involved in the constituent intermolecular interactions (*i.e.* switching from imidazole to benzimidazole, varying the positions of these heterocyclic moieties in molecules, and by replacing the H2 hydrogen atom on the benzimidazol-1-yl moiety with a methyl group). By understanding these scenarios we can develop a library of reliable supramolecular synthons that can, in principle, find applications in more sophisticated biological systems *e.g.* cytochrome *c* peroxidase[11] and CGS 14796C[17] in order to better understand the nature and roles of relevant intermolecular interactions.

When carboxylic acids interact with Im and Bzim the solid state outcome is often an organic salt, not a co-crystal, as a result of proton transfer.[16] A co-crystal can form, however, if a carboxylic acid interacts with an imidazol-1-yl or benzimidazol-1-yl moiety

as noted in the crystal structure of 1,4-*bis*-[(imidazol-1-yl)methyl]-cyclohexane succinic acid, a 1:1 co-crystal (CGS 14796C, an active non-steroidal aromatase inhibitor).[17] An O–H···N hydrogen bond is formed between the carboxylic acid group on succinic acid and the imidazol-1-yl nitrogen atom.

In this chapter, we present the syntheses of six closely related symmetric ditopic *bis*-imidazol-1-yl/*bis*-benzimidazol-1-yl compounds, and the crystal structures of three of them, **7**-**9**. We will subsequently test the limits and limitations of COOH···Im/COOH···Bzim interactions through a systematic structural study of eleven molecular co-crystals composed of dicarboxylic acids and these ditopic *N*-heterocyclic compounds; 1,4-*bis*-[(imidazol-1-yl)methyl]-benzene *trans*-3-hexenedioic acid (**10**), 1,4-*bis*-[(imidazol-1-yl)methyl]-benzene fumaric acid (**11**), 1,4-*bis*-[(imidazol-1-yl)methyl]-benzene succinic acid (**12**), 1,4-*bis*-[(imidazol-1-yl)methyl]-benzene *iso*phthalic acid (**13**), 1,4-*bis*-[(benzimidazol-1-yl)methyl]-benzene fumaric acid (**14**), 1,4-*bis*-[(benzimidazol-1-yl)methyl]-benzene malonic acid (**15**), 1,4-*bis*-[(benzimidazol-1-yl)methyl]-benzene *iso*phthalic acid $EtOH_{0.5}$ (**16**), 1,4-*bis*-[(benzimidazol-1-yl)methyl]-benzene 5-amino*iso*phthalic acid $EtOH_{0.5}$ (**17**), 1,3-*bis*-[(benzimidazol-1-yl)methyl]-benzene malonic acid (**18**), 1,4-*bis*-[(2-methylbenzimidazol-1-yl)methyl]-benzene *trans*-3-hexenedioic acid (**19**), and 1,4-*bis*-[(2-methylbenzimidazol-1-yl)methyl]-benzene adipic acid (**20**).

N-substituted symmetric ditopic imidazoles and benzimidazoles can be prepared by substituting the N1 atom on the Im and Bzim moieties with an alkyl group, Scheme 3.2.

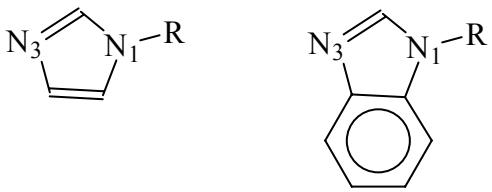

Scheme 3.2 *N*-substituted imidazoles and benzimidazoles denoting labeled nitrogen atoms.

We will also investigate the nature of the C–H···O interaction that can arise from the COOH···Im and COOH···Bzim synthons. Since an O–H···N hydrogen bond would

involve the best hydrogen-bond donor (the acidic OH group of the carboxylic acid) and the best hydrogen-bond acceptor (the heterocyclic nitrogen atom), we can, therefore, expect this hydrogen bond to be the primary intermolecular force. In co-crystals of carboxylic acids and 4,4'-bipyridine, a secondary C–H···O interaction arises from the C–H group on the C2 carbon of 4,4'-bipyridine and the carbonyl oxygen atom of the carboxylic acid. However, since 4,4'-bipyridine is symmetric about the nitrogen atoms, the *ortho*- C–H groups are equivalent. This is not the case in the COOH···Im and COOH···Bzim synthons because the *ortho*- C–H groups possess different acidities. Thus, our study will allow us to establish if the carbonyl oxygen atom on the acid shows a preference for the more acidic of the two C–H options,[18] Scheme 3.3.

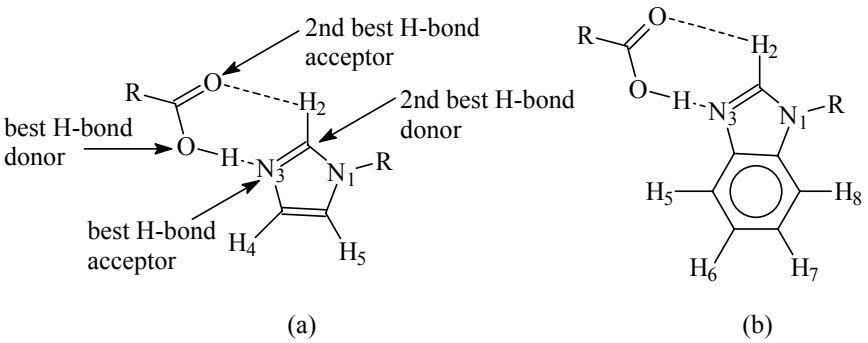

Scheme 3.3 The (a) COOH···Im and (b) COOH···Bzim synthons indicating the best and second-best hydrogen-bond donor/acceptor couples.

3.2 Experimental

3.2.1 Synthesis

All starting materials were purchased from Aldrich and used without further purification. Melting points were determined on a Fisher-Johns melting point apparatus and are uncorrected.

3.2.1.1 Synthesis of 1,4-*bis*-[(imidazol-1-yl)methyl]-benzene dihydrate[19]

α,α'-Dichloro-*p*-xylene (3.90 g, 22.3 mmol) and imidazole (15.8 g, 232 mmol) were dissolved in 250 mL of methanol with stirring in a 500-mL round-bottomed flask. A reflux condenser was attached, and the clear, colorless solution was heated and stirred

under reflux. The reaction was followed by TLC. After 17 h, the mixture was cooled and concentrated *via* rotary evaporation to afford a yellow syrup. A K_2CO_3 solution (31.2 g in 300 mL of distilled water) was then added to the flask containing the yellow syrup immediately producing white microcrystals, which were collected by vacuum filtration. The microcrystalline solid was recrystallized from 600 mL of hot distilled water to yield long, white needles, which was filtered *via* vacuum filtration, collected, and dried. Yield 4.17 g (68%); m.p. 128-131˚C; ^{1}H NMR (DMSO-d_6, 400 MHz) δ 5.16 (s, 4H), 6.88 (s, 2H), 7.15 (s, 2H), 7.23 (s, 4H), 7.72 (s, 2H).

3.2.1.2 Synthesis of 1,3-*bis*-[(imidazol-1-yl)methyl]-benzene

α,α'-Dichloro-*m*-xylene (2.00 g, 11.0 mmol) and imidazole (7.76 g, 114 mmol) were dissolved in 100 mL of methanol with stirring in a 250-mL round-bottomed flask. A reflux condenser was attached, and the clear, colorless solution was heated and stirred under reflux. The reaction progress was followed by TLC. After 42 h, the mixture was cooled and concentrated *via* rotary evaporation to produce a yellow syrup. A K_2CO_3 solution (15.4 g in 100 mL of distilled water) was added to form a clear, pale yellow solution. A fine and white solid precipitated within 30 min, and was filtered *via* vacuum filtration, collected, and dried. Yield 2.06 g (78.8%); m.p. 45-48˚C; ^{1}H NMR (DMSO-d_6, 400 MHz) δ 5.17 (s, 4H), 6.90 (s, 2H), 7.14 (d, 4H, J = 6.4 Hz), 7.20 (s, 1H), 7.34 (t, 1H, J = 7.6 Hz), 7.72 (s, 2H).

3.2.1.3 Synthesis of 1,4-bis-[(2-methylimidazol-1-yl)methyl]-benzene

α,α'-Dichloro-*p*-xylene (2.00 g, 11.0 mmol) and 2-methylimidazole (9.77 g, 119 mmol) were dissolved in 100 mL of methanol with stirring in a 250-mL round-bottomed flask. A reflux condenser was attached, and the clear, colorless solution was heated and stirred under reflux. The reaction progress was monitored by TLC. After 24 h, the mixture was cooled and concentrated *via* rotary evaporation to afford a white microcrystalline solid. A K_2CO_3 solution (15.4 g in 125 mL of distilled water) was added to produce a clear, colorless solution. Within 2 h, a white microcrystalline solid formed, which was filtered *via* vacuum filtration, collected, and dried. Yield 2.18 g (74.6%); m.p. 150-153˚C; ^{1}H

NMR (DMSO-d_6, 400 MHz) δ 2.20 (s, 6H), 5.11 (s, 4H), 6.74 (d, 2H, J = 1.2 Hz), 7.09 (d, 2H, J = 1.2 Hz), 7.11 (s, 4H).

3.2.1.4 Synthesis of 1,4-*bis*-[(benzimidazol-1-yl)methyl]-benzene, **7**

α,α'-Dichloro-*p*-xylene (1.00 g, 5.70 mmol) and benzimidazole (7.03 g, 59.5 mmol) were dissolved in 60 mL of methanol with stirring in a 250-mL round-bottomed flask. A reflux condenser was attached, and the clear, dark brown mixture was heated and stirred under reflux. The reaction progress was monitored by TLC. After 22 h, the mixture was cooled and concentrated *via* rotary evaporation to obtain a dark brown syrup that soon solidified. The solid was then washed with 100 mL of acetone and filtered by vacuum filtration. The remaining solid was further washed with 75 mL of distilled water by heating and stirring the suspension under reflux for 1 h. The resulting pale brown solid, was filtered *via* vacuum filtration, collected, and dried. Slow evaporation of the product from absolute ethanol produced orange plates, **7**. Yield 1.31 g (67.8%); m.p. 187-191˚C; ^{1}H NMR (DMSO-d_6, 400 MHz) δ 5.45 (s, 4H), 7.17 (m, 4H), 7.26 (s, 4H), 7.46 (m, 2H), 7.64 (m, 2H), 8.36 (s, 2H).

3.2.1.5 Synthesis of 1,3-*bis*-[(benzimidazol-1-yl)methyl]-benzene

α,α'-Dichloro-*m*-xylene (2.00 g, 11.0 mmol) and benzimidazole (13.6 g, 115 mmol) were dissolved in 100 mL of methanol with stirring in a 250-mL round-bottomed flask. A reflux condenser was attached, and the clear, dark brown solution was heated and stirred under reflux. The reaction progress was monitored *via* TLC. The reaction was cooled after 24 h and concentrated by rotary evaporation to produce a dark brown solid. The solid was then washed with 150 mL of acetone and filtered *via* vacuum filtration. The clear, brown filtrate was concentrated by rotary evaporation to obtain a brown solid. This solid was washed with 150 mL of distilled water by heating and stirring the suspension under reflux for 1.5 h. The remaining brown solid was filtered *via* vacuum filtration, collected, and dried. Slow evaporation of the product from absolute ethanol produced amber prisms, **8**. Yield 2.09 g (56.1%); m.p. 70-75˚C; ^{1}H NMR (DMSO-d_6, 400 MHz) δ 5.46 (s, 4H), 7.17 (m, 5H), 7.28 (t, 1H, J = 8 Hz), 7.43 (m, 4H), 7.65 (dd, 2H, J_1 = 6.4 Hz, J_2 = 1.6 Hz), 8.38 (s, 2H).

3.2.1.6 Synthesis of 1,4-*bis*-[(2-methylbenzimidazol-1-yl)methyl]-benzene, **9**

α,α'-Dichloro-*p*-xylene (0.50 g, 2.86 mmol) and 2-methylbenzimidazole (3.93 g, 29.8 mmol) were dissolved in 30 mL of methanol with stirring in a 100-mL round-bottomed flask. A reflux condenser was attached, and the clear, yellow solution was heated and stirred under reflux. The reaction progress was followed by TLC. After 24 h, the mixture was cooled and concentrated by rotary evaporation to obtain an off-white solid. The solid was washed with 40 mL of distilled water by heating and stirring the suspension under reflux for 1 h. The remaining off-white solid was filtered *via* vacuum filtration. The solid was then washed with 10 mL of cold acetone, and a fine, white solid was obtained upon vacuum filtration. The white solid was further washed with 150 mL of distilled water by heating and stirring the suspension under reflux for 1 h. The resulting white solid was immediately filtered by vacuum filtration, washed with small amounts of distilled water, collected, and dried. Colorless plates of **9** were obtained upon recrystallization from absolute ethanol. Yield 0.32 g (30.7%); m.p. 255-258˚C; ^{1}H NMR (DMSO-d_6, 400 MHz) δ 2.48 (s, 6H), 5.41 (s, 4H), 7.08 (s, 4H), 7.12 (m, 4H), 7.41 (m, 2H), 7.52 (m, 2H).

3.2.2 Syntheses of co-crystals[20]

3.2.2.1 Synthesis of 1,4-*bis*-[(imidazol-1-yl)methyl]-benzene *trans*-3-hexenedioic acid, **10**

1,4-*bis*-[(imidazol-1-yl)methyl]-benzene (0.05 g, 0.18 mmol) was dissolved in 1 mL of methanol. To this solution was added an ethanolic solution containing *trans*-3-hexenedioic acid (0.03 g, 0.18 mmol). Colorless prisms were obtained after one week of slow evaporation of the solvent. M.p. 171-176˚C; IR (KBr pellet) ν 2450 cm^{-1}, 1928 cm^{-1} (O–H···N, br), 1700 cm^{-1} (C=O, s).

3.2.2.2 Synthesis of 1,4-*bis*-[(imidazol-1-yl)methyl]-benzene fumaric acid, **11**

1,4-*bis*-[(imidazol-1-yl)methyl]-benzene (0.05 g, 0.18 mmol) was dissolved in 1 mL of methanol. To this solution was added fumaric acid (0.02 g, 0.18 mmol) in ethanol.

Colorless prisms were afforded after one week of slow evaporation of the solvent. M.p. 175-178˚C; IR (KBr pellet) *v* 2472 cm^{-1}, 1931 cm^{-1} (O–H···N, br), 1695 cm^{-1} (C=O, s).

3.2.2.3 Synthesis of 1,4-*bis*-[(imidazol-1-yl)methyl]-benzene succinic acid, **12**

1,4-*bis*-[(imidazol-1-yl)methyl]-benzene (0.05 g, 0.18 mmol) was dissolved in 1 mL of methanol. An ethanolic solution of succinic acid (0.02 g, 0.18 mmol) was added to this solution. Colorless prisms were obtained after one week upon evaporation of the solvent. M.p. 159-161˚C; IR (KBr pellet) *v* 2423 cm^{-1}, 1952 cm^{-1} (O–H···N, br), 1700 cm^{-1} (C=O, s).

3.2.2.4 Synthesis of 1,4-*bis*-[(imidazol-1-yl)methyl]-benzene *iso*phthalic acid, **13**

1,4-*bis*-[(imidazol-1-yl)methyl]-benzene (0.05 g, 0.18 mmol) was dissolved in 1 mL of methanol. To this solution was added *iso*phthalic acid (0.03 g, 0.18 mmol) in ethanol. Colorless prisms were afforded after one week of slow evaporation of the solvent. M.p. 174-178˚C; IR (KBr pellet) *v* 2448 cm^{-1}, 1927 cm^{-1} (O–H···N, br), 1691 cm^{-1} (C=O, s).

3.2.2.5 Synthesis of 1,4-*bis*-[(benzimidazol-1-yl)methyl]-benzene fumaric acid, **14**

1,4-*bis*-[(benzimidazol-1-yl)methyl]-benzene (0.05 g, 0.15 mmol) was dissolved in 1 mL of ethanol. To this solution was added an ethanolic solution containing fumaric acid (0.020 g, 0.15 mmol). Orange plates were afforded after 24 h of slow evaporation of the solvent. M.p. 234-238˚C (decomp.); IR (KBr pellet) *v* 2450 cm^{-1}, 1917 cm^{-1} (O–H···N, br), 1700 cm^{-1} (C=O, s).

3.2.2.6 Synthesis of 1,4-*bis*-[(benzimidazol-1-yl)methyl]-benzene malonic acid, **15**

1,4-*bis*-[(benzimidazol-1-yl)methyl]-benzene (0.05 g, 0.15 mmol) was dissolved in 1 mL of ethanol. To this solution was added malonic acid (0.02 g, 0.15 mmol) in ethanol. Orange prisms were obtained after six days of slow evaporation of the solvent. M.p. 175-180˚C; IR (KBr pellet) *v* 2500 cm^{-1}, 1942 cm^{-1} (O–H···N, br), 1700 cm^{-1} (C=O, s).

3.2.2.7 Synthesis of 1,4-bis-[(benzimidazol-1-yl)methyl]-benzene *iso*phthalic acid $EtOH_{0.5}$, **16**

1,4-*bis*-[(benzimidazol-1-yl)methyl]-benzene (0.05 g, 0.15 mmol) was dissolved in 1 mL of ethanol. To this solution was added an ethanolic solution containing *iso*phthalic acid (0.03 g, 0.15 mmol). Orange prisms were obtained after two weeks of slow evaporation of the solvent. M.p. 177-180˚C; IR (KBr pellet) *v* 2494 cm^{-1}, 1918 cm^{-1} (O–H···N, br), 1696 cm^{-1} (C=O, s).

3.2.2.8 Synthesis of 1,4-*bis*-[(benzimidazol-1-yl)methyl]-benzene 5-amino*iso*phthalic acid $EtOH_{0.5}$, **17**

1,4-*bis*-[(benzimidazol-1-yl)methyl]-benzene (0.05 g, 0.15 mmol) was dissolved in 1 mL of ethanol. To this solution was added a solution containing 5-amino*iso*phthalic acid (0.03 g, 0.15 mmol) in ethanol. Orange plates were afforded after two weeks of slow evaporation of the solvent. M.p. 230-234˚C; IR (KBr pellet) *v* 2438 cm^{-1}, 1917 cm^{-1} (O–H···N, br), 1700 cm^{-1} (C=O, s).

3.2.2.9 Synthesis of 1,3-*bis*-[(benzimidazol-1-yl)methyl]-benzene malonic acid, **18**

1,3-*bis*-[(benzimidazol-1-yl)methyl]-benzene (0.02 g, 0.06 mmol) was dissolved in 1 mL of ethanol. To this solution was added a solution of malonic acid (0.01 g, 0.06 mmol) in ethanol. Colorless plates were obtained after two weeks of slow evaporation of the solvent. M.p. 175-179˚C; IR (KBr pellet) *v* 2515 cm^{-1}, 1918 cm^{-1} (O–H···N, br), 1700 cm^{-1} (C=O, s).

3.2.2.10 Synthesis of 1,4-*bis*-[(2-methylbenzimidazol-1-yl)methyl]-benzene *trans*-3-hexenedioic acid, **19**

1,4-*bis*-[(2-methylbenzimidazol-1-yl)methyl]-benzene (0.02 g, 0.05 mmol) was dissolved in 1 mL of ethanol. To this solution was added *trans*-3-hexenedioic acid (0.01 g, 0.05 mmol) in ethanol. Colorless plates were obtained after two days of slow evaporation of the solvent. M.p. 215-220˚C; IR (KBr pellet) *v* 2525 cm^{-1}, 1918 cm^{-1} (O–H···N, br), 1700 cm^{-1} (C=O, s).

3.2.2.11 Synthesis of 1,4-*bis*-[(2-methylbenzimidazol-1-yl)methyl]-benzene adipic acid, **20**

1,4-*bis*-[(2-methylbenzimidazol-1-yl)methyl]-benzene (0.02 g, 0.05 mmol) was dissolved in 1 mL of ethanol. To this solution was added an ethanolic solution containing adipic acid (0.01 g, 0.05 mmol). Colorless plates were afforded after one week of slow evaporation of the solvent. M.p. 184-187˚C; IR (KBr pellet) ν 2514 cm^{-1}, 1946 cm^{-1} (O–H···N, br), 1696 cm^{-1} (C=O, s).

3.2.3 X-ray crystallography

X-ray data were collected on a Bruker SMART 1000 four-circle CCD diffractometer using a fine-focus molybdenum Kα tube. Data were collected using SMART.[21] Initial cell constants were found by small widely separated "matrix" runs. Preliminary Laué symmetry was determined from axial images. Generally, an entire hemisphere of reciprocal space was collected regardless of Laué symmetry. Scan speed and scan width were chosen based on scattering power and peak rocking curves.

Unit cell constants and orientation matrix were improved by least-squares refinement of reflections thresholded from the entire dataset. Integration was performed with SAINT,[22] using this improved unit cell as a starting point. Precise unit cell constants were calculated in SAINT from the final merged dataset. Lorenz and polarization corrections were applied, but data were generally not corrected for absorption. Laué symmetry, space group, and unit cell contents were found with XPREP.

Data were reduced with SHELXTL.[23] The structures were solved in all cases by direct methods without incident. In general, hydrogens were assigned to idealized positions and were allowed to ride. Where possible, the coordinates of hydrogen-bonding hydrogens were allowed to refine. Heavy atoms, other than those of the guests, were refined with anisotropic thermal parameters. Additional experimental details: **10** The carboxylic acid hydrogen and the imidazole C-2 hydrogen were allowed to refine; all other hydrogens were located at calculated positions; **11** The carboxylic acid hydrogens and the imidazole C-5 hydrogen were allowed to refine; all other hydrogens were located at calculated positions; **12** The carboxylic acid hydrogens and the imidazole C-5 hydrogen were allowed to refine; all other hydrogens were located at calculated positions; **13** The carboxylic acid hydrogens and the imidazole C-2 hydrogen were allowed to refine; all other hydrogens were located at calculated positions; **14** The carboxylic acid

hydrogens and the imidazole C-2 hydrogen were allowed to refine; all other hydrogens were located at calculated positions; **16** A disordered solvent ethanol was located in the difference Fourier map. The molecule was located on an inversion center, the two occupancies were constrained so that their sum equalled 0.50, and the two species were each assigned a free variable for their thermal motion. The geometry of the two ethanol species was constrained with 'DFIX' distance constraints. For neither of these species was the hydroxyl hydrogen located. The carboxylic acid hydrogens were allowed to refine; **17** A disordered solvent ethanol was located in the difference Fourier map. The molecule was located on an inversion center, the two occupancies were constrained so that their sum equalled 0.50, and the geometry of the two ethanol species was constrained with 'DFIX' distance constraints; **19** Highly anisotropic thermal parameters for the two carboxylate oxygens suggested the presence of disorder. Two –COOH moieties were introduced into the structural model, representing a small "wobble" about the C–COOH bond. The two species refined to approximately a 3:1 ratio. Because of this disorder, the carboxylate hydrogens were included in calculated positions.

3.2.4 Powder X-ray diffraction

Powder XRD data for **13** and **14** were collected on a Bruker/Nonius D8 ADVANCE diffractometer with Bragg-Brentano geometry. A step size of 0.04˚ and step time of 60 sec per step were used. Data were processed using EVA v8.0.[24]

3.3 Results

Relevant crystallographic data for **7-20** are given in Tables A7-A20, hydrogen-bond parameters for **10-20** are provided in Table 3.1, and thermal ellipsoids and labeling schemes for **7-20** are shown in Figure 3.1.

Table 3.1 Hydrogen-bond geometries for **10**-**20**.

Compound	D-H A	D-H/Å	H...A/Å	D...A/Å	<(DHA)/°	generator for A
10	O31 H31 N13	1.03(2)	1.60(2)	2.6245(16)	175.2(16)	–
11	O31 H31 N13	1.042(18)	1.523(19)	2.5624(15)	174.3(15)	–
12	O31 H31 N13	0.962(17)	1.648(18)	2.6077(14)	174.5(15)	–
13	O37 H37 N13	0.985(17)	1.633(17)	2.6126(15)	173.1(16)	–
14	O31 H31 N13	1.125(17)	1.487(17)	2.6096(14)	174.9(13)	–
15	O51 H51A N33 O53 H53 N13	1.10(7) 1.01(3)	1.52(7) 1.59(3)	2.615(3) 2.597(3)	178(6) 178(3)	– –
16	O57 H57 N33 O59 H59 N13	1.07(2) 0.92(2)	1.54(2) 1.74(2)	2.6080(18) 2.6463(16)	171.2(18) 166(2)	– –
17	O51 H51 N43 O53 H53 N23 N55 H55B O53	1.03(2) 1.020(18) 0.97(2)	1.57(2) 1.592(18) 2.25(2)	2.5852(17) 2.6041(15) 3.189(2)	171.2(15) 170.8(17) 163.9(16)	– – x-1, y, z
18	O41 H41 N33 O43 H43 N23	0.952(17) 0.907(18)	1.690(17) 1.747(18)	2.6407(15) 2.6508(15)	176.0(15) 174.6(15)	– x, y+1, z-1
19	O31 H31 N13	1.07(2)	1.59(2)	2.644(2)	168.3(18)	–
20	O31 H31 N13	1.05(2)	1.61(2)	2.652(2)	171.4(19)	–

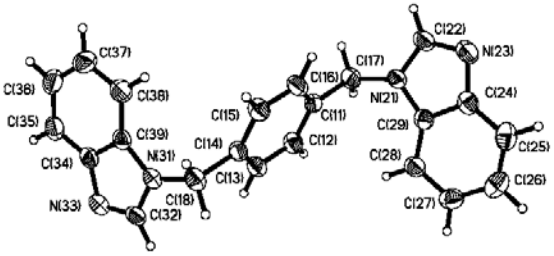

(a)

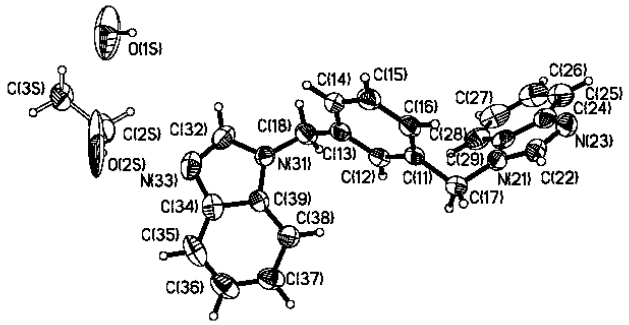

(b)

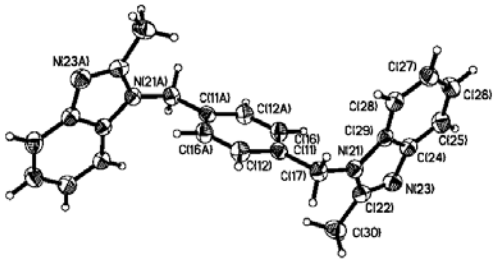
N(23A)
N(21A)
C(11A)
C(12A)
C(16)
C(11)
C(16A)
C(12)
C(17)
N(21)
C(27)
C(28)
C(26)
C(29)
C(25)
C(24)
N(23)
C(22)
C(30)

(c)

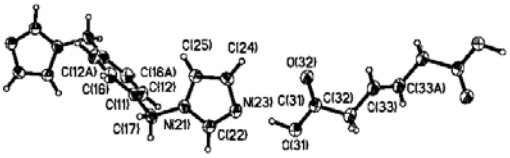
C(25)
C(24)
C(12A)
C(16A)
C(16)
C(12)
C(11)
C(17)
N(21)
C(22)
N(23)
O(32)
C(31)
C(32)
C(33A)
O(31)

(d)

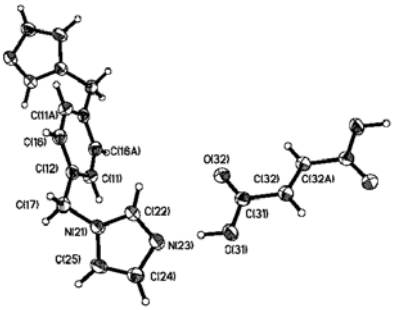
C(11A)
C(16)
C(16A)
C(12)
C(11)
C(17)
C(22)
N(21)
N(23)
C(25)
C(24)
O(32)
C(32)
C(32A)
C(31)
O(31)

(e)

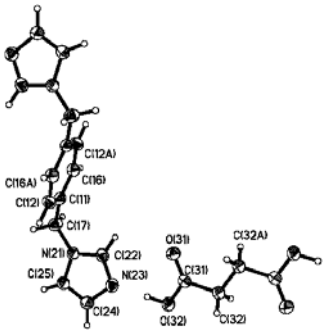
C(12A)
C(16A)
C(16)
C(12)
C(11)
C(17)
N(21)
C(22)
C(25)
N(23)
C(24)
O(31)
C(32A)
C(31)
O(32)
C(32)

(f)

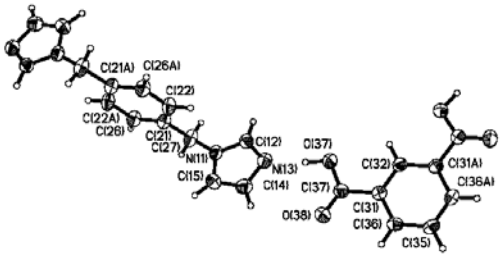
C(21A)
C(26A)
C(22)
C(22A)
C(26)
C(21)
C(27)
N(11)
C(15)
C(12)
N(13)
C(14)
C(37)
O(38)
C(32)
C(31A)
C(36A)
C(31)
C(36)
C(35)

(g)

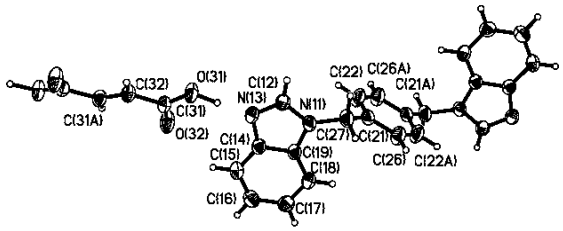
C(32)
O(31)
C(31A)
C(31)
O(32)
C(12)
N(13)
N(11)
C(22)
C(26A)
C(21A)
C(27)
C(21)
C(14)
C(15)
C(19)
C(18)
C(26)
C(22A)
C(16)
C(17)

(h)

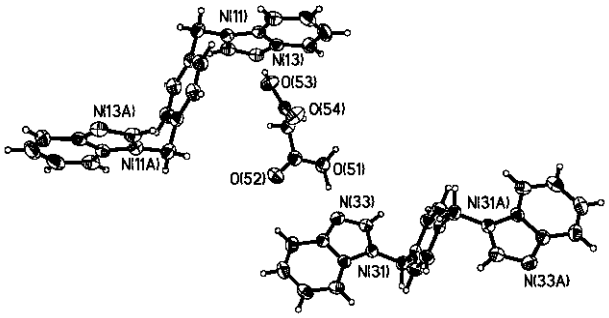
N(11)
N(13)
O(53)
O(54)
N(13A)
N(11A)
O(52)
O(51)
N(33)
N(31A)
N(31)
N(33A)

(i)

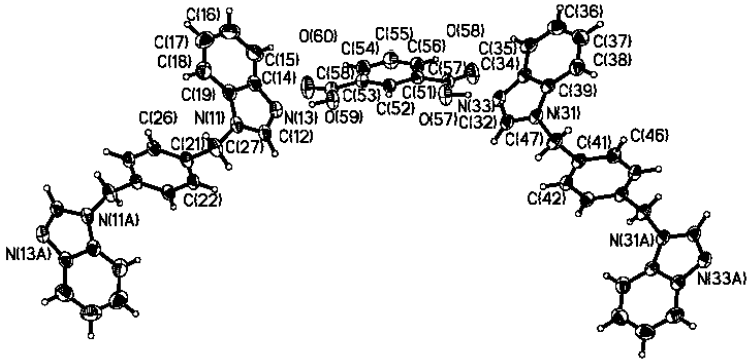
C(16)
C(17)
C(18)
C(15)
C(14)
C(19)
C(26)
N(11)
N(13)
C(12)
C(21)
C(27)
C(22)
N(11A)
N(13A)
O(60)
C(55)
C(54)
C(56)
O(58)
C(36)
C(35)
C(37)
C(34)
C(38)
C(58)
C(57)
C(53)
C(51)
C(39)
C(52)
N(33)
O(59)
O(57)
C(32)
N(31)
C(47)
C(41)
C(46)
C(42)
N(31A)
N(33A)

(j)

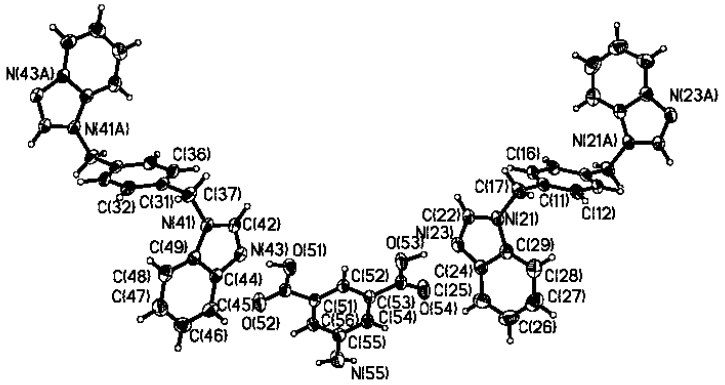
N(43A)
N(41A)
C(36)
C(32)
C(31)
C(37)
N(41)
C(42)
C(49)
N(43)
O(51)
C(48)
C(44)
C(47)
C(45)
O(52)
C(46)
C(52)
C(51)
C(53)
C(54)
C(56)
C(55)
N(55)
O(53)
N(23)
C(22)
C(24)
C(25)
O(54)
N(23A)
N(21A)
C(16)
C(17)
C(11)
C(12)
N(21)
C(29)
C(28)
C(27)
C(26)

(k)

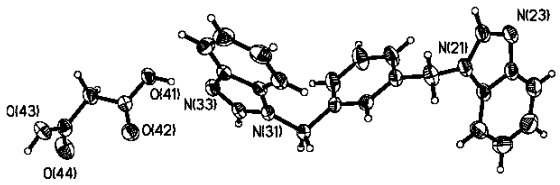

(l)

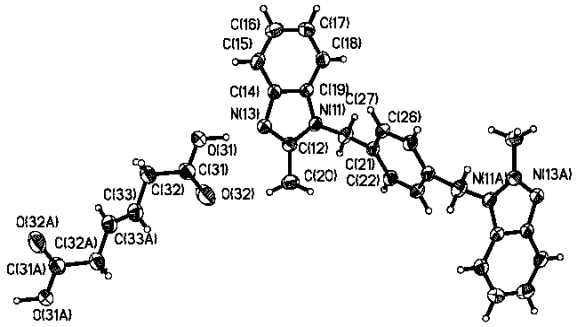

(m)

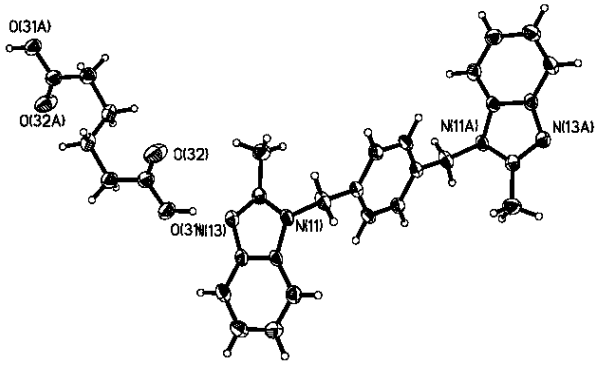

(n)

Figure 3.1 Thermal ellipsoid plots (50% probabilities) and labeling schemes for **7**-**20** (a-n).

3.3.1 Crystal structure of 1,4-bis-*[(benzimidazol-1-yl)methyl]-benzene,* **7**

No significant intermolecular interactions are present in the crystal structure of **7**, Figure 3.1a; molecules pack mainly *via* π···π interactions.

3.3.2 Crystal structure of 1,3-bis-*[(benzimidazol-1-yl)methyl]-benzene hydrate ethanol,* **8**

Water and disordered ethanol solvent molecules are present in the crystal structure of **8**, Figure 3.1b, and hydrogen bonds between 1,3-*bis*-[(benzimidazol-1-yl)methyl]-benzene molecules and these solvent molecules could not be identified.

3.3.3 Crystal structure of 1,4-bis-*[(2-methylbenzimidazol-1-yl)methyl]-benzene,* **9**

Similarly to **7**, there are no noteworthy intermolecular interactions in the crystal structure of **9**, Figure 3.1c, and 1,4-*bis*-[(2-methylbenzimidazol-1-yl)methyl]-benzene molecules are mainly stabilized by π···π interactions.

3.3.4 Crystal structure of 1,4-bis-*[(imidazol-1-yl)methyl]-benzene* trans-*3-hexenedioic acid,* **10**

The asymmetric unit of **10** consists of half a molecule each of 1,4-*bis*-[(imidazol-1-yl)methyl]-benzene and *trans*-3-hexenedioic acid, Figure 3.1d. The desired O–H···N hydrogen bond is formed by the O–H group on the dicarboxylic acid and the imidazol-1-yl nitrogen atom, (O31···N13, 2.6245(16) Å), and no proton transfer has occurred between the acid and the base. This hydrogen bond is accompanied by a C–H···O contact involving H14 on Im and O32 on the COOH carbonyl oxygen atom (C14···O32, 3.34 Å) in which the imidazole-carboxylic acid moieties are co-planar. This heteromeric synthon further propagates the acid and the base into an infinite one-dimensional zig-zag chain, Figure 3.2.

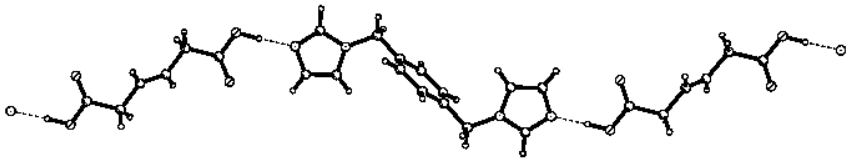

Figure 3.2 Extended 1-D chain in **10**.

Neighboring one-dimensional chains are stacked in an antiparallel fashion through C–H···O contacts between H12 on Im and O32 on carbonyl oxygen atoms of adjacent dicarboxylic acids (C12···O32, 3.12 Å).

3.3.5 Crystal structure of 1,4-bis-*[(imidazol-1-yl)methyl]-benzene fumaric acid,* **11**

The principal O–H···N hydrogen bond in **11** is formed between the acid and the base, and therefore a co-crystal is produced (O31···N13, 2.5624(15) Å), Figure 3.1e. A C–H···O contact also accompanies the O–H···N hydrogen bond, this time utilizing H12 on Im and O32 on the COOH carbonyl oxygen atom (C12···O32, 3.40 Å). The extended supramolecular architecture is an infinite one-dimensional undulating chain, Figure 3.3.

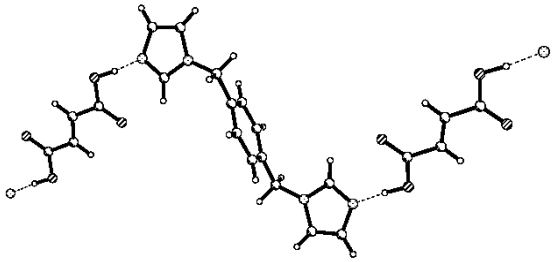

Figure 3.3 Extended 1-D supramolecular chain in **11**.

Adjacent one-dimensional chains are further held together by C–H···O contacts between H15 on Im and O32 on carbonyl oxygen atoms of neighboring fumaric acid molecules (C15···O32, 3.20 Å).

3.3.6 Crystal structure of 1,4-bis-*[(imidazol-1-yl)methyl]-benzene succinic acid,* **12**

The expected O–H···N interaction was afforded in **12** through the O–H group on the dicarboxylic acid and the imidazol-1-yl nitrogen atom (O31···N13, 2.6077(14) Å) and no proton transfer from the acid to the base took place, Figure 3.1f. The O–H···N hydrogen bond is accompanied by a C–H···O contact involving H12 on Im and O32 on the COOH carbonyl oxygen atom (C12···O32, 3.40 Å). This heteromeric synthon in turn connects the molecular components into an infinite one-dimensional undulating chain, Figure 3.4.

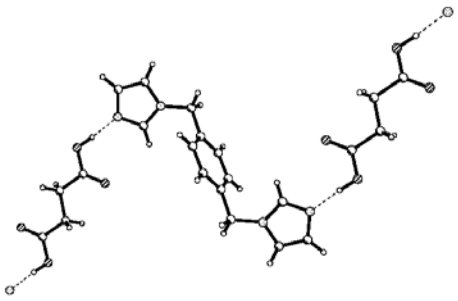

Figure 3.4 Infinite hydrogen-bonded 1-D chain in **12**.

Neighboring chains are further held together by C–H···O contacts between H15 on Im and O32 on carbonyl oxygen atoms of adjacent succinic acid molecules (C15···O32, 3.26 Å).

3.3.7 Crystal structure of 1,4-bis-*[(imidazol-1-yl)methyl]-benzene* iso*phthalic acid,* **13**

The intended infinite one-dimensional chain was produced in **13** *via* COOH···Im hydrogen bonds (O37···N13, 2.6126(15) Å, Figures 3.1g and 3.5.

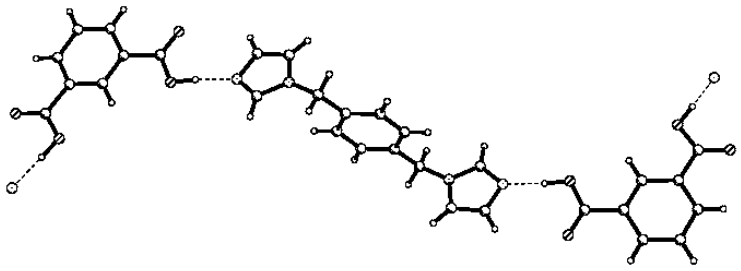

Figure 3.5 Infinite hydrogen-bonded chain in **13**.

The COOH···Im hydrogen bond is accompanied by a C–H···O contact utilizing H14 on Im and O38 on the COOH carbonyl oxygen atom (C14···O38, 3.32 Å). Adjacent chains are organized in a parallel manner through C–H···O contacts between H12 on Im and O38 on carbonyl oxygen atoms of neighboring *iso*phthalic acid molecules (C12···O38, 3.15 Å).

3.3.8 Crystal structure of 1,4-bis-*[(benzimidazol-1-yl)methyl]-benzene fumaric acid,* **14**

The expected O–H···N hydrogen bond is produced in **14** from the interaction between the COOH-Bzim moieties (O31···N13, 2.6096(14) Å), Figure 3.1h. This hydrogen bond co-exists with a C–H···O contact arising from H15 on Bzim and O32 on the COOH carbonyl oxygen atom (C15···O32, 3.32 Å). The resulting O–H···N/C–H···O heteromeric synthon propagates the acid and the base into an infinite one-dimensional chain, Figure 3.6.

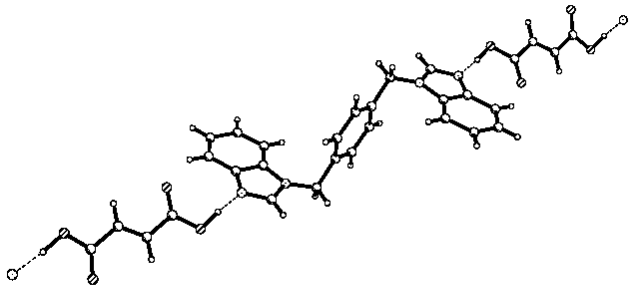

Figure 3.6 1-D hydrogen-bonded chain in **14**.

Neighboring chains are stacked in an alternating parallel/antiparallel fashion *via* C–H···O contacts between H12 and H16 respectively on Bzim and O32 on carbonyl oxygen atoms of adjacent fumaric acid molecules (C12···O32, 3.17 Å; C16···O32, 3.45 Å). Proximal chains are further stabilized by π···π interactions between the benzene core of the ditopic base of one layer and the Bzim aromatic ring of the ditopic base of another layer.

3.3.9 Crystal structure of 1,4-bis-*[(benzimidazol-1-yl)methyl]-benzene malonic acid,* **15**

The asymmetric unit of **15** shows the presence of two crystallographically unique molecules of 1,4-*bis*-[(benzimidazol-1-yl)methyl]-benzene and one molecule of malonic acid, Figure 3.1i. These components interact through two different O–H···N hydrogen bonds (O51···N33, 2.615(3) Å; O53···N13, 2.597(3) Å). One of these heteromeric interactions is accompanied by a C–H···O contact (C35···O52, 3.48 Å). The primary COOH···Bzim hydrogen bonds combine to produce an undulating 1-D chain, Figure 3.7.

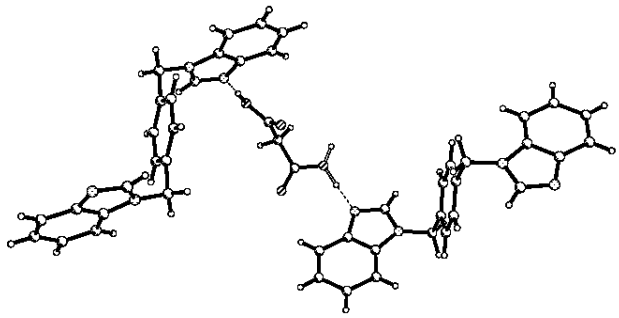

Figure 3.7 1-D chain in **15**.

Adjacent chains are stabilized by C–H···O interactions between a C–H proton on the benzene ring of the ditopic base and the carbonyl oxygen atom of proximal malonic acid molecules (C42···O54, 3.36 Å), as well as between H12 on Bzim and phenolic oxygen atoms on COOH moieties (C12···O51, 3.33 Å).

3.3.10 Crystal structure of 1,4-bis-*[(benzimidazol-1-yl)methyl]-benzene* iso*phthalic acid* $EtOH_{0.5}$, **16**

The asymmetric unit of **16** contains two crystallographically unique halves of 1,4-*bis*-[(benzimidazol-1-yl)methyl]-benzene, one *iso*phthalic acid molecule, and half a disordered ethanol molecule, Fig. 3.1j. Two O–H···N hydrogen bonds are produced as a result of the interaction between the COOH-Bzim moieties (O57···N33, 2.6080(18) Å; O59···N13, 2.6463(16) Å). No C–H···O contacts accompany the primary O–H···N hydrogen bonds, and as a consequence, the COOH···Bzim hydrogen bonds interconnect the acid and the base into an infinite one-dimensional undulating chain, Figure 3.8.

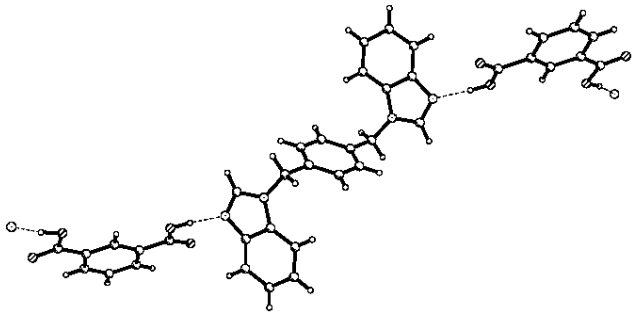

Figure 3.8 Primary hydrogen-bonded motif in **16**.

Adjacent chains are arranged in a parallel fashion by C–H···O contacts involving H32 and H12 on Bzim and O58 and O60 respectively on carbonyl oxygen atoms of neighboring *iso*phthalic acid molecules (C32···O58, 3.20 Å; C12···O60, 3.20 Å).

3.3.11 Crystal structure of 1,4-bis-*[(benzimidazol-1-yl)methyl]-benzene 5-amino*iso*phthalic acid* $EtOH_{0.5}$, **17**

The asymmetric unit of **17** consists of two crystallographically distinct halves of 1,4-*bis*-[(benzimidazol-1-yl)methyl]-benzene, one 5-amino*iso*phthalic acid molecule, and half of a disordered ethanol solvent molecule, Figure 3.1k. Two inequivalent O–H···N hydrogen bonds result from the interactions between the COOH···Bzim moieties (O51···N43, 2.5852(17) Å; O53···N23, 2.6041(15) Å). No C–H···O contacts accompany the primary O–H···N hydrogen bonds. As a result, the COOH···Bzim hydrogen bonds connect the acid and the base into an infinite one-dimensional undulating chain. Proximal chains are further stabilized in a parallel fashion by N–H···O hydrogen bonds (N55···O53, 3.189(2) Å) to afford a two-dimensional sheet, Figure 3.9.

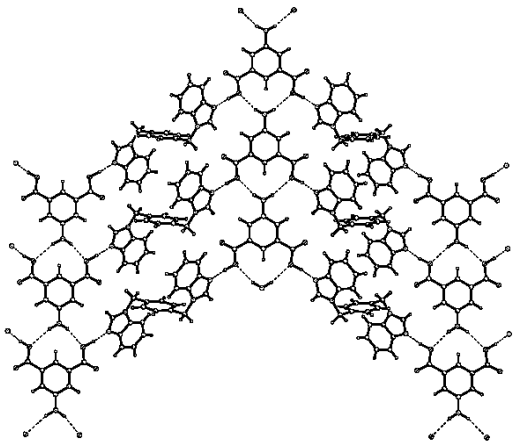

Figure 3.9 Infinite two-dimensional sheet in **17** resulting from N–H···O hydrogen bonds between 5-amino*iso*phthalic acid molecules in adjacent one-dimensional chains.

3.3.12 Crystal structure of 1,3-bis-*[(benzimidazol-1-yl)methyl]-benzene malonic acid,* **18**

There is one molecule each of 1,3-*bis*-[(benzimidazol-1-yl)methyl]-benzene and malonic acid in the asymmetric unit of **18**, Figure 3.1l, that together display two distinct

heteromeric O–H···N hydrogen bonds (O41···N33, 2.6407(15) Å; O43···N23, 2.6508(15) Å). No C–H···O interactions co-exist with these primary hydrogen bonds and, thus, the principal supramolecular motif is an infinite 1-D chain, Figure 3.10.

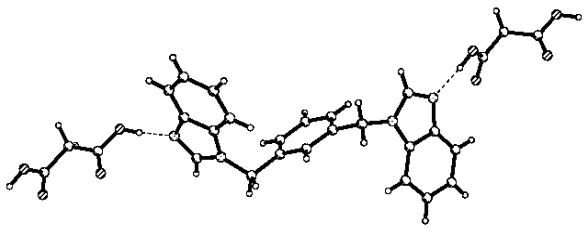

Figure 3.10 Extended chain in the crystal structure of **18**.

These chains are stacked in an antiparallel manner *via* C–H···O contacts involving the phenylic C–H protons on the ditopic base and O42 of neighboring diacids (C12···O42, 3.32 Å) and π···π interactions between adjacent Bzim moieties (about 3.3 Å).

3.3.13 Crystal structure of 1,4-bis-*[(2-methylbenzimidazol-1-yl)methyl]-benzene* trans-*3-hexenedioic acid,* **19**

The dominant O–H···N hydrogen bond in **19** is produced *via* the interaction of COOH···Bzim moieties (O31···N13, 2.644(2) Å), Figure 3.1m. A C–H···O contact co-exists with the primary O–H···N hydrogen bond, which uses H20C on Bzim and O32 on the COOH carbonyl oxygen atom (C20···O32, 3.44 Å). The resulting heteromeric synthon connects the acid and the base into an infinite one-dimensional zig-zag chain, Figure 3.11.

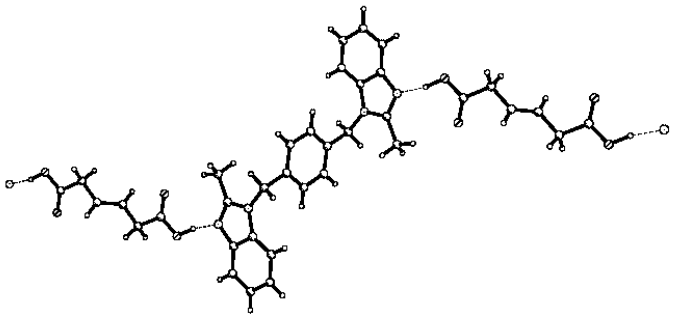

Figure 3.11 Extended supramolecular chain in **19**.

Adjacent chains are stabilized in a parallel manner through C–H···O contacts between H22 from the benzene core on the ditopic base and O32 on carbonyl oxygen atoms of neighboring *trans*-3-hexenedioic acid molecules (C22···O32, 3.31 Å).

3.3.14 Crystal structure of 1,4-bis-*[(2-methylbenzimidazol-1-yl)methyl]-benzene adipic acid,* **20**

The acid and the base in **20** interact through O–H···N hydrogen bonds (O31···N13, 2.652(2) Å), Figure 3.1n, and no C–H···O interactions are present in the primary motif, an infinite undulating 1-D chain, Figure 3.12.

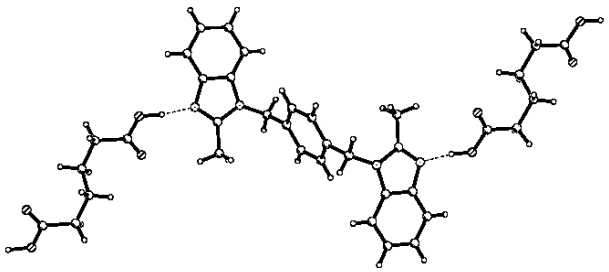

Figure 3.12 1-D supramolecular assembly in **20**.

Two types of C–H···O contacts are identified between neighboring chains, involving phenylic and Bzim C–H protons and carbonyl oxygen atoms of COOH moieties (C18···O32, 3.39 Å; C22···O32, 3.30 Å).

3.4 Discussion

Crystal structures of **10**-**20** all display the primary O–H···N hydrogen-bond interaction between COOH-Im/Bzim moieties in which no protons have been transferred from the acid to the base. This observation is unambiguously supported by the C–O bond lengths as determined by single crystal X-ray crystallography. Furthermore, IR information of these compounds suggests that co-crystals were afforded and not salts, since the C=O stretches in **10**-**20** correspond to the carboxylic acid instead of the carboxylate (see Experimental section). Characteristic broad O–H···N bands at around 2500 cm^{-1} and 1900 cm^{-1} also reinforce the presence of extensive strong O–H···N hydrogen bonds in the IR spectra of co-crystals **10**-**20**.[16a] Co-crystals were obtained for all eleven structures

despite the fact that experimental pK_b values for the Im/Bzim *N*-methylated analogs and Im/Bzim are almost identical.[25,26] Based upon information extracted from the Cambridge Structural Database (CSD),[27] there is a strong bias towards co-crystal formation, in preference to organic salts, when a carboxylic acid is allowed to react with a symmetric ditopic base such as 4,4'-bipyridine. Out of the 43 total crystal structures retrieved from the CSD containing 4,4'-bipyridine and a carboxylic acid, 34 are co-crystals (79%).[28] Of these co-crystals, there are 13 monocarboxylic acids, 17 dicarboxylic acids, and 4 tricarboxylic acids. Therefore, co-crystal formation involving symmetric ditopic bases does not seem to require a symmetric carboxylic acid.

The thermal stabilities of co-crystals **10**-**20** were modulated by increasing the molecular mass of the heterocyclic base from imidazole to benzimidazole. The melting points of the co-crystals corresponding to the imidazol-1-yl base were below 200˚C while employing the benzimidazol-1-yl base in general imparted a greater thermal stability in the resulting co-crystals, since their melting points were above 200˚C; co-crystals **15**, **16**, **18**, and **20** had melting points lower than 200˚C.

We also examined the structural homogeneity of bulk samples of **13** and **14** through a comparison of experimental and simulated powder X-ray diffraction (XRD) patterns. The experimental patterns correlate favorably with the simulated ones generated from single crystal X-ray diffraction data, Figure 3.13.

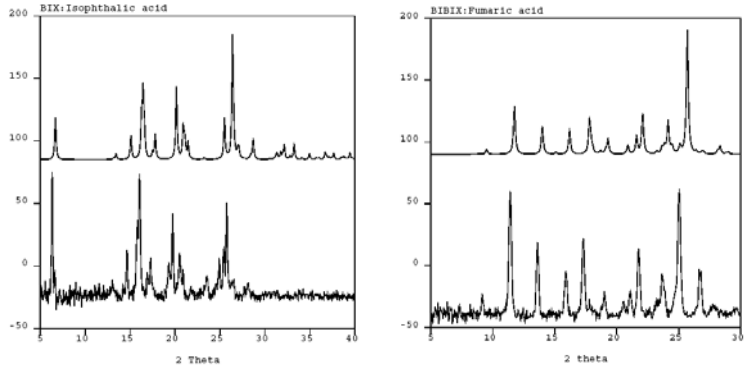

(a) (b)

Figure 3.13 Representative powder XRD patterns of co-crystals in (a) **13** and (b) **14**. The top and bottom patterns in each case correspond to simulated and experimental respectively.[29]

All these supramolecular reactions were carried out in the presence of potentially disruptive solvent molecules such as water and ethanol. In addition, hydrogen-bond interactions also faced potential competition from the requirements of a variety of π···π interactions between *bis*-Bzim moieties. We also induced changes in molecular shape by switching from Im to Bzim, and by introducing substituent groups in the case of **19** and **20** in order to put the COOH···Im and COOH···Bzim synthons to the test. The results clearly indicate that these synthons are very robust, and the primary intermolecular interactions, the O–H···N hydrogen bonds, remain intact even in the presence of an $–NH_2$ moiety (as in **17**). Consequently, the best donor/acceptor guideline is clearly evident in this case since the O–H···N hydrogen bond is the best donor/acceptor couple while the secondary N–H···O interaction involves the second-best donor and second-best acceptor. The infinite one-dimensional motif was the same in all crystal structures, propagated by the heteromeric COOH···Im and COOH···Bzim synthons. We have furthermore demonstrated that the COOH···Bzim synthon is invariant to changes in molecular isomerism in **15** and **18** (1,3- vs. 1,4-substituted *bis*-benzimidazol-1-yl supramolecular reagents).[30] In all, the success of transforming the dicarboxylic acids and the ditopic bases into co-crystals with predictable connectivities can be equated to a high supramolecular yield (100%) of the COOH···Im and COOH···Bzim synthons.

While the O–H···N hydrogen bond involves the best donor and best acceptor we also observed that the C–H···O interaction does not necessarily utilize the most acidic C–H proton. A statistical analysis of crystal structures **10**-**20** reveals that out of the eleven structures ten of them employ C–H···O interactions while one does not. Of the ten structures that involve C–H···O contacts seven of them contain *intra*chain interactions, which utilize either H2 or other protons on the Im/Bzim moieties. Thus we can formulate alternative heteromeric O–H···N/C–H···O patterns compared to the suggestions shown in Scheme 3.3 for the COOH···Im and COOH···Bzim interactions, Scheme 3.4.

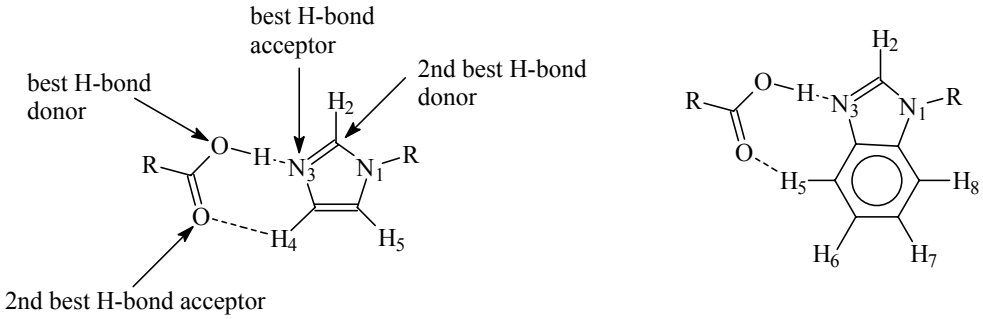

Scheme 3.4 Alternative heteromeric O–H···N/C–H···O motifs in the (a) COOH···Im and (b) COOH···Bzim intrachain interactions.

We furthermore noted that C–H···O interactions *between* adjacent 1-D chains also occurred in most of our crystal structures, Scheme 3.5.

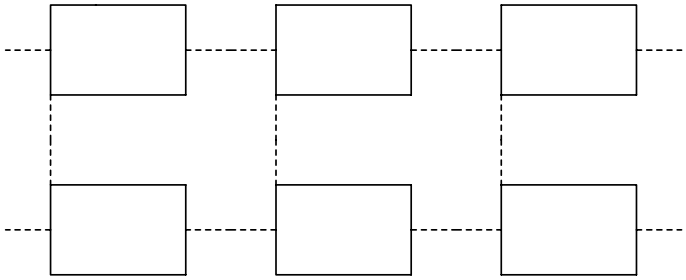

Scheme 3.5 Intrachain (horizontal) and interchain (vertical) C–H···O contacts represented by dashed lines.

How important are these *inter*chain C–H···O interactions? To establish if these contacts were merely the result of "close packing" or if they displayed directionalities that could be readily rationalized, we examined the geometries of both intrachain and interchain C–H···O interactions by studying the relationship between the C=O···H angles and C···O distances, Figure 3.14.

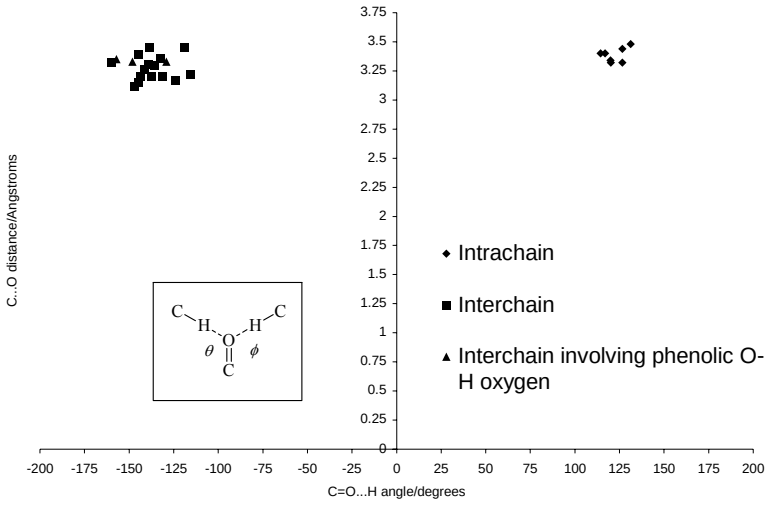

Figure 3.14 Relationship between intrachain and interchain C=O···H angles versus C···O distances in crystal structures **10**-**20**. Inset: The angular dependence of intrachain and interchain C–H···O interactions as defined by ϕ and θ respectively.

Figure 3.14 shows two highly localized regions corresponding to intrachain and interchain C–H···O interactions. The data points describing intrachain C–H···O interactions range from 120 to 131˚ and 3.3 to 3.5 Å, whereas the corresponding data points for the interchain C–H···O contacts range from -160 to -116˚ and 3.1-3.5 Å. The tight clustering of both sets of data and the fact that ϕ and θ are centered around 120˚ and -120˚ respectively (coinciding with regions of maximum electron density around the oxygen atom), indicate that intra- and interchain C–H···O hydrogen bonds are of equal importance and principally driven by electrostatic considerations.[31] Crystal structures **11**, **12**, and **15** also contain interchain C–H···O interactions in which the phenolic O–H oxygen atom on the COOH moiety acts as the hydrogen-bond acceptor (C–O···H angle *ca.* -120˚), and were therefore also incorporated into this study.

Interchain C–H···O interactions are responsible for the assembly of secondary structures in co-crystals **10**-**16** and **18**-**20** while the principal O–H···N hydrogen bond directs the assembly of ditopic base and dicarboxylic acid molecules into the primary one-dimensional motifs. In the case of **17**, no significant C–H···O interactions are present because the N–H···N hydrogen bond acts as the secondary intermolecular force. Figure

3.14 also indicates that there is no selectivity towards one particular C–H proton in C–H···O interactions in this set because there are cases when these interactions involve a phenylic C–H proton on the ditopic base. This behavior can be rationalized based on the electrostatics of the C–H···O interaction. The carbonyl oxygen atom, which acts as the hydrogen-bond acceptor, has a greater electrostatic charge density than any of the C–H protons; consequently, even if C–H protons possess varying acidities, the product of the charges between the proton and the carbonyl oxygen atom would not vary significantly.

3.5 Conclusions

This systematic structural study has demonstrated that the O–H···N hydrogen bond is the primary intermolecular force in a family of structures containing the COOH···Im and COOH···Bzim synthons. These interactions are responsible for the high-yielding supramolecular assembly of ditopic imidazoles/benzimidazoles and dicarboxylic acids into co-crystals, not salts, with desired connectivities. The O–H···N hydrogen bond remains intact in every case despite competition from π···π interactions and the presence of solvent molecules while the auxiliary C–H···O interaction is less robust and can be replaced by a suitable hydrogen-bond donor such as an amino moiety. Two types of C–H···O hydrogen bonds were observed, intra- and interchain interactions, and based upon their geometric preferences they seem to be of equal structural importance.

The results presented in this chapter indicate that the strength and directionality of the O–H···N hydrogen bond between carboxylic acids and ditopic imidazoles/benzimidazoles are sufficient to bring about the formation of binary co-crystals despite the proclivity for solid-state selfishness displayed by the vast majority of molecular species. It is very likely that the primary intermolecular interactions observed in **10**-**20** can be employed in practical and transferable supramolecular synthetic strategies in co-crystal formation involving a range of biologically relevant residues.

References

[1] Steed, J. W.; Atwood, J. L. *Supramolecular Chemistry*; John Wiley & Sons, Ltd.: Chichester, 2000.

[2] Desiraju, G. R. *Crystal Engineering: The Design of Organic Solids*; Elsevier Science Publishers B. V.: Amsterdam, 1989.

[3] Desiraju, G. R. *The Crystal as a Supramolecular Entity*; John Wiley & Sons, Ltd., 1996.

[4] Desiraju, G. R. *Angew. Chem. Int. Ed. Engl.* **1995**, *34*, 2311.

[5] Aakeröy, C. B.; Beatty, A. M.; Helfrich, B. A. *Angew. Chem. Int. Ed. Engl.* **2001**, *40*, 3240.

[6] (a) Shan, N.; Bond, A. D.; Jones, W. *Cryst. Eng.* **2002**, *5*, 9. (b) Shan, N.; Bond, A. D.; Jones, W. *New J. Chem.* **2003**, *2*, 365. (c) Shan, N.; Batchelor, E.; Jones, W. *Tetrahedron Lett.* **2002**, *43*, 8721. (d) Liu, R.; Valiyaveettil, S.; Mok, K.-F.; Vittal, J. J.; Hoong, A. K. M. *CrystEngComm* **2002**, *4*, 574.

[7] (a) Sharma, C. V. K.; Zaworotko, M. J. *Chem. Commun.* **1996**, 2655. (b) Zaworotko, M. J. *Chem. Commun.* **2001**, 1. (c) Bhogala, B. R.; Vishweshwar, P.; Nangia, A. *Cryst. Growth Des.* **2002**, *2*, 325. (d) Bhogala, B. R.; Nangia, A. *Cryst. Growth Des.* **2003**, *3*, 547. (e) Ma, B.-Q.; Coppens, P. *Chem. Commun.* **2003**, 2290.

[8] (a) Arora, K. K.; Pedireddi, V. R. *J. Org. Chem.* **2003**, *68*, 9177. (b) Vishweshwar, P.; Nangia, A.; Lynch, V. M. *J. Org. Chem.* **2002**, *67*, 556.

[9] Sundberg, R. J.; Yilmaz, I.; Mente, D. C. *Inorg. Chem.* **1977**, *16*, 1470.

[10] Santoro, S. W.; Joyce, G. F.; Sakthivel, K.; Gramatikova, S.; Barbas, C. F. *J. Am. Chem. Soc.* **2000**, *122*, 2433.

[11] (a) Zarić, S. D.; Popović, D. M.; Knapp, E.-W. *Biochemistry* **2001**, *40*, 7914. (b) Hirst, J.; Wilcox, S. K.; Williams, P. A.; Blankenship, J.; McRee, D. E.; Goodin, D. B. *Biochemistry* **2001**, *40*, 1265. (c) Hirst, J.; Wilcox, S. K.; Ai, J.; Moënne-Loccoz, P.; Loehr, T. M.; Goodin, D. B. *Biochemistry* **2001**, *40*, 1274.

[12] Deschamps, P.; Kulkarni, P. P.; Sarkar, B. *Inorg. Chem.* **2003**, *42*, 7366.

[13] (a) Arrowsmith, J.; Jennings, S. A.; Clark, A. S.; Stevens, M. F. G. *J. Med. Chem.* **2002**, *45*, 5458. (b) Betti, L.; Botta, M.; Corelli, F.; Floridi, M.; Giannaccini, G.; Maccari, L.; Manetti, F.; Strappaghetti, G.; Tafi, A.; Corsano, S. *J. Med. Chem.* **2002**, *45*, 3603. (c) Cole, C.; Reigan, P.; Gbaj, A.; Edwards, P. N.; Douglas, K. T.; Stratford, I. J.; Freeman, S.; Jaffar, M. *J. Med. Chem.* **2003**, *46*, 207.

[14] Hay, M. P.; Anderson, R. F.; Ferry, D. M.; Wilson, W. R.; Denny, W. A. *J. Med. Chem.* **2003**, *46*, 5533.

[15] (a) Kendi, E.; Özbey, S.; Göker, H. *Acta Crystallogr.* **1999**, *C55*, 243. (b) Wurtz, N. R.; Pomerantz, D. B.; Dervan, P. B. *Biochemistry* **2002**, *41*, 7604.

[16] (a) Trivedi, D. R.; Ballabh, A.; Dastidar, P. *CrystEngComm* **2003**, *5*, 358. (b) MacDonald, J. C.; Dorrestein, P. C.; Pilley, M. M. *Cryst. Growth Des.* **2001**, *1*, 29. (c) Overgaard, J.; Schiøtt, B.; Larsen, F. K.; Schultz, A. J.; MacDonald, J. C.; Iversen, B. B. *Angew. Chem. Int. Ed. Engl.* **1999**, *38*, 1239. (d) Aakeröy, C. B.; Hughes, D. P.; Nieuwenhuyzen, M. *J. Am. Chem. Soc.* **1996**, *118*, 10134.

[17] Roey, P. V.; Bullion, K. A.; Osawa, Y. *Acta Crystallogr.* **1991**, *C47*, 1015.

[18] Etter, M. C. *J. Phys. Chem.* **1991**, *95*, 4601.

[19] Hoskins, B. F.; Robson, R.; Slizys, D. A. *J. Am. Chem. Soc.* **1997**, *119*, 2952.

[20] Methanol/ethanol mixtures were used in these co-crystallization reactions since the reagents displayed similar solubilities in MeOH/EtOH, thus minimizing the unwanted premature precipitation of one of the two reagents. It is always conceivable that polymorphs would have appeared with other solvent systems

but we did employ powder X-ray diffraction to ensure that the samples that were produced under the specified reaction conditions were structurally homogeneous.

[21] SMART v5.060; Bruker Analytical X-ray Systems: Madison, WI, 1997 – 1999.

[22] SAINT v6.02; Bruker Analytical X-ray Systems: Madison, WI, 1997 – 1999.

[23] SHELXTL v5.10; Bruker Analytical X-ray Systems: Madison, WI, 1997.

[24] EVA v8.0; Bruker AXS Gmbh: Karlsruhe, West Germany, 1997 – 2002.

[25] pK_b values of *N*-substituted imidazoles and benzimidazoles were compared to the pK_{b1} values of the free bases: imidazole, 7.04; 1-methylimidazole, 7.05; benzimidazole, 8.45; 1-methylbenzimidazole, 8.46.

[26] Perrin, D. D. *Dissociation Constants of Organic Bases in Aqueous Solution*; Butterworth & Co., Ltd.: London, 1965.

[27] Allen, F. A. *Acta Crystallogr., Sect. B.* **2002**, *58*, 380.

[28] Out of the remaining nine structures (21%), eight are salts containing the monoprotonated 4,4'-bipyridinium cation (19%) and one is a salt containing the diprotonated 4,4'-bipyridinium cation (2%).

[29] In each case a new phase had formed and no peaks corresponding to starting materials were present indicating that the reactions proceeded in near quantitative yields.

[30] Aakeröy, C. B.; Desper, J.; Elisabeth, E.; Helfrich, B. A.; Levin, B.; Urbina, J. F. *Zeit. Kristallogr.* **2005**, *220*, 325.

[31] Steiner, T. *Angew. Chem. Int. Ed. Engl.* **2002**, *41*, 48.

Chapter 4

[(Benzimidazol-1-yl)methyl]-benzamides as supramolecular reagents for binary and ternary co-crystals

4.1 Introduction

A central part of crystal engineering employs molecular recognition events for the directed assembly of discrete or extended supramolecular architectures.[1,2,3] This type of supramolecular synthesis is frequently based upon a library of hydrogen-bond based synthons, Scheme 4.1, and can offer rational and versatile strategies for the directed assembly of molecular co-crystals.

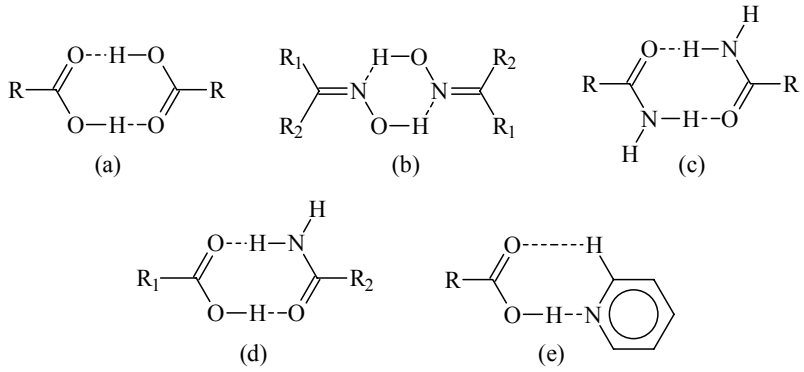

Scheme 4.1 A few examples of hydrogen-bond based synthons employed in crystal engineering.

Co-crystallization reactions provide helpful means for probing the importance of, and balance between, different intermolecular interactions and, thus, offer invaluable information for developing new methodologies in supramolecular synthesis. However, the synthesis of new co-crystals can also be an important goal in and of itself, especially within the pharmaceutical industry, since co-crystal formation may provide a tool for fine-tuning a variety of relevant physical properties like solubility, hygroscopicity, thermal stability, and processability.[4]

Even though synthesis that relies on reversible and relatively weak intermolecular interactions provide many unusual challenges, previous efforts have shown that it is possible to prepare a variety of binary co-crystals through a judicious choice of molecular

building blocks;[5] more complex systems (ternary, quaternary, *etc*), however, are very rare.

We are particularly interested in formulating reliable supramolecular synthetic strategies as well as in identifying suitable supramolecular reagents that will allow for the directed assembly of ternary and higher-order supermolecules or co-crystals with predetermined intermolecular connectivities. This study is derived from results that were obtained with *iso*nicotinamide, a relatively simple molecule that contains two distinctly different "binding sites", Scheme 4.2a, which allows it to act as a central hub for the assembly of ternary supermolecules. The synthetic protocol for these reactions relies on a best donor-acceptor/second-best donor-acceptor approach,[2(b),6] which, in the case of *iso*nicotinamide, consistently directs a stronger carboxylic acid towards the pyridyl nitrogen atom whereas a weaker carboxylic acid is left to complete the ternary supermolecule through a heteromeric carboxylic acid···carboxamide synthon, Scheme 4.2b.[7,8]

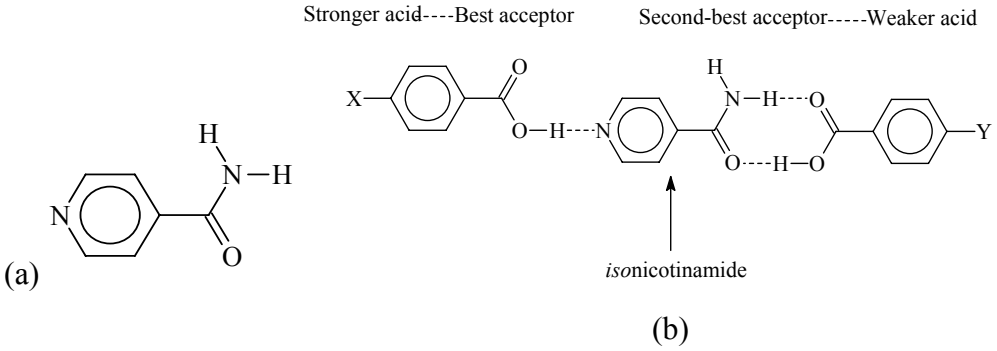

Scheme 4.2 (a) *Iso*nicotinamide, a supramolecular reagent. (b) Ternary supermolecules formed from a "strong" carboxylic acid, *iso*nicotinamide, and a "weak" carboxylic acid through carboxylic acid···pyridine and carboxamide···carboxylic acid hydrogen bonds.

We have employed a similar approach in the design of a family of new structurally versatile supramolecular reagents for the assembly of ternary co-crystals. These reagents, [(benzimidazol-1-yl)methyl]-benzamides, possess several attractive features when compared to *iso*nicotinamide, Scheme 4.3.

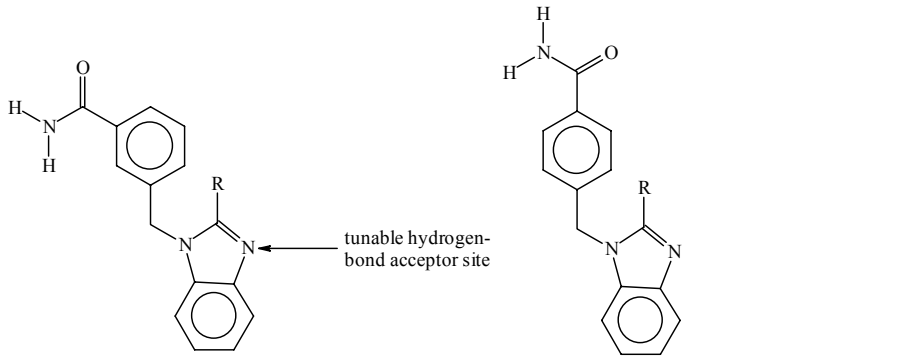

R = H (**4.2.1.7**), CH_3 (**4.2.1.9**), Cl (**4.2.1.11**) R = H (**4.2.1.8**), CH_3 (**4.2.1.10**), Cl (**4.2.1.12**)

(a) (b)

Scheme 4.3 New supramolecular reagents based on (a) 3- and (b) 4-substituted [(benzimidazol-1-yl)methyl]-benzamides.

First, the two different binding sites are uncoupled, which allows us to fine-tune the electronic nature of the benzimidazol-1-ylmethyl nitrogen atoms without affecting the electronic environment of the carboxamide moiety by varying the substituent group (H, CH_3, Cl) in the 2-position of the benzimidazol-1-yl ring. Second, the inclusion of a bridging methylene group expands the solubility of these reagents, which is of considerable concern in co-crystal synthesis. Third, the commercial availability of different isomers (3- and 4-substituted starting materials) provides the opportunity to synthesize a family of closely related compounds and thus to explore their ability to act as suitable supramolecular reagents in a systematic fashion.

In this chapter we present the syntheses of six [(benzimidazol-1-yl)methyl]-benzamide molecules that can, in principle, act as supramolecular reagents for ternary supermolecules. We also present crystal structures for five of these molecules, as well as crystal structures of two binary co-crystals, and a 1:1:1 ternary supermolecule in order to begin understanding how these reagents respond to the presence of one or more carboxylic acids.

4.2 Experimental

4.2.1 Synthesis

All starting materials were purchased from Aldrich and used without further purification. Melting points were determined on a Fisher-Johns melting point apparatus and are uncorrected.

4.2.1.1 Synthesis of 3-[(benzimidazol-1-yl)methyl]-benzonitrile

Benzimidazole (0.60 g, 5.10 mmol) was dissolved in 100 mL of dry THF with stirring in a 250-mL round-bottomed flask. To the clear and colorless solution was added NaOH (2.13 g, 53.3 mmol), and the resulting mixture was stirred for 2 h at room temperature under a N_2 atmosphere. To this mixture was added a 40-mL dry THF solution containing α-bromo-*m*-tolunitrile (1.00 g, 5.10 mmol), which immediately turned the mixture into an off-white and cloudy suspension. Stirring was continued at room temperature for 12 h under a N_2 atmosphere. 50 mL of distilled water was added to the reaction mixture to dissolve the NaOH pellets and NaBr that had formed upon reaction of the two starting materials, and two layers formed. The two layers were separated using a separatory funnel, and the THF layer was dried over anhydrous Na_2SO_4 overnight. The Na_2SO_4 was filtered by vacuum filtration, and the filtrate was concentrated *via* rotary evaporation to produce a pale brown, microcrystalline solid. Recrystallization of the solid from hot acetonitrile afforded large, pale brown plates. Yield 1.02 g (85.4%); m.p. 93-96˚C; ^{1}H NMR (DMSO-d_6, 400 MHz) δ 5.57 (s, 2H), 7.21 (m, 2H), 7.55 (m, 2H), 7.61 (d, 1H, J = 6.4 Hz), 7.66 (dd, 1H, J_1 = 7.6 Hz, J_2 = 2.4 Hz), 7.77 (d, 1H, J = 7.6 Hz), 7.86 (s, 1H), 8.44 (s, 1H); IR (KBr pellet) ν 2234 cm^{-1} (C≡N).

4.2.1.2 Synthesis of 4-[(benzimidazol-1-yl)methyl]-benzonitrile

Benzimidazole (0.60 g, 5.10 mmol) was dissolved in 100 mL of dry THF with stirring in a 250-mL round-bottomed flask. To this solution was added NaOH (2.13 g, 53.3 mmol) and allowed to stir for 2 h at room temperature under a N_2 atmosphere. Then, α-bromo-*p*-tolunitrile (1.00 g, 5.10 mmol) in 40 mL of dry THF was added to the stirring reaction mixture, which immediately turned into an off-white and cloudy suspension. This mixture was allowed to stir for 12 h at room temperature under a N_2 atmosphere. 50 mL of distilled water was added to the clear, yellow heterogeneous reaction mixture, and

stirred to dissolve the NaOH pellets and NaBr that had formed during the reaction to form a biphasic system. The two phases were separated using a separatory funnel, and the THF layer was dried over anhydrous Na_2SO_4 overnight. The Na_2SO_4 was filtered *via* vacuum filtration, and the filtrate was concentrated by rotary evaporation to obtain a pale brown solid. Recrystallization of the solid from hot ethyl acetate produced colorless plates. Yield 1.13 g (95.0%); m.p. 81-85˚C; ^{1}H NMR (DMSO-d_6, 400 MHz) δ 5.63 (s, 2H), 7.21 (m, 2H), 7.44 (d, 2H, J = 8.4 Hz), 7.48 (m, 1H), 7.67 (m, 1H), 7.81 (d, 2H, J = 8.4 Hz), 8.43 (s, 1H); IR (KBr pellet) v 2227 cm^{-1} (C≡N).

4.2.1.3 Synthesis of 3-[(2-methylbenzimidazol-1-yl)methyl]-benzonitrile

2-Methylbenzimidazole (0.67 g, 5.10 mmol) was dissolved in 100 mL of dry THF with stirring in a 250-mL round-bottomed flask. To this clear and colorless solution was added NaOH (2.13 g, 53.3 mmol) and continued to stir for 2 h at room temperature under a N_2 atmosphere. Then, α-bromo-*m*-tolunitrile (1.00 g, 5.10 mmol) in 40 mL of dry THF was added to the reaction mixture, which immediately formed an off-white, cloudy suspension. The mixture was consequently allowed to stir for 12 h at room temperature under a N_2 atmosphere. 50 mL of distilled water was added to the clear, yellow heterogeneous reaction mixture to dissolve the NaOH pellets and NaBr that had precipitated during the reaction, and two layers were obtained. The two layers were separated by using a separatory funnel, and the THF layer was dried over anhydrous Na_2SO_4 overnight. Upon vacuum filtration of Na_2SO_4, the filtrate was concentrated *via* rotary evaporation to give a white powder. The white powder was recrystallized from hot acetonitrile to produce a white, microcrystalline solid. Yield 1.17 g (93.1%); m.p. 110-115˚C; ^{1}H NMR (CD_3CN, 400 MHz) δ 2.51 (s, 3H), 5.42 (s, 2H), 7.18 (m, 2H), 7.27 (dd, 1H, J_1 = 7.2 Hz, J_2 = 2.4 Hz), 7.34 (d, 1H, J = 9.2 Hz), 7.45 (s, 1H), 7.48 (t, 1H, J = 5.2 Hz), 7.60 (dd, 1H, J_1 = 8.4 Hz, J_2 = 2 Hz), 7.64 (d, 1H, J = 8 Hz); IR (KBr pellet) v 2232 cm^{-1} (C≡N).

4.2.1.4 Synthesis of 4-[(2-methylbenzimidazol-1-yl)methyl]-benzonitrile

2-Methylbenzimidazole (0.67 g, 5.10 mmol) was dissolved in 100 mL of dry THF with stirring in a 250-mL round-bottomed flask. To this clear and colorless solution was

added NaOH (2.13 g, 53.3 mmol), and the resulting mixture was allowed to stir for 2 h at room temperature under a N_2 atmosphere. Then, α-bromo-*p*-tolunitrile (1.00 g, 5.10 mmol) in 40 mL of dry THF was added to the stirring mixture, and a cloudy, pale yellow suspension was immediately formed. This mixture was stirred for 12 h at room temperature under a N_2 atmosphere. 50 mL of distilled water was then added to the clear, yellow heterogeneous reaction mixture, and stirred to dissolve the NaOH pellets and NaBr that had formed during the reaction. Two layers formed, which were separated by means of a separatory funnel, and the THF layer was dried over anhydrous Na_2SO_4 overnight. The Na_2SO_4 was filtered by vacuum filtration, and the filtrate was concentrated *via* rotary evaporation to produce a yellow, microcrystalline solid. The solid was recrystallized from hot acetonitrile to afford off-white, fine needles. Yield 0.85 g (67.1%); m.p. 120-122˚C; ^{1}H NMR (CD_3CN, 400 MHz) δ 2.49 (s, 3H), 5.45 (s, 2H), 7.19 (d, m, 4H, J = 7.2 Hz), 7.25 (dd, 1H, J_1 = 6 Hz, J_2 = 2.4 Hz), 7.59 (dd, 1H, J_1 = 8 Hz, J_2 = 2 Hz), 7.66 (d, 2H, J = 8.4 Hz); IR (KBr pellet) ν 2222 cm^{-1} (C≡N).

4.2.1.5 Synthesis of 3-[(2-chlorobenzimidazol-1-yl)methyl]-benzonitrile

2-Chlorobenzimidazole (0.78 g, 5.10 mmol) was dissolved in 75 mL of dry THF with stirring in a 250-mL round-bottomed flask. To the clear and colorless solution was added NaOH (2.13 g, 53.3 mmol), and stirring was continued for 2 h at room temperature under a N_2 atmosphere. α-Bromo-*m*-tolunitrile (1.00 g, 5.10 mmol) dissolved in 75 mL of dry THF was then added to the reaction mixture, which immediately produced a white and cloudy suspension. This mixture was consequently allowed to stir for 12 h at room temperature under a N_2 atmosphere. 60 mL of distilled water was added to the reaction mixture to dissolve the NaOH pellets and NaBr that had formed from the reaction, and a biphasic system was attained. The two layers were separated using a separatory funnel, and the THF layer was dried over anhydrous Na_2SO_4 overnight. The Na_2SO_4 was then filtered by vacuum filtration, and the filtrate was concentrated *via* rotary evaporation to obtain a fluffy white solid. Recrystallization of the white powder from hot ethyl acetate afforded colorless plates. Yield 1.06 g (77.6%); m.p. 146-148˚C; ^{1}H NMR (DMSO-d_6, 400 MHz) δ 5.61 (s, 2 H), 7.29 (m, 2H), 7.46 (d, 1H, J = 8 Hz), 7.56 (t, 1H, J = 8 Hz), 7.64 (m, 2H), 7.79 (s, d, 2 H, J = 8.8 Hz); IR (KBr pellet) ν 2233 cm^{-1}(C≡N).

4.2.1.6 Synthesis of 4-[(2-chlorobenzimidazol-1-yl)methyl]-benzonitrile

2-Chlorobenzimidazole (0.78 g, 5.10 mmol) was dissolved in 100 mL of dry THF with stirring in a 250-mL round-bottomed flask. To the clear and colorless solution was added NaOH (2.13 g, 53.3 mmol) and continued to stir for 2 h at room temperature under a N_2 atmosphere. Then, a 40-mL dry THF solution containing α-bromo-*p*-tolunitrile (1.00 g, 5.10 mmol) was added to the reaction mixture, which immediately produced a white and cloudy suspension. This mixture was allowed to stir for 12 h at room temperature under a N_2 atmosphere. 50 mL of distilled water was then added to the clear, yellow heterogeneous mixture, and stirred to dissolve the NaOH pellets and NaBr that had formed upon reaction of the two starting materials, to form two layers. The two layers were separated by means of a separatory funnel, and the THF layer was dried over anhydrous Na_2SO_4 overnight. The Na_2SO_4 was then filtered *via* vacuum filtration, and the filtrate was concentrated by rotary evaporation to produce a yellow solid. The solid was recrystallized from hot ethyl acetate to give pale yellow plates. Yield 1.07 g (78.4%); m.p. 138-141˚C; ^{1}H NMR (DMSO-d_6, 400 MHz) δ 5.66 (s, 2H), 7.29 (m, 2H), 7.34 (d, 2H, J = 8.8 Hz), 7.60 (dd, 1H, J_1 = 7.2 Hz, J_2 = 2 Hz), 7.65 (dd, 1H, J_1 = 7.6 Hz, J_2 = 2.4 Hz), 7.83 (d, 2H, J = 8.4 Hz); IR (KBr pellet) ν 2233 cm^{-1} (C≡N).

4.2.1.7 Synthesis of 3-[(benzimidazol-1-yl)methyl]-benzamide, **21**

3-[(Benzimidazol-1-yl)methyl]-benzonitrile (1.00 g, 4.29 mmol) was dissolved in 4 mL of DMSO with stirring in a 100-mL three-necked flask under a N_2 atmosphere. The reaction flask was then cooled in an ice-water bath, and anhydrous K_2CO_3 (0.090 g, 0.62 mmol) was added to the reaction mixture. 9 mL of 30 wt % H_2O_2 solution was syringed dropwise into the reaction mixture, and an off-white, fine solid formed almost immediately. The reaction was consequently allowed to warm to room temperature with continued stirring for 1 h while wrapped in aluminum foil. 5 mL of distilled water was added to the reaction mixture, and cooling in an ice-water bath was applied to result in an off-white, cloudy suspension. An off-white solid was obtained upon vacuum filtration, which was washed with small portions of distilled water and dried. Recrystallization of the solid from hot acetonitrile gave colorless plates. Yield 0.85 g (79.2%); m.p. 181-184˚C; ^{1}H NMR (DMSO-d_6, 400 MHz) δ 5.54 (s, 2H), 7.20 (m, 2H), 7.41 (m, 3H), 7.50

(m, 1H), 7.66 (m, 1H), 7.78 (d, 1H, J = 7.2 Hz), 7.85 (s, 1H), 7.99 (s, 1H), 8.43 (s, 1H); IR (KBr pellet) ν 1679 cm^{-1} (C=O, s), 3142 cm^{-1} (N-H, broad), 3284 cm^{-1} (N-H, broad).

4.2.1.8 Synthesis of 4-[(benzimidazol-1-yl)methyl]-benzamide

4-[(Benzimidazol-1-yl)methyl]-benzonitrile (0.50 g, 2.15 mmol) was dissolved in 2 mL of DMSO with stirring in a 100-mL three-necked flask under a N_2 atmosphere. The reaction flask was then placed in an ice-water bath, and anhydrous K_2CO_3 (0.04 g, 0.31 mmol) was added to the reaction mixture. 5 mL of 30 wt % H_2O_2 solution was syringed dropwise into the reaction mixture, and a white, chalky solid precipitated almost immediately. The reaction was then allowed to warm to room temperature with continued stirring for 1 h while covered in aluminum foil. 2.5 mL of distilled water was added to the reaction mixture, cooling in an ice-water bath was applied, and the solid was filtered by vacuum filtration. The solid was then washed with small amounts of distilled water and dried. The solid was recrystallized from hot acetonitrile to afford colorless needles. Yield 0.34 g (63.5%); m.p. 203-206˚C; ^{1}H NMR (DMSO-d_6, 400 MHz) δ 5.56 (s, 2H), 7.19 (m, 2H), 7.35 (s, d, 3H, J = 8.4 Hz), 7.49 (m, 1H), 7.66 (m, 1H), 7.82 (d, 2H, J = 8.4 Hz), 7.92 (s, 1H), 8.42 (s, 1H); IR (KBr pellet) ν 1690 cm^{-1} (C=O, s), 3148 cm^{-1} (N-H, broad), 3293 cm^{-1} (N-H, broad).

4.2.1.9 Synthesis of 3-[(2-methylbenzimidazol-1-yl)methyl]-benzamide, **22**

3-[(2-Methylbenzimidazol-1-yl)methyl]-benzonitrile (1.00 g, 4.05 mmol) was dissolved in 5 mL of DMSO with stirring in a 100-mL three-necked flask under a N_2 atmosphere. The reaction flask was then placed in an ice-water bath, and anhydrous K_2CO_3 (0.080 g, 0.59 mmol) was added to the reaction mixture. 8 mL of 30 wt % H_2O_2 solution was syringed dropwise into the reaction mixture, and an off-white solid formed almost immediately. The mixture was then warmed to room temperature with continued stirring for 1 h while covered in aluminum foil. 5mL of distilled water was added to the reaction mixture, cooling in an ice-water bath was applied, and the solid was filtered *via* vacuum filtration. The solid was then washed with small amounts of distilled water and dried. The solid was recrystallized from hot acetonitrile/ethyl acetate (95:5) to afford colorless plates. Yield 0.68 g (63.6%); m.p. 236-239˚C; ^{1}H NMR (DMSO-d_6, 400 MHz) δ 2.52 (s,

3H), 5.51 (s, 2H), 7.14 (m, 2H), 7.23 (d, 1H, J = 7.6 Hz), 7.42 (m, 3H), 7.55 (dd, 1H, J_1 = 6 Hz, J_2 = 3.2 Hz), 7.68 (s, 1H), 7.77 (d, 1H, J = 8 Hz), 7.99 (s, 1H); IR (KBr pellet) v 1682 cm^{-1} (C=O, s), 3144 cm^{-1} (N-H, broad), 3300 cm^{-1} (N-H, broad).

4.2.1.10 Synthesis of 4-[(2-methylbenzimidazol-1-yl)methyl]-benzamide, **23**

4-[(2-Methylbenzimidazol-1-yl)methyl]-benzonitrile (0.82 g, 3.32 mmol) was dissolved in 5 mL of DMSO with stirring in a 100-mL three-necked flask under a N_2 atmosphere. The reaction flask was then cooled in an ice-water bath, and anhydrous K_2CO_3 (0.070 g, 0.48 mmol) was added to the reaction mixture. 8 mL of 30 wt % H_2O_2 solution was syringed dropwise into the reaction mixture, and an off-white, chalky solid formed almost immediately. The mixture was then allowed to warm to room temperature with continued stirring for 1 h while wrapped in aluminum foil. 5 mL of distilled water was added to the reaction mixture, cooling in an ice-water bath was applied, and the solid was filtered *via* vacuum filtration. The solid was then washed with small portions of distilled water and dried. Recrystallization from hot acetonitrile afforded colorless needles. Yield 0.63 g (71.1%); m.p. 224-227˚C; ^{1}H NMR (DMSO-d_6, 400 MHz) δ 2.51 (s, 3H), 5.53 (s, 2H), 7.16 (m, 4H), 7.34 (s, 1H), 7.44 (dd, 1H, J_1 = 6 Hz, J_2 = 3.2 Hz), 7.55 (dd, 1H, J_1 = 6Hz, J_2 = 3.2 Hz), 7.81 (d, 2H, J = 8.8 Hz), 7.92 (s, 1H); IR (KBr pellet) v 1685 cm^{-1} (C=O, s), 3148 cm^{-1} (N-H, broad), 3322 cm^{-1} (N-H, broad).

4.2.1.11 Synthesis of 3-[(2-chlorobenzimidazol-1-yl)methyl]-benzamide, **24**

3-[(2-Chlorobenzimidazol-1-yl)methyl]-benzonitrile (0.85 g, 3.18 mmol) was dissolved in 8 mL of DMSO with stirring in a 100-mL three-necked flask under a N_2 atmosphere. The reaction flask was then placed in an ice-water bath, and anhydrous K_2CO_3 (0.06 g, 0.46 mmol) was added to the reaction mixture. 7 mL of 30 wt % H_2O_2 solution was syringed dropwise into the stirring reaction mixture, and a white solid formed almost immediately. The reaction was then allowed to warm to room temperature for 1 h while covered in aluminum foil. 5 mL of distilled water was added to the mixture, cooling in an ice-water bath was applied, and the solid was filtered *via* vacuum filtration. The solid was then washed with small amounts of distilled water and dried. Recrystallization of the solid from hot acetonitrile afforded the pure product. Colorless prisms were obtained

upon crystallization from methanol. Yield 0.67 g (73.6%); m.p. 222-224˚C; ^{1}H NMR (DMSO-d_6, 400 MHz) δ 5.58 (s, 2H), 7.28 (m, 2H), 7.42 (s, t, 2H, J = 7.6 Hz), 7.60 (dd, 1H, J_1 = 6.6 Hz, J_2 = 2 Hz), 7.64 (dd, 1H, J_1 = 6.2 Hz, J_2 = 2.4 Hz), 7.75 (s, 1H), 7.79 (d, 1H, J = 7.6 Hz), 8.00 (s, 1H); IR (KBr pellet) ν 1680 cm^{-1} (C=O, s), 3161 cm^{-1} (N-H, broad), 3351 cm^{-1} (N-H, broad).

4.2.1.12 Syntheses of 4-[(2-chlorobenzimidazol-1-yl)methyl]-benzamide, and 4-[2-chlorobenzimidazol-1-yl)methyl]-benzamide monohydrate, **25**

4-[(2-Chlorobenzimidazol-1-yl)methyl]-benzonitrile (0.70 g, 2.61 mmol) was dissolved in 7 mL of DMSO with stirring in a 100-mL three-necked flask under a N_2 atmosphere. The reaction flask was then placed in an ice-water bath, and anhydrous K_2CO_3 (0.05 g, 0.38 mmol) was added to the reaction mixture. 7 mL of 30 wt % H_2O_2 solution was syringed dropwise into the reaction mixture, and an off-white, chalky solid formed almost immediately. The reaction was then allowed to warm to room temperature for 1 h while wrapped in aluminum foil. 5 mL of distilled water was added to the reaction mixture, cooling in an ice-water bath was applied, and the solid was filtered *via* vacuum filtration. The solid was then washed with small portions of distilled water and dried. Recrystallization of the solid from hot acetonitrile gave a first crop as white microcrystals, which formed almost immediately, and harvested. Yield of microcrystals 0.60 g (80.8%); m.p. 185-190˚C; ^{1}H NMR of microcrystals (DMSO-d_6, 400 MHz) δ 5.59 (s, 2H), 7.25 (d, 2H, J = 8.8 Hz), 7.28 (m, 2H), 7.36 (s, 1H), 7.61 (dd, 1H, J_1 = 6.6 Hz, J_2 = 2.8 Hz), 7.64 (dd, 1H, J_1 = 6.6 Hz, J_2 = 2.4 Hz), 7.82 (d, 2H, J = 8.4 Hz), 7.93 (s, 1H); IR (KBr pellet) ν 1684 cm^{-1} (C=O, s), 3176 cm^{-1} (N-H, broad), 3336 cm^{-1} (N-H, broad). Slow evaporation of the mother liquor afforded colorless prisms as the second crop, **25**. Yield of prisms 0.16 g (19.8%); m.p. 124-127˚C; IR (KBr pellet) ν 1671 cm^{-1} (C=O, s), 3195 cm^{-1} (N-H, broad), 3350 cm^{-1} (N-H, broad), 3100-3500 cm^{-1} (O-H, very broad).

4.2.2 Syntheses of binary co-crystals

4.2.2.1 Synthesis of 3-[(benzimidazol-1-yl)methyl]-benzamide 4-nitrobenzoic acid, **26**

3-[(Benzimidazol-1-yl)methyl]-benzamide (0.020 g, 0.080 mmol) was dissolved in 2 mL of ethanol. To this solution was added an ethanolic solution containing 4-nitrobenzoic

acid (0.013 g, 0.080 mmol). The resulting solution was allowed to evaporate slowly under ambient conditions for six days whereupon colorless prisms were obtained. M.p. 219-222˚C.[9]

4.2.2.2 Synthesis of 3-[(2-methylbenzimidazol-1-yl)methyl]-benzamide 4-nitrobenzoic acid, **27**

3-[(2-Methylbenzimidazol-1-yl)methyl]-benzamide (0.020 g, 0.075 mmol) was dissolved in 3 mL of ethanol. A solution of 4-nitrobenzoic acid (0.013 g, 0.075 mmol) in ethanol was added to this solution. Colorless plates formed after six days of slow evaporation of the solvent under ambient conditions. M.p. 223-227˚C.[9]

4.2.3 Syntheses of ternary co-crystals

4.2.3.1 Synthesis of 4-[(2-methylbenzimidazolium-1-yl)methyl]-benzamide 2,6-dichlorobenzoate 4-nitrobenzoic acid, **28**

4-[(2-Methylbenzimidazol-1-yl)methyl]-benzamide (0.020 g, 0.075 mmol) was dissolved in 2 mL of ethanol, which was added to a 3 mL ethanolic solution containing 2,6-dichlorobenzoic acid (0.014 g, 0.075 mmol) and 4-nitrobenzoic acid (0.013 g, 0.075 mmol). The resulting solution was slowly evaporated under ambient conditions for one month until colorless prisms formed. M.p. 176-178˚C.

4.2.4 X-ray crystallography

X-ray data were collected on a Bruker SMART 1000 four-circle CCD diffractometer using a fine-focus molybdenum Kα tube. Data were collected using SMART.[10] Initial cell constants were found by small widely separated "matrix" runs. Preliminary Laué symmetry was determined from axial images. Generally, an entire hemisphere of reciprocal space was collected regardless of Laué symmetry. Scan speed and scan width were chosen based on scattering power and peak rocking curves. Unless otherwise noted, data were collected at -70 °C, using 0.2° scan width.

Unit cell constants and orientation matrix were improved by least-squares refinement of reflections "thresholded" from the entire dataset. Integration was performed with SAINT,[11] using this improved unit cell as a starting point. Precise unit cell constants were

calculated in SAINT from the final merged dataset. Lorenz and polarization corrections were applied, but data were generally not corrected for absorption. Laué symmetry, space group, and unit cell contents were found with XPREP.

Data were reduced with SHELXTL.[12] The structures were solved in all cases by direct methods without incident. In general, hydrogen atoms were assigned to idealized positions and were allowed to ride. Where possible, the coordinates of hydrogen-bonding hydrogen atoms were allowed to refine. Heavy atoms, other than those of the guests, were refined with anisotropic thermal parameters. None of the datasets were corrected for absorption. Linear absorption coefficients for the strongest absorbers, **24** and **25**, were 0.294 mm^{-1} and 0.273 mm^{-1}, respectively. Merging R for these two datasets were 4.9% and 5.2%, respectively. **24:** Coordinates for the amide hydrogen atoms were allowed to refine. **25:** This compound crystallizes in the noncentrosymmetric space group $P2_12_12_1$, with the asymmetric unit containing one molecule of the benzimidazole compound and one molecule of water. Coordinates for the amide hydrogen atoms and water hydrogen atoms were allowed to refine. The structure was refined as a racemic twin and converged to an approximately 28:72 ratio of the two enantiomorphs. **21:** This compound crystallizes with two formula units per asymmetric unit. A scan width of 0.3 °C was chosen for data collection. Coordinates for the amide hydrogen atoms were allowed to refine. **23:** Coordinates for the amide hydrogen atoms were allowed to refine. **26:** Coordinates for the amide hydrogens and carboxylic acid hydrogens were allowed to refine. **27:** Data were collected at -100 °C. Coordinates for the amide and carboxylic acid hydrogen atoms were allowed to refine.

4.2.5 Powder X-ray diffraction

Powder XRD data were collected on a Bruker/Nonius D8 ADVANCE diffractometer with Bragg-Brentano geometry. A step size of 0.04˚ and step time of 5 sec per step were used. Data for **26** and **27** were obtained over 5-50˚ and 2-50˚ 2-θ ranges respectively. Data were then processed using EVA v8.0.[13]

4.3 Results

A summary of the crystallographic information for each compound is displayed in Tables A21-A28, all hydrogen-bond geometries are listed in Table 4.1, and the relevant labeling schemes and thermal ellipsoids are shown in Figure 4.1.

Table 4.1 Hydrogen-bond geometries for **21-28**.

Compound	**D-H A**	**D-H/Å**	**H…A/Å**	**D…A/Å**	**<(DHA)/°**	**generator for A**
21	N27 H27A N33	0.91(2)	2.07(2)	2.962(2)	166.3(17)	–
	N27 H27B O47	0.90(2)	2.04(2)	2.926(2)	168.7(19)	–
	N47 H47A O27	0.91(2)	2.00(2)	2.898(2)	170.3(19)	–
	N47 H47B N13	0.84(2)	2.21(2)	3.030(2)	163.1(18)	–
22	N27 H27A O47	0.95(3)	1.99(3)	2.929(4)	171(3)	–
	N47 H47A O27	0.99(3)	1.90(3)	2.889(3)	174(3)	–
	N27 H27B N33	0.95(3)	2.12(3)	2.996(3)	153(3)	x, y-1, z
	N47 H47B N13	0.92(3)	2.14(3)	3.009(3)	156(3)	x, y+1, z
23	N27 H27A N13	0.88(3)	2.17(3)	3.014(3)	162(2)	x, -y-1/2, z-1/2
	N27 H27B O27	0.97(3)	1.93(3)	2.888(3)	168(2)	x, -y-1/2, z-1/2
24	N27 H27A O47	0.90(2)	1.97(2)	2.869(2)	174(2)	–
	N47 H47A O27	0.89(2)	2.02(2)	2.909(2)	174(2)	–
	N27 H27B N33	0.95(2)	2.12(2)	3.022(2)	158(2)	–
	N47 H47B N13	0.90(2)	2.20(2)	3.060(2)	159.7(19)	–
25	N27 H27A O1S	0.86(2)	2.07(2)	2.885(3)	158(2)	-x+1/2, -y, z+1/2
	N27 H27B O1S	0.92(2)	2.01(2)	2.858(3)	153(2)	-x, y+1/2, z+1/2
	O1S H1B N13	0.85(2)	1.98(3)	2.803(3)	162(2)	–
	O1S H1A O27	0.82(3)	1.95(3)	2.750(2)	163(2)	-x, y+1/2, z+1/2
26	O47 H47 N13	1.11(2)	1.49(2)	2.5808(18)	165.2(16)	–
	N27 H27A O27	1.00(2)	1.95(2)	2.944(2)	174(2)	-x, -y, -z
	N27 H27B O48	1.09(2)	1.94(2)	2.989(2)	161.1(17)	-x, -y, -z
27	O31 H31 O27	0.94(2)	1.64(2)	2.571(2)	172(2)	–
	O41 H41 N13	1.07(2)	1.53(2)	2.591(2)	170.8(19)	–
	N27 H27A O32	0.96(2)	1.92(3)	2.873(3)	169(2)	–
	N27 H27B O41	0.86(2)	2.57(2)	3.342(3)	149(2)	-x, -y, -z
28	N13 H13 O31	1.24(2)	1.31(2)	2.533(2)	169.5(18)	–
	O41 H41 O27	0.82(2)	1.75(2)	2.562(2)	169(2)	–
	N27 H27A O42	0.90(3)	2.01(3)	2.875(2)	160(2)	–
	N27 H27B O32	0.90(3)	2.09(3)	2.918(2)	152(2)	-x+1, y-1/2, -z+1/2

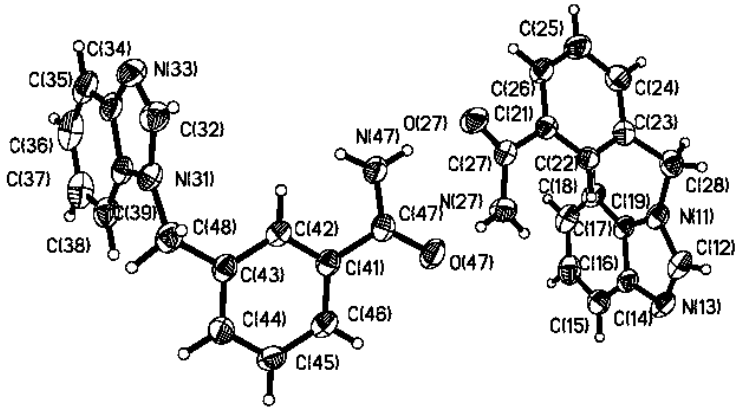
C(34)
N(33)
C(35)
C(32)
C(36)
N(31)
C(37)
C(39)
C(38)
C(48)
C(42)
C(47)
N(47)
O(27)
C(43)
C(41)
O(47)
C(44)
C(46)
C(45)
C(25)
C(26)
C(24)
C(21)
C(23)
C(27)
C(22)
C(28)
C(18)
C(19)
N(27)
C(17)
N(11)
C(12)
C(16)
C(15)
C(14)
N(13)

(a)

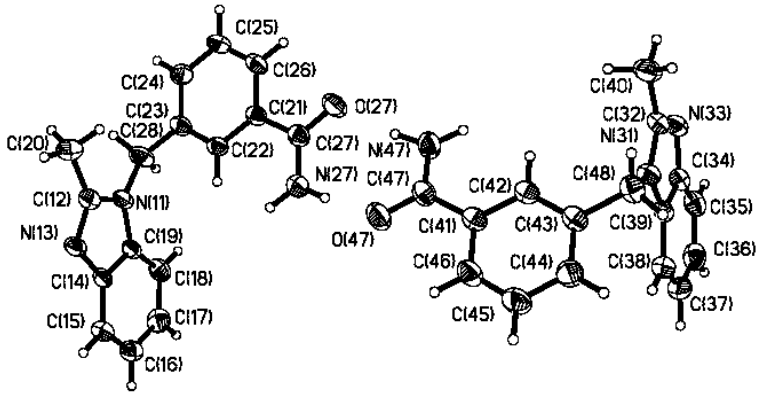
C(25)
C(26)
C(24)
C(23)
C(21)
O(27)
C(28)
C(22)
C(27)
N(47)
C(20)
C(47)
N(27)
C(12)
N(11)
C(42)
C(48)
C(40)
C(32)
N(33)
N(31)
C(34)
C(35)
N(13)
C(19)
C(41)
C(43)
C(39)
O(47)
C(36)
C(14)
C(18)
C(46)
C(44)
C(38)
C(15)
C(17)
C(45)
C(37)
C(16)

(b)

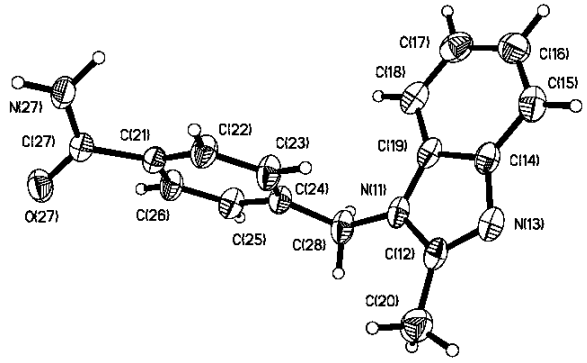
C(17)
C(16)
C(18)
C(15)
N(27)
C(19)
C(27)
C(21)
C(22)
C(23)
C(14)
C(24)
N(11)
O(27)
C(26)
N(13)
C(25)
C(28)
C(12)
C(20)

(c)

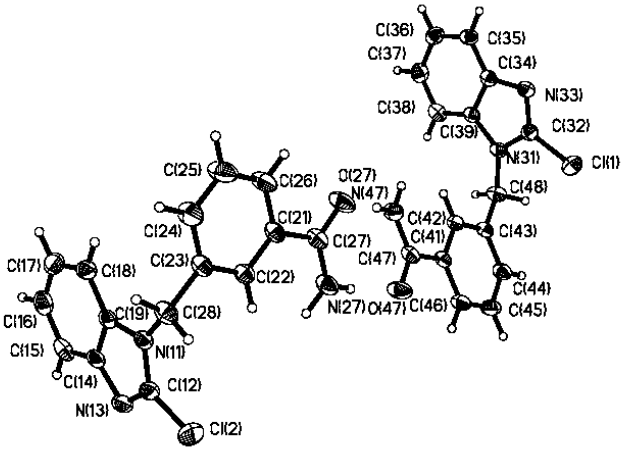
C(36)
C(35)
C(37)
C(34)
N(33)
C(38)
C(39)
C(32)
N(31)
Cl(1)
C(48)
C(25)
C(26)
O(27)
N(47)
C(42)
C(24)
C(21)
C(27)
C(41)
C(43)
C(17)
C(18)
C(23)
C(22)
C(47)
C(44)
C(19)
C(28)
N(27)
O(47)
C(46)
C(45)
C(16)
C(15)
N(11)
C(14)
C(12)
N(13)
Cl(2)

(d)

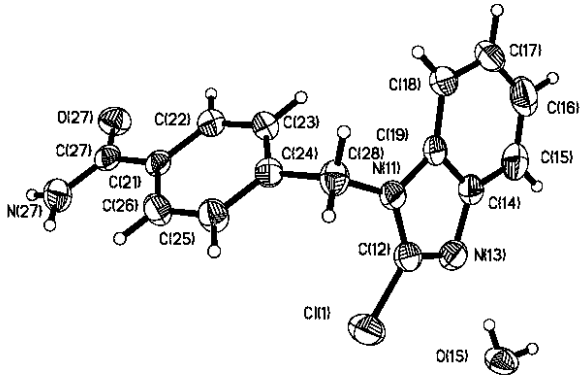
C(17)
C(18)
C(16)
O(27)
C(22)
C(23)
C(19)
C(15)
C(27)
C(24)
C(28)
N(11)
C(21)
C(14)
N(27)
C(26)
C(25)
C(12)
N(13)
Cl(1)
O(15)

(e)

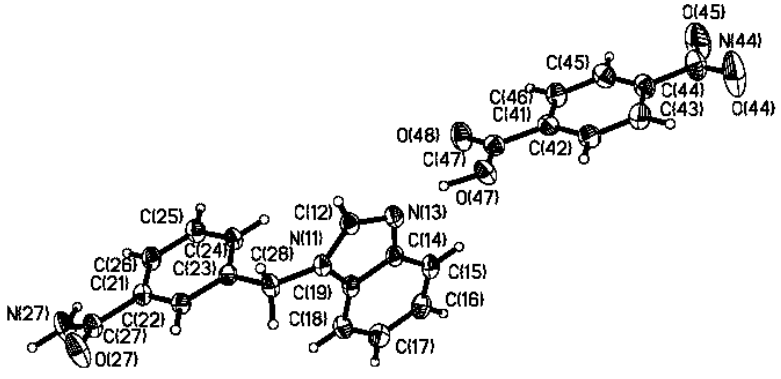
O(45)
N(44)
C(45)
C(46)
C(44)
C(41)
C(43)
O(44)
O(48)
C(42)
C(47)
O(47)
C(25)
C(12)
N(13)
C(24)
N(11)
C(14)
C(26)
C(28)
C(23)
C(15)
C(21)
C(19)
C(16)
N(27)
C(22)
C(18)
C(27)
C(17)
O(27)

(f)

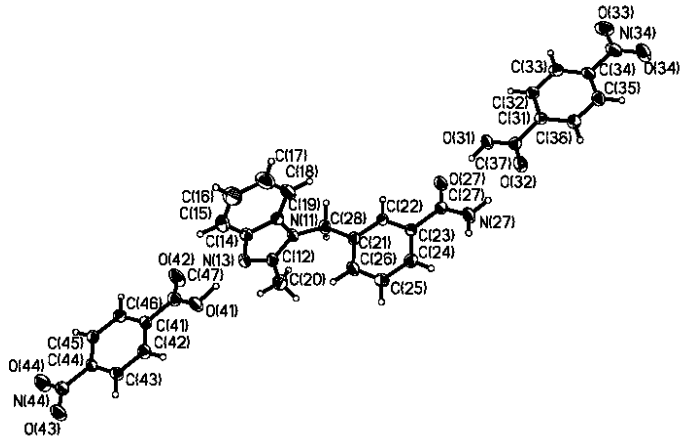

(g)

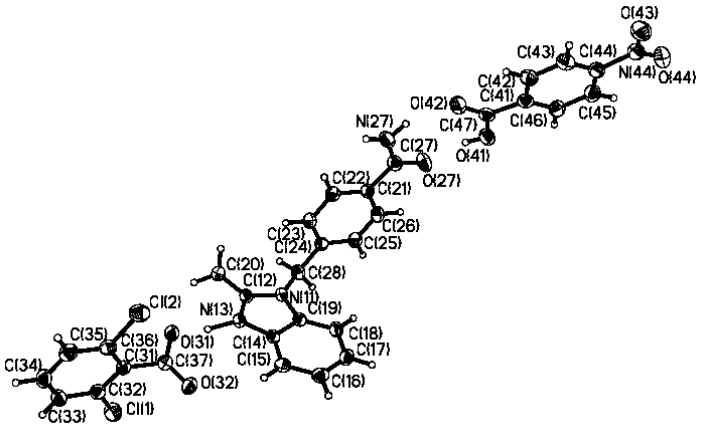

(h)

Figure 4.1a-h Thermal ellipsoid plots (50% probabilities) and labeling schemes for **21**-**28**.

4.3.1 Crystal structure of 3-[(benzimidazol-1-yl)methyl]-benzamide, **21**

The crystal structure of **21** contains two molecules of 3-[(benzimidazol-1-yl)methyl]-benzamide in the asymmetric unit, Figure 4.1a. These molecules interact through two different N–H···O hydrogen bonds in which the *syn*- N–H protons of carboxamide moieties interact with carbonyl oxygen atoms of carboxamide moieties on adjacent molecules (N27···O47, 2.926(2) Å; N47···O27, 2.898(2) Å), Figure 4.2. The dimeric units are propagated into an infinite 1-D ribbon through two crystallographically

inequivalent N–H···N hydrogen bonds between the *anti*- N–H proton of a carboxamide moiety and the benzimidazol-1-yl nitrogen atom of another molecule (N27···N33, 2.962(2) Å; N47···N13, 3.030(2) Å.

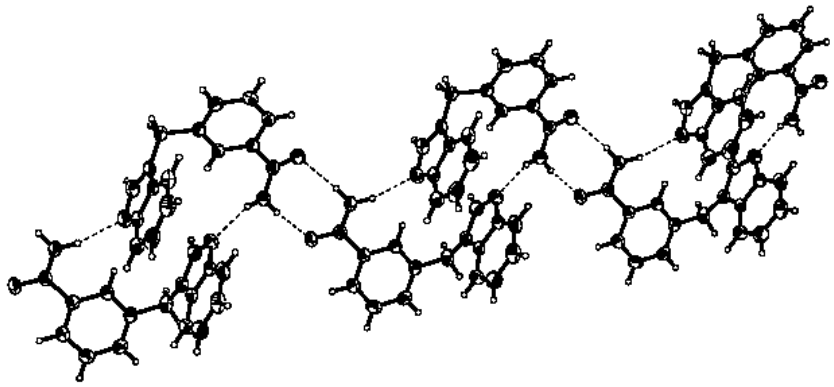

Figure 4.2 Infinite 1-D ribbon in the crystal structure of **21**.

4.3.2 Crystal structure of 3-[(2-methylbenzimidazol-1-yl)methyl]-benzamide, **22**

Similarly to **21**, the crystal structure determination of **22** revealed the presence of two molecules of 3-[(2-methylbenzimidazol-1-yl)methyl]-benzamide in the asymmetric unit, Figure 4.1b, that interact *via* head-to-head $R_2^2(8)$ carboxamide···carboxamide hydrogen bonds (N27···O47, 2.929(4) Å; N47···O27, 2.889(3) Å), Figure 4.3. This dimeric unit is further extended into an infinite 1-D ribbon through N–H···N interactions involving the *anti*- N–H proton of one carboxamide moiety and the 2-methylbenzimidazol-1-yl moiety of an adjacent molecule (N27···N33, 2.996(3) Å; N47···N13, 3.009(3) Å).

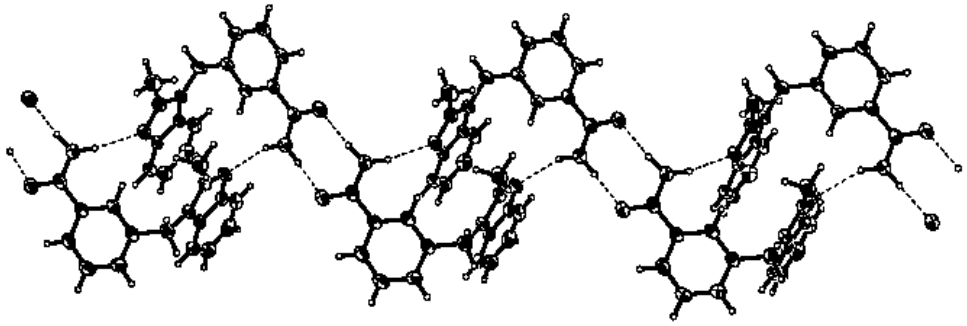

Figure 4.3 Extended 1-D motif in the crystal structure of **22**.

4.3.3 Crystal structure of 4-[(2-methylbenzimidazol-1-yl)methyl]-benzamide, **23**

The asymmetric unit of **23** contains one 4-[(2-methylbenzimidazol-1-yl)methyl]-benzamide molecule, Figure 4.1c, which extends into an infinite two-dimensional puckered sheet through N–H···O and N–H···N hydrogen bonds, Figure 4.4.

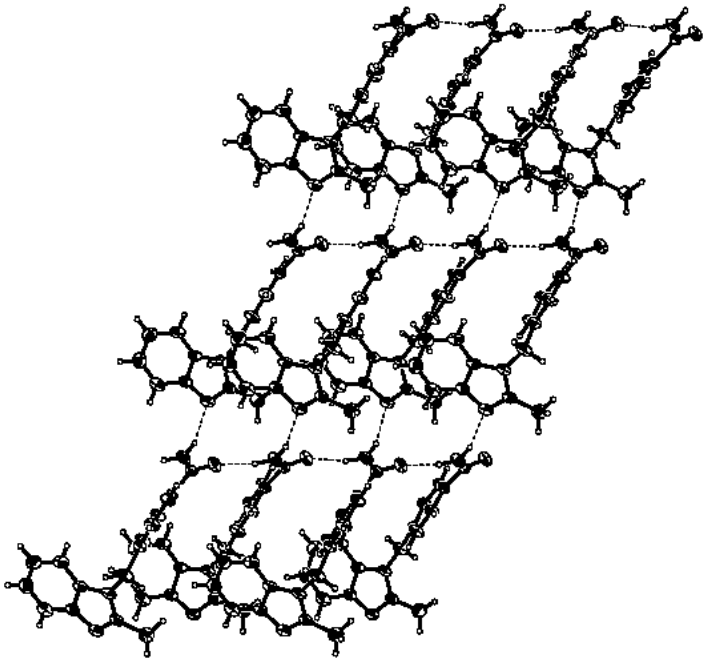

Figure 4.4 Extended 2-D sheet in the crystal structure of **23**.

The N–H···O hydrogen bonds arise from catemeric C(4) carboxamide···carboxamide interactions between the *anti*- N–H proton of a carboxamide moiety on one molecule and the carbonyl oxygen atom of a neighboring molecule (N27···O27, 2.888(3) Å). The second component of the sheet is the "head-to-tail" N–H···N hydrogen bond between the *syn*- N–H proton of a carboxamide moiety and the 2-methylbenzimidazol-1-yl nitrogen atom of an adjacent molecule (N27···N13, 3.014(3) Å).

4.3.4 Crystal structure of 3-[(2-chlorobenzimidazol-1-yl)methyl]-benzamide, **24**

The crystal structure of **24** contains two molecules of 3-[(2-chlorobenzimidazol-1-yl)methyl]-benzamide in the asymmetric unit, Figure 4.1d. These molecules interact through two crystallographically inequivalent N–H···O hydrogen bonds involving the *syn*- N–H proton of one carboxamide moiety and the carbonyl oxygen atom of another

carboxamide moiety (N27···O47, 2.869(2) Å; N47···O27, 2.909(2) Å). These dimeric units are then propagated into the expected infinite 1-D undulating ribbons through hydrogen bonds between the *anti*- N–H protons and the 2-chlorobenzimidazol-1-yl nitrogen atoms of adjacent molecules (N27···N33, 3.022(2) Å; N47···N13, 3.060(2) Å), Figure 4.5.

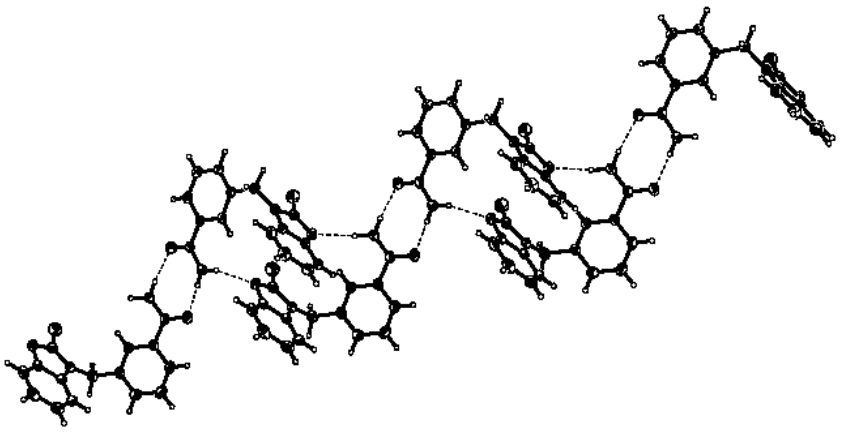

Figure 4.5 Extended 1-D ribbon in **24**.

4.3.5 Crystal structure of 4-[2-chlorobenzimidazol-1-yl)methyl]-benzamide monohydrate, **25**

The asymmetric unit in the crystal structure of **25** consists of one molecule of 4-[(2-chlorobenzimidazol-1-yl)methyl]-benzamide and one water molecule, Figure 1e. These interact *via* an O–H···N hydrogen bond involving the 2-chlorobenzimidazol-1-yl nitrogen atom (O1S···N13, 2.803(3) Å). Expansion of the asymmetric unit reveals the presence of an aggregate that can be described as a water-bridged hydrogen-bonded $R_4^3(10)$ hexameric unit, Figure 4.6.

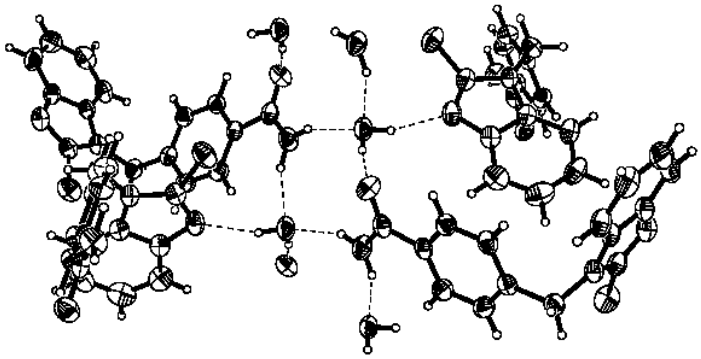

Figure 4.6 Local environment around a water-bridged $R_4^3(10)$ hexameric unit in the crystal structure of **25** generated by hydrogen bonds between 4-[(2-chlorobenzimidazol-1-yl)methyl]-benzamide and water molecules.

The water-bridged $R_4^3(10)$ motif arises from a combination of N–H···O and O–H···O hydrogen bonds. The first N–H···O interaction involves the *syn*- N–H proton of a carboxamide moiety on one 4-[(2-chlorobenzimidazol-1-yl)methyl]-benzamide molecule and the oxygen atom of a water molecule (N27···O1S, 2.885(3) Å) whereas the second N–H···O hydrogen bond takes place between the *anti*- N–H proton of the same carboxamide and the oxygen atom of another water molecule (N27···O1S, 2.858(3) Å). The O–H···O hydrogen bond is formed between H1A of a water molecule and the carbonyl oxygen atom of an adjacent carboxamide moiety (O1S···O27, 2.750(2) Å). This local environment, when extended further, results in an extended 2-D corrugated sheet, Figure 4.7, which is formed from ladders of interconnected $R_4^3(10)$ hydrogen-bond units. Adjacent sheets are interconnected in a parallel fashion through O–H···O hydrogen bonds involving O–H donors of water molecules on one layer and carbonyl oxygen atoms of carboxamide moieties in another layer (O1S···O27, 2.750(2) Å) to afford a three-dimensional network.

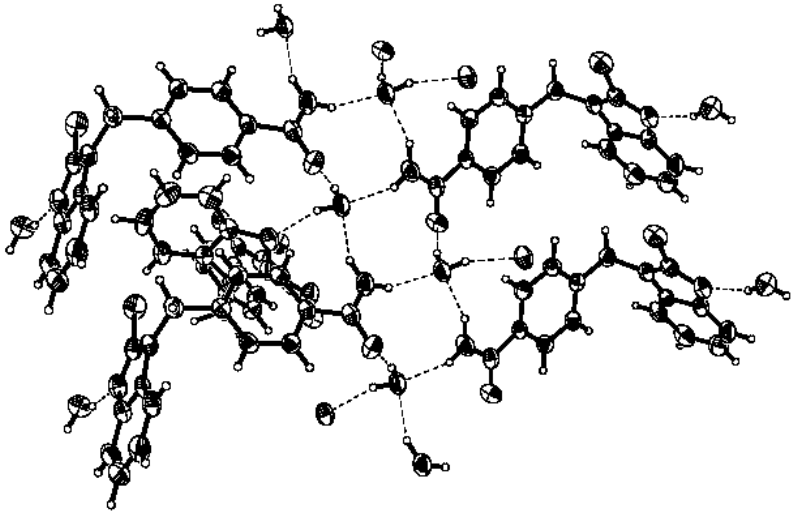

Figure 4.7 Extended view of the crystal structure of **25** showing the interconnections of $R_4^3(10)$ motifs.

4.3.6 Crystal structure of 3-[(benzimidazol-1-yl)methyl]-benzamide 4-nitrobenzoic acid, **26**

The crystal structure of **26** contains one molecule each of 4-nitrobenzoic acid and 3-[(benzimidazol-1-yl)methyl]-benzamide in the asymmetric unit, Figure 4.1f. The two molecules interact *via* an O–H···N hydrogen bond between the carboxylic acid O–H moiety of 4-nitrobenzoic acid and the benzimidazol-1-yl nitrogen atom of 3-[(benzimidazol-1-yl)methyl]-benzamide (O47···N13, 2.5808(18) Å). The two molecules are extended into a four-component supermolecule consisting of two molecules each of 4-nitrobenzoic acid and 3-[(benzimidazol-1-yl)methyl]-benzamide related by an inversion center through self-complementary "head-to-head" $R_2^2(8)$ N–H···O hydrogen bonds involving *syn*- N–H protons and carbonyl oxygen atoms (N27···O27, 2.944(2) Å), Figure 4.8.

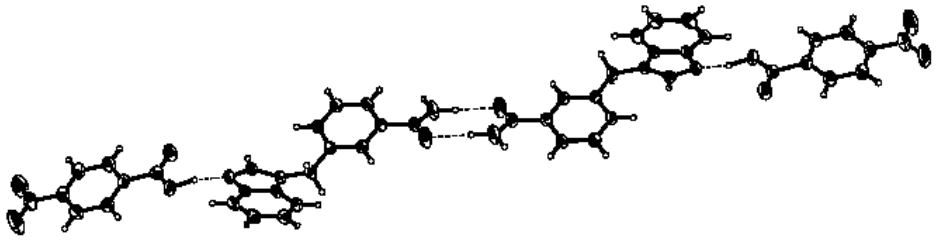

Figure 4.8 Hydrogen-bond driven assembly of a four-component supermolecule in the crystal structure of **26**.

Adjacent supermolecules are connected into an infinite 1-D ladder motif through N–H···O hydrogen bonds between the *anti*- N–H proton of a carboxamide moiety and a carbonyl oxygen atom of a 4-nitrobenzoic acid molecule on a neighboring layer (N27···O48, 2.989(2) Å), Figure 4.9.

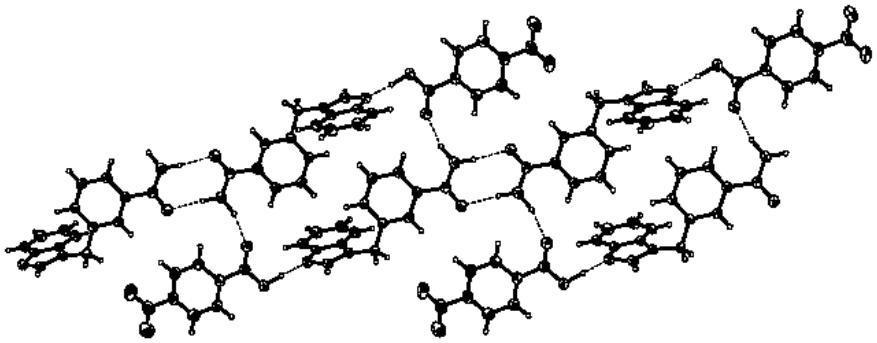

Figure 4.9 Infinite 1-D ladder motif in the crystal structure of **26** showing interactions between neighboring supermolecules.

4.3.7 Crystal structure of 3-[(2-methylbenzimidazol-1-yl)methyl]-benzamide 4-nitrobenzoic acid, **27**

In contrast to the crystal structure of **26**, the asymmetric unit of **27** consists of two 4-nitrobenzoic acid molecules and one 3-[(2-methylbenzimidazol-1-yl)methyl]-benzamide molecule. The latter is therefore a 2:1 molecular co-crystal Figure 4.1g. The molecules interact through an O–H···N hydrogen bond between the carboxylic acid O–H moiety of the first 4-nitrobenzoic acid molecule and the 2-methylbenzimidazol-1-yl nitrogen atom of 3-[(2-methylbenzimidazol-1-yl)methyl]-benzamide (O41···N13, 2.591(2) Å) and a "head-to-head" carboxylic acid···carboxamide interaction consisting of O–H···O and

N–H···O hydrogen bonds, (O31···O27, 2.571(2) Å; N27···O32, 2.873(3) Å), Figure 4.10. Adjacent supermolecules are interconnected in an antiparallel fashion through N–H···O hydrogen bonds involving the *anti*- N–H proton of a carboxamide moiety in one layer and a 4-nitrobenzoic acid molecule in a neighboring layer (N27···O41, 3.342(3) Å).

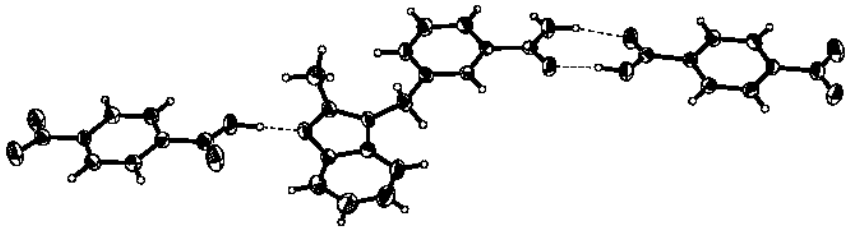

Figure 4.10 Trimeric supermolecule in the crystal structure of **27**.

4.3.8 Crystal structure of 4-[(2-methylbenzimidazolium-1-yl)methyl]-benzamide 2,6-dichlorobenzoate 4-nitrobenzoic acid, **28**

In the crystal structure of **28**, a 1:1:1 ternary compound had formed between the stronger carboxylic acid (as determined by pK_a values),[14] 2,6-dichlorobenzoic acid, 4-[(2-methylbenzimidazol-1-yl)methyl]-benzamide, and the weaker acid, 4-nitrobenzoic acid, Figure 4.1h. The stronger acid seeks out the best acceptor, the 2-methylbenzimidazol-1-yl nitrogen atom, to form an ionic N^+–H···O^- hydrogen bond (N13···O31, 2.533(2) Å), while the weaker carboxylic acid forms a heteromeric acid···amide synthon with the second-best acceptor, the carboxamide moiety (O41···O27, 2.562(2) Å; N27···O42, 2.875(2) Å), Figure 4.11.

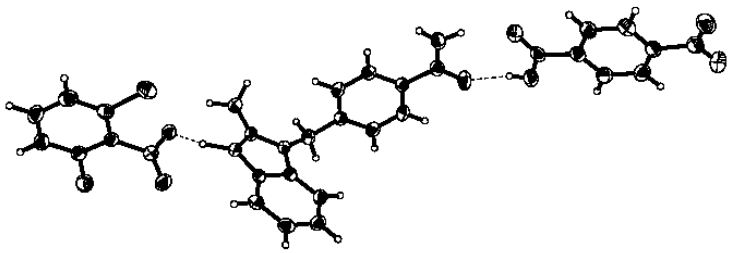

Figure 4.11 Ternary compound in the crystal structure of **28**.

Neighboring compounds are interconnected into an infinite undulating 1-D chain through N–H···O hydrogen bonds involving the *anti*- N–H protons on carboxamide moieties and

carbonyl oxygen atoms of 2,6-dichlorobenzoic acid molecules on adjacent compounds (N27···O32, 2.918(2) Å), Figure 4.12.

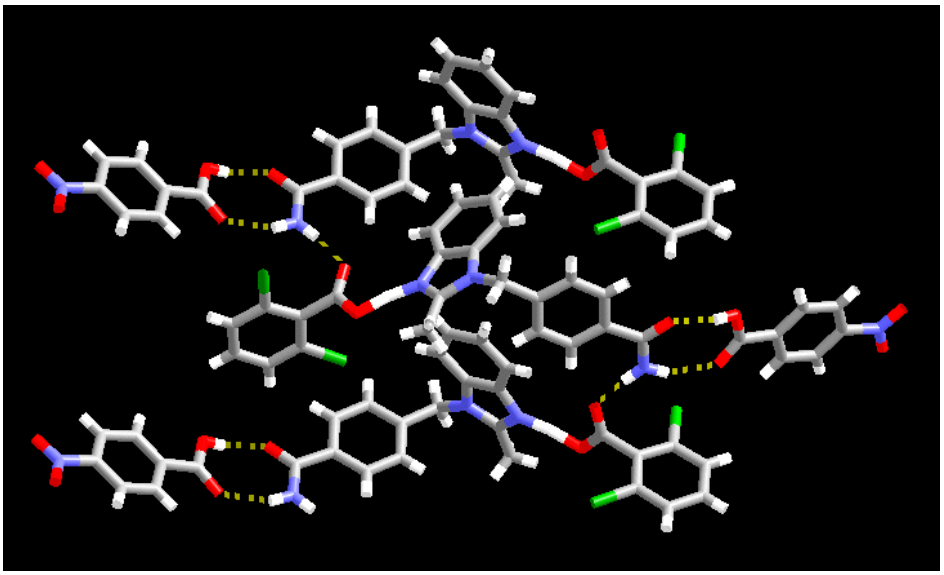

Figure 4.12 1-D chain in **28** resulting from interactions between adjacent ternary compounds.

4.4 Discussion

All (benzimidazol-1-yl)methylbenzonitrile precursors **4.2.1.1**-**4.2.1.6** were synthesized in good yields by allowing the appropriate α-bromotolunitrile and benzimidazole to react under alkaline conditions[15] employing a slightly modified procedure. Their formation is supported by ^{1}H NMR spectroscopy in which the chemical shifts corresponding to the methylene protons on the α-bromotolunitrile compared to those of the coupled products are significantly different. IR spectra of these precursors also indicate the presence of C≡N stretches demonstrating that the nitrile groups remain intact upon reaction of the two starting materials. Hydrolysis of **4.2.1.1**-**4.2.1.6** with 30 wt % H_2O_2 in DMSO[16] afforded the desired benzamides **4.2.1.7**-**4.2.1.12** in good yields. The chemical shifts, splitting patterns, and integration in the ^{1}H NMR spectra correlate well with the molecular structures of the desired products, and there were no traces of starting material in the spectra. Furthermore, characteristic C=O and N-H stretches as a result of carboxamide formation were observed in the IR spectra of the products.

Recrystallization of benzamides **4.2.1.7-4.2.1.12** from either hot acetonitrile, ethyl acetate, or methanol afforded crystals suitable for X-ray crystallography except for **4.2.1.8**. In the case of **4.2.1.12**, recrystallization from hot acetonitrile yielded microcrystals that were too small for X-ray crystallography. Slow evaporation of the mother liquor, however, produced colorless prisms suitable for X-ray crystallography, **25**. IR spectroscopy of these prisms shows a characteristic broad O–H stretch at 3100-3500 cm^{-1}, which is due to the presence of water. This broad stretch is not observed in the IR spectrum of **4.2.1.12**. Structural analysis of these prisms subsequently confirms the presence of water molecules in the crystal structure of **25**. The crystal structures of the other benzamide compounds do not incorporate solvent molecules. The non-hydrated compounds **4.2.1.7-4.2.1.12** are thermally stable from 181-239˚C. The melting point of **25**, however, is much lower (124-127˚C) than that of the non-hydrated form in **4.2.1.12** (185-190˚C). The workup and purification/recrystallization of **4.2.1.7-4.2.1.12** show that these compounds have overall very good solubility, which is a desirable attribute for effective and versatile co-crystal formation.

An examination of the crystal structures of **21-24** reveals two well-known hydrogen-bond motifs. In **21**, **22**, and **24**, the same infinite 1-D motif, constructed from N–H···N and N–H···O hydrogen bonds, is observed. The self-complementary carboxamide···carboxamide interactions create a dimeric arrangement, Scheme 4.4a.

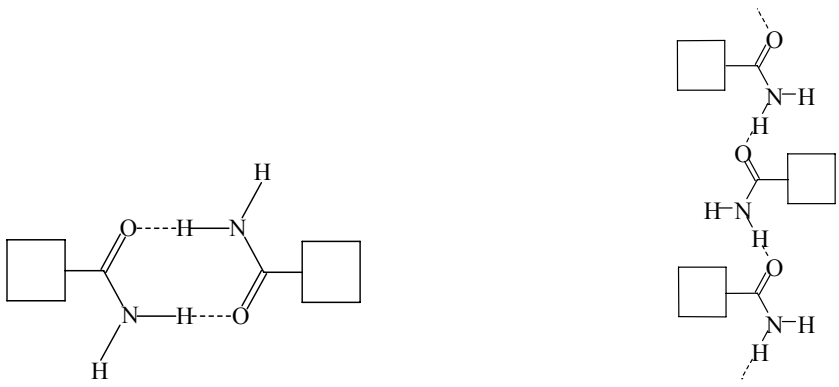

(a) (b)

Scheme 4.4 Possible hydrogen-bond motifs between carboxamide moieties, (a) dimer and (b) catemer.

The crystal structure of **23** contains a different hydrogen-bond motif, however, as the self-complementary carboxamide···carboxamide interactions generate a catemeric structure, Scheme 4.4b. Both the dimer and the catemer motif can be expected in these molecules, since they are common hydrogen-bond patterns encountered in carboxamide moieties, and are robust enough to be employed as supramolecular tools in the solid state.

The hydrogen-bond patterns in the crystal structure of **25** are very different due to the presence of a water molecule. The appearance of hydrated structures tends to be highly unpredictable, and it is clear that even the reasonably robust carboxamide···carboxamide interactions can be disrupted by a suitable solvent molecule, resulting in an unexpected structural outcome.

As mentioned previously, these supramolecular reagents (SR's) were prepared with the ultimate goal of generating ternary co-crystals by taking advantage of the best donor/best acceptor concept in a series of reactions between suitable SR's and two different carboxylic acids. However, unless a binary solid can be obtained in some rational manner there would be little point in pursuing ternary co-crystals. Therefore we prepared two binary co-crystals, **26** and **27**, by allowing 4-nitrobenzoic acid to react with **4.2.1.7** and **4.2.1.9**, respectively. Although co-crystallization attempts employing **4.2.1.12** with 4-nitrobenzoic acid and 3,5-dinitrobenzoic acid in each case did not yield single crystals of sufficient quality, the IR spectra of both powdery materials displayed broad O–H···N stretches typical of co-crystal formation between carboxylic acids and nitrogen-containing heterocycles *via* hydrogen bonding.[17,18] Both **26** and **27** are molecular co-crystals and not salts since no proton transfer between carboxylic acid and the benzimidazol-1-yl moiety has taken place. This conclusion is based upon the observed C–O bond lengths as determined by single crystal X-ray crystallography. The formation of molecular solids in reactions between *N*-substituted benzimidazole and carboxylic acids is also consistent with previous results gathered from a systematic structural study of symmetric ditopic *N*-substituted imidazoles/benzimidazoles and dicarboxylic acids.[19]

The crystal structure of **26** is typical of binary co-crystals between heterocyclic-based carboxamides such as *iso*nicotinamide and carboxylic acids[6] in that the carboxylic acid (the best donor) interacts with the heterocyclic nitrogen atom (the best acceptor), thus

leaving the carboxamide moiety to form self-complementary hydrogen bonds. The crystal structure of **27**, however, exhibits a somewhat different scenario in that the self-complementary carboxamide···carboxamide interaction present in **26** is disrupted by a second 4-nitrobenzoic acid molecule in favor of a heteromeric carboxylic acid···carboxamide hydrogen-bond interaction. This disruption is, in fact, welcome as it indicates that this particular supramolecular reagent can simultaneously form hydrogen bonds with carboxylic acids at both its binding sites; the next phase will involve exploring the selectivity of these supramolecular reagents when confronted with two different carboxylic acids.

We also examined the structural homogeneity of the products that were obtained in the syntheses of **26** and **27** through an analysis of bulk samples using powder X-ray diffraction (XRD) data. Bulk samples were collected and analyzed in two stages and were obtained from reactions between [benzimidazol-1-yl)methyl]-benzamides and 4-nitrobenzoic acid that were set up in 1:1 and 1:2 stoichiometric ratios. The first crop of crystals was harvested immediately upon precipitation, and the second crop was obtained upon complete evaporation of the solvent.

The powder XRD patterns of both the first and second crop resulting from the 1:1 reaction between 3-[(benzimidazol-1-yl)methyl]-benzamide and 4-nitrobenzoic acid are essentially the same and correspond very well to the X-ray powder pattern simulated from the single-crystal data of the crystal structure of **26**, Figure 4.13a. When the same reaction is carried out in a 1:2 ratio, the first crop still has a powder pattern that corresponds to the crystal structure of the 1:1 co-crystal, **26**. The experimental powder pattern of the second crop only shows the presence of unreacted 4-nitrobenzoic acid,[20] Figure 4.13b. Both crops are homogeneous and show the presence of only one phase in each case. The only new compound that is formed in the reaction between 3-[(benzimidazol-1-yl)methyl]-benzamide and 4-nitrobenzoic acid, regardless of initial ratio, is the 1:1 molecular co-crystal. Furthermore, the reaction is quantitative and none of the limiting reactant is left behind.

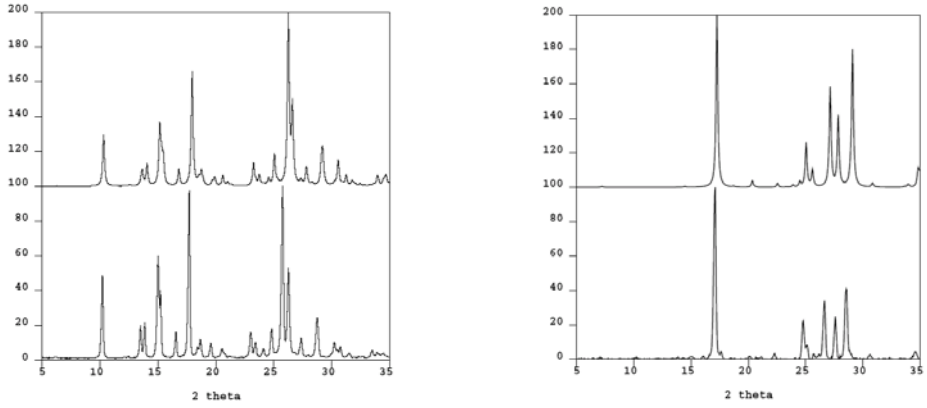

(a) (b)

Figure 4.13 Simulated (top) and experimental (bottom) powder XRD patterns for (a) **26** (first crop) and (b) **26** (second crop). The reaction was carried out in a 1:2 stoichiometry, and the only material left over is unreacted 4-nitrobenzoic acid.

In the 1:1 reaction between 3-[(2-methylbenzimidazol-1-yl)methyl]-benzamide and 4-nitrobenzoic acid, the powder pattern of the first crop of crystals corresponds exclusively to that simulated from the single-crystal data of **27**, a molecular co-crystal with a 1:2 composition. The second crop from this reaction corresponds exclusively to the pattern simulated from that of the crystal structure of the SR by itself (which is expected as 4-nitrobenzoic acid is now the limiting reactant). When a starting ratio of 1:2 is employed, only the 1:2 supramolecular product, **27**, is attained (100 % conversion) in both first and second crops as demonstrated by the experimental powder patterns, Figures 4.14a and 4.14b, respectively.

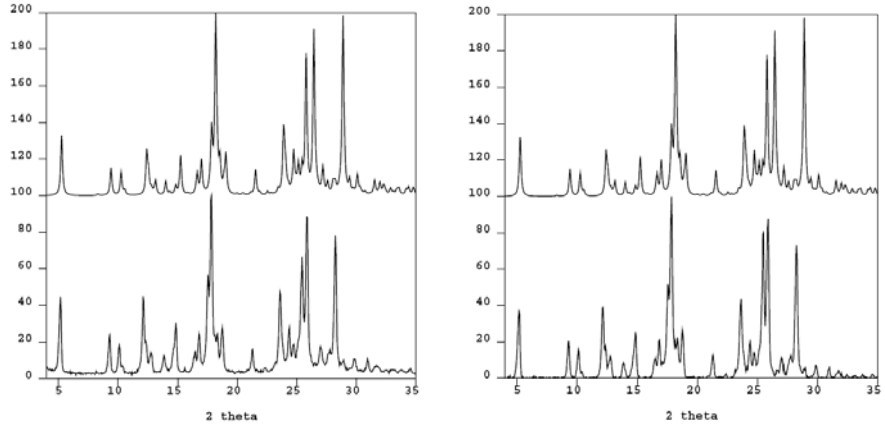

(c) (d)

Figure 4.14 Simulated (top) and experimental (bottom) powder XRD patterns for (a) **27** (first crop) and (b) **27** (second crop).

When 4-[(2-methylbenzimidazol-1-yl)methyl]-benzamide was allowed to react with two different carboxylic acids, 2,6-dichlorobenzoic acid and 4-nitrobenzoic acid, it effectively produced a 1:1:1 ternary supermolecule, **28**, with predetermined connectivity. The stronger carboxylic acid, 2,6-dichlorobenzoic acid, interacted with the best hydrogen-bond acceptor while the weaker acid, 4-nitrobenzoic acid, formed a carboxamide···carboxylic acid synthon. Although the heterocyclic moiety on the SR was protonated, the structural selectivity in **28** still followed the best donor–best acceptor/second-best donor–second-best acceptor concept.

4.5 Conclusions

A family of closely related [(benzimidazol-1-yl)methyl]-benzamide compounds was synthesized in good yields through a two-step procedure. These molecules were characterized by ^{1}H NMR and IR spectroscopy, and the crystal structures of **21**-**25** were obtained *via* single-crystal X-ray crystallography. Analyses of these crystal structures revealed self-complementary dimeric $R_2^2(8)$ and catemeric C(4) hydrogen-bond motifs between carboxamide moieties in combination with the expected amide···heterocycle N-H···N hydrogen bond. These compounds have two independent binding sites suitable for two different intermolecular interactions, and they are also soluble in a range of polar solvents. Two of them, 3-[(benzimidazol-1-yl)methyl]-benzamide and 3-[(2-methylbenzimidazol-1-yl)methyl]-benzamide, have already been shown to be capable of co-crystal formation with a carboxylic acid. The co-crystallization reactions proceed in a quantitative manner, as evidenced by powder XRD. The potential effectiveness of these compounds as reliable and versatile supramolecular reagents for the assembly of ternary supermolecules was also shown in **28**, employing 4-[(2-methylbenzimidazol-1-yl)methyl]-benzamide and two different carboxylic acids. The structural and electronic aspects in this family of SR's are readily tunable (1,3- and 1,4- isomers and different substituents), which provide opportunities for the formation of more ternary co-crystals. These examples would then serve to gain a better command over the competition and balance of intermolecular forces as a result of a transferable and modular non-covalent synthetic approach.

References

[1] (a) Desiraju, G. R. *Crystal Engineering: The Design of Organic Solids*; Elsevier Science Publishers B. V.: Amsterdam, 1989. (b) Steed, J. W.; Atwood, J. L. *Supramolecular Chemistry*; John Wiley & Sons, Ltd.: Chichester, 2000. (c) Desiraju, G. R. *The Crystal as a Supramolecular Entity*; John Wiley & Sons, Ltd.: 1996. (d) Desiraju, G. R. *Angew. Chem. Int. Ed. Engl.* **1995**, *34*, 2311. (e) Etter, M. C. *Acc. Chem. Res.* **1990**, *23*, 120. (f) Sharma, C. V. K.; Panneerselvam, K.; Pilati, T.; Desiraju, G. R. *J. Chem. Soc., Perkin Trans. 2* **1993**, 2209. (g) Aakeröy, C. B.; Desper, J.; Elisabeth, E.; Helfrich, B. A.; Levin, B.; Urbina, J. F. *Zeit. Kristallogr.* **2005**, *220*, 325.

[2] (a) Aakeröy, C. B. *Acta Crystallogr.* **1997**, *B53*, 569. (b) Etter, M. C. *J. Phys. Chem.* **1991**, *95*, 4601.

[3] (a) Shan, N.; Bond, A. D.; Jones, W. *Cryst. Eng.* **2002**, *5*, 9. (b) Shan, N.; Bond, A. D.; Jones, W. *New J. Chem.* **2003**, *2*, 365. (c) Shan, N.; Batchelor, E.; Jones, W. *Tetrahedron Lett.* **2002**, *43*, 8721. (d) Liu, R.; Valiyaveettil, S.; Mok, K.-F.; Vittal, J. J.; Hoong, A. K. M. *CrystEngComm.* **2002**, *4*, 574. (e) Sharma, C. V. K.; Zaworotko, M. J. *Chem. Commun*. **1996**, 2655. (f) Bhogala, B. R.; Vishweshwar, P.; Nangia, A. *Cryst. Growth Des.* **2002**, *2*, 325. (g) Bhogala, B. R.; Nangia, A. *Cryst. Growth Des.* **2003**, *3*, 547. (h) Arora, K. K.; Pedireddi, V. R. *J. Org. Chem.* **2003**, *68*, 9177. (i) Vishweshwar, P.; Nangia, A.; Lynch, V. M. *J. Org. Chem.* **2002**, *67*, 556.

[4] Almarsson, Ö.; Zaworotko, M. J. *Chem. Commun.* **2004**, 1889.

[5] (a) Bailey Walsh, R. D.; Bradner, M. W.; Fleischman, S.; Morales, L. A.; Moulton, B.; Rodriguez-Hornedo, N.; Zaworotko, M. J. *Chem. Commun*. **2003**, 186. (b) MacGillivray, L. R.; Reid, J. L.; Ripmeester, J. A. *J. Am. Chem. Soc.* **2000**, *122*, 7817. (c) Vishweshwar, P.; Thaimattam, R.; Jaskolski, M.; Desiraju, G. R. *Chem. Commun.* **2002**, 1830. (d) Zerkowski, J. A.; MacDonald, J. C.; Whitesides, G. M. *Chem. Mater*. **1997**, *9*, 1933. (e) Kane, J. J.; Liao, R.-F.; Lauher, J. W.; Fowler, F. W. *J. Am. Chem. Soc.* **1995**, *117*, 12003. (f) Lehn, J.-M.; Mascal, M.; DeCian, A.; Fischer, J. *J. Chem. Soc., Chem. Commun.* **1990**, 479. (g) Vishweshwar, P.; Nangia, A.; Lynch, V. M. *CrystEngComm*, **2003**, *5*, 164. (h) Aakeröy, C. B.; Desper, J.; Helfrich, B. A. *CrystEngComm* **2004**, *6*, 19. (i) Dale, S. H.; Elsegood, M. R. J.; Hemmings, M.; Wilkinson, A. L. *CrystEngComm* **2004**, *6*, 207. (j) Pedireddi, V. R.; PrakashaReddy, J.; Arora, K. K. *Tetrahedron Lett* **2003**, *44*, 4857.

[6] Aakeröy, C. B.; Beatty, A. M.; Helfrich, B. A. *J. Am. Chem. Soc.* **2002**, *124*, 14425.

[7] Aakeröy, C. B.; Beatty, A. M.; Helfrich, B. A. *Angew. Chem. Int. Ed. Engl.* **2001**, *40*, 3240.

[8] Other examples of heteromeric carboxylic acid···carboxamide interactions include: (a) Leiserowitz, L.; Nader, F. *Acta Crystallogr.* **1977**, *B33*, 2719. (b) Leiserowitz, L. *Acta Crystallogr.* **1976**, *B32*, 775.

[9] Almost quantitative yields for **13** and **14** were determined by powder X-ray diffraction.

[10] SMART v5.060; Bruker Analytical X-ray Systems: Madison, WI, 1997 – 1999.

[11] SAINT v6.02; Bruker Analytical X-ray Systems: Madison, WI, 1997 – 1999.

[12] SHELXTL v5.10; Bruker Analytical X-ray Systems: Madison, WI, 1997.

[13] EVA v8.0; Bruker AXS Gmbh: Karlsruhe, West Germany, 1997 – 2002.

[14] (a) pK_a values were calculated using Advanced Chemistry Development (ACD/Labs) Software Solaris v4.76; ACD/Labs, 1994-2005. (b) pK_a of 2,6-dichlorobenzoic acid: 1.69 ± 0.20; pK_a of 4-nitrobenzoic acid: 3.42 ± 0.20.

[15] (a) Zhou, C. H.; Guo, S. J.; Xie, R. G.; Zhao, H. M. *Chin. Chem. Lett.* **1996**, *7*, 321. (b) Liu, H. K.; Sun, W. Y.; Zhu, H. L.; Yu, K. B.; Tang, W. X. *Inorg. Chim. Acta* **1999**, *295*, 129.

[16] Katritzky, A. R.; Pilarski, B.; Urogdi, L. *Synthesis* **1989**, 949.

[17] The observed O–H···N stretches in the IR spectra for these materials correspond to (a) **4.2.1.12**/4-nitrobenzoic acid (2512 and 1918 cm^{-1}) and (b) **4.2.1.12**/3,5-dinitrobenzoic acid (2466 and 1869 cm^{-1}).

[18] Trivedi, D. R.; Ballabh, A.; Dastidar, P. *CrystEngComm* **2003**, *5*, 358.

[19] Aakeröy, C. B.; Desper, J.; Leonard, B.; Urbina, J. F. *Cryst. Growth Des.* **2005**, DOI: 10.1021/cg049682i.

[20] Groth, P. *Acta Chem. Scand. A* **1980**, *34*, 229.

Chapter 5

[(Benzimidazol-1-yl)methyl]-benzamides as ligands for high-yielding inorganic-organic supramolecular synthesis

5.1 Introduction

The supramolecular synthesis of extended metal-ligand frameworks with predetermined metrics and connectivities is a rapidly expanding area of crystal engineering.[1] Many of these architectures are constructed from rigid linkers (multi-topic ligands) and can possess a high degree of structural integrity even though they may display open structures with pores and channels. Some of the most popular building blocks in the synthesis of coordination polymers are ditopic ligands such as 4,4'-bipyridine that can be combined in different stoichiometries with metal ions of different coordination modes.[2] Recently, a number of coordination polymers built from flexible ditopic[3] and tritopic[4] *N*-substituted imidazole/benzimidazole ligands, Scheme 5.1, have also been reported which demonstrates that such *N*-heterocycles are also useful building blocks of extended metal-containing networks.

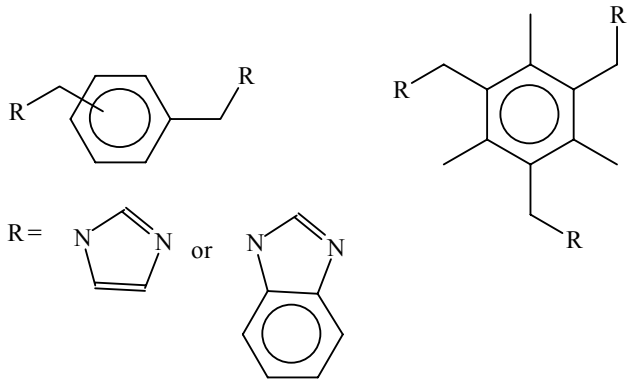

Scheme 5.1 Ditopic and tritopic imidazol-1-yl/benzimidazol-1-yl ligands used in the construction of coordination polymers.

Imidazol-1-yl and benzimidazol-1-yl-containing ligands may turn out to be more versatile that their pyridyl counterparts mainly due to their smaller C–N–C angles (108˚ vs 120˚ respectively) which alleviate steric crowding at the metal center upon

coordination. Consequently, five-membered *N*-heterocycles can readily be accommodated in an octahedral geometry around a suitable metal ion, an arrangement that is extremely rare for pyridyl-based ligands, Scheme 5.2. Better access to symmetric octahedral building blocks provides opportunities for the construction of porous networks in a more controlled manner; the geometry of the metal node can be propagated simultaneously in 3-D with only one type of ligand, which reduces potential structural interference.

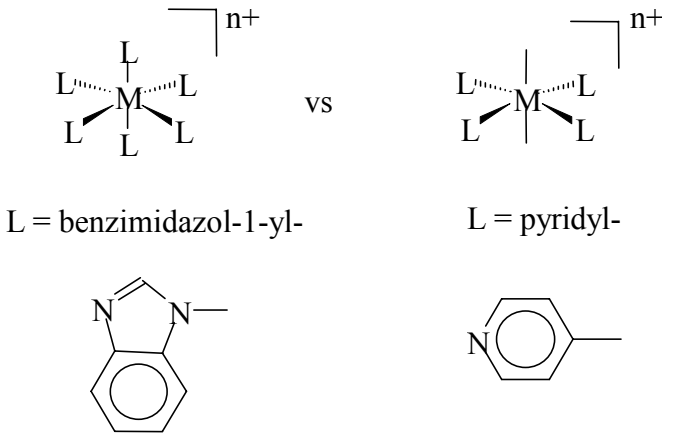

(a) C–N–C angle = 108˚ (b) C–N–C angle = 120˚

Scheme 5.2 Comparison of C–N–C angles in (a) benzimidazol-1-yl- and (b) pyridyl-containing ligands.

Another supramolecular synthetic strategy for the construction of extended metal-containing networks combines a suitable ligand moiety (for metal coordination) with an appropriate self-complementary hydrogen-bond functionality (for the supramolecular chemistry).[5] An example of such a coordinating/hydrogen-bonding ligand is *iso*nicotinamide,[6,7] which typically binds to a metal ion *via* the pyridyl moiety and also employs an $R_2^2(8)$ carboxamide···carboxamide hydrogen bond to propagate the inherent geometry of the complex ion into extended networks. The self-complementarity of the amide moiety essentially produces a supramolecular dimer that is topologically equivalent to the ditopic 4,4'-(1,4-phenylene)*bis*-pyridine,[8] Scheme 5.3.

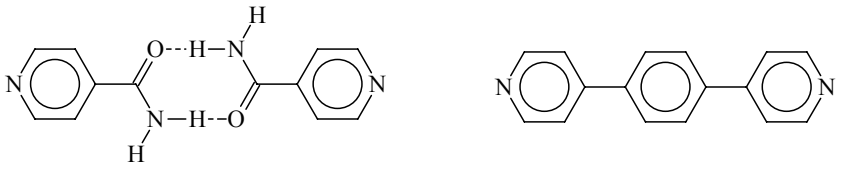

Scheme 5.3 (a) Hydrogen-bond linked and (b) covalently-linked extended ligands.

At times, supramolecular ligands may provide some advantages compared to their covalent counterparts. Representatives from the latter group may require significant synthetic efforts, and extended rigid aromatic ligands frequently suffer from poor solubility, which can be a drawback during the synthesis of the extended metal-containing network. It is frequently necessary to employ harsher and (at times) more unpredictable reaction conditions such as solvothermal methods, whereas hydrogen-bonded ligands are typically more soluble in a range of solvents.

The choice of hydrogen-bonding moiety is typically governed by its ability to form consistent and predictable supramolecular motifs but it is also important that it does not compete with the *N*-heterocycle for the metal ion itself. The carboxamide moiety frequently forms either dimeric or catemeric hydrogen-bonded patterns in the presence of potentially disruptive species (counterions, solvent molecules, etc.), and it is less likely to coordinate directly to the metal ion than are pyridyl- or imidazol-1-yl moieties. These attributes combine to make the carboxamide functionality a useful connector in inorganic-organic supramolecular synthesis. Even though flexible [(imidazol-1-yl)methyl]-benzoic acid ligands have been employed in coordination chemistry,[9] the carboxylic acid moiety is less reliable than the carboxamide moiety. This is due to the propensity of the carboxylate moiety to bind directly to the metal ion *via* one of many possible coordination modes in which case the outcome is most likely a coordination polymer.

Based on the versatility of five-membered *N*-heterocycles as coordination sites in inorganic supramolecular synthesis, coupled with the robust self-complementarity of the carboxamide functionality, we have previously synthesized (in Chapter 4) a new family

of ligands for the directed assembly of extended metal-containing networks, [(benzimidazol-1-yl)methyl]-benzamides,[10] Scheme 5.4.

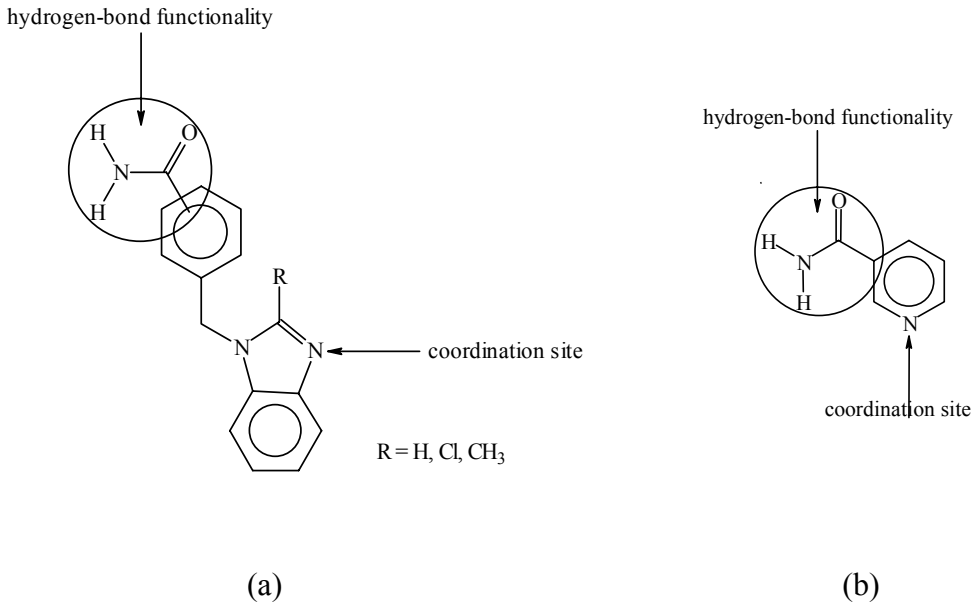

Scheme 5.4 Comparison of (a) [(benzimidazol-1-yl)methyl]-benzamide ligands and (b) nicotinamide.

In comparison with previously utilized nicotinamide and *iso*nicotinamide, these ligands would provide greater space between the nodes (metal ions) in the structure, which can increase porosity. Furthermore, the conformational flexibility resulting from the methylene bridge imparts an expanded solubility in a wide range of solvents without compromising the intended supramolecular assembly process. In addition, these ligands can be readily prepared through common synthetic procedures to generate a family of closely related ligands, which allows us to examine solid-state assembly and structure in a systematic manner.

In this chapter, we will begin to explore the inorganic-organic supramolecular chemistry of [(benzimidazol-1-yl)methyl]-benzamide ligands by allowing them to react with a variety of Ag(I) salts. Silver(I) provides a good starting point thanks to its propensity for simple linear coordination. The intention is, therefore, to establish how reliably we can propagate the inherent linear geometry of the complex ion into infinite 1-D chains with the aid of self-complementary ligand-ligand based hydrogen-bond

interactions. The necessary presence of various counterions also allows for an examination of the structural complications that these counterions may present vis-a-vi the desired supramolecular assembly process. In this way, we will be able to assess the supramolecular yield, the capacity of this family of ligands to form specific and reproducible architectures through the use of self-complementary intermolecular interactions.

5.2 Experimental

5.2.1 Syntheses of Ag(I) complexes

The syntheses of [(2-methylbenzimidazol-1-yl)methyl]-benzamide ligands are reported elsewhere.[10] Silver(I) tetrafluoroborate, silver(I) hexafluoroarsenate, and silver(I) hexafluoroantimonate were purchased from Aldrich and used without further purification. Melting points were determined on a Fisher-Johns melting point apparatus and are uncorrected.

5.2.1.1 Synthesis of *bis*-[4-(2-methylbenzimidazol-1-yl)methylbenzamide]silver(I) tetrafluoroborate hydrate methanol, **29**

4-[(2-methylbenzimidazol-1-yl)methyl]-benzamide (0.020 g, 0.075 mmol) was dissolved in 3 mL of methanol with heat in a small beaker and cooled to room temperature. To this solution was added a methanolic solution containing silver(I) tetrafluoroborate (0.007 g, 0.038 mmol) and the beaker with the resulting solution covered in Al foil and stored in the dark. Pale-yellow needles were obtained after 5 days. M.p. 172˚C (decomp.).

5.2.1.2 Synthesis of *bis*-[3-(2-methylbenzimidazol-1-yl)methylbenzamide]silver(I) tetrafluoroborate, **30**

3-[(2-methylbenzimidazol-1-yl)methyl]-benzamide (0.020 g, 0.075 mmol) was dissolved in 3 mL of methanol with heat in a small beaker and cooled to room temperature. To this solution was added silver(I) tetrafluoroborate (0.007 g, 0.038 mmol) in methanol and the beaker containing the resulting solution covered in Al foil and stored in the dark. Colorless plates were afforded after 5 days. M.p. 264-266˚C (decomp.).

5.2.1.3 Synthesis of *bis*-[4-(2-methylbenzimidazol-1-yl)methylbenzamide]silver(I) hexafluoroarsenate methanol, **31**

4-[(2-methylbenzimidazol-1-yl)methyl]-benzamide (0.030 g, 0.113 mmol) was dissolved in 5 mL of methanol with heat in a small beaker and cooled to room temperature. To this solution was added a methanolic solution containing silver(I) hexafluoroarsenate (0.017 g, 0.057 mmol) and the beaker with the resulting solution covered in Al foil and stored in the dark. Colorless needles appeared after 2 days. M.p. 195-197˚C.

5.2.1.4 Synthesis of *bis*-[3-(2-methylbenzimidazol-1-yl)methylbenzamide]silver(I) hexafluoroarsenate methanol$_{0.5}$, **32**

3-[(2-methylbenzimidazol-1-yl)methyl]-benzamide (0.030 g, 0.113 mmol) was dissolved in 5 mL of methanol with heat in a small beaker and cooled to room temperature. To this solution was added silver(I) hexafluoroarsenate (0.017 g, 0.057 mmol) in methanol and the beaker containing the resulting solution covered in Al foil and stored in the dark. Colorless microcrystals formed after 1 day, which were too small for X-ray crystallography. The experiment was repeated, this time adding a few microcrystals from the previous experiment to the reaction mixture as seed crystals. Colorless plates were obtained after 1 day. M.p. 248-250˚C (decomp.).

5.2.1.5 Synthesis of *bis*-[4-(2-methylbenzimidazol-1-yl)methylbenzamide]silver(I) hexafluoroantimonate, **33**

4-[(2-methylbenzimidazol-1-yl)methyl]-benzamide (0.030 g, 0.113 mmol) was dissolved in 5 mL of methanol with heat in a small beaker and cooled to room temperature. To this solution was added a methanolic solution containing silver(I) hexafluoroantimonate (0.019 g, 0.057 mmol) and the beaker with the resulting solution covered in Al foil and stored in the dark. Colorless plates formed after 2 days. M.p. 238-241˚C.

5.2.1.6 Synthesis of *bis*-[3-(2-methylbenzimidazol-1-yl)methylbenzamide]silver(I) hexafluoroantimonate, **34**

3-[(2-methylbenzimidazol-1-yl)methyl]-benzamide (0.030 g, 0.113 mmol) was dissolved in 5 mL of methanol with heat in a small beaker and cooled to room temperature. To this solution was added silver(I) hexafluoroantimonate (0.019 g, 0.057 mmol) in methanol

and the beaker containing the resulting solution covered in Al foil and stored in the dark. Colorless plates were afforded after 2 days. M.p. 235-238˚C (decomp.).

5.2.2 X-ray crystallography

X-ray data were collected on a Bruker SMART 1000 four-circle CCD diffractometer (**29**, **30**, and **32**) or SMART APEX CCD diffractometer (**31**, **33**, and **34**) using a fine-focus molybdenum K_α tube. Data were collected using SMART.[11] Initial cell constants were found by small widely separated "matrix" runs. Generally, an entire hemisphere of reciprocal space was collected regardless of Laué symmetry. Scan speed and scan width were chosen based on scattering power and peak rocking curves. Datasets were collected under an N_2 stream at the temperature indicated in Tables A29-A34.

Unit cell constants and orientation matrix were improved by least-squares refinement of reflections thresholded from the entire dataset. Integration was performed with SAINT,[12] using this improved unit cell as a starting point. Precise unit cell constants were calculated in SAINT from the final merged dataset. Lorenz and polarization corrections were applied. Laué symmetry, space group, and unit cell contents were found with XPREP.

Data were reduced with SHELXTL.[13] The structures were solved in all cases by direct methods without incident. In general, hydrogen atoms were assigned to idealized positions and were allowed to ride. Where possible, the coordinates of the amide hydrogens were allowed to refine. Heavy atoms were refined with anisotropic thermal parameters. Unless otherwise noted, data were corrected for absorption.

29 Amide hydrogen atoms were inserted in calculated positions and were allowed to ride. Three peaks in the difference Fourier were assigned as water oxygen atoms; hydrogen atoms for these molecules could not be located. Occupancies for these oxygen atoms were allowed to refine during initial least-squares cycles and were fixed during the last cycle. Two [BF_4] anions were located in the difference Fourier map. The fluorine atoms for the major species were refined using anisotropic thermal parameters; isotropic thermal motion for the remaining five atoms was modeled with an overall free variable. The geometry of the major species was restrained using DFIX commands. The geometry of the minor species was linked to that of the major species with the SAME command.

30 Two [BF_4] anions were refined using DFIX commands to restrain their geometries. The two boron atoms shared anisotropic thermal parameters (using the EADP command). The fluorine atoms for the major species were allowed anisotropic thermal parameters; those on the minor species were given isotropic thermal parameters. Data were not corrected for absorption.

31 Amide hydrogen atoms were inserted in calculated positions and were allowed to ride. Peaks in the difference Fourier map were assigned to four closely-spaced methanol molecules. Occupancies for these four species were allowed to refine during early least-squares cycles and were fixed for final refinement. Carbon and oxygen atoms for the four molecules were refined using isotropic thermal parameters and restrained geometry (using the DFIX command). Two closely located [AsF_6] anions were refined using pairwise linked thermal parameters (using the EADP command). The arsenic atom and five of the six fluorine atoms were given anisotropic thermal parameters. The geometry of the minor species was linked to that of the major species with the SAME command.

32 Amide hydrogen atoms were inserted in calculated positions and were allowed to ride. One of the two amide groups was best treated as two closely located "wobble" conformers differing in C(aryl)-C(carbonyl) torsion angle. Peaks in the difference Fourier map were assigned to a single well-behaved methanol molecule. A single AsF_6 counter-ion was included in the structural model.

33 Amide hydrogen atoms were inserted in calculated positions and were allowed to ride. Three peaks in the difference Fourier were assigned to water molecules; the hydrogen atoms could not be located. The three water oxygen atoms were allowed full occupancy and refined successfully with anistropic thermal parameters. Two closely located SbF_6 anions were refined using restrained geometry. Atoms in the major species were allowed anisotropic thermal parameters. Thermal parameters for the minor antimony atom were linked (using EADP) to those of the major antimony atom; the remaining atoms were given isotropic thermal parameters. The geometry of the minor species was linked to that of the major species with the SAME command.

34 A single well-behaved [SbF_6] was included in the structural model.

5.3 Results

Crystallographic data are given in Tables A29-A34, selected bond distances and angles in Table 5.1, hydrogen-bond geometries in Table 5.2, and thermal ellipsoids and labeling schemes are shown in Figure 5.1.

Table 5.1 Selected bond distances and angles for **29**-**34**.

Compound	Ag–N (Å)	< N–Ag–N (˚)
29	Ag1–N13, 2.070(3)	N13–Ag1–N13, 180.00(10)
30	Ag1–N13, 2.085(2) Ag1–N33, 2.086(2)	N13–Ag1–N33, 173.38(9)
31	Ag1–N13, 2.073(2) Ag1–N33, 2.070(2)	N13–Ag1–N33, 173.67(7)
32	Ag1–N13, 2.102(3) Ag1–N33, 2.103(3)	N13–Ag1–N33, 171.38(13)
33	Ag1–N13, 2.066(4) Ag1–N33, 2.086(4)	N13–Ag1–N33, 173.97(13)
34	Ag1–N13, 2.1025(17) Ag1–N33, 2.0995(18)	N13–Ag1–N33, 174.06(7)

Table 5.2 Hydrogen-bond geometries for **29**-**34**.

Compound	D-H A	H…A/Å	D…A/Å	<(DHA)/°	generator for A
29	N27 H27A O27	2.03	2.911(5)	173.9	-x+1, -y-1, -z+1
	N27 H27B O1S	2.28	2.96(3)	133.1	–
30	N27 H27A F12	2.02(4)	2.918(4)	166(3)	-x, -y+1, -z-1
	N27 H27A F16	2.08(4)	2.982(18)	167(3)	-x, -y+1, -z-1
	N27 H27B F11	2.26(3)	3.090(4)	160(3)	–
	N27 H27B F15	2.03(4)	2.834(12)	152(3)	–
	N47 H47A O47	2.10(3)	2.881(3)	177(3)	-x, -y, -z+2
	N47 H47B O27	2.14(3)	2.866(3)	149(3)	x, y-1, z+1
31	N27 H27A F3A	2.29	3.124(3)	158.3	x+1, y+1, z
	N47 H47A F2B	2.22	3.027(18)	152.7	x+1, y, z
	N27 H27B O47	2.12	2.962(3)	159.4	-x+2, y+1/2, -z+1/2
	N47 H47B O27	2.11	2.977(3)	166.2	x, y-1, z
	O1S H1S O27	2.17	2.818(8)	134.1	–
32	N27A H27A O27A	2.07	2.930(6)	172.0	-x+1, -y+1, -z+2
	N27B H27C O27B	2.05	2.88(2)	159.2	-x+1, -y+1, -z+2
	N47 H47A F1	2.15	2.898(5)	143.6	-x+1, -y, -z
	N47 H47B F3	2.36	3.181(6)	157.9	x, y, z-1
	O1S H1S O47	2.22	3.021(9)	162.3	–
33	N27 H27B O47	2.16	3.023(4)	165.6	x, y-1, z
	N47 H47B O27	2.13	2.969(4)	158.9	-x+2, y+1/2, -z+1/2
34	N27 H27A O27	2.04(3)	2.907(3)	171(3)	-x-1, -y+2, -z+2
	N47 H47A F1	2.15(4)	2.959(3)	165(3)	–

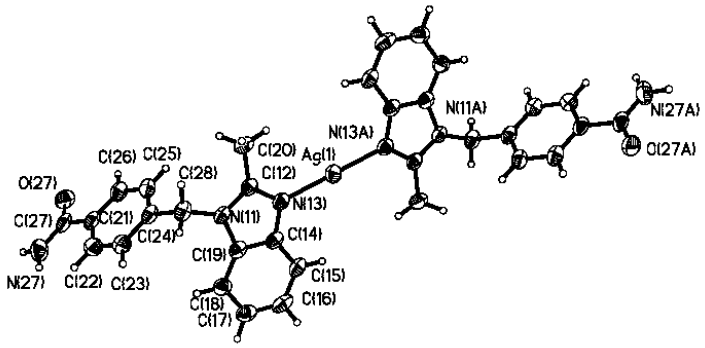
N(11A)
N(27A)
N(13A)
O(27A)
C(26)
C(25)
C(20)
Ag(1)
C(28)
C(12)
O(27)
N(13)
C(27)
C(21)
N(11)
C(24)
C(14)
C(19)
C(15)
N(27)
C(22)
C(23)
C(18)
C(16)
C(17)

(a)

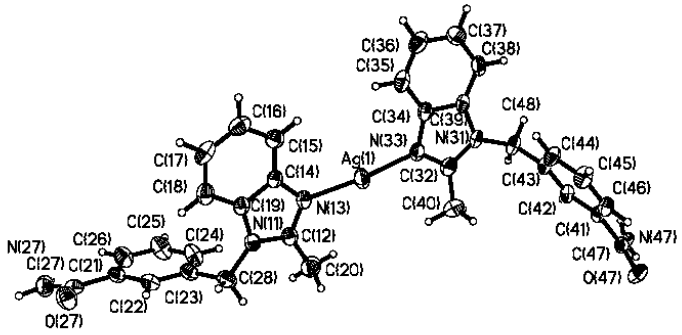
C(37)
C(36)
C(38)
C(35)
C(16)
C(34)
C(39)
C(48)
C(15)
N(33)
N(31)
C(44)
C(17)
Ag(1)
C(14)
C(32)
C(43)
C(45)
C(18)
C(19)
N(13)
C(40)
C(46)
C(42)
C(25)
N(11)
C(12)
C(41)
N(47)
N(27)
C(26)
C(24)
C(27)
C(21)
C(47)
C(28)
C(20)
C(23)
O(47)
C(22)
O(27)

(b)

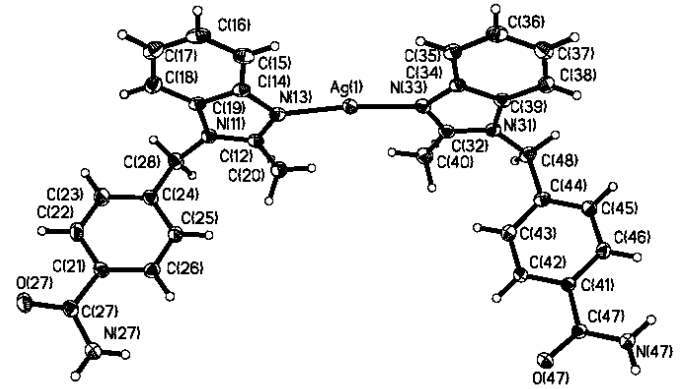
C(16)
C(36)
C(17)
C(15)
C(35)
C(37)
C(18)
C(14)
C(34)
C(38)
N(13)
Ag(1)
N(33)
C(19)
N(11)
C(39)
C(28)
C(12)
C(32)
N(31)
C(40)
C(48)
C(20)
C(23)
C(24)
C(44)
C(22)
C(25)
C(45)
C(43)
C(46)
C(21)
C(26)
C(42)
O(27)
C(41)
C(27)
C(47)
N(27)
N(47)
O(47)

(c)

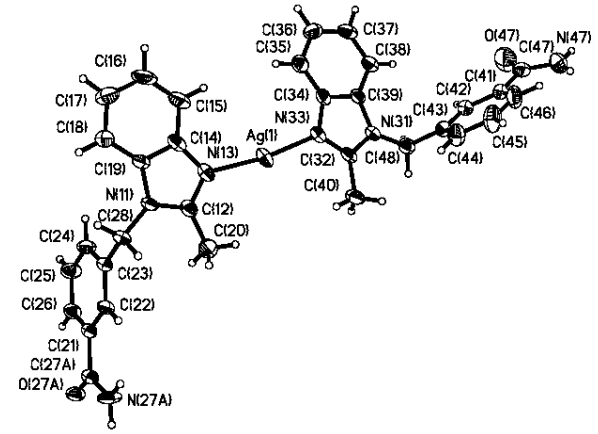

(d)

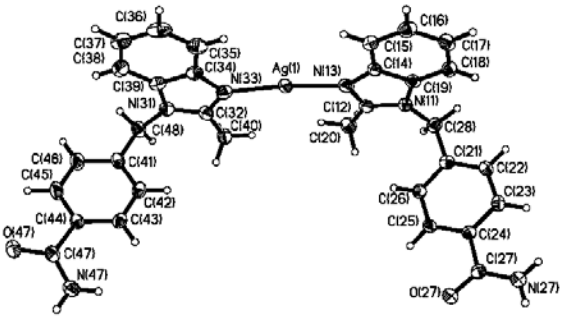

(e)

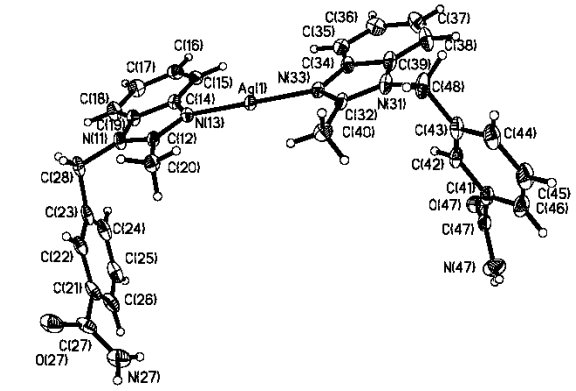

(f)

Figure 5.1 Thermal ellipsoid plots (50% probabilities) and labeling scheme for **29**-**34** (a-f).

5.3.1 Crystal structure of bis-*[4-(2-methylbenzimidazol-1-yl)methylbenzamide]silver(I) tetrafluoroborate hydrate methanol,* **29**

The crystal structure determination of **29** revealed that water and methanol had been incorporated into the lattice. The silver ion is coordinated to two 4-[(2-methylbenzimidazol-1-yl)methyl]-benzamide ligands in a linear fashion, Figure 5.1a, and this geometry is propagated through symmetry-related head-to-head $R_2^2(8)$ carboxamide···carboxamide hydrogen bonds (N27···O27, 2.911(5) Å) to produce an infinite undulating one-dimensional chain, Figure 5.2.

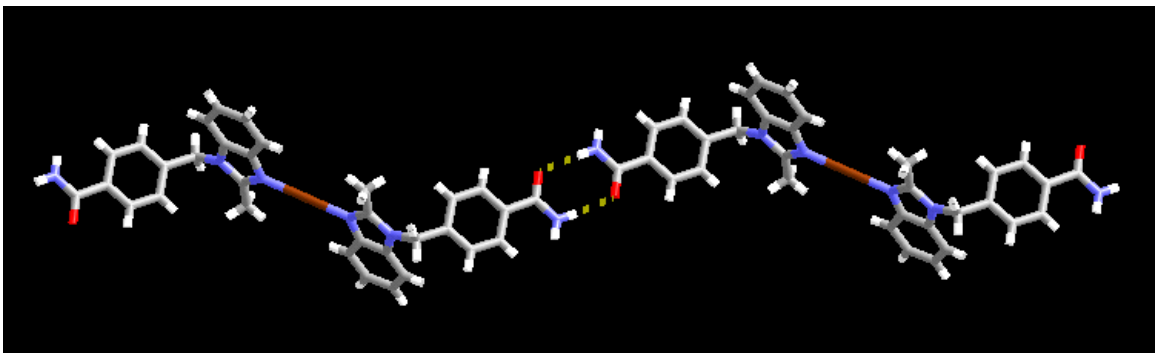

Figure 5.2 Linear cationic assembly in **29**. Tetrafluoroborate anions and solvent molecules are omitted for clarity.

Anti-N–H protons of carboxamide groups form N–H···O hydrogen bonds with disordered methanol molecules (N27···O1S, 2.96(3) Å) while the tetrafluoroborate anions do not form any significant interactions with the cationic chains. The shortest through space intra-chain distance between Ag(I) ions is approximately 23.6 Å.

5.3.2 Crystal structure of bis-*[3-(2-methylbenzimidazol-1-yl)methylbenzamide]silver(I) tetrafluoroborate,* **30**

The asymmetric unit of **30** contains a disordered anion in addition to two crystallographically unique molecules of 3-[(2-methylbenzimidazol-1-yl)methyl]-benzamide coordinated to a central silver(I) cation in a near-linear fashion through their benzimidazol-1-yl nitrogen atoms, Figure 5.1b. Neighboring complexes are interconnected through self-complementary head-to-head $R_2^2(8)$ motifs (N47···O47,

2.881(3) Å) as well as through catemeric C(4) N–H···O motifs (N47···O27, 2.866(3) Å) to produce an infinite one-dimensional ladder, Figure 5.3.

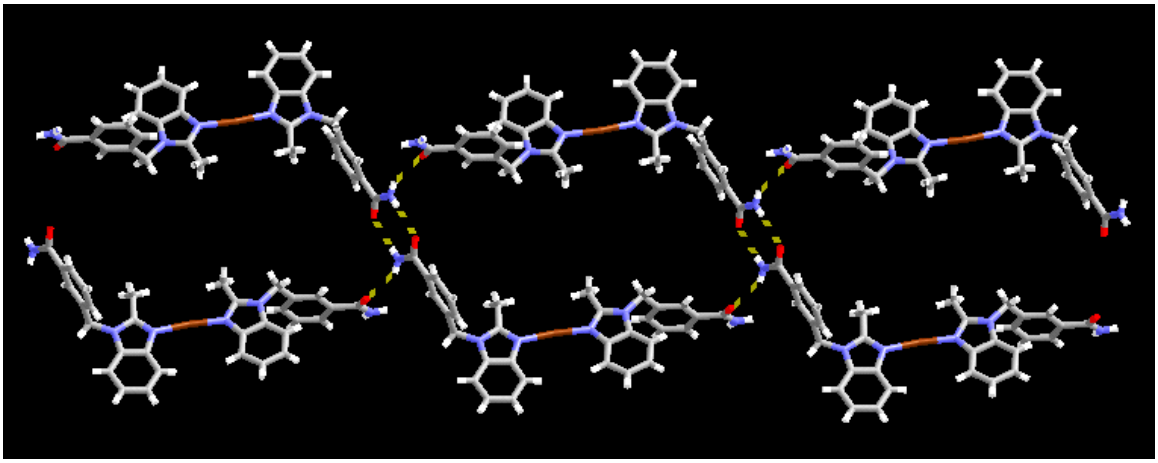

Figure 5.3 Extended one-dimensional ladder motif in **30**. $[BF_4]^-$ anions removed for clarity.

N–H protons of the carboxamide moieties also display short contacts to adjacent anions, thereby providing a bridge between cationic ribbons (N27···F11, 3.090(4) Å; N27···F15, 2.834(12) Å; N27···F12, 2.918(4) Å; N27···F16, 2.982(18) Å), Figure 5.4. The shortest through space intra-chain distance between Ag(I) ions is approximately 21.5 Å.

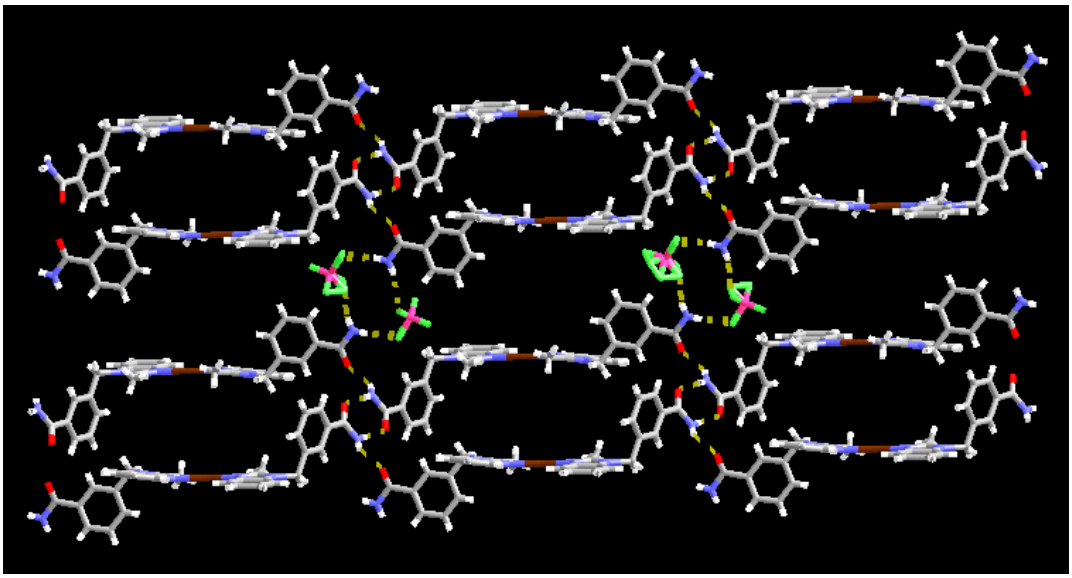

Figure 5.4 Interconnection of adjacent one-dimensional ladders in **30** through disordered tetrafluoroborate anions.

5.3.3 Crystal structure of bis-*[4-(2-methylbenzimidazol-1-yl)methylbenzamide]silver(I) hexafluoroarsenate methanol,* **31**

The crystal structure of **31** contains linear complex ions composed of silver ions and two crystallographically unique 4-[(2-methylbenzimidazol-1-yl)methyl]-benzamide ligands. The counterions are disordered, and there is also a disordered methanol molecule in the lattice, Figure 5.1c. Neighboring complex ions are connected through catemeric C(4) N–H···O hydrogen bonds (N27···O47, 2.962(3) Å; N47···O27, 2.977(3) Å) to afford infinite undulating chains. Pairs of chains are then linked through additional C(4) N-H···O hydrogen bonds to produce one-dimensional ribbons. Neighboring ribbons are held together by π···π interactions (3.4 Å) to generate a two-dimensional sheet, Figure 5.5.

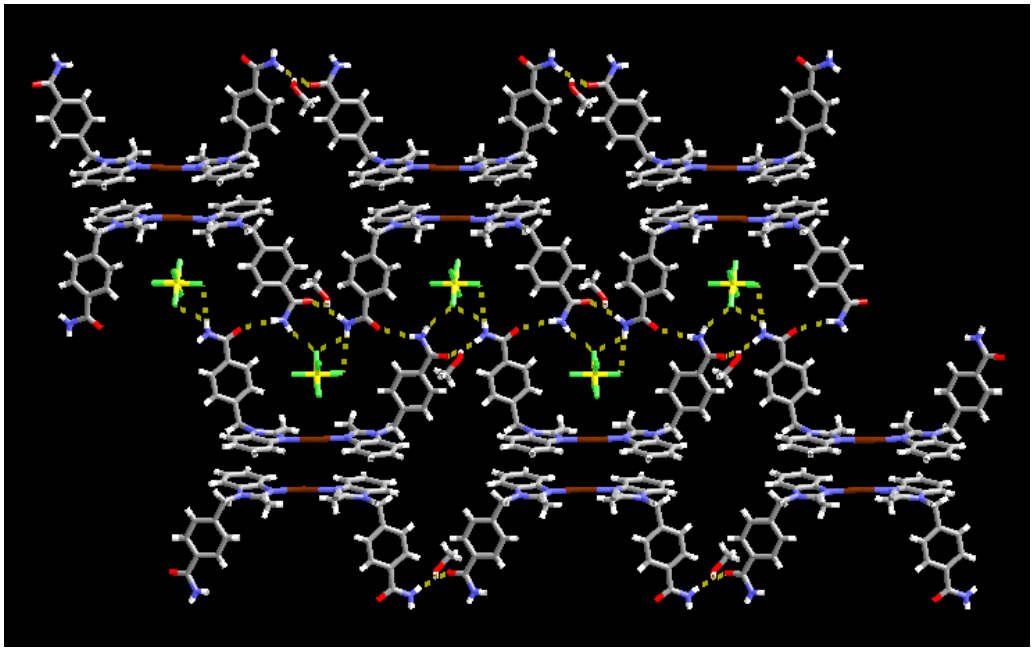

Figure 5.5 Infinite two-dimensional sheet in **31** formed from catemeric carboxamide···carboxamide hydrogen bonds and π···π interactions.

Hexafluoroarsenate anions are positioned inside the pores of the sheet *via* interactions between *syn*- N–H protons of carboxamide moieties and fluorine atoms (N27···F3A, 3.124(3) Å; N47···F2B, 3.027(18) Å). Methanol molecules also interact with carbonyl oxygen atoms of the carboxamide groups in the two-dimensional sheet (O1S···O27, 2.818(8) Å).

5.3.4 Crystal structure of bis-*[3-(2-methylbenzimidazol-1-yl)methylbenzamide]silver(I) hexafluoroarsenate methanol$_{0.5}$,* **32**

The crystal structure of **32** contains two crystallographically unique molecules of 3-[(2-methylbenzimidazol-1-yl)methyl]-benzamide coordinated in a linear geometry to a central silver(I) cation through their benzimidazol-1-yl nitrogen atoms. One of the carboxamide moieties is disordered and there is also disordered methanol in the lattice, Figure 5.1d. The geometry of the complex ion is propagated into an infinite one-dimensional chain by dimeric head-to-head $R_2^2(8)$ N–H···O hydrogen bonds between neighboring carboxamide moieties on one side of the metal complex (N27A···O27A, 2.930(6) Å; N27B···O27B, 2.88(2) Å). In addition, there are O–H···O hydrogen bonds between the O–H groups of methanol and carbonyl oxygen atoms of carboxamide moieties (O1S···O47, 3.021(9) Å) to produce an alternating N–H···O/O–H···O hydrogen-bonded pattern, Figure 5.6.

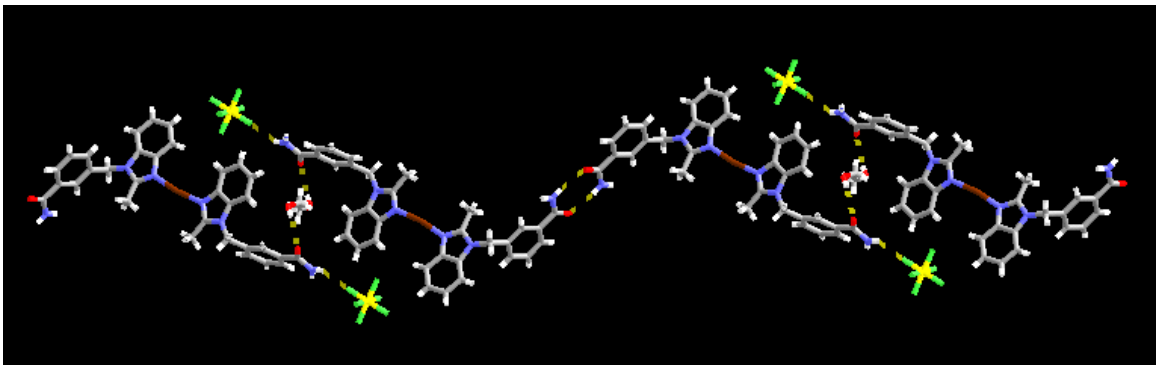

Figure 5.6 Infinite 1-D chain in **32** formed from N–H···O/O–H···O hydrogen bonds.

Syn- and *anti*- N–H protons of carboxamide groups on the methanol side of the complex ion interact with anions (N47···F1, 2.898(5) Å and N47···F3, 3.181(6) Å respectively).

5.3.5 Crystal structure of bis-*[4-(2-methylbenzimidazol-1-yl)methylbenzamide]silver(I) hexafluoroantimonate,* **33**

The crystal structure determination of **33** reveals the presence of two crystallographically unique 4-[(2-methylbenzimidazol-1-yl)methyl]-benzamide ligands coordinated to a silver(I) cation in a near-linear geometry *via* their benzimidazol-1-yl nitrogen atoms, as well as a disordered hexafluoroantimonate anion, Figure 5.1e.

Adjacent units are held together by catemeric N–H···O hydrogen bonds (N27···O47, 3.023(4) Å; N47···O27, 2.969(4) Å) to produce an infinite undulating one-dimensional chain. Neighboring chains are connected by catemeric N–H···O hydrogen bonds to generate an infinite ribbon. Adjacent ribbons interact *via* π···π interactions (3.3 Å) between benzimidazol-1-yl moieties to generate a two-dimensional sheet, Figure 5.7, similar to the extended structure in **31**. The anions reside within the pores of the sheet.

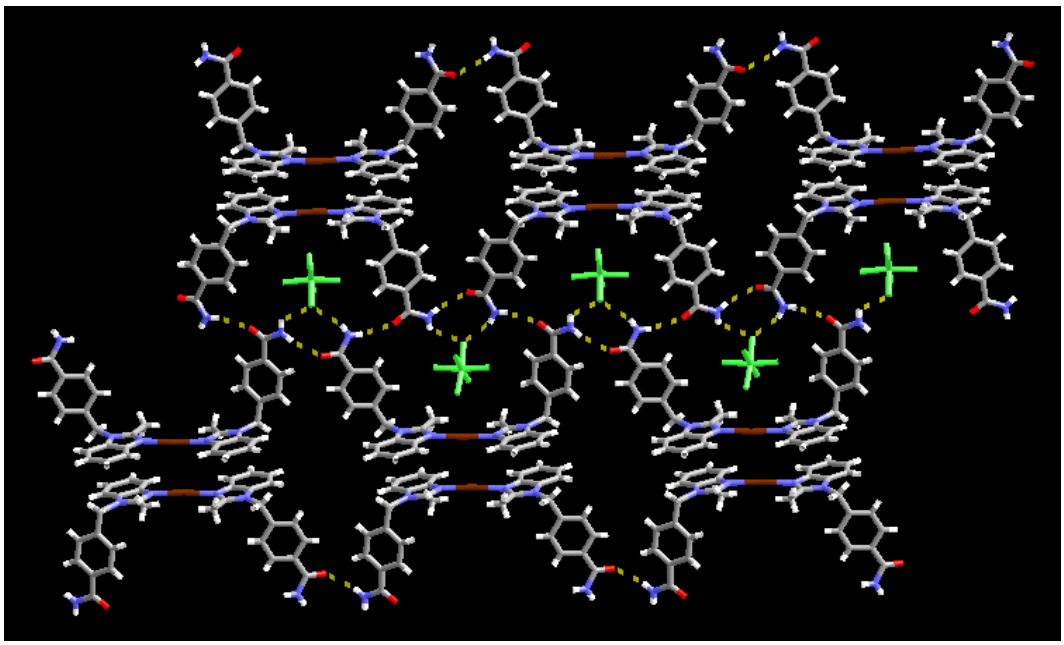

Figure 5.7 2-D sheet in **33** formed from N-H···O hydrogen bonds and π···π interactions.

5.3.6 Crystal structure of bis-*[3-(2-methylbenzimidazol-1-yl)methylbenzamide]silver(I) hexafluoroantimonate*, **34**

The crystal structure of **34** contains two crystallographically distinct 3-[(2-methylbenzimidazol-1-yl)methyl]-benzamide ligands molecules coordinated to a silver(I) ion in a near-linear manner, Figure 5.1f. Adjacent ions are interconnected through dimeric head-to-head $R_2^2(8)$ N–H···O hydrogen bonds on one side of the metal complex (N27···O27, 2.907(3) Å) whereas the carboxamide moieties on the other side are capped by interactions with hexafluoroantimonate anions (N47···F1, 2.959(3) Å). Neighboring dimeric units interact through π···π interactions (3.6 Å) between benzimidazol-1-yl moieties resulting in a one-dimensional assembly, Figure 5.8.

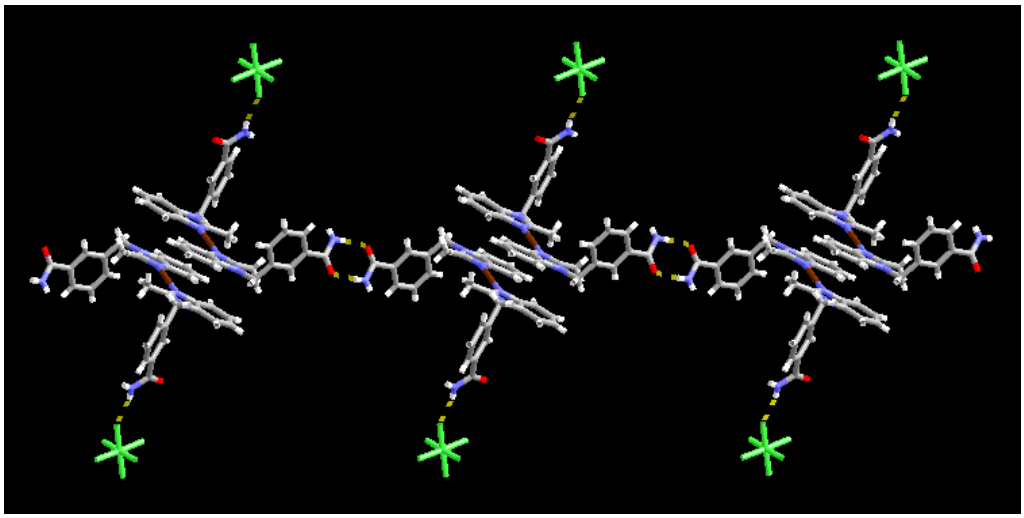

Figure 5.8 Extended 1-D assembly in **34** held together by dimeric carboxamide···carboxamide hydrogen bonds and π···π interactions.

5.4 Discussion

Six inorganic-organic coordination complexes with Ag(I) ions and [(benzimidazol-1-yl)methyl]-benzamide ligands were characterized using single-crystal X-ray diffraction in order to establish if this family of ligands is capable of facilitating high-yielding supramolecular synthesis.

In each structure, **29**-**34**, the Ag(I) ion is coordinated in a linear manner by two ligands and the ligand-metal interaction invariably takes place through the accessible nitrogen atom of the benzimidazol-1-yl moiety. The amide moiety does not bind directly to the metal ion in any case which leaves it open to engage in the supramolecular assembly process. With six linear complexes there are twelve amide moieties that need to be classified according to the type of hydrogen-bond interactions that they participate in. Ligand-ligand based hydrogen bonds (either $R_2^2(8)$ or C(4) motifs) will lead to extended assemblies, whereas hydrogen bonding to counterions and/or solvent molecules represents loss of control and directionality and is considered a failed assembly event. In this family of compounds, adjacent amides produced five $R_2^2(8)$ motifs and five C(4) motifs. Only on two occasions were the intended supramolecular ligand···ligand interactions disrupted, once by an $[SbF_6]^-$ anion (in **34**) and once by a methanol molecule (in **32**). The ligands are therefore capable of propagating the inherent linear geometry of

the metal complex in four of the six structures – a supramolecular yield of 67%. Since each structure necessarily contains potentially disruptive counterions and, on three occasions, included solvent molecules, a supramolecular assembly strategy of extended metal-containing architectures using this family of ligands is likely to be quite successful. The fact that ligand-based amide···amide hydrogen bonds are capable of maneuvering complex ions of substantial size, also bodes well for the transferability and versatility of these ligands.

Since there was only one occasion when an anion disrupted an intended recognition event it is not possible to rank the potential structural interference from the anions used in this structural study: $[BF_4]^-$, $[AsF_6]^-$, and $[SbF_6]^-$. Based upon charge-size ratio one might expect the tetrafluoroborate anion to be most likely to cause problems by competing as an alternative hydrogen-bond acceptor, but that was not the case in **29**-**34**. It should be noted that these six compounds represent most of the complexes in this family of compounds that have been crystallographically characterized to date.[14] With an increased number of structural data points we do not expect to find any marked deviations from the supramolecular yield that we have found so far.

Secondary intermolecular interactions are responsible for organizing 1-D assemblies with respect to each other, and these forces can principally be classified as π···π contacts. The asymmetric charge distribution in heterocyclic compounds can strengthen such interactions, and there were several examples of short π···π distances (3.3-3.6 Å) in these structures, indicative of attractive forces that further stabilized the extended structures.

5.5 Conclusions

At this stage, it is clear that ligands, such as those described herein, can be used effectively for the directed assembly of complex ions into desired extended motifs even in the presence of a variety of structurally disruptive counterions and solvent molecules. We are currently synthesizing 2-D and 3-D inorganic-organic hybrid systems employing [(benzimidazol-1-yl)methyl]-benzamide ligands and metal ions with preferences for higher coordination numbers in order to take advantage of the coordinating versatility of five-membered *N*-substituted heterocyclic moieties for the construction of open architectures. Furthermore, we are also synthesizing even longer ligands, with the same

coordinating and hydrogen-bonding sites, to determine how the supramolecular yield is affected by an increase in molecular weight of the constituent building blocks in the assembly process.

References

[1] (a) Eddaoudi, M.; Moler, D. B.; Li, H.; Chen, B.; Reineke, T. M.; O'Keeffe, M.; Yaghi, O. M. *Acc. Chem. Res.* **2001**, *34*, 319. (b) Plévert, J.; Gentz, T. M.; Laine, A.; Li, H.; Young, V. G.; Yaghi, O. M.; O'Keeffe, M. *J. Am. Chem. Soc.* **2001**, *123*, 12706. (c) Chae, H. K.; Eddaoudi, M.; Kim, J.; Hauck, S. I.; Hartwig, J. F.; O'Keeffe, M.; Yaghi, O. M. *J. Am. Chem. Soc.* **2001**, *123*, 11482. (d) Eddaoudi, M.; Li, H.; Yaghi, O. M. *J. Am. Chem. Soc.* **2000**, *122*, 1391. (e) Chen, B.; Eddaoudi, M.; Reineke, T. M.; Kampf, J. W.; O'Keeffe, M.; Yaghi, O. M. *J. Am. Chem. Soc.* **2000**, *122*, 11559. (f) Yaghi, O. M.; Li, H.; Davis, C.; Richardson, D.; Groy, T. L. *Acc. Chem. Res.* **1998**, *31*, 474. (g) Yaghi, O. M.; Li, H.; Groy, T. L. *J. Am. Chem. Soc.* **1996**, *118*, 9096. (h) Brammer, L. *Chem. Soc. Rev.* **2004**, *33*, 476.

[2] (a) Yaghi, O. M.; Li, H. *J. Am. Chem. Soc.* **1996**, *118*, 295. (b) Yaghi, O. M.; Li, G. *Angew. Chem., Int. Ed. Engl.* **1995**, *34*, 207. (c) Subramanian, S.; Zaworotko, M. J. *Angew. Chem., Int. Ed. Engl.* **1995**, *34*, 2127. (d) Fujita, M.; Kwon, Y. -J.; Osamu, S.; Yamaguchi, K.; Ogura, K. *J. Am. Chem. Soc.* **1995**, *117*, 7287. (e) Zaworotko, M. J. *Chem. Soc. Rev.* **1994**, *23*, 283. (f) Copp, S. B.; Subramanian, S.; Zaworotko, M. J. *J. Am. Chem. Soc.* **1992**, *114*, 8719.

[3] (a) Barszcz, B.; Glowiak, T.; Detka, K. *Polyhedron* **2003**, 1329. (b) Ma, J. -F.; Yang, J.; Zheng, G. -L.; Li, L.; Liu, J. -F. *Inorg. Chem.* **2003**, *42*, 7531. (c) Su, C. -Y.; Smith, M. D.; Loye, H. -C. *Angew. Chem., Int. Ed. Engl.* **2003**, *42*, 4085. (d) Abrahams, B. F.; Hoskins, B. F.; Robson, R.; Slizys, D. A. *CrystEngComm* **2002**, *4*, 478. (e) Sui, B.; Fan, J.; Okamura, T.; Sun, W. -Y.; Ueyama, N. *New J. Chem.* **2001**, *25*, 1379. (f) Liu, H. -K.; Hu, J.; Wang, T. -W.; Yu, X. -L.; Liu, J.; Kang, B. -S. *J. Chem. Soc., Dalton Trans.* **2001**, 3534. (g) Ma, J. -F.; Liu, J. -F.; Liu, Y. -C.; Xing, Y.; Jia, H. -Q.; Lin, Y. -H. *New J. Chem.* **2000**, *24*, 759. (h) Ma, J. -F.; Liu, J. -F.; Xing, Y.; Jia, H. -Q.; Lin, Y. -H. *J. Chem. Soc., Dalton Trans.* **2000**, 2403. (i) Fei, B. -L.; Sun, W. -Y.; Zhang, Y. -A.; Yu, K. -B.; Tang, W. -X. *J. Chem. Soc., Dalton Trans.* **2000**, 2345. (j) Shen, H. -Y.; Liao, D. -Z.; Jiang, Z. -H.; Yan, S. -P.; Wang, G. -L.; Yao, X. -K.; Wang, H. -G. *Acta Chem. Scand.* **1999**, *53*, 387. (k) Mago, G.; Hinago, M.; Miyasaka, H.; Matsumoto, N.; Okawa, H. *Inorg. Chim. Acta* **1997**, *254*, 145. (l) Hoskins, B. F.; Robson, R.; Slizys, D. A. *Angew. Chem., Int. Ed. Engl.* **1997**, *36*, 2336. (m) Hoskins, B. F.; Robson, R.; Slizys, D. A. *J. Am. Chem. Soc.* **1997**, *119*, 2952. (n) Zhu, H. -F.; Fan, J.; Okamura, T. -A.; Sun, W. -Y.; Ueyama, N. *Cryst. Growth Des.* ASAP. (o) Zhang, L.; Lü, X. -Q.; Chen, C. -L.; Tan, H. -Y.; Zhang, H. -X.; Kang, B. -S. *Cryst. Growth Des.* ASAP.

[4] (a) Su, C. -Y.; Cai, Y. -P.; Chen, C. -L.; Smith, M. D.; Kaim, W.; Loye, H. -C. *J. Am. Chem. Soc.* **2003**, *125*, 8595. (b) Liu, H. -K.; Sun, W. -Y.; Tang, W. -X.; Tan, H. -Y.; Zhang, H. -X.; Tong, Y. -X.; Yu, X. -L.; Kang, B. -S. *J. Chem. Soc., Dalton Trans.* **2002**, 3886. (c) Wan, S. -Y.; Fan, J.; Okamura, T. -A.; Zhu, H. -F.; Ouyang, X. -M.; Sun, W. -Y.; Ueyama, N. *Chem. Commun.* **2002**, 2520. (d) Fan, J.; Sui, B.; Okamura, T. -A.; Sun, W. -Y.; Tang, W. -X.; Ueyama, N. *J. Chem. Soc., Dalton Trans.* **2002**, 3868. (e) Sun, W. -Y.; Fan, J.; Okamura, T. -A.; Xie, J.; Yu, K. -B.; Ueyama, N. *Chem. Eur. J.* **2001**, *7*, 2557. (f) Liu, H. -K.; Tan, H. -Y.; Cai, J. -W.; Zhou, Z. -Y.; Chan, A. S. C.; Liao, S.; Xiao, W.; Zhang, H. -X.; Yu, X. -L.; Kang, B. -S. *Chem. Commun.* **2001**, 1008. (g) Liu, H. -K.; Sun, W. -Y.; Ma, D. -J.; Yu, K. -B.; Tang, W. -X. *Chem. Commun.* **2000**, 591. (h) Liu, H. -K.; Sun, W. -Y.; Zhu, H. -L.; Yu, K. -B.; Tang, W. -X. *Inorg. Chim. Acta* **1999**, *295*, 129. (i) Liu, H. -K.; Sun, W. -Y.; Tang, W. -X.; Yamamoto, T.; Ueyama, N. *Inorg. Chem.* **1999**, *38*, 6313. (j) Cai, Y. -P.; Su, C. -Y.; Chen, C. -L.; Li, Y. -M.; Kang, B. -S.; Chan, A. S. C.; Kaim, W. *Inorg. Chem.* ASAP. (k) Yang, X. -P.; Kang, B. -S.; Wong, W. -K.; Su, C. -Y.; Liu, H. -Q. *Inorg. Chem.* ASAP.

[5] (a) Aakeröy, C. B.; Desper, J.; Valdés-Martínez, J. *CrystEngComm* **2004**, *6*, 413. (b) Aakeröy, C. B.; Beatty, A. M.; Desper, J.; O'Shea, M.; Valdés-Martínez, J. *Dalton Trans.* **2003**, 3956. (c) Beatty, A. M. *CrystEngComm* **2001**, *51*, 243. (d) Aakeröy, C. B.; Beatty, A. M. *Aust. J. Chem.* **2001**, *54*, 409. (e)

Aakeröy, C. B.; Beatty, A. M.; Lorimer, K. R. *J. Chem. Soc., Dalton Trans.* **2000**, 3869. (f) Aakeröy, C. B.; Beatty, A. M.; Leinen, D. S. *CrystEngComm* **2000**, *27*, 1. (g) Aakeröy, C. B.; Beatty, A. M.; Leinen, D. S.; Lorimer, K. R. *Chem. Commun.* **2000**, 935. (h) Aakeröy, C. B.; Beatty, A. M.; Leinen, D. S. *Angew. Chem., Int. Ed. Engl.* **1999**, *38*, 1815. (i) Aakeröy, C. B.; Beatty, A. M.; Helfrich, B. A. *J. Chem. Soc., Dalton Trans.* **1998**, 1943. (j) Aakeröy, C. B.; Beatty, A. M.; Leinen, D. S. *J. Am. Chem. Soc.* **1998**, *120*, 7383. (k) Uemura, K.; Kitagawa, S.; Kukui, K.; Saito, K. *J. Am. Chem. Soc.* ASAP.

[6] Aakeröy, C. B.; Beatty, A. M. *Chem. Commun.* **1998**, 1067.

[7] (a) Oertel, C. M.; Sweeder, R. D.; Patel, S.; Downie, C. M.; DiSalvo, F. J. *Inorg. Chem*. **2005**, *44*, 2287. (b) Brammer, L.; Rivas, J. C. M.; Atencio, R.; Fang, S.; Pigge, C. F. *Dalton Trans.* **2000**, 3855. (c) Qin, Z.; Jennings, M. C.; Puddephatt, R. J. *Inorg. Chem*. **2001**, *40*, 6220.

[8] Angeloni, A.; Orpen, A. G. *Chem. Commun*. **2001**, 343.

[9] (a) Fan, J.; Zhang, Y. -A.; Okamura, T. -A.; Zou, Z. -H.; Ueyama, N.; Sun, W. -Y. *Inorg. Chem. Commun.* **2001**, *4*, 501. (b) Sun, W. -Y.; Zhang, Y. -A.; Okamura, T. -A.; Ye, T.; Ueyama, N. *Chem. Lett.* **2000**, 1222.

[10] Aakeröy, C. B.; Desper, J.; Urbina, J. F. *Cryst. Growth Des.* **2005**, DOI: 10.1021/cg049579t.

[11] SMART v5.060; Bruker Analytical X-ray Systems: Madison, WI, 1997–1999.

[12] SAINT v6.02; Bruker Analytical X-ray Systems: Madison, WI, 1997–1999.

[13] SHELXTL v5.10; Bruker Analytical X-ray Systems: Madison, WI, 1997.

[14] Aakeröy, C. B.; Desper, J.; Smith, M. M.; Urbina, J. F. *Dalton Trans.* **2005**, submitted.

Chapter 6

Organizing M(II)(acac)$_2$ complexes into infinite 1-D chains using ditopic imidazole/benzimidazole ligands and hydrogen-bond analogues

6.1 Introduction

Synthetic inorganic supramolecular chemistry frequently begins with metal ions with predictable (or at least preferential) coordination geometries, followed by the application of a reliable method for propagating the shape or dimensionality of the complex ion into an extended architecture. An example of such a strategy is the combination of metal ions that tend to adopt a linear geometry (e.g. Ag(I)), with rigid ditopic ligands, such as 4,4'-bipyridine – the inherent symmetry of the metal center is readily extrapolated into an infinite 1-D chain.[1] Challenges to such approaches are frequently encountered when the metal ion can adopt a multitude of geometries and coordination numbers, or when potentially disruptive species such as coordinating counterions are present in order to maintain charge neutrality.

One way of gaining better control over the coordination geometry of a metal ion is to employ chelating ligands, which tend to yield more predictable results due to relatively limited binding modes of a rigid multitopic ligand compared to most of their monodentate counterparts. The potential supramolecular problems that arise due to competition from counterions can also be eliminated by ensuring that the complex ion itself is electrically neutral.

We are interested in developing robust and versatile methods for practical inorganic supramolecular synthesis, and a helpful starting point for testing the reliability and supramolecular effectiveness of new ligands is a discrete, low-dimensional and charge-neutral coordination complex.

For example, linear building blocks are readily obtained by preparing metal complexes derived from acetylacetonato (acac) ligands,[2] where two of these "capping" ligands coordinate to octahedral M(II) centers in the equatorial positions, thus leaving the axial sites accessible for additional ligands that can form a bridge between adjacent complex ions, Scheme 6.1.

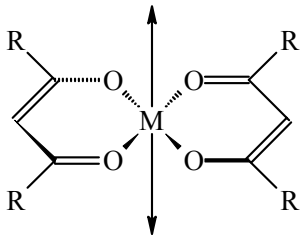

R = CH_3, CF_3, phenyl
M = Cu(II), Co(II), Ni(II)

Scheme 6.1 M(II)$(acac)_2$ complexes showing accessible axial coordination sites.

Not only do the two acac ligands create opportunities for the assembly of infinite chains, but they also produce an overall neutral metal complex, thus eliminating possible structural interference from counterions. Consequently, we will employ various M(II)$(acac)_2$ complexes (M = Cu, Co, and Ni) as starting points in our supramolecular assembly. Both Co(II) and Ni(II) adopt octahedral geometries whereas in Cu(II) the coordination mode is usually less predictable. In addition to acac, the chelating ligands will include hexafluoroacetylacetonato (hfacac) and dibenzoylmethanato (DBM).

Interlinking of discrete metal complexes into extended networks is typically achieved either with only coordinate-covalent bonds,[3] or through a combination of metal-ligand coordination and intermolecular ligand···ligand hydrogen-bond interactions.[4] We intend to explore both strategies in this study. First, we will use symmetric ditopic bridging ligands based upon *N*-substituted imidazoles/benzimidazoles,[5] Scheme 6.2, since they are capable of coordinating to metal ions without significant steric hindrance due to their smaller C–N–C angles (108˚) compared to their bipyridyl counterparts (120˚).

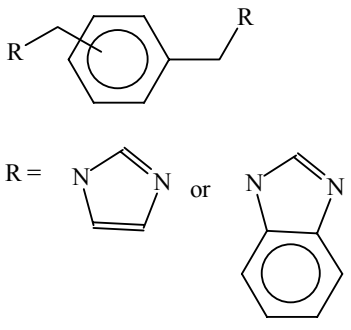

Scheme 6.2 Ditopic imidazol-1-yl/benzimidazol-1-yl ligands used in coordination chemistry.

Specifically, we will utilize a previously synthesized ditopic *bis*-imidazole ligand, 1,4-*bis*-[(imidazol-1-yl)methyl]-benzene (bix), [5m,6] and imidazol-1-yl/benzimidazol-1-yl analogues thereof in an attempt to produce infinite 1-D chains of M(II)(acac)$_2$ complexes using only coordinate covalent bonds as our supramolecular tools.

Second, in order to vary the metrics in these metal-containing 1-D chains, it is necessary to alter the distance between metal centers, a task that can be achieved by changing the length of the bridging ligand. This can be accomplished by covalently adding rigid spacers between heterocycles but this frequently requires significant synthetic efforts and the resulting extended ditopic ligand may be considerably less soluble than its shorter analogue, which may prove to be an obstacle for the supramolecular assembly. Alternatively, an extended ligand can be obtained through self-complementary hydrogen-bond interactions, and such species may also have the added benefit of better solubility compared to their covalent analogues. We have previously shown in Chapter 5 that [(benzimidazol-1-yl)methyl]-benzamide ligands can be employed in the assembly of linear Ag(I) complexes into infinite chains through self-complementary ligand···ligand hydrogen bonds.[7] In this chapter we intend to compare the metrics and supramolecular reliability of assembly processes that are driven by (a) coordinate covalent bonds (symmetric ditopic imidazole/benzimidazole), and (b) hydrogen bonds (4-[(2-methylbenzimidazol-1-yl)methyl]-benzamide), Scheme 6.3.

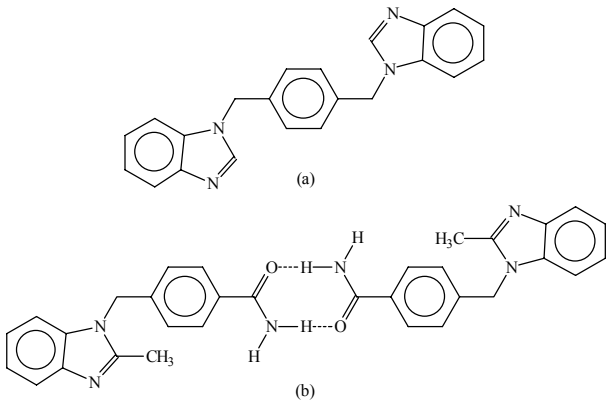

Scheme 6.3 A comparison between (a) a ditopic benzimidazol-1-yl ligand and (b) a hydrogen bond-linked analogue based upon a 4-[(2-methylbenzimidazol-1-yl)methyl]-benzamide supramolecular dimer.

Herein we present the crystal structures of five M(II)$(acac)_2(L)_x$ (L = ditopic imidazol-1-yl/benzimidazol-1-yl ligand) structures, **35-39**, that we obtained in our attempts at organizing different M(II)$(acac)_2$ blocks into infinite 1-D chains.

6.2 Experimental

6.2.1 Synthesis

All starting materials were purchased from Aldrich and used without further purification. *Bis*-(dibenzoylmethanato)cobalt(II) (Co(II)$(DBM)_2$) and *bis*-(dibenzoylmethanato)nickel(II) (Ni(II)$(DBM)_2$) were prepared according to the literature.[8] The syntheses of *bis*-imidazol-1-yl/benzimidazol-1-yl ligands are described in Chapter 3. The synthesis of 4-[(2-methylbenzimidazol-1-yl)methyl]-benzamide is presented in Chapter 4.[9] Melting points were determined on a Fisher-Johns melting point apparatus and are uncorrected.

6.2.2 Syntheses of M(II)$(acac)_2$ complexes

6.2.2.1 Synthesis of [1,4-*bis*-(2-methylbenzimidazol-1-yl)methylbenzene]$_{0.5}$*bis*-(acetylacetonato)copper(II) hydrate, **35**

1,4-*Bis*-[(2-methylbenzimidazol-1-yl)methyl]-benzene (0.110 g, 0.300 mmol) was dissolved in 20 mL of methanol in a small beaker. *Bis*-(acetylacetonato)copper(II) (0.026 g, 0.100 mmol) dissolved in 5 mL of chloroform was then added to the ligand solution and the resulting solution heated for 15 min, and the solvent allowed to evaporate to dryness. After three days, blue-green plates formed that correspond to **35**, as well as crystals of excess ligand and unreacted Cu(II)$(acac)_2$. M.p. of blue-green plates 212-216˚C (decomp.).

6.2.2.2 Synthesis of [1,4-*bis*-(imidazol-1-yl)methylbenzene]*bis*-(hexafluoroacetylacetonato)copper(II), **36**

1,4-*Bis*-[(imidazol-1-yl)methyl]-benzene dihydrate (0.082 g, 0.300 mmol) was dissolved in 4 mL of absolute ethanol in a small beaker. To this solution was added a solution containing *bis*-(hexafluoroacetylacetonato)copper(II) (0.048 g, 0.100 mmol) in 5 mL of

chloroform. The combined solutions were subsequently heated for 15 min and the solvent evaporated to dryness. Blue-green rods, **36**, formed after six days, along with crystals of excess ligand and unreacted Cu(II)(hfacac)$_2$. M.p. of blue-green rods 205-209˚C (decomp.).

6.2.2.3 Synthesis of [1,4-*bis*-(2-methylbenzimidazol-1-yl)methylbenzene]*bis*-(dibenzoylmethanato)copper(II), **37**

1,4-*Bis*-[(2-methylbenzimidazol-1-yl)methyl]-benzene (0.030 g, 0.082 mmol) and *bis*-(dibenzoylmethanato)copper(II) (0.014 g, 0.027 mmol) were dissolved in 6 mL of DMF with heat in a small beaker. The solvent was then allowed to evaporate for twelve days under ambient conditions, upon which green prisms, **37**, formed. M.p. 243-245˚C (decomp.).

6.2.2.4 Synthesis of [4-(2-methylbenzimidazol-1-yl)methylbenzamide]*bis*-(dibenzoylmethanato)cobalt(II) THF, **38**

4-[(2-methylbenzimidazol-1-yl)methyl]-benzamide (0.040 g, 0.153 mmol) was dissolved in 7 mL of dry tetrahydrofuran with heat in a small vial and cooled to room temperature. To this solution was added a solution (3 mL) containing *bis*-(dibenzoylmethanato)cobalt(II) (0.039 g, 0.076 mmol) in dry acetonitrile with the resulting solution covered and allowed to stand under ambient conditions. Orange plates, **38**, were grown after four days. M.p. >300˚C.

6.2.2.5 Synthesis of [4-(2-methylbenzimidazol-1-yl)methylbenzamide]*bis*-(dibenzoylmethanato)nickel(II) THF, **39**

4-[(2-methylbenzimidazol-1-yl)methyl]-benzamide (0.040 g, 0.153 mmol) was dissolved in 7 mL of dry tetrahydrofuran with heat in a small vial and cooled to room temperature. To this solution was added *bis*-(dibenzoylmethanato)nickel(II) (0.039 g, 0.076 mmol) dissolved in 3 mL of dry acetonitrile. The resulting solution was covered and allowed to stand under ambient conditions. Green plates corresponding to **39** were obtained after two weeks. M.p. 283-287˚C (decomp.).

6.2.3 X-ray crystallography

X-ray data were collected on a Bruker SMART 1000 four-circle CCD diffractometer using a fine-focus molybdenum Kα tube. Data were collected using SMART.[10] Initial cell constants were found by small widely separated "matrix" runs. Preliminary Laué symmetry was determined from axial images. Generally, an entire hemisphere of reciprocal space was collected regardless of Laué symmetry. Scan speed and scan width were chosen based on scattering power and peak rocking curves. Unless otherwise noted, data were collected at low temperatures, using a scan width appropriate for the crystal's mosaic spread.

Unit cell constants and orientation matrix were improved by least-squares refinement of reflections thresholded from the entire dataset. Integration was performed with SAINT,[11] using this improved unit cell as a starting point. Precise unit cell constants were calculated in SAINT from the final merged dataset. Lorenz and polarization corrections were applied. Laué symmetry, space group, and unit cell contents were found with XPREP.

Data were reduced with SHELXTL.[12] The structures were solved in all cases by direct methods without incident. In general, hydrogens were assigned to idealized positions and were allowed to ride. Where possible, the coordinates of hydrogen-bonding hydrogens were allowed to refine. Heavy atoms were refined with anisotropic thermal parameters. Strongly absorbing atoms such as transition metals were corrected for absorption.

6.3 Results

A summary of the crystallographic information for **35-39** is displayed in Tables A35-A39. Bond distances and angles for these compounds are given in Table 6.1, hydrogen-bond geometries for **38** and **39** are listed in Table 6.2, and thermal ellipsoid plots and labeling schemes are provided in Figure. 6.1.

Table 6.1 Selected bond distances and angles for **35**-**39**.

Compound	M(II)–N (Å)	< N–M(II)–N (˚)
35	Cu1–N13, 2.280(2)	–
36	Cu1–N23, 1.991(2)	N13–Cu1–N23, 180.00(10)
37	Cu1–N13, 2.535(2)	N13–Cu1–N13, 180.00
38	Co1–N13, 2.175(2)	N13–Co1–N13, 179.999(2)
39	Ni1–N13, 2.114(4)	N13–Ni1–N13, 180.000(1)

Table 6.2 Hydrogen-bond geometries for **38** and **39**.

Compound	D-H A	D-H/Å	H…A/Å	D…A/Å	<(DHA)/°	generator for A
38	N27 H27A O27	0.87	2.09	2.954(4)	171.4	-x+2, -y, -z
	N27 H27B O1A	0.87	2.11	2.932(7)	156.8	-x+2, -y+1, -z
39	N27 H27A O27	0.87	2.06	2.922(6)	171.9	-x+2, -y, -z
	N27 H27B O1A	0.87	2.17	2.975(8)	153.9	-x+2, -y+1, -z

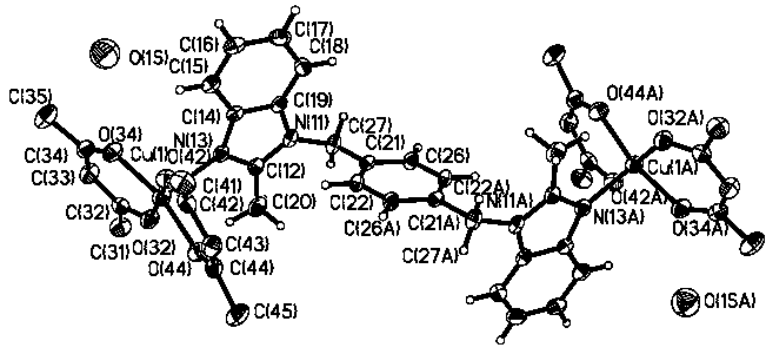

(a)

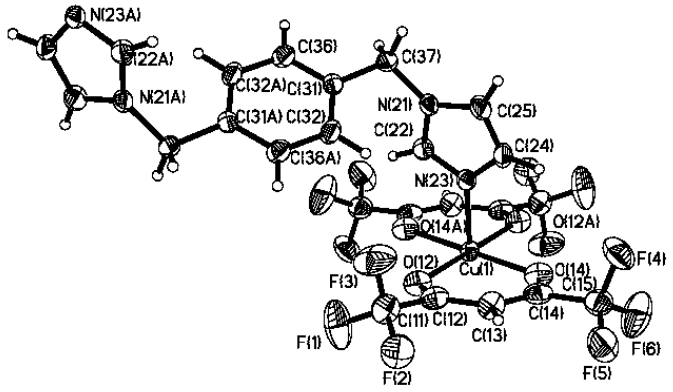

(b)

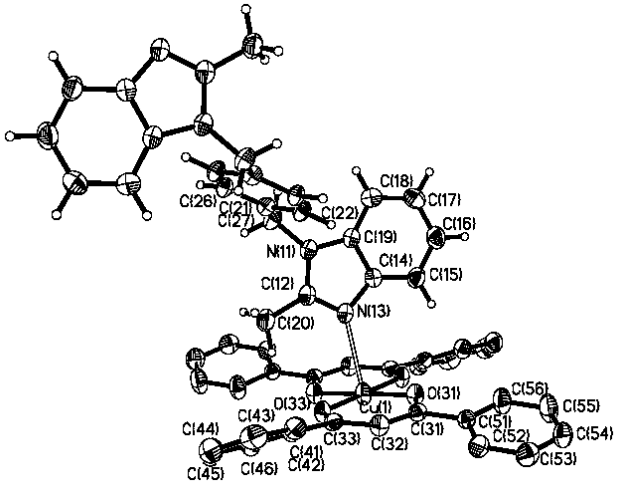

(c)

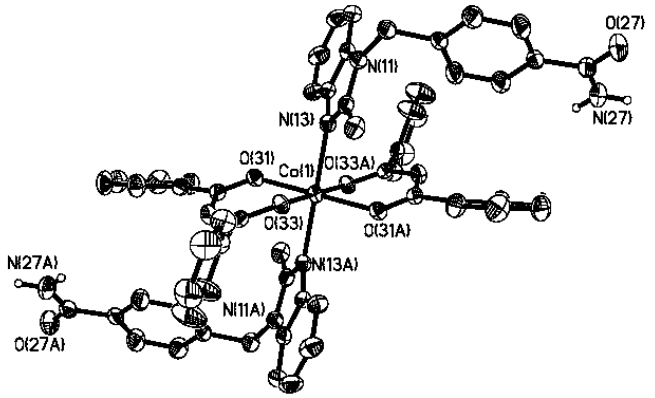

(d)

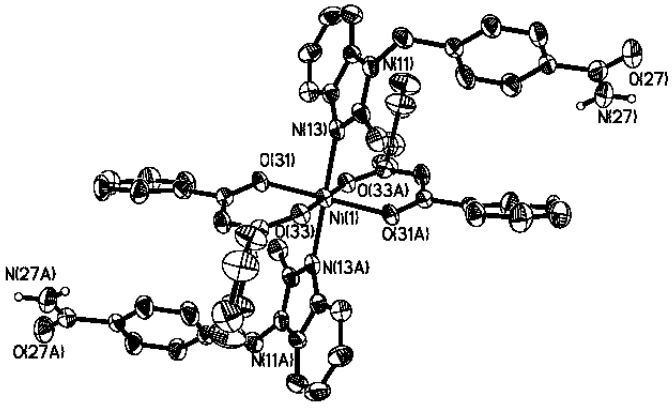

(e)

Figure 6.1 Thermal ellipsoid plots (50% probabilities) and labeling scheme for **35**-**39** (a-e). Whenever appropriate, hydrogen atoms were removed for clarity.

*6.3.1 Crystal structure of [1,4-*bis*-(2-methylbenzimidazol-1-yl)methylbenzene]$_{0.5}$bis-(acetylacetonato)copper(II) hydrate,* **35**

The geometry around the copper(II) center in **35** is five-coordinate square pyramidal and thus only one of the two available axial sites (Cu1–N13, 2.280(2) Å) is occupied, Figure 6.1a. The result is a 0-D structure consisting of two Cu(II)(acac)$_2$ complexes bridged by one ditopic ligand, Figure 6.2.

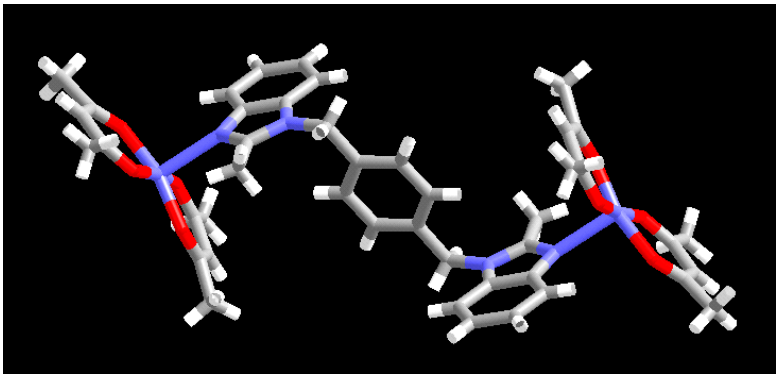

Figure 6.2 0-D structure in **35** formed by two Cu(II)(acac)$_2$ complexes bridged by one 1,4-*bis*-[(2-methylbenzimidazol-1-yl)methyl]-benzene ligand.

The through-space intrachain Cu(II) distance is about 14.2 Å. Acetylacetonato oxygen atoms on adjacent metal complexes are connected by hydrogen bonds involving water molecules (hydrogen atoms could not be located), to form an infinite 1-D ladder, Figure 6.3.

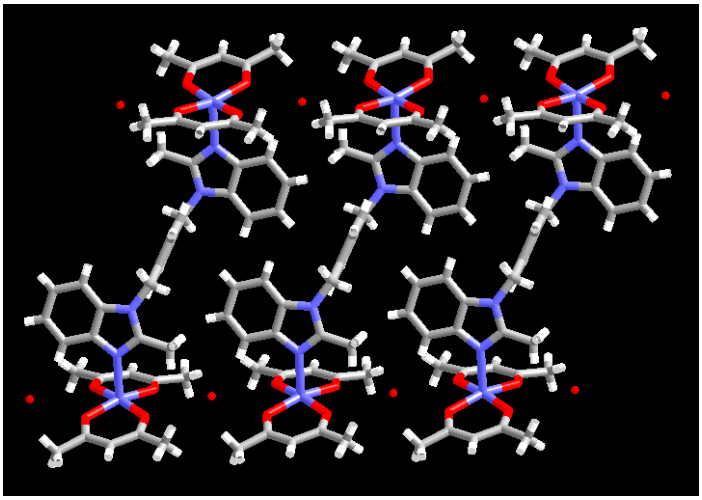

Figure 6.3 Infinite 1-D ladder in **35** obtained through interactions between acetylacetonato oxygen atoms and bridging water molecules.

*6.3.2 Crystal structure of [1,4-*bis*-(imidazol-1-yl)methylbenzene]*bis-*(hexafluoroacetylacetonato)copper(II),* **36**

The crystal structure of **36** reveals an infinite undulating 1-D coordination polymer where bridging 1,4-*bis*-[(imidazol-1-yl)methyl]-benzene ligands coordinate to the copper(II) ions through their imidazol-1-yl nitrogen atoms in a linear fashion (Cu1–N23, 1.991(2) Å; < N23–Cu1–N23, 180.00(10)˚), Figures 6.1b and 6.4. Each metal ion possesses an octahedral geometry, and both axial sites are engaged in coordination to the bridging ligands. Through-space intrachain Cu(II)-Cu(II) distances are approximately 13.1 Å.

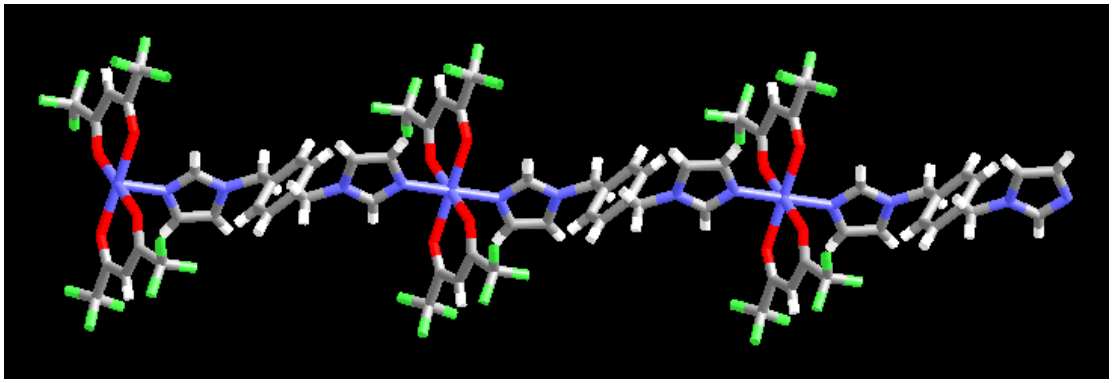

Figure 6.4 Infinite 1-D coordination polymer in **36** formed through coordination of bridging ligands and Cu(II)$(hfacac)_2$ centers.

*6.3.3 Crystal structure of [1,4-*bis*-(2-methylbenzimidazol-1-yl)methylbenzene]*bis-*(dibenzoylmethanato)copper(II),* **37**

In the crystal structure of **37**, an infinite zig-zag 1-D coordination polymer is generated where bridging 1,4-*bis*-[(2-methylbenzimidazol-1-yl)methyl]-benzene ligands coordinate through the accessible axial sites of octahedral copper(II) ions in a linear manner (Cu1–N13, 2.535(2) Å; < N13–Cu1–N13, 180.00˚), Figures 6.1c and 6.5. Through-space intrachain Cu–Cu distances are about 15.3 Å.

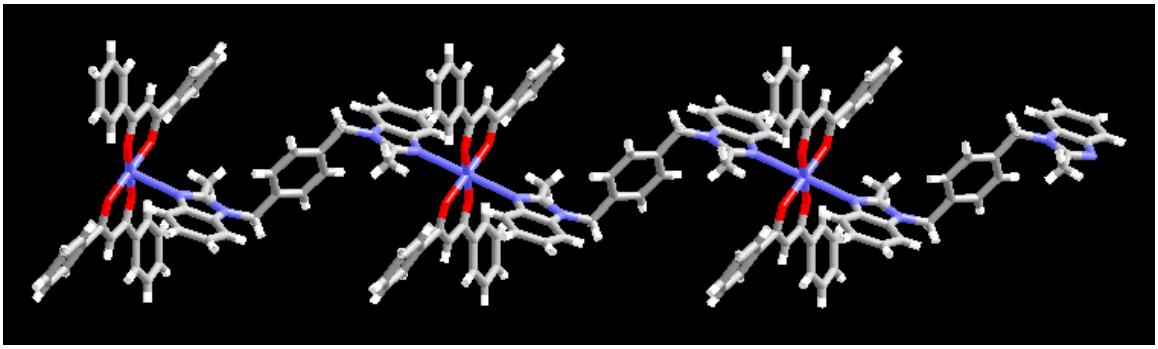

Figure 6.5 Extended 1-D coordination polymer in **37** afforded through coordination of bridging ligands to the axial sites of Cu(II)$(DBM)_2$ centers.

Adjacent 1-D chains interact *via* π···π stacking involving the aromatic rings of 2-methylbenzimidazol-1-yl moieties, Figure 6.6, with distances averaging about 3.5 Å.

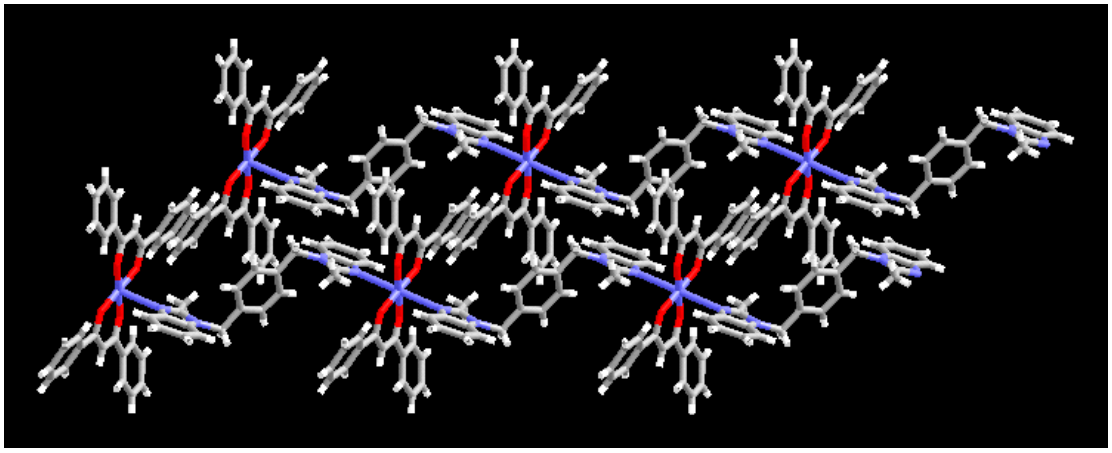

Figure 6.6 Extended view of **37** showing π···π interactions between the aromatic rings of 2-methylbenzimidazol-1-yl moieties of adjacent 1-D chains.

*6.3.4 Crystal structure of [4-(2-methylbenzimidazol-1-yl)methylbenzamide]*bis-*(dibenzoylmethanato)cobalt(II) THF,* **38**

The crystal structure of **38** contains dibenzoylmethanato (DBM) ligands coordinated to a cobalt(II) ion while the axial coordination sites on the metal ion are occupied by two 4-[(2-methylbenzimidazol-1-yl)methyl]-benzamide ligands through their heterocyclic nitrogen atoms (Co1–N13, 2.175(2) Å; < N13–Co1–N13, 179.999(2)°) resulting in an octahedral metal complex, Figure 6.1d. Neighboring complexes are interconnected through dimeric head-to-head $R_2^2(8)$ N–H···O hydrogen bonds between carboxamide

moieties using their *syn*- N–H protons and carbonyl oxygen atoms (N27···O27, 2.954(4) Å) to generate an infinite l-D chain, Figure 6.7.

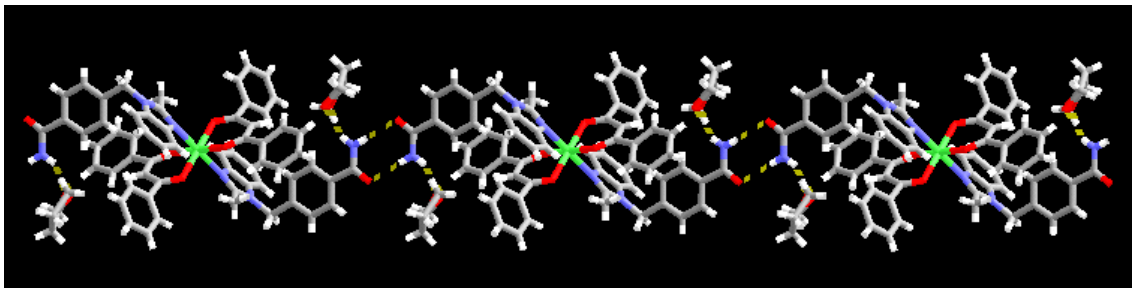

Figure 6.7 1-D chain in **38** formed by dimeric carboxamide···carboxamide hydrogen bonds. THF molecules interact with *anti*- N–H protons of carboxamide moieties.

Additionally, the *anti*- N–H protons of carboxamide moieties interact with oxygen atoms of THF molecules (N27···O1A, 2.932(7) Å). Cobalt(II) ions within the chain are separated by approximately 21.0 Å.

*6.3.5 Crystal structure of [4-(2-methylbenzimidazol-1-yl)methylbenzamide]*bis-*(dibenzoylmethanato)nickel(II) THF*, **39**

The crystal structure of **39** comprises DBM ligands coordinated to a central nickel(II) ion with the axial sites of the metal ion coordinated by the benzimidazol-1-yl nitrogen atoms of two 4-[(2-methylbenzimidazol-1-yl)methyl]-benzamide ligands (Ni1–N13, 2.114(4) Å; < N13–Ni1–N13, 180.0(1)˚) resulting in an octahedral metal complex, Figure 6.1e. The extended structure is isostructural with that of **38** – neighboring metal complexes are linked by dimeric head-to-head $R_2^2(8)$ N–H···O hydrogen bonds utilizing the *syn*- N–H protons and carbonyl oxygen atoms of carboxamide moieties (N27···O27, 2.922(6) Å) to produce an infinite one-dimensional chain, Figure 6.8, while the *anti*- N–H protons are capped through interactions with oxygen atoms of tetrahydrofuran solvent molecules also present in the crystal structure (N27···O1A, 2.975(8) Å). Intrachain Ni–Ni distances are about 21.0 Å.

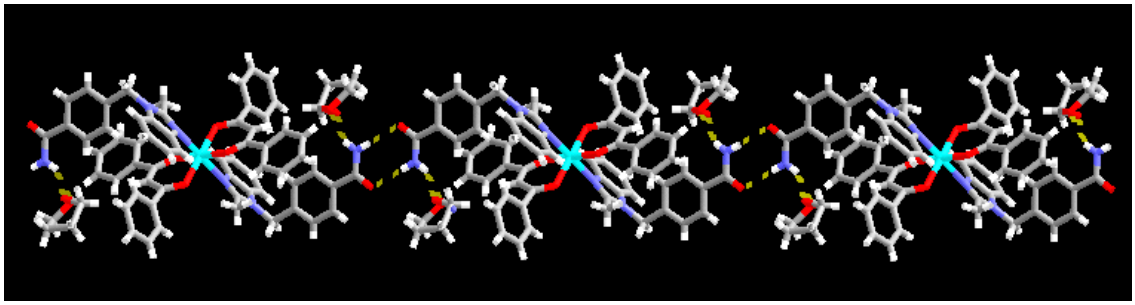

Figure 6.8 One-dimensional supramolecular chain in **39** showing interactions with THF solvent molecules.

6.4 Discussion

Compounds **35-39** were obtained as a result of coordination from either ditopic imidazol-1-yl/benzimidazol-1-yl ligands or their hydrogen bond-linked analogues, with various M(II)$(acac)_2$ complexes. The intended supramolecular strategy, seeking different means of propagating M(II)$(acac)_2$ complexes through ditopic imidazol-1-yl/benzimidazol-1-yl or hydrogen bond-linked ligands into infinite 1-D chains, turned out to be highly effective, as four of the five structures displayed the desired motif – an 80% supramolecular yield. In the case of **35**, however, a 0-D motif was obtained, due to the square pyramidal geometry adopted by the Cu ion which serves to illustrate the unpredictability of the coordination chemistry of Cu(II). The remaining two Cu(II) complexes, **36** and **37**, are however extended 1-D chains built upon octahedral Cu(II) centers.

The infinite chains observed in **38** and **39** were generated through the combination of metal-ligand coordination (involving the 2-methylbenzimidazol-1-yl moiety) and a head-to-head amide-amide hydrogen-bonded dimer. The use of this ligand allowed for the separation of metal centers to increase to approx. 21.0 Å, compared to Cu(II)-Cu(II) separations of 13.1-15.3 Å in the structures of **35-37**.

The lack of counterions may certainly have contributed in a positive way to the high supramolecular yield that was observed in this study. Neither the coordinate covalent bonds nor the primary hydrogen bonds were disrupted by the presence of solvent molecules (THF in the case of **38** and **39**), and despite opportunities for extensive π···π interactions in these systems, no discernable patterns involving ligand-ligand stacking were observed.

A similar supramolecular strategy as the one employed here was previously reported in the directed assembly of Co(II) and Ni(II)$(DBM)_2$ complexes into infinite chains.[4a] The supramolecular chemistry was then performed by *iso*nicotinamide as a bridging ligand and it also produced the primary 1-D motifs observed in **38** and **39**. In these complexes, the metal-metal separation, bridged by *iso*nicotinamide ligands *via* amide···amide hydrogen bonds, is about 17 Å, which is comparable with those using the [(benzimidazol-1-yl)methyl]-benzamide dimer. A possible reason for this similarity is that the [(benzimidazol-1-yl)methyl-benzamide ligands are "bent" due to the bridging methylene groups, thereby shortening the through-space intrachain distances between metal centers.

The propensity of Cu(II)$(acac)_2$ complexes to form five-coordinate or octahedral geometries using nitrogen-containing ligands was further examined through a CSD search,[13,14] Table 6.3.

Acac ligand	Five-coordinate	Six-coordinate
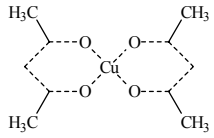		
(a) axial nitrogen-containing ligands	7	1
(b) axial imidazole/benzimidazole-containing ligands	0	0
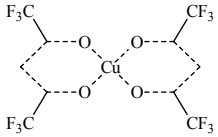		
(a) axial nitrogen-containing ligands	21	88
(b) axial imidazole/benzimidazole-containing ligands	15	4
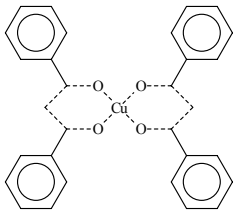		
(a) axial nitrogen-containing ligands	0	1
(b) axial imidazole/benzimidazole-containing ligands	0	0

Table 6.3 Five-coordinate versus six-coordinate Cu$(acac)_2$ complexes in the CSD with axial nitrogen-containing ligands.

There are only seven five-coordinate and one six-coordinate $Cu(acac)_2$ structures with nitrogen donors in the axial positions. Of the five-coordinate structures, three of them utilize monotopic *N*-ligands (*e.g.* cyano and quinoline) while the remaining four structures involve ditopic *N*-ligands (piperazine, pyrazine, and 4,4'-bipyridine). No examples in either five- or six-coordinate $Cu(acac)_2$ complexes contain imidazoles as *N*-ligands; compound **35**, therefore, is the first example of a five-coordinate $Cu(acac)_2$ complex that consists of a *bis*-imidazol-1-yl ligand. Based on these search results, it also seems that there is a greater tendency of acac to produce a five-coordinate complex when it is employed as the "capping" ligand.

In the case of $Cu(II)(hfacac)_2$ complexes, the odds are stacked favorably towards an octahedral geometry (88 octahedral structures over 21 five-coordinate structures) when a nitrogen-containing ligand is used. Of the 88 structures, only four structures involve imidazole ligands and their derivatives (one chelating *bis*-imidazole, two bridging imidazoles, and one non-bridging imidazole). On the other hand, fifteen of the 21 five-coordinate structures contain imidazole and their derivatives as bridging ligands (ten imidazoles, three ditopic imidazole/pyrazole ligands, and two ditopic imidazole/pyridine ligands). We were also able to generate the first octahedral *bis*-imidazol-1-yl-containing $Cu(II)(hfacac)_2$ complex in **36** that extends into an infinite 1-D architecture.

Only one octahedral $Cu(II)(DBM)_2$ structure exists in the CSD, which involves a *N*-ligand (the DBM ligands in this structure contain an acetonitrile functionality), whereas there are no five-coordinate examples. Compound **37**, thus, is the first example of an octahedral $Cu(II)(DBM)_2$ complex consisting of a *bis*-*N*-heterocyclic ligand.

6.5 Conclusions

In this chapter we have employed a cooperative supramolecular strategy combining imidazol-1-yl/benzimidazol-1-yl bridging ligands and various $M(II)(acac)_2$ complexes into infinite 1-D chains resulting in a high supramolecular yield. The use of acac ligands with octahedral metal ions led to the formation of well-defined building blocks whose resulting linear geometry consists of readily accessible axial coordination sites. At the same time, possible competition from counterions is avoided. Additionally, the metrics of the ditopic ligand was deliberately increased with a hydrogen bond-linked ligand,

which also proved to be essential in further separating M(II)$(acac)_2$ units. We are currently employing this approach to form more elaborate supramolecular architectures in conjunction with metal ions containing higher accessible coordination sites (square planar, octahedral, etc.) with the goal of producing highly porous extended frameworks.

References

[1] Blake, A. J.; Champness, N. R.; Crew, M.; Larsons, S. *New J. Chem.* **1999**, *23*, 13.

[2] (a) Yasui, M.; Ishikawa, Y.; Ishida, T.; Nogami, T.; Iwasaki, F. *Acta Crystallogr., Sect. B* **2001**, *57*, 772. (b) Li, B.; Zhu, L.; Wang, S.; Lang, J.; Zhang, Y. *J. Coord. Chem.* **2003**, *56*, 933. (c) Fursova, E.; Romanenko, G.; Ikorski, V.; Ovcharenko, V. *Polyhedron* **2003**, *22*, 1957. (d) Bailey, N. A.; Fenton, D. E.; Gonzalez, M. S. L. *Inorg. Chim. Acta* **1984**, *88*, 125. (e) Shu, S.; Yuanzhi, X. *Chinese J. Struct. Chem.* **1985**, *4*, 38. (f) Papaefstathiou, G. S.; Hamilton, T. D.; Friscic, T.; MacGillivray, L. R. *Chem. Commun.* **2004**, 270.

[3] (a) Yaghi, O. M.; Li, H. *J. Am. Chem. Soc.* **1996**, *118*, 295. (b) Yaghi, O. M.; Li, G. *Angew. Chem., Int. Ed. Engl.* **1995**, *34*, 207. (c) Subramanian, S.; Zaworotko, M. J. *Angew. Chem., Int. Ed. Engl.* **1995**, *34*, 2127. (d) Fujita, M.; Kwon, Y. -J.; Osamu, S.; Yamaguchi, K.; Ogura, K. *J. Am. Chem. Soc.* **1995**, *117*, 7287. (e) Zaworotko, M. J. *Chem. Soc. Rev.* **1994**, *23*, 283. (f) Copp, S. B.; Subramanian, S.; Zaworotko, M. J. *J. Am. Chem. Soc.* **1992**, *114*, 8719.

[4] (a) Aakeröy, C. B.; Desper, J.; Valdés-Martínez, J. *CrystEngComm* **2004**, *6*, 413. (b) Aakeröy, C. B.; Beatty, A. M.; Desper, J.; O'Shea, M.; Valdés-Martínez, J. *Dalton Trans.* **2003**, 3956. (c) Beatty, A. M. *CrystEngComm* **2001**, *51*, 243. (d) Aakeröy, C. B.; Beatty, A. M. *Aust. J. Chem.* **2001**, *54*, 409. (e) Aakeröy, C. B.; Beatty, A. M.; Lorimer, K. R. *J. Chem. Soc., Dalton Trans.* **2000**, 3869. (f) Aakeröy, C. B.; Beatty, A. M.; Leinen, D. S. *CrystEngComm* **2000**, *27*, 1. (g) Aakeröy, C. B.; Beatty, A. M.; Leinen, D. S.; Lorimer, K. R. *Chem. Commun.* **2000**, 935. (h) Aakeröy, C. B.; Beatty, A. M.; Leinen, D. S. *Angew. Chem., Int. Ed. Engl.* **1999**, *38*, 1815. (i) Aakeröy, C. B.; Beatty, A. M.; Helfrich, B. A. *J. Chem. Soc., Dalton Trans.* **1998**, 1943. (j) Aakeröy, C. B.; Beatty, A. M.; Leinen, D. S. *J. Am. Chem. Soc.* **1998**, *120*, 7383. (k) Uemura, K.; Kitagawa, S.; Kukui, K.; Saito, K. *J. Am. Chem. Soc.* **2004**, *126*, 3817.

[5] (a) Barszcz, B.; Glowiak, T.; Detka, K. *Polyhedron* **2003**, 1329. (b) Ma, J. -F.; Yang, J.; Zheng, G. -L.; Li, L.; Liu, J. -F. *Inorg. Chem.* **2003**, *42*, 7531. (c) Su, C. -Y.; Smith, M. D.; Loye, H. -C. *Angew. Chem., Int. Ed. Engl.* **2003**, *42*, 4085. (d) Abrahams, B. F.; Hoskins, B. F.; Robson, R.; Slizys, D. A. *CrystEngComm* **2002**, *4*, 478. (e) Sui, B.; Fan, J.; Okamura, T.; Sun, W. -Y.; Ueyama, N. *New J. Chem.* **2001**, *25*, 1379. (f) Liu, H. -K.; Hu, J.; Wang, T. -W.; Yu, X. -L.; Liu, J.; Kang, B. -S. *J. Chem. Soc., Dalton Trans.* **2001**, 3534. (g) Ma, J. -F.; Liu, J. -F.; Liu, Y. -C.; Xing, Y.; Jia, H. -Q.; Lin, Y. -H. *New J. Chem.* **2000**, *24*, 759. (h) Ma, J. -F.; Liu, J. -F.; Xing, Y.; Jia, H. -Q.; Lin, Y. -H. *J. Chem. Soc., Dalton Trans.* **2000**, 2403. (i) Fei, B. -L.; Sun, W. -Y.; Zhang, Y. -A.; Yu, K. -B.; Tang, W. -X. *J. Chem. Soc., Dalton Trans.* **2000**, 2345. (j) Shen, H. -Y.; Liao, D. -Z.; Jiang, Z. -H.; Yan, S. -P.; Wang, G. -L.; Yao, X. -K.; Wang, H. -G. *Acta Chem. Scand.* **1999**, *53*, 387. (k) Mago, G.; Hinago, M.; Miyasaka, H.; Matsumoto, N.; Okawa, H. *Inorg. Chim. Acta* **1997**, *254*, 145. (l) Hoskins, B. F.; Robson, R.; Slizys, D. A. *Angew. Chem., Int. Ed. Engl.* **1997**, *36*, 2336. (m) Hoskins, B. F.; Robson, R.; Slizys, D. A. *J. Am. Chem. Soc.* **1997**, *119*, 2952. (n) Zhu, H. -F.; Fan, J.; Okamura, T. -A.; Sun, W. -Y.; Ueyama, N. *Cryst. Growth Des.* **2005**, *5*, 289. (o) Zhang, L.; Lü, X. -Q.; Chen, C. -L.; Tan, H. -Y.; Zhang, H. -X.; Kang, B. -S. *Cryst. Growth Des.* **2005**, 5, 283.

[6] B. F. Abrahams; Hoskins, B. F.; Robson, R.; Slizys, D. A. *Acta Crystallogr.* **1998**, *C54*, 1666.

[7] Aakeröy, C. B.; Desper, J.; Smith, M. M.; Urbina, J. F. *Dalton Trans.* submitted.

[8] Soldatov, D. V.; Ripmeester, J. A. *Chem. Eur. J.* **2001**, *7*, 2979.

[9] Aakeröy, C. B.; Desper, J.; Urbina, J. F. *Cryst. Growth Des.* **2005**, DOI: 10.1021/cg049579t.

[10] SMART v5.060; Bruker Analytical X-ray Systems: Madison, WI, 1997–1999.

[11] SAINT v6.02; Bruker Analytical X-ray Systems: Madison, WI, 1997–1999.

[12] SHELXTL v5.10; Bruker Analytical X-ray Systems: Madison, WI, 1997.

[13] Search hits as of April, 2005.

[14] Allen, F. A. *Acta Crystallogr.*, *Sect. B.* **2002**, *58*, 380.

Chapter 7

Asymmetric supramolecular reagents for binary and ternary co-crystals

7.1 Introduction

Many elegant studies have shown that extended supramolecular architectures can be synthesized with the aid of complementary intermolecular interactions.[1] When such assemblies are constructed from neutral molecular building blocks they are typically homomeric, which is consistent with the observation that *"most crystals are built from identical (or enantiomeric) copies of the same molecule"*.[2] Despite an abundance of papers dealing with design and assembly of organic extended networks with desirable connectivities and shapes, it remains exceedingly difficult to bring more than two different molecular species into one crystalline lattice in a predictable manner, without making or breaking covalent bonds.[3,4,5] In fact, recent work with *iso*nicotinamide remains the only reported successful strategy for the reliable construction of ternary supermolecules.[6,7,8,9,10,11] In a typical reaction, *iso*nicotinamide is allowed to react with two carboxylic acids resulting in ternary supermolecules with two primary supramolecular synthons;[12] (1) the heteromeric carboxylic acid···pyridine hydrogen bond and (2) the heteromeric amide···acid hydrogen bond. In Chapter 4 it was also shown that [(benzimidazol-1-yl)methyl]-benzamides can act as supramolecular reagents for the directed assembly of ternary supermolecules. The supramolecular targets are assembled using a synthetic strategy based upon a hierarchical view of intermolecular forces -- the stronger acid (as determined by pK_a values) interacts preferentially with the best hydrogen-bond acceptor (the pyridyl or benzimidazol-1-yl nitrogen atom), and the weaker acid binds to the amide moiety.[13]

Despite its success, *iso*nicotinamide is not an ideal supramolecular reagent. First, it is capable of forming self-complementary amide···amide and amide···pyridine hydrogen bonds, which makes it inherently difficult to combine it with molecules that lack moieties that can compete successfully with the hydrogen-bonding capabilities of the amide functionality. Second, since the two binding sites on *iso*nicotinamide are attached to the same delocalized backbone, it is not possible to tune the electronics of the two sites independently, which reduces versatility.

In order to bring supramolecular synthesis in the solid state (crystal engineering) to a new level of complexity we are now developing supramolecular reagents (SR's) that can be refined in such a way that they offer more opportunities for structural selectivity and specificity.

This chapter describes the rationale behind, and synthesis of, a family of pyridyl/benzimidazol-1-yl and pyrimidyl/benzimidazol-1-yl-based SR's, Scheme 7.1, and the subsequent modular assembly of ternary co-crystals (1:1:1).

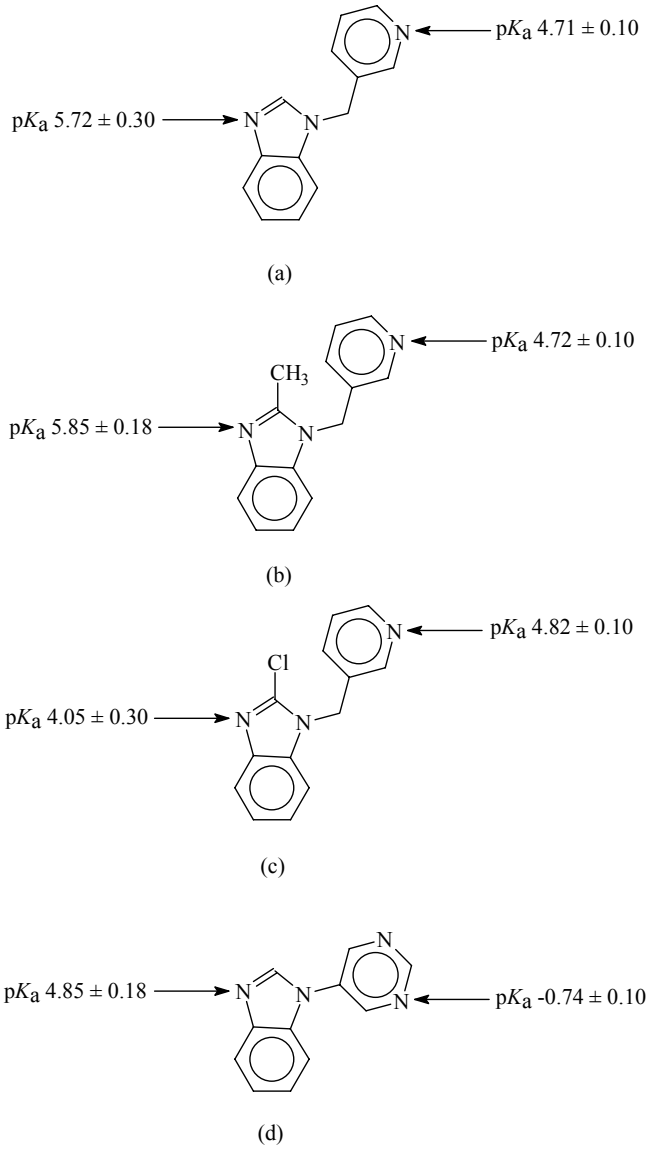

Scheme 7.1 Proposed strategy for ternary supermolecules based upon asymmetric (a)-(c) pyridyl-benzimidazol-1-yl and (d) pyrimidyl-benzimidazol-1-yl supramolecular reagents (SR's).

Our approach is based upon hydrogen-bond interactions in the context of the best-donor/best-acceptor, second-best donor/second-best acceptor concept. [6,14,15] The SR's in this study are built around asymmetric *bis*-heterocycles where two binding sites (hydrogen-bond acceptor sites) are linked by a methylene bridge (in the case of pyridyl/benzimidazol-1-yl SR's) in order to provide increased solubility in a range of solvents. The binding sites have significantly different basicities,[16] which means that their abilities to accept hydrogen bonds vary. They also lack strong hydrogen-bond donors and, consequently, any self-complementary intermolecular interaction will be weak and less likely to disrupt the desired heteromeric interactions.

Even though pK_a/pK_b values do not provide direct measures of hydrogen-bond strength, hydrogen bond abilities and free energies of complexation have been correlated with pK_a values, and within closely related classes of compounds, such comparisons frequently yield correct qualitative results.[17] Finally, the basicity of each heterocycle can be independently altered through suitable covalent substituents on each ring, which thereby provides an effective handle for fine-tuning differences in intermolecular reactivity between the two binding sites. The latter is highly significant as it creates a supramolecular reagent with the potential for a high degree of versatility and transferability. Ditopic *bis*-imidazoles/*bis*-benzimidazoles are also known to form binary co-crystals with a variety of dicarboxylic acids as presented earlier in Chapter 2.[18]

The ability of these supramolecular reagents to form binary co-crystals with monocarboxylic acids was first investigated, as these results provide valuable information about the selectivity and specificity of these SR's. Subsequently, our strategy for the directed assembly of ternary supermolecules with predictable connectivity employing these SR's was put to the test by allowing each SR to react with pairs of carboxylic acids with different pK_a values[19] in a 1:1:1 ratio.

7.2 Experimental

7.2.1 Synthesis

Starting materials were obtained from Aldrich and used without further purification. Melting points were determined on a Fisher-Johns melting point apparatus and are uncorrected.

7.2.1.1 Synthesis of 3-(benzimidazol-1-yl)methylpyridine and synthesis of 3-(benzimidazol-1-yl)methylpyridine hydrate, **40**

Benzimidazole (4.25 g, 36.0 mmol) was dissolved in 18 mL of anhydrous DMF with stirring under a N_2 atmosphere. To the clear, light-brown solution was added NaH (0.86 g, 36.0 mmol) inside a glove bag under a N_2 atmosphere. Effervescence was immediately observed, and once fizzing had subsided, the mixture was heated and stirred under reflux for 1 h under a N_2 atmosphere. After 1 h, the mixture was cooled to room temperature. To this solution was added dropwise a solution of 3-picolyl chloride hydrochloride (2.95 g, 18.0 mmol) in 36 mL of anhydrous DMF. The resulting mixture was heated and stirred under reflux under a N_2 atmosphere and monitored by TLC. After 48 h, the brown mixture was cooled to room temperature. NaCl that had formed during the reaction was filtered *via* vacuum filtration, and the clear, brown filtrate was concentrated by rotary evaporation to obtain a brown syrup. The syrup was purified by column chromatography using silica gel (200-425 mesh), and ethyl acetate : hexanes 1:1, ethyl acetate, followed by methanol as eluents. Concentration of the appropriate fractions *via* rotary evaporation afforded the pure product as a pale yellow crystalline solid. The monohydrate, **40**, was obtained as colorless plates suitable for X-ray crystallography upon slow evaporation of the pure product in ethyl acetate after 24 h. Yield 1.99 g (52.9%); m.p. 48-51˚C; ^{1}H NMR (DMSO-d_6, 400 MHz) δ 5.56 (s, 2H), 7.21 (m, 2 H), 7.35 (dd, 1H, J_1 = 7.6 Hz, J_2 = 4.8 Hz), 7.57 (m, 1H), 7.68 (m, 2H), 8.45 (s, 1H), 8.49 (dd, 1H, J_1 = 5 Hz, J_2 = 1.6 Hz), 8.64 (s, 1H).

7.2.1.2 Synthesis of 3-(2-methylbenzimidazol-1-yl)methylpyridine

2-Methylbenzimidazole (8.06 g, 61.0 mmol) was dissolved in 61 mL of anhydrous DMF with stirring under a N_2 atmosphere. To the clear, light-brown solution was added NaH (1.46 g, 61.0 mmol) inside a glove bag under a N_2 atmosphere. Effervescence was immediately observed, and once fizzing had subsided, the mixture was heated and stirred under reflux for 1 h under a N_2 atmosphere. After 1 h, the mixture was cooled to room temperature. To this solution was added dropwise a solution of 3-picolyl chloride hydrochloride (5.00 g, 30.5 mmol) in 61 mL of anhydrous DMF. The resulting mixture was heated and stirred under reflux under a N_2 atmosphere and monitored by TLC. After

96 h, the brown mixture was cooled to room temperature. NaCl that had formed during the reaction was filtered via vacuum filtration, and the clear, brown filtrate was concentrated by rotary evaporation to obtain a brown syrup. The syrup was purified by column chromatography using silica gel (200-425 mesh), and ethyl acetate : hexanes 1:2 followed by ethyl acetate as eluents. Concentration of the appropriate fractions via rotary evaporation afforded the pure product as a pale brown microcrystalline solid. Yield 1.43 g (21.0%); m.p. 91-93˚C; ^{1}H NMR (CD_3OD, 400 MHz) δ 2.60 (s, 3H), 5.55 (s, 2H), 7.25 (m, 2H), 7.39 (m, 2H), 7.52 (d, 1H, J = 8.8 Hz), 7.61 (m, 1H), 8.42 (s, 1H), 8.47 (dd, 1H, J_1 = 4.8 Hz, J_2 = 1.6 Hz).

7.2.1.3 Synthesis of 3-(2-chlorobenzimidazol-1-yl)methylpyridine and synthesis of 3-(2-chlorobenzimidazol-1-yl)methylpyridine hydrate, **41**

2-Chlorobenzimidazole (3.00 g, 19.7 mmol) was dissolved in 300 mL of dry THF with stirring in a 1000 mL round-bottomed flask under a N_2 atmosphere. To the pale brown solution was added NaOH pellets (8.24 g, 205.9 mmol) and the resulting suspension stirred at room temperature under a N_2 atmosphere for 2 h whereupon the suspension turned yellowish-green. After 2 h, a suspension of 3-picolyl chloride hydrochloride (3.23 g, 19.7 mmol) in 400 mL of dry THF was added all at once to the stirring reaction mixture, and the resulting pale yellow-brown suspension was heated and stirred under reflux under a N_2 atmosphere and monitored by TLC. After one week, the dark red-brown mixture was cooled to room temperature. Distilled water (100 mL) was then added to the suspension to dissolve the NaOH pellets and NaCl that had formed during the reaction to obtain two layers. The THF layer was separated and dried over anhydrous Na_2SO_4, the suspension filtered, and the filtrate concentrated by rotary evaporation to afford the crude product as a brown syrup. The syrup was purified by column chromatography using silica gel (200-425 mesh), and hexanes : ethyl acetate 10:1 as the eluent. Concentration of the appropriate fractions *via* rotary evaporation afforded the pure product as an off-white solid. Colorless prisms of the hydrate, **41**, were afforded after 24 h upon slow evaporation of the pure product in ethyl acetate. Yield 3.16 g (65.8%); m.p. 95-97˚C; ^{1}H NMR (DMSO-d_6, 400 MHz) δ 5.60 (s, 2H), 7.29 (m, 2 H),

7.37 (dd, 1H, J_1 = 8 Hz, J_2 = 4.8 Hz), 7.58 (d, 1H, J = 8 Hz), 7.64 (d, 1H, J = 7.2 Hz), 7.69 (d, 1H, J = 6.8 Hz), 8.51 (d, 1H, J = 4.8 Hz), 8.57 (s, 1H).

7.2.1.4 Synthesis of 5-(benzimidazol-1-yl)-pyrimidine

Benzimidazole (1.06 g, 9.00 mmol) was dissolved in 9 mL of anhydrous DMF with stirring under a N_2 atmosphere. To the clear, light brown solution was added NaH (0.25 g, 10.5 mmol) inside a glove bag under a N_2 atmosphere. Effervescence was immediately observed, and once the fizzing had subsided, the cloudy, dark brown mixture was heated and stirred under reflux for 1 h. The clear, brown mixture was then cooled to room temperature, and to it was added dropwise a solution of 5-bromopyrimidine (1.43 g, 9.00 mmol) in 9 mL of anhydrous DMF. The resulting mixture was allowed to heat and stir under reflux under a N_2 atmosphere, and its progress monitored by TLC. After 48 h, the red-orange mixture was cooled to room temperature, and the NaBr that had formed during the reaction was filtered via vacuum filtration and the clear, red-orange filtrate was concentrated by rotary evaporation to afford the crude product as a pale brown solid. The crude product was purified upon recrystallization from 30 mL of hot water, and an off-white solid formed upon cooling, which was filtered *via* vacuum filtration, dried, and collected. Yield 1.13 g (64.2%); m.p. 137-138˚C; ^{1}H NMR (DMSO-d_6, 400 MHz) δ 7.37 (m, 2H), 7.74 (m, 1H), 7.81 (m, 1H), 8.70 (s, 1H), 9.27 (s, 2H), 9.32 (s, 1H).

7.2.2 Syntheses of binary co-crystals and salts

7.2.2.1 Synthesis of 4-nitrobenzoic acid 3-(benzimidazol-1-yl)methylpyridine, **42**

To an ethanolic solution (4 mL) of 4-nitrobenzoic acid (0.032 g, 0.191 mmol) was added a solution containing 3-(benzimidazol-1-yl)methylpyridine (0.020 g, 0.096 mmol) in 1 mL of absolute ethanol. Colorless blocks resulted from slow evaporation of the solvent after 5 days. M.p. 178-181˚C.

7.2.2.2 Synthesis of 2,3-dimethylbenzoic acid 3-(benzimidazol-1-yl)methylpyridine, **43**

2,3-Dimethylbenzoic acid (0.014 g, 0.096 mmol) was dissolved in 2 mL of absolute ethanol. To this solution was added 3-(benzimidazol-1-yl)methylpyridine (0.020 g, 0.096 mmol) dissolved in 1 mL of absolute ethanol. The solvent was evaporated slowly upon which colorless blocks formed after 3 weeks. M.p. 100-103˚C.

*7.2.2.3 Synthesis of 3-*N,N*-dimethylaminobenzoic acid 3-(2-methylbenzimidazol-1-yl)methylpyridine,* **44**

3-*N*,*N*-dimethylaminobenzoic acid (0.012 g, 0.072 mmol) was dissolved in 1 mL of absolute ethanol. To this solution were added 4-nitrobenzoic acid (0.012 g, 0.072 mmol) in 2 mL of absolute ethanol and 3-(2-methylbenzimidazol-1-yl)methylpyridine (0.016 g, 0.072 mmol) in 1 mL of absolute ethanol. The resulting solution was evaporated slowly for one month until amber prisms of **44** formed. M.p. 162-165˚C.

7.2.2.4 Synthesis of 3-(2-methylbenzimidazolium-1-yl)methylpyridine 3,5-dinitrobenzoate 3,5-dinitrobenzoic acid, **45**

3,5-Dinitrobenzoic acid (0.030 g, 0.144 mmol) was dissolved in 2 mL of absolute ethanol. An ethanolic solution (1 mL) containing 3-(2-methylbenzimidazol-1-yl)methylpyridine (0.016 g, 0.072 mmol) was then added to the first solution. Slow evaporation of the solvent yielded colorless plates after 10 days. M.p. 170-173˚C.

7.2.2.5 Synthesis of 3-(benzimidazolium-1-yl)methylpyridine pentamethylbenzoate pentamethylbenzoic acid, **46**

An ethanolic solution (1 mL) of 3-(benzimidazol-1-yl)methylpyridine (0.020 g, 0.096 mmol) was added to a 2 mL ethanolic solution containing pentamethylbenzoic acid (0.036 g, 0.191 mmol). The resulting solution was evaporated slowly for 3 weeks until colorless blocks of **46** formed. M.p. 152-155˚C.

7.2.2.6 Synthesis of 3-(benzimidazolium-1-yl)methylpyridine 3,5-dinitrobenzoate 3,5-dinitrobenzoic acid, **47**

3,5-Dinitrobenzoic acid (0.040 g, 0.191 mmol) was dissolved in 2 mL of absolute ethanol. To this solution was added 3-(benzimidazol-1-yl)methylpyridine (0.020 g, 0.096

mmol) in 1 mL of absolute ethanol. The combined solution was evaporated slowly for 6 days until colorless prisms formed. M.p. 158-161˚C.

7.2.2.7 Synthesis of 3-(2-methylbenzimidazolium-1-yl)methylpyridine 4-nitrobenzoate 4-nitrobenzoic acid hydrate, **48**

4-Nitrobenzoic acid (0.024 g, 0.144 mmol) was dissolved in 4 mL of absolute ethanol. An ethanolic solution (1 mL) containing 3-(2-methylbenzimidazol-1-yl)methylpyridine (0.016 g, 0.072 mmol) was then added to the first solution. Colorless plates formed upon slow evaporation of the solvent after 1 week. M.p. 163-166˚C.

7.2.2.8 Synthesis of 3,5-dinitrobenzoic acid 5-(benzimidazol-1-yl)-pyrimidine, **49**

To an ethanolic solution (2 mL) containing 3,5-dinitrobenzoic acid (0.032 g, 0.153 mmol) was added 5-(benzimidazol-1-yl)-pyrimidine (0.015 g, 0.077 mmol) in 2 mL of absolute ethanol. Amber rods of **49** were obtained after 24 h upon slow evaporation of the solvent. M.p. 172-174˚C.

7.2.2.9 Synthesis of 4-nitrobenzoic acid 5-(benzimidazol-1-yl)-pyrimidine, **50**

4-Nitrobenzoic acid (0.026 g, 0.153 mmol) was dissolved in 4 mL of absolute ethanol. To this solution was added 5-(benzimidazol-1-yl)-pyrimidine (0.015 g, 0.077 mmol) in 2 mL of absolute ethanol. Slow evaporation of the solvent yielded yellow prisms of **50** after 3 weeks. M.p. 168-170˚C.

7.2.3 Syntheses of ternary co-crystals

7.2.3.1 Synthesis of 3,5-dinitrobenzoic acid 3-(benzimidazol-1-yl)methylpyridine 4-nitrobenzoic acid, **51**

3,5-Dinitrobenzoic acid (0.020 g, 0.10 mmol) was dissolved in 1 mL of absolute ethanol and added to a 2 mL ethanolic solution containing 4-nitrobenzoic acid (0.016 g, 0.10 mmol). To the resulting solution was added 3-(benzimidazol-1-yl)methylpyridine (0.020 g, 0.10 mmol) in 1 mL of absolute ethanol. Slow evaporation of the solvent after two weeks yielded colorless plates. TLC of individual crystals showed spots corresponding to all three components. M.p. 133-136˚C.[20]

*7.2.3.2 Synthesis of 3,5-dinitrobenzoic acid 3-(benzimidazol-1-yl)methylpyridine 3-*N,N*-dimethylaminobenzoic acid,* **52**

3,5-Dinitrobenzoic acid (0.020 g, 0.10 mmol) was dissolved in 1 mL of absolute ethanol and added to a 1 mL ethanolic solution containing 3-*N,N*-dimethylaminobenzoic acid (0.016 g, 0.10 mmol). To the resulting solution was added 3-(benzimidazol-1-yl)methylpyridine (0.020 g, 0.10 mmol) in 1 mL of ethanol. Slow evaporation of the solvent yielded a crop of yellow prisms after two weeks.[21] A few days later, a second crop consisting of red prisms formed. TLC of individual red crystals showed spots corresponding to all three components. M.p. 110-113˚C.

7.2.3.3 Synthesis of 3,5-dinitrobenzoic acid 3-(benzimidazol-1-yl)methylpyridine 4-cyanobenzoic acid, **53**

3,5-Dinitrobenzoic acid (0.02 g, 0.10 mmol) was dissolved in 1 mL of absolute ethanol and added to a 1 mL ethanolic solution containing 4-cyanobenzoic acid (0.02 g, 0.10 mmol). To the resulting solution was added 3-(benzimidazol-1-yl)methylpyridine (0.02 g, 0.10 mmol) in 1 mL of ethanol. Slow evaporation of the solvent after two weeks yielded colorless plates. TLC of the crystals showed spots corresponding to all three components. M.p. 145-150˚C.

7.2.3.4 Synthesis of 3,5-dinitrobenzoic acid 3-(2-methylbenzimidazol-1-yl)methylpyridine 4-nitrobenzoic acid, **54**

3,5-Dinitrobenzoic acid (0.015 g, 0.070 mmol) was dissolved in 1 mL of absolute ethanol and added to a 2 mL ethanolic solution containing 4-nitrobenzoic acid (0.012 g, 0.070 mmol). To the resulting solution was added 3-(2-methylbenzimidazol-1-yl)methylpyridine (0.016 g, 0.070 mmol) in 1 mL of ethanol. Slow evaporation of the solvent after two weeks yielded colorless plates. TLC of individual crystals showed spots corresponding to all three components. M.p. 158-161˚C.[22]

7.2.3.5 Synthesis of 4-nitrobenzoic acid 3-(2-chlorobenzimidazol-1-yl)methylpyridine 4-cyanobenzoic acid, **55**

4-Nitrobenzoic acid (0.014 g, 0.082 mmol) and 4-cyanobenzoic acid (0.012 g, 0.082 mmol) were dissolved in 2 mL of absolute ethanol. To this solution was added an

ethanolic solution (1 mL) containing 3-(2-chlorobenzimidazol-1-yl)methylpyridine (0.020 g, 0.082 mmol), and the resulting solution evaporated slowly under ambient conditions upon which colorless blocks formed after 12 days. M.p. 150-153˚C.[23]

7.2.4 X-ray crystallography

X-ray data were collected on a Bruker SMART 1000 four-circle CCD diffractometer using a fine-focus molybdenum Kα tube. Data were collected using SMART.[24] Initial cell constants were found by small widely separated "matrix" runs. Preliminary Laué symmetry was determined from axial images. Generally, an entire hemisphere of reciprocal space was collected regardless of Laué symmetry. Scan speed and scan width were chosen based on scattering power and peak rocking curves. Unless otherwise noted, data were collected at low temperatures, using a scan width appropriate for the crystal's mosaic spread.

Unit cell constants and orientation matrix were improved by least-squares refinement of reflections thresholded from the entire dataset. Integration was performed with SAINT,[25] using this improved unit cell as a starting point. Precise unit cell constants were calculated in SAINT from the final merged dataset. Lorenz and polarization corrections were applied. Laué symmetry, space group, and unit cell contents were found with XPREP.

Data were reduced with SHELXTL.[26] The structures were solved in all cases by direct methods without incident. In general, hydrogens were assigned to idealized positions and were allowed to ride. Where possible, the coordinates of hydrogen-bonding hydrogens were allowed to refine. Heavy atoms were refined with anisotropic thermal parameters.

7.3 Results

Crystallographic data for **40**-**55** are given in Tables A40-A55. Hydrogen-bond geometries for **40**-**55** are presented in Table 7.1. Thermal ellipsoid plots, showing numbering schemes, hydrogen bonds, and molecular geometries, are displayed in Figures 7.1-7.18.

Table 7.1 Hydrogen-bond geometries for **40**-**55**.

Compound	D-H A	D-H/Å	H…A/Å	D…A/Å	<(DHA)/°	generator for A
40	O1S H1A N13	0.87(2)	1.98(2)	2.8486(14)	174(2)	–
	O1S H1B O1S	1.00(5)	1.98(5)	2.976(3)	171(4)	-x+1, -y, -z+2
	O1S H1C O1S	0.93(4)	2.09(4)	2.999(3)	167(3)	-x+1, y, -z+3/2
41	O1S H1A N13	0.85(2)	2.13(2)	2.9837(18)	175(2)	–
	O1S H1B N21	0.85(2)	2.02(2)	2.8667(19)	172(2)	-x+1, -y+1, -z
42	O31 H31 N13	1.078(16)	1.500(16)	2.5717(11)	172.2(14)	–
	O41 H41 N21	1.031(15)	1.550(15)	2.5747(12)	171.8(14)	–
43	O31 H31 N13	0.972(16)	1.657(16)	2.6263(12)	174.5(15)	–
44	O31 H31 N13	0.92(3)	1.71(3)	2.622(2)	169(2)	–
45	O41 H41 N21	0.99(2)	1.57(2)	2.5551(19)	173(2)	–
	N13 H13 O31	1.197(19)	1.340(19)	2.5337(19)	174.2(16)	–
46	N13 H13 O41	1.019(15)	1.557(15)	2.5750(12)	176.9(15)	–
	O61 H61 O41	0.942(19)	1.65(2)	2.5823(12)	171.6(18)	–
47	O31 H31 O41	1.13(2)	1.32(2)	2.4501(17)	176(2)	–
	N13 H13 N21	1.14(2)	1.50(2)	2.6287(18)	171.5(19)	x, -y+3/2, z+1/2
48	N13 H13 O31	1.08(3)	1.49(3)	2.560(2)	173(2)	–
	O41 H41 O1S	0.89(3)	1.68(3)	2.559(2)	169(3)	–
	O1S H1A N21	0.95(3)	1.84(3)	2.779(3)	169(3)	–
	O1S H1B O32	0.74(3)	2.10(3)	2.842(3)	173(3)	x-1,y+1,z
49	O31 H31 N13	0.926(19)	1.719(19)	2.6398(15)	172.5(18)	–
50	O31 H31 N21	0.901(15)	1.801(15)	2.7007(11)	176.1(14)	–
	O41 H41 N13	0.945(15)	1.719(15)	2.6569(11)	171.4(14)	–
51	O31 H31 N13	1.024(18)	1.559(18)	2.5762(17)	171.0(16)	–
	O71 H71 N53	1.044(19)	1.502(19)	2.5455(18)	177.4(15)	–
	O41 H41 N21	1.018(18)	1.594(19)	2.6081(18)	173.6(16)	–
	O81 H81 N61	1.06(2)	1.55(2)	2.6057(19)	174.2(16)	–
52	O47 H47 N13	0.94(3)	1.71(3)	2.652(3)	175(3)	–
	O37 H37 N21	0.90(3)	1.78(3)	2.665(3)	166(3)	–
53	O37 H37 N21	1.09(3)	1.53(3)	2.611(3)	172(2)	–
	O47 H47 N13	1.10(3)	1.44(3)	2.544(3)	175(2)	–
	O77 H77 N61	0.96(3)	1.61(3)	2.568(3)	176(3)	–
	O87 H87 N53	1.02(3)	1.55(3)	2.571(3)	179(3)	–
54	O47 H47 N13	1.01(3)	1.55(3)	2.553(3)	170(2)	x+1, y+1, z
	O37 H37 N21	1.08(3)	1.56(3)	2.641(3)	179(2)	–
55	O31 H31 N13	0.84	1.84	2.6764(14)	175.3	–
	O41 H41 N21	0.84	1.82	2.6551(14)	174.4	–

7.3.1 Crystal structure of 3-(benzimidazol-1-yl)methylpyridine hydrate, **40**

The crystal structure of **40** displays a hydrated molecule of 3-(benzimidazol-1-yl)methylpyridine, with one disordered water molecule hydrogen-bonded to the benzimidazol-1-yl nitrogen atom of the SR through O–H···N interactions (O1S···N13, 2.8486(14) Å), Figure 7.1. The other protons on the water molecule interact with the

oxygen atoms of neighboring water molecules. No significant intermolecular interactions involve the pyridyl nitrogen atom of the SR.

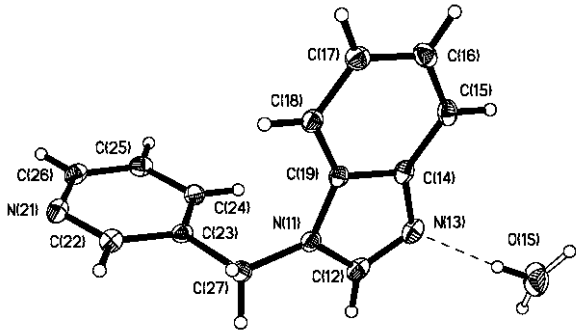

Figure 7.1 Hydrogen bonding between the disordered water molecule and 3-(benzimidazol-1-yl)methylpyridine in **40**.

7.3.2 Crystal structure of 3-(2-chlorobenzimidazol-1-yl)methylpyridine hydrate, **41**

The crystal structure determination of **41** reveals a hydrate of 3-(2-chlorobenzimidazol-1-yl)methylpyridine in which a proton of the water molecule interacts with the 2-chlorobenzimidazol-1-yl nitrogen site *via* O–H···N hydrogen bonds (O1S···N13, 2.9837(18) Å), Figure 7.2.

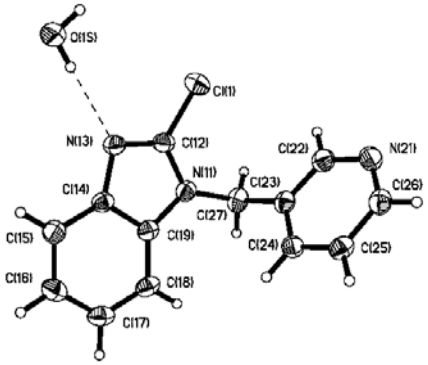

Figure 7.2 Hydrogen-bonded unit in **41**.

The pyridyl nitrogen atom also partakes in hydrogen bonding with the second proton of the water molecule (O1S···N21, 2.8667(19) Å). The combined interactions produce a $R_4^4(20)$ hydrogen-bond motif composed of alternating molecules of 3-(2-chlorobenzimidazol-1-yl)methylpyridine and water molecules, Figure 7.3.

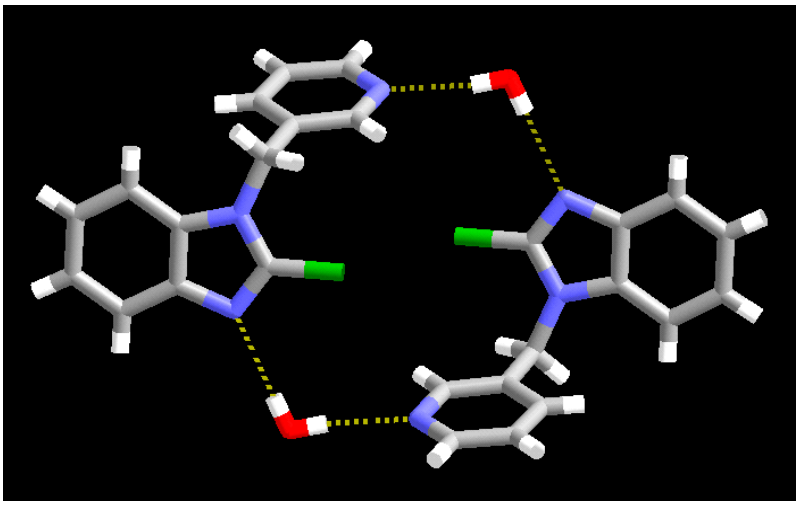

Figure 7.3 Four membered ring formed in **41**.

7.3.3 Crystal structure of 3-(benzimidazol-1-yl)methylpyridine 4-nitrobenzoic acid, **42**

A 2:1 molecular co-crystal is formed in **42** where the two 4-nitrobenzoic acid molecules interact at both heterocyclic nitrogen sites of 3-(benzimidazol-1-yl)methylpyridine through two different O–H···N hydrogen bonds (O31···N13, 2.5717(11) Å; O41···N21, 2.5747(12) Å), Figure 7.4; no proton transfer is observed. There are also no significant C–H···O interactions accompanying these primary hydrogen bonds as the carboxylic acid moieties are not co-planar with respect to the two heterocycles.

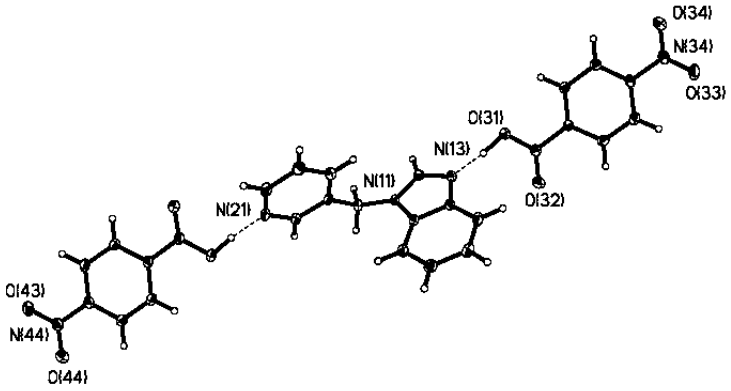

Figure 7.4 Three-component hydrogen-bonded motif in **42**.

7.3.4 Crystal structure of 3-(benzimidazol-1-yl)methylpyridine 2,3-dimethylbenzoic acid, **43**

A 1:1 co-crystal is evidenced in the crystal structure of **43** involving 3-(benzimidazol-1-yl)methylpyridine and 2,3-dimethylbenzoic acid, Figure 7.5. The primary O–H···N hydrogen bond (O31···N13, 2.6263(12) Å) involves the carboxylic acid and the more basic benzimidazol-1-yl nitrogen site while no interactions occur at the less basic pyridyl nitrogen atom. As in **42**, there is no C–H···O interaction that accompanies this hydrogen bond, nor is there any proton transfer.

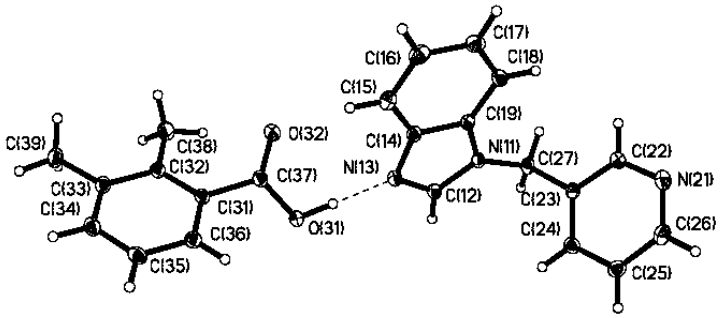

Figure 7.5 1:1 Binary co-crystal in **43**.

*7.3.5 Crystal structure of 3-(2-methylbenzimidazol-1-yl)methylpyridine 3-*N,N*-dimethylaminobenzoic acid,* **44**

A 1:1 co-crystal between 3-(2-methylbenzimidazol-1-yl)methylpyridine and 3-*N*,*N*-dimethylaminobenzoic acid is formed in **44**, with the same connectivity as that in **43**, Figure 7.6. A single O–H···N hydrogen bond is formed between the carboxylic acid and the more basic 2-methylbenzimidazol-1-yl nitrogen atom (O31···N13, 2.622(2) Å). Again, the pyridyl nitrogen atom of the SR does not engage in any noteworthy intermolecular interactions, and no C–H···O contacts were identified as the carboxylic acid and 2-methylbenzimidazol-1-yl moieties are not coplanar.

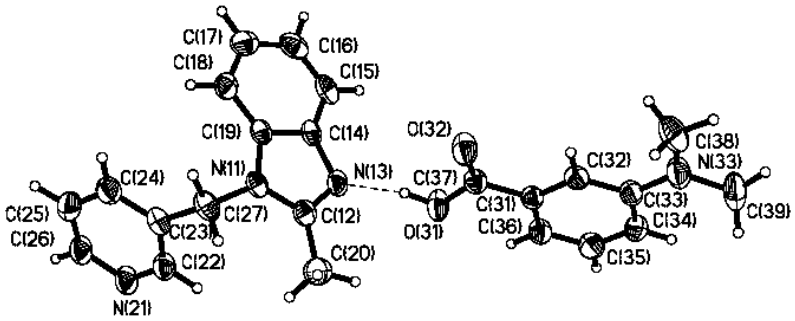

Figure 7.6 Primary motif in the crystal structure of **44**.

7.3.6 Crystal structure of 3-(2-methylbenzimidazolium-1-yl)methylpyridine 3,5-dinitrobenzoate 3,5-dinitrobenzoic acid, **45**

The crystal structure of **45** consists of a 3,5-dinitrobenzoic acid molecule, 3-(2-methylbenzimidazolium-1-yl)methylpyridine, and a 3,5-dinitrobenzoate anion, Figure 7.7. The SR is protonated at the more basic 2-methylbenzimidazol-1-yl nitrogen atom resulting in an N^+–H···O^- hydrogen bond (N13···O31, 2.5337(19) Å) whereas the pyridyl site forms a neutral O–H···N hydrogen bond with the second 3,5-dinitrobenzoic acid molecule (O41···N21, 2.5551(19) Å). No C–H···O interactions augment these primary hydrogen bonds.

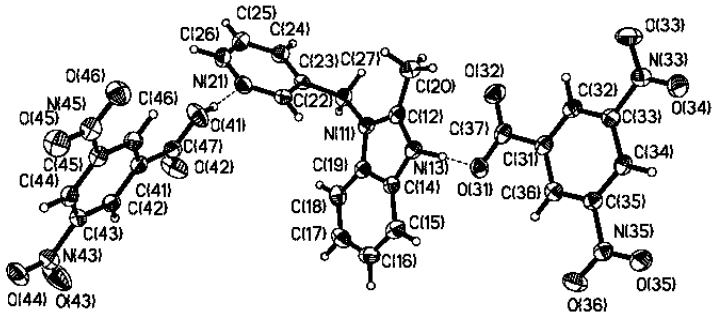

Figure 7.7 Hydrogen-bond motif in **45**.

7.3.7 Crystal structure of 3-(benzimidazolium-1-yl)methylpyridine pentamethylbenzoate pentamethylbenzoic acid, **46**

An ionic compound is also produced in **46**, Figure 7.8, comprising a pentamethylbenzoate anion, a pentamethylbenzoic acid molecule, and 3-

(benzimidazolium-1-yl)methylpyridine. Proton transfer occurs to the more basic site of the SR (the benzimidazol-1-yl moiety) (N13···O41, 2.5750(12) Å). A C–H···O contact also accompanies the N–H···O hydrogen bond involving the most acidic C–H proton of the benzimidazol-1-yl moiety in the SR and the carboxylate oxygen group of the pentamethylbenzoate anion (C12–H12···O42, 3.48 Å). The pentamethylbenzoic acid molecule forms an O–H···O hydrogen bond with the carboxylate functionality of the pentamethylbenzoate anion (O61···O41, 2.5823(12) Å). The pyridyl nitrogen atom does not participate in any principal intermolecular interactions.

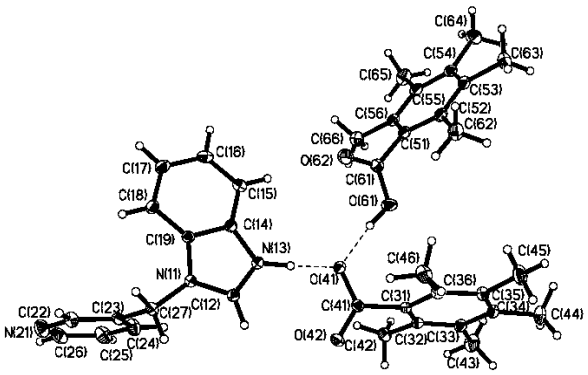

Figure 7.8 Ionic compound in the crystal structure of **46**.

7.3.8 Crystal structure of 3,5-dinitrobenzoic acid 3-(benzimidazolium-1-yl)methylpyridine 3,5-dinitrobenzoate, **47**

In the crystal structure of **47**, a molecule of 3,5-dinitrobenzoic acid, a 3,5-dinitrobenzoate anion, and 3-(benzimidazol-1-yl)methylpyridine form an ionic compound with a different connectivity pattern to that of **46**, Figure 7.9. Although the more basic site of the SR is protonated (the benzimidazol-1-yl nitrogen atom), it forms an N^{+}–H···N hydrogen bond with the pyridyl nitrogen atom of a neighboring SR (N13···N21, 2.6287(18) Å) resulting in an infinite 1-D chain. The anion interacts with the neutral carboxylic acid through an O–H···O hydrogen bond (O31···O41, 2.4501(17) Å). The 3,5-dinitrobenzoic acid molecule furthermore interacts through π···π stacking interactions (~3.5 Å) with the benzimidazol-1-yl moiety of the SR.

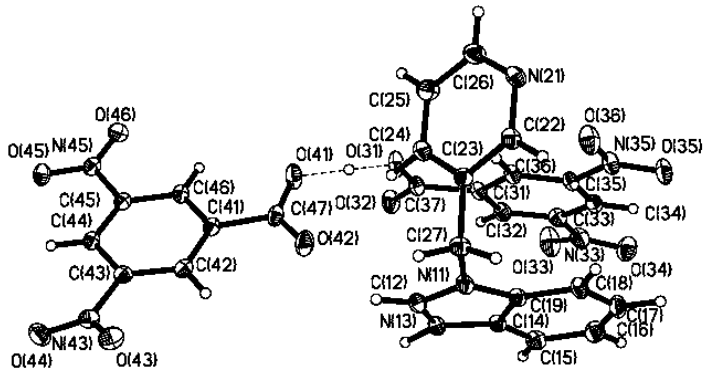

Figure 7.9 Charged-assisted hydrogen bonds and π···π interactions in the crystal structure of **47**.

7.3.9 Crystal structure of 3-(2-methylbenzimidazolium-1-yl)methylpyridine 4-nitrobenzoate 4-nitrobenzoic acid hydrate, **48**

The crystal structure determination of **48** reveals a hydrogen-bonded motif involving 4-nitrobenzoic acid, 4-nitrobenzoate, 3-(2-methylbenzimidazolium-1-yl)methylpyridine, and a water molecule, Figure 7.10. The carboxylate moiety formed due to proton transfer to the 2-methylbenzimidazol-1-yl nitrogen atom to produce a charge-assisted N^{+}–H···O^{-} hydrogen bond (N13···O31, 2.560(2) Å). The carboxylic acid is bridged by the water molecule through an O–H···O hydrogen bond (O41···O1S, 2.559(2) Å). An additional O–H···N hydrogen bond between the water molecule and the pyridyl nitrogen atom of the SR also forms part of the crystal structure of **48** (O1S···N21, 2.779(3) Å).

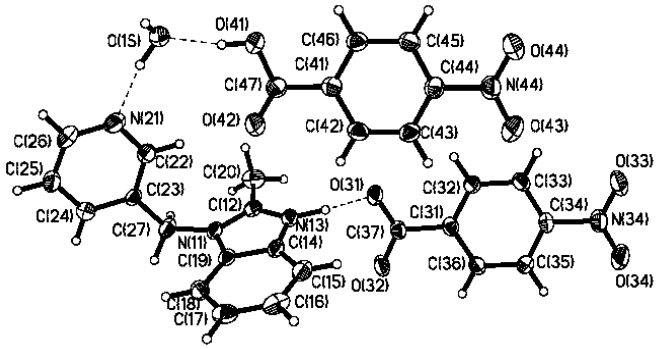

Figure 7.10 Hydrogen-bonded pattern in **48**. A water molecule provides a hydrogen-bond bridge between one carboxylic acid moiety and the pyridyl nitrogen atom of the SR.

The resulting extended structure of **48**, an infinite 1-D chain, is afforded through O–H···O hydrogen bonds between the bridging water molecule and the carboxylate moiety of a neighboring anion (O1S···O32, 2.842(3) Å), Figure 7.11.

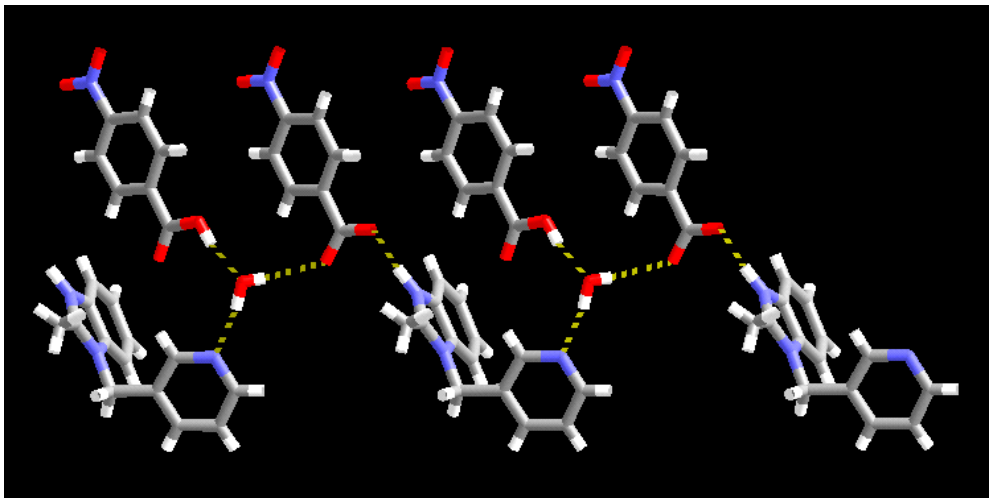

Figure 7.11 1-D chain in the crystal structure of **48**.

7.3.10 Crystal structure of 3,5-dinitrobenzoic acid 5-(benzimidazol-1-yl)-pyrimidine, **49**

A 1:1 co-crystal, **49**, is afforded between 5-(benzimidazol-1-yl)-pyrimidine and 3,5-dinitrobenzoic acid, Figure 7.12. As in the previous 1:1 co-crystals, the carboxylic acid forms an O–H···N hydrogen bond with the benzimidazol-1-yl nitrogen site (the stronger base) (O31···N13, 2.6398(15) Å). In addition, a C–H···O interaction accompanies this hydrogen bond utilizing the most acidic C–H proton of the benzimidazol-1-yl moiety and the carbonyl oxygen atom of the carboxylic acid (C12–H12···O32, 3.02 Å). The pyrimidyl nitrogen sites, however, are not involved in any primary intermolecular interactions.

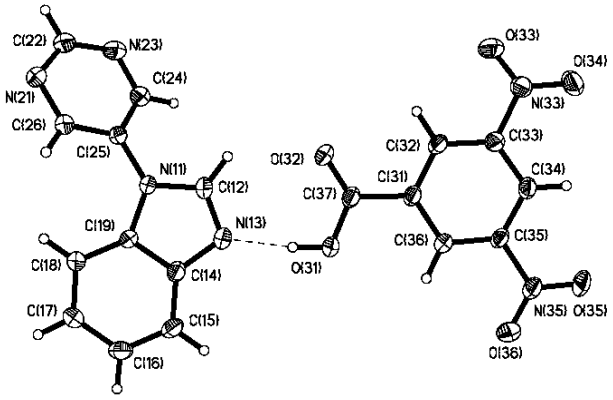

Figure 7.12 1:1 Motif in the crystal structure of **49**.

7.3.11 Crystal structure of 4-nitrobenzoic acid 5-(benzimidazol-1-yl)-pyrimidine, **50**

The crystal structure of **50** displays a 2:1 stoichiometry between 4-nitrobenzoic acid and 5-(benzimidazol-1-yl)-pyrimidine, Figure 7.13. Consequently, two unique O–H···N hydrogen bonds are formed, involving both benzimidazol-1-yl (O41···N13, 2.6569(11) Å) and pyrimidyl (O31···N21, 2.7007(11) Å) sites. The O–H···N hydrogen bond that incorporates the benzimidazol-1-yl site is further accompanied by a C–H···O interaction (C12–H12···O42, 3.68 Å).

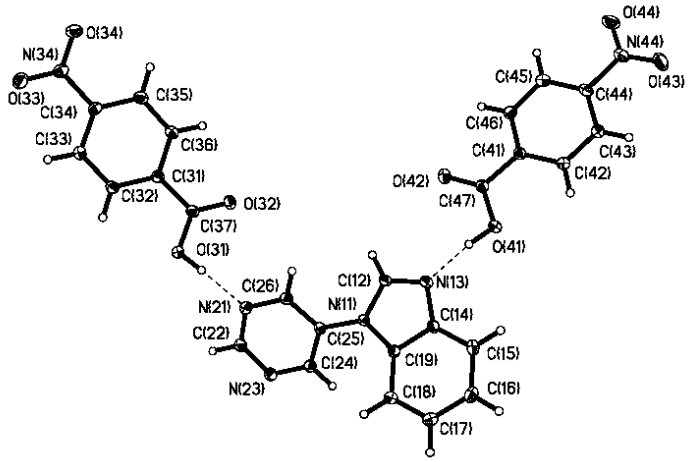

Figure 7.13 2:1 Co-crystal in **50**.

7.3.12 Crystal structure of 3,5-dinitrobenzoic acid 3-(benzimidazol-1-yl)methylpyridine 4-nitrobenzoic acid, **51**

The crystal structure of **51** consists of two crystallographically inequivalent sets of ternary supermolecules with identical connectivity, Figure 7.14.

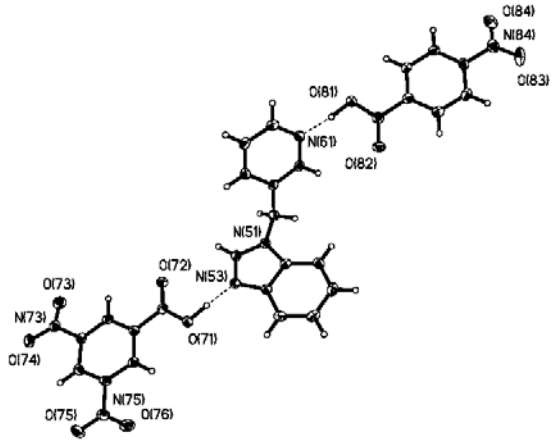

Figure 7.14 One of two ternary supermolecules in the crystal structure of **51** (both have the same connectivity). The best hydrogen-bond donor binds to the best hydrogen-bond acceptor and the second-best donor binds to the second-best acceptor.

The primary synthons in this structure are (a) the O–H···N hydrogen bonds from the stronger acid (3,5-dinitrobenzoic acid) to the most basic nitrogen atom located on the benzimidazol-1-yl ring (O31···N13, 2.5762(17) Å and O71···N53, 2.5455(18) Å), and (b) the O–H···N hydrogen bonds from the weaker acid (4-nitrobenzoic acid) to the less basic nitrogen atom located on the pyridyl moiety (O41···N21, 2.6081(18) Å and O81···N61, 2.6057(19) Å).

*7.3.13 Crystal structure of 3,5-dinitrobenzoic acid 3-(benzimidazol-1-yl)methylpyridine 3-*N,N*-dimethylaminobenzoic acid,* **52**

The crystal structure determination of **52** also reveals a ternary 1:1:1 supermolecule with the same connectivity as found in **51**, Figure 7.15.

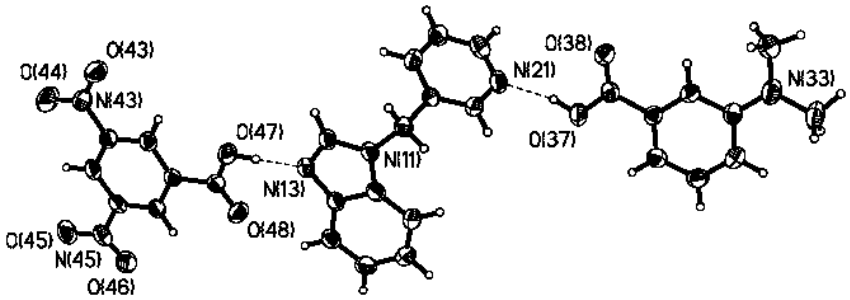

Figure 7.15 The ternary supermolecule in the crystal structure of **52**. The best hydrogen-bond donor binds to the best hydrogen-bond acceptor and the second-best donor binds to the second-best acceptor.

The primary synthons comprise (a) an O–H···N hydrogen bond between the stronger acid, 3,5-dinitrobenzoic acid, and the most basic heterocyclic moiety (O47···N13, 2.652(3) Å), and (b) another O–H···N interaction between the weaker acid, 3-*N*,*N*-dimethylaminobenzoic acid, and the second-best hydrogen-bond acceptor, the pyridyl moiety (O37···N21, 2.665(3) Å).

7.3.14 Crystal structure of 3,5-dinitrobenzoic acid 3-(benzimidazol-1-yl)methylpyridine 4-cyanobenzoic acid, **53**

A 1:1:1 ternary co-crystal is also observed in the crystal structure of **53**, which contains two inequivalent sets of supermolecules with the intended connectivity, Figure 7.16.

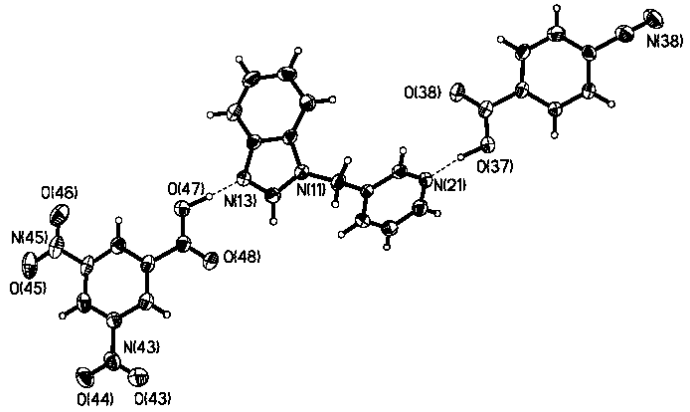

Figure 7.16 One of the two sets of ternary supermolecule in **53**, which contains the expected hydrogen-bond connectivities.

Once again the two principal O–H···N hydrogen bonds involve (a) an interaction between the stronger carboxylic acid (3,5-dinitrobenzoic acid) and the more basic benzimidazol-1-yl nitrogen atom (O47···N13, 2.544(3) Å and O87···N53, 2.571(3) Å), and (b) the weaker acid, 4-cyanobenzoic acid, interacting with the less basic pyridyl site (O37···N21, 2.611(3) Å and O77···N61, 2.568(3) Å).

7.3.15 Crystal structure of 3,5-dinitrobenzoic acid 3-(2-methylbenzimidazol-1-yl)methylpyridine 4-nitrobenzoic acid, **54**

The crystal structure of **54** contains the desired 1:1:1 supermolecule with the expected connectivity, Figure 7.17.

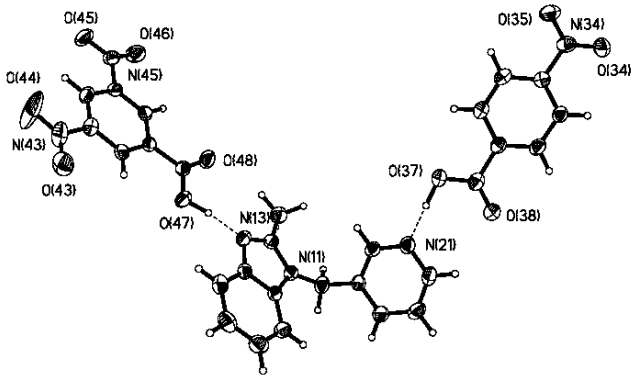

Figure 7.17 The ternary supermolecule in the crystal structure of **54**. The best hydrogen-bond donor binds to the best hydrogen-bond acceptor and the second-best donor binds to the second-best acceptor.

The best acceptor, the 2-methylbenzimidazol-1-yl moiety, forms an O–H···N hydrogen bond with the best donor, the stronger acid, 3,5-dinitrobenzoic acid (O47···N13, 2.553(3) Å). The second-best acceptor, the pyridyl moiety, binds to the weaker acid (4-nitrobenzoic acid) *via* an O–H···N hydrogen bond (O37···N21, 2.641(3) Å).

7.3.16 Crystal structure of 4-nitrobenzoic acid 3-(2-chlorobenzimidazol-1-yl)methylpyridine 4-cyanobenzoic acid, **55**

The crystal structure determination of **55** reveals a disordered 1:1:1 ternary co-crystal, Figure 7.18, where the 4-cyanobenzoic acid molecule is 60% occupied. The remaining 40% occupancy is completed by 4-nitrobenzoic acid.

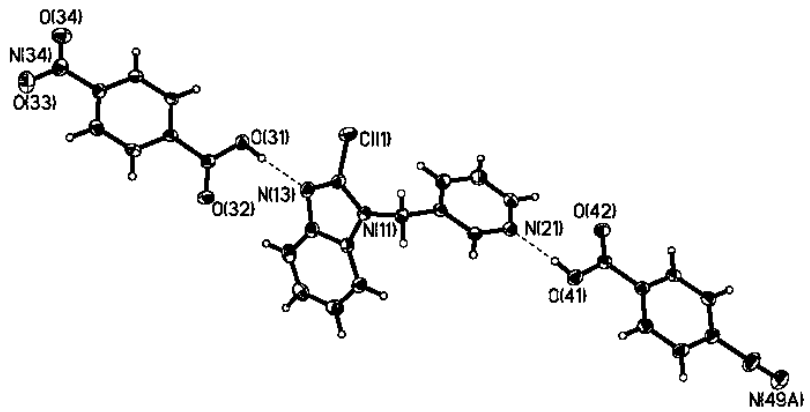

Figure 7.18 Ternary co-crystal in **55**.

The stronger acid, 4-nitrobenzoic acid, hydrogen-bonds to the 2-chlorobenzimidazol-1-yl nitrogen site (O31···N13, 2.6764(14) Å), thereby leaving the weaker acid (4-cyanobenzoic acid) to interact with the pyridyl nitrogen atom (O41···N21, 2.6551(14) Å).

7.4 Discussion

Asymmetric pyridyl-benzimidazol-1-yl and pyrimidyl-benzimidazol-1-yl SR's readily formed several binary co-crystals/hydrates and salts, **42**-**50**, with carboxylic acids and water molecules, Scheme 7.2.

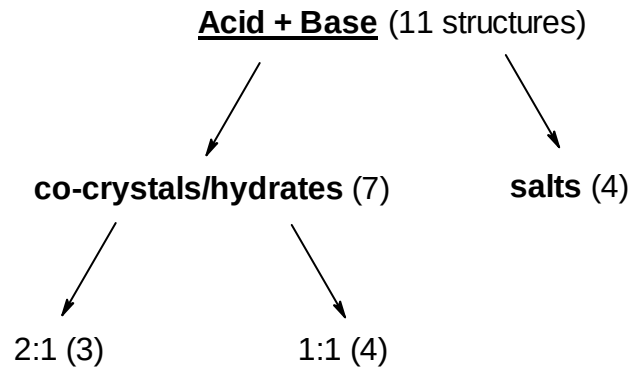

Scheme 7.2 Classification of binary structures resulting from supramolecular reactions between carboxylic acids and asymmetric pyridyl-benzimidazol-1-yl and pyrimidyl-benzimidazol-1-yl SR's. The values in parentheses indicate the number of structures obtained in each case.

The presence of only one co-crystallizing agent determined either a 1:1 (four structures) or 2:1 (three structures) co-crystal/hydrate, or salt (four structures). Formation of salts led to unpredictable motifs, as the carboxylate moieties possess more diffuse electrostatic regions, thereby becoming a strong hydrogen-bond acceptor. Both 1:1 and 2:1 compositions are obtained for co-crystals and hydrates. When a 1:1 co-crystal/hydrate is formed, the correct selectivity is displayed in all four structures, with preference for the benzimidazol-1-yl nitrogen atom of the SR (a 100% supramolecular yield).

Since these SR's were specifically designed for the construction of ternary supermolecules, structures **51**-**55** were obtained through the deliberate use of directional intermolecular synthetic operations. Each SR has two binding sites that differ primarily in their basicity but neither site is otherwise biased or predisposed towards interacting preferentially with either of the two competing carboxylic acids. The differences in basicity are translated into supramolecular reactivity and selectivity that subsequently carry over into the solid state, which demonstrates that supramolecular assembly can be controlled by fine-tuning individual binding sites. It seems, therefore, that when the basicities of the two heterocycles are significantly different, as in 3-(benzimidazol-1-yl)methylpyridine and 3-(2-methylbenzimidazol-1-yl)methylpyridine (by about one pK_a unit), the desired selectivity is witnessed. This raises the possibility that a solution to the problem of making non-covalent one-pot synthesis "sequential" may be to devise modular assembly processes based upon a hierarchy of intermolecular interactions derived from molecular properties and structural trends.

It should be emphasized that ternary co-crystals are extremely rare and that the supramolecular reagents presented in this chapter contribute to high-yielding reactions -- in a supramolecular sense, this translates to high frequency of occurrence of a particular intermolecular binding pattern in the presence of potentially disruptive intermolecular interactions. All four ternary co-crystals obtained in this study display the intended selectivity (**51**-**54**), a 100% supramolecular yield.

The only SR possessing moieties of similar basicities is 3-(2-chlorobenzimidazol-1-yl)methylpyridine (Scheme 7.1c), with the pyridyl moiety in this case displaying a slightly greater basicity than the 2-chlorobenzimidazol-1-yl nitrogen acceptor. This

situation, in principle, may lead to a lack of selectivity in this SR and, consequently, to a mixture of supramolecular products in the presence of two different carboxylic acids.[20] The structural selectivity in **55** cannot be ascertained due to disorder about the 4-cyanobenzoic acid molecule.

7.5 Conclusions

The SR's presented in this chapter were able to form ternary co-crystals with a high degree of selectivity and specificity using a "hierarchical" concept of non-covalent interactions. These SR's will at some point undoubtedly generate results that do not acquiesce to the proposed assembly principles. However, through covalent synthesis we have unlimited opportunities for modulating the electronic and geometric details of each binding site on a supramolecular reagent such that a variety of chemical functionalities can be targeted for binding. In this way we can build a team of SR's where each member is capable of affecting the assembly of new supermolecules with a high degree of specificity and reliability, thereby clearing a path towards practical and transferable guidelines for versatile supramolecular synthesis. We are currently probing the limits and limitations of this hierarchical approach to non-covalent synthesis by examining the structural reactivity of libraries of supramolecular reagents containing multiple binding sites with easily adjustable differences in hydrogen-bonding donating/accepting capabilities. We will therefore continue to investigate this hierarchical strategy in Chapters 8 and 9.

References

[1] (a) Aakeröy, C. B. *Acta Crystallogr. Sect. B*. **1997**, *53*, 569. (b) Moulton, B.; Zaworotko, M. J. *Chem. Rev*. **2001**, *101*, 1629. (c) Desiraju, G. R. *Acc. Chem. Res*. **2002**, *35*, 565. (d) Hosseini, M. W. *CrystEngComm* **2004**, *6*, 318. (e) MacGillivray, L. R. *CrystEngComm* **2004**, *6*, 77. (f) Brammer, L. *Chem. Soc. Rev*. **2004**, *33*, 476. (g) Aakeröy, C. B.; Beatty, A. M. *Aus. J. Chem.* **2001**, *54*, 409. (h) Lehn, J. –M. *Supramolecular Chemistry*; VCH: Weinheim, 1995. (i) Caulder, D. L.; Raymond, K. N. *Acc. Chem. Res.* **1999**, *32*, 975. (j) Reinhoudt, D. N.; Crego-Calama, M. *Science* **2002**, *295*, 2403. (k) Lehn, J. –M. *Science* **2002**, *295*, 2400. (l) Braga, D.; Desiraju, G.; Miller, J. S.; Orpen, A. G.; Price, S. L. *CrystEngComm* **2002**, *4*, 500. (m) Braga, D.; Maini, L.; Polito, M.; Grepioni, F. *Structure and Bonding* **2004**, *111*, 1. (n) Lewis, G.; Orpen, A. G. *Chem. Commun*. **1998**, 1873. (o) Prins, L. J.; Reinhoudt, D. N.; Timmerman, P. *Angew. Chem. Int. Ed.* **2001**, *40*, 2382. (p) Zimmerman, S. C.; Corbin, P. S. *Struct. Bond.* **2000**, *96*, 63.

[2] Dunitz, J. D. *Perspectives in Supramolecular Chemistry: The Crystal as a Supramolecular Entity*; ed. Desiraju, G. R.; Wiley, 1995.

[3] Many binary co-crystals based on principles of molecular recognition have, however, been reported *e.g*. (a) Shan, S.; Batchelor, E.; Jones, W. *Tetrahedron Lett.* **2002**, *43*, 8721. (b) Bailey Walsh, R. D.; Bradner, M. W.; Fleischman, S.; Morales, L. A.; Moulton, B.; Rodriguez-Hornedo, N.; Zaworotko, M. J. *Chem. Commun*. **2003**, 186. (c) MacGillivray, L. R.; Reid, J. L.; Ripmeester, J. A. *J. Am. Chem. Soc.* **2000**, *122*, 7817. (d) Vishweshwar, P.; Thaimattam, R.; Jaskolski, M.; Desiraju, G. R. *Chem. Commun.* **2002**, 1830. (e) Zerkowski, J. A.; MacDonald, J. C.; Whitesides, G. M. *Chem. Mater*. **1997**, *9*, 1933. (f) Kane, J. J.; Liao, R. –F.; Lauher, J. W.; Fowler, F. W. *J. Am. Chem. Soc.* **1995**, *117*, 12003. (g) Lehn, J. –M.; Mascal, M.; DeCian, A.; Fischer, J. *J. Chem. Soc., Chem. Commun.* **1990**, 479. (h) Almarsson, Ö.; Zaworotko, M. J. *Chem. Commun*. **2004**, 1889.

[4] (a) Desiraju, G. R.; Sarma, J. A. R. P. *Chemical Comm*. **1983**, 45. (b) Huang, C.; Leiserowitz, L.; Schmidt, G. M. *J. Chem. Soc., Perkin Trans. 2* **1973**, 503. (c) Pan, F.; Wong, W. S.; Gramlich, V.; Bosshard, C.; Gunter, P. *Chem. Commun.* **1996**, 2. (d) Pedireddi, V. R.; Jones, W.; Chorlton, A. P.; Docherty, R. *Chem. Commun*. **1996**, 997. (e) Vishweshwar, P.; Nangia, A.; Lynch, V. M. *J. Org. Chem.* **2002**, *67*, 556. (f) Aakeröy, C. B.; Beatty, A. M.; Nieuwenhuyzen, M.; Zou, M. *Tetrahedron* **2000**, *56*, 6693. (g) Dale, S. H.; Elsegood, M. R. J.; Hemmings, M.; Wilkinson, A. L. *CrystEngComm* **2004**, *6*, 207. (h) Remenra, J. F.; Morisette, S. L.; Peterson, M. L.; Moulton, B.; MacPhee, J. M.; Guzman, H. R.; Almarsson, Ö. *J. Am. Chem. Soc.* **2003**, *125*, 8456.

[5] Aakeröy, C. B.; Desper, J.; Helfrich, B. A. *CrystEngComm* **2004**, *6,* 19.

[6] Aakeröy, C. B.; Beatty, A. M.; Helfrich, B. A. *Angew. Chem. Int. Ed*. **2001**, *40*, 3240.

[7] Aakeröy, C. B.; Beatty, A. M.; Helfrich, B. A.; Nieuwenhuyzen, M. *Cryst. Growth Des.* **2003**, *3*, 159.

[8] Koefler's complex is a solvate (pyridine), and its preparation was not based upon an explicit supramolecular strategy. Bernstein, J.; Regev, H.; Herbstein, F. H. *Acta Crystallogr. Sect. B* **1980**, *36*, 1170.

[9] A three-component co-crystal based on isomorphous replacement with acridine in a 2:3 2,2'-dihydroxybiphenyl phenazine co-crystal has been reported. This approach relies on molecular complementarity and recognition and may be effective in the design of other ternary systems. Smolka, T.; Boese, R.; Sustmann, R. *Struct. Chem.* **1999**, *10*, 429.

[10] A 3:1:1 ternary co-crystal has been reported previously although no explicit design strategy was evident. Lynch, D. E.; Smith, G.; Byriel, K. A.; Kennard, C. H. L. *J. Chem. Soc., Chem. Commun.* **1992**, 300.

[11] The term "ternary supermolecule" indicates a discrete species with predictable and desirable connectivity, constructed from three different molecular species and assembled *via* directional non-covalent forces. Thus, ternary systems formed by ionic interactions (salts) or by incorporation of solvent molecules within a lattice (*e.g*. clathrates, solvates, or inclusion compounds) are distinctly different from the supermolecules that we discuss in this chapter.

[12] Desiraju, G. R. *Angew. Chem. Int. Ed. Engl*. **1995**, *34*, 2311.

[13] To date, more than ten ternary co-crystals based around *iso*nicotinamide or nicotinamide with two different carboxylic acids are known, and the stronger acid binds to the pyridine moiety, and the weaker acids binds to the amide functionality in each case.

[14] (a) Etter, M. C. *Acc. Chem. Res.* **1990**, *23*, 120. (b) Etter, M. C. *J. Phys. Chem*. **1991**, *95*, 4601.

[15] Approaches such as this are also predicated upon the idea that a small number of specific intermolecular interactions can provide a significant part of the stabilization energy of molecular crystals. Dauber, P.; Hagler, A. T. *Acc. Chem. Res.* **1980**, *13*, 105.

[16] The calculations were performed using ACD/Solaris v4.76; Advanced Chemistry Development, Inc.: Toronto, ON, Canada, www.acdlabs.com, 1994–2005.

[17] (a) Laurence, C.; Berthelot, M. *Persp. Drug Disc. Design* **2000**, *18*, 39. (b) Abraham, M. H. *Chem. Soc. Rev.* **1993**, *22*, 73. (c) Shan, S.; Loh, S.; Herschlag, D. *Science* **1996**, *272*, 97.

[18] Aakeröy, C. B.; Desper, J.; Leonard, B.; Urbina, J. F. *Cryst. Growth Des*. **2005**, DOI: 10.1021/cg049682i.

[19] 3,5-dinitrobenzoic acid (pK_a = 2.8); 4-nitrobenzoic acid (pK_a = 3.44); 3-*N,N*-dimethylaminobenzoic acid (pK_a = 4.30); 4-cyanobenzoic acid (pK_a = 3.55). Kartum, G.; Vogel, W.; Andrussov, K. *Dissociation constants of organic acids in aqueous solution*, 1961.

[20] Due to the fact that all these co-crystallization reactions may yield crystals of each reagent by itself, five possible binary co-crystals (the SR plus one of the two carboxylic acids in either 1:1 or 1:2 stoichiometry, or a heteromeric acid···acid co-crystal), or of the desired 1:1:1 ternary product, it is important to carry out analysis of individual crystallites. The combination of TLC and NMR, when performed on individual crystals, will give information about which of the three species are present as well as their relative ratios. Single-crystal X-ray crystallography is required in order to determine the connectivity of the supermolecule (and hence the selectivity of the supramolecular reagent).

[21] A binary compound of the strong acid and the SR as determined by TLC and NMR.

[22] The overall yield of **52** was approximately 50% and significantly higher for the other ternary co-crystals.

[23] TLC analysis of individual crystallites showed only two spots, one for the SR and the other as a streak.

[24] SMART v5.060; Bruker Analytical X-ray Systems: Madison, WI, 1997–1999.

[25] SAINT v6.02; Bruker Analytical X-ray Systems: Madison, WI, 1997–1999.

[26] SHELXTL v5.10; Bruker Analytical X-ray Systems: Madison, WI, 1997.

Chapter 8

A continued study of binary and ternary co-crystals using asymmetric supramolecular reagents

8.1 Introduction

As shown in Chapter 7, asymmetric pyridyl/benzimidazol-1-yl supramolecular reagents (SR's) can guide the supramolecular assembly of ternary co-crystals when introduced to two carboxylic acids with different pK_a values according to the best donor/best acceptor, second-best donor/second-best acceptor concept.[1] Furthermore, imidazol-1-yl- and benzimidazol-1-yl-based SR's are each capable of forming co-crystals with a variety of hydrogen-bond donors (Chapters 3, 5, and 7). Thus, we reasoned that SR's with *both* heterocyclic moieties attached to the same backbone could, in principle, give rise to ternary supermolecules in the presence of two different carboxylic acids. In this chapter, we will explore the structural selectivity and specificity of asymmetric SR's 4-[(benzimidazol-1-yl)methyl]-imidazol-1-ylbenzene, Scheme 8.1a, and 4-[(2-methylbenzimidazol-1-yl)methyl]-imidazol-1-ylbenzene, Scheme 8.1b.

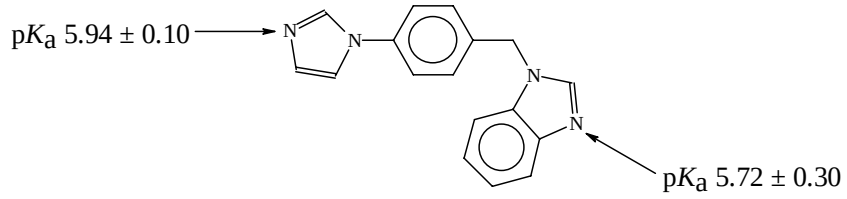

(a)

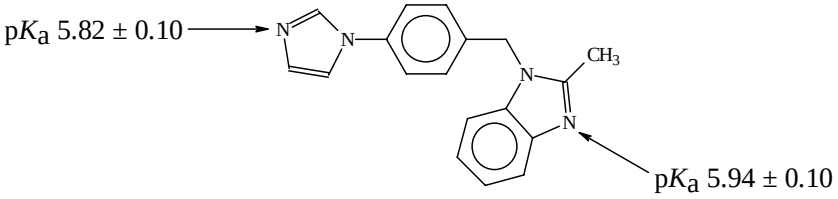

(b)

Scheme 8.1 Asymmetric SR's, (a) 4-[(benzimidazol-1-yl)methyl]-imidazol-1-ylbenzene, and (b) 4-[(2-methylbenzimidazol-1-yl)methyl]-imidazol-1-ylbenzene.

As in pyridyl/benzimidazol-1-yl SR's, the two acceptor sites are uncoupled, which provides the opportunity to independently fine-tune their basicities through electron-donating and electron-withdrawing substituents. The pK_a values of each SR were also calculated in the same manner as in Chapter 7,[2] but they now in each case indicate a much smaller difference in basicity between the two heterocyclic nitrogen sites. It is still useful, however, to determine whether these SR's can facilitate the formation of ternary co-crystals. Similarly to pyridyl/benzimidazol-1-yl SR's, the benzimidazol-1-yl moieties in each case are linked to a central phenyl ring through a methylene bridge in order to enhance solubility.

As shown in Chapter 3, a useful indication of co-crystal formation can be obtained through IR spectroscopy, particularly the presence of heteromeric O–H···N hydrogen bonds between O–H donors and N-heterocyclic moieties. These relevant interactions have been studied in carboxylic acid-pyridine,[3] carboxylic acid-benzimidazole,[4] and carboxylic acid-imidazol-1-yl/benzimidazol-1-yl[5] systems, all of which show two characteristic broad O–H···N stretches, one between 2600-2500 cm^{-1}, and the other at about 1900 cm^{-1}. Strictly speaking, co-crystal formation could also be driven by other intermolecular interactions,[6] *e.g.* π···π stacking, even though the molecular components are intended to form heteromeric interactions, and as such the expected IR stretches would not be observed.

We will carry out IR analyses of binary and ternary co-crystallization experiments using 4-[(benzimidazol-1-yl)methyl]-imidazol-1-ylbenzene and 4-[(2-methylbenzimidazol-1-yl)methyl]-imidazol-1-ylbenzene each with various co-crystallizing agents to detect the presence of these "marker" bands. Through these analyses we will determine the supramolecular yields (the frequency or occurrence of O–H···N hydrogen-bond formation in each set of experiments) of the two SR's and, thus, attempt to establish their supramolecular efficiencies.

8.2 Experimental

8.2.1 Synthesis

All starting materials were obtained from Aldrich and used without further purification. Melting points were determined on a Fisher-Johns melting point apparatus and are uncorrected.

8.2.1.1 Synthesis of 4-[(benzimidazol-1-yl)methyl]-bromobenzene

Benzimidazole (1.42 g, 12.0 mmol) was dissolved in 100 mL of dry THF with stirring at room temperature in a 250 mL round-bottomed flask. To this solution was added NaOH pellets (6.40 g, 160 mmol), and the reaction mixture was stirred for 2 h under a N_2 atmosphere. 4-Bromobenzyl bromide (3.00 g, 12.0 mmol) was then added all at once to the reaction mixture to immediately produce a white suspension. This mixture was stirred for 12 h at room temperature under a N_2 atmosphere. Distilled water (100 mL) was then added to it to dissolve excess NaOH pellets and NaBr that had formed during the reaction, and formed two layers, which were separated by using a separatory funnel. The THF layer was dried over anhydrous Na_2SO_4 overnight, the Na_2SO_4 filtered by vacuum filtration, and the filtrate concentrated *via* rotary evaporation to give the crude product as an off-white solid. The crude product was then washed with cold distilled water and dried to afford the pure product as a pale yellow solid. Yield 2.97 g (86.2%); m.p. 83-85˚C; ^{1}H NMR (DMSO-d_6, 400 MHz) δ 5.49 (s, 2H), 7.20 (m, 2H), 7.26 (d, 2H, J = 8.4 Hz), 7.49 (m, 1H), 7.53 (d, 2H, J = 8.4 Hz), 7.66 (m, 1H), 8.40 (s, 1H).

8.2.1.2 Synthesis of 4-[(2-methylbenzimidazol-1-yl)methyl]-bromobenzene

2-Methylbenzimidazole (1.59 g, 12.0 mmol) was dissolved in 100 mL of dry THF with stirring at room temperature in a 250 mL round-bottomed flask. To this solution was added NaOH pellets (6.40 g, 160 mmol) and the resulting mixture stirred for 2 h under a N_2 atmosphere. 4-Bromobenzyl bromide (3.00 g, 12.0 mmol) was then added all at once to the reaction mixture upon which a pale yellow suspension formed immediately. Stirring was continued for 12 h at room temperature under a N_2 atmosphere. Distilled water (100 mL) was then added to the mixture to dissolve the excess NaOH pellets, as well as NaBr that had formed during the reaction, to produce two layers. These layers were separated using a separatory funnel and the THF layer dried over anhydrous Na_2SO_4 overnight. The Na_2SO_4 was filtered by vacuum filtration and the pale yellow filtrate was

concentrated *via* rotary evaporation to afford the pure product as a pale yellow-brown syrup, which turned into a microcrystalline pale yellow-brown solid. Yield 2.81 g (78.1%); m.p. 66-70˚C; ^{1}H NMR (DMSO-d_6, 400 MHz) δ 2.50 (s, 3H), 5.44 (s, 2H), 7.07 (d, 2H, J = 8.8 Hz), 7.15 (m, 2H), 7.43 (m, 1H), 7.52 (d, 2H, J = 8.4 Hz), 7.55 (m, 1H).

8.2.1.3 Synthesis of 4-[(benzimidazol-1-yl)methyl]-imidazol-1-ylbenzene[7]

4-[(Benzimidazol-1-yl)methyl]-bromobenzene (5.00 g, 17.4 mmol) was dissolved in 25 mL of anhydrous 1,4-dioxane with stirring in a 100 mL three-necked flask under a N_2 atmosphere. Imidazole (1.42 g, 20.9 mmol), anhydrous K_2CO_3 (5.06 g, 36.6 mmol), *trans*-1,2-cyclohexanediamine (0.40 g, 3.49 mmol), and CuI (0.33 g, 1.74 mmol) were then added to the reaction mixture, which immediately formed a bright blue suspension. This mixture was heated and stirred at 110˚C under a N_2 atmosphere and continuously monitored by TLC. After 5 days, the reaction mixture was cooled to room temperature and purified by column chromatography using silica gel (200-425 mesh), and ethyl acetate : hexanes 1:3, 1:2, and ethyl acetate as eluents. Rotary evaporation of the ethyl acetate fractions yielded the pure product as a dark brown solid. Yield 1.03 g (21.6%); m.p. 125-130˚C; ^{1}H NMR (DMSO-d_6, 400 MHz) δ 5.55 (s, 2H), 7.08 (s, 1H), 7.20 (m, 2H), 7.46 (d, 2H, J = 8.8 Hz), 7.56 (m, 1H), 7.62 (d, 2H, J = 8.4 Hz), 7.66 (m, 1H), 7.70 (s, 1H), 8.21 (s, 1H), 8.45 (s, 1H).

8.2.1.4 Synthesis of 4-[(2-methylbenzimidazol-1-yl)methyl]-imidazol-1-ylbenzene[7]

4-[(2-Methylbenzimidazol-1-yl)methyl]-bromobenzene (1.00 g, 3.32 mmol) was dissolved in 3.4 mL of anhydrous 1,4-dioxane with stirring in a 100 mL three-necked flask under a N_2 atmosphere. To this solution was added imidazole (0.27 g, 3.99 mmol), anhydrous K_2CO_3 (0.96 g, 6.98 mmol), *trans*-1,2-cyclohexanediamine (0.08 g, 0.66 mmol), and CuI (0.03 g, 0.17 mmol). The suspension turned bright blue and was heated and stirred at 110˚C under a N_2 atmosphere. Monitoring by TLC indicated that the reaction was complete after 72 h, and at this point the dark brown reaction mixture was cooled to room temperature. The mixture was then diluted with 3 mL of ethyl acetate and filtered through a plug of silica gel with continuous amounts of ethyl acetate until the filtrate turned colorless. The filtrate was then concentrated by rotary evaporation to give

the crude product. Purification of the crude product by column chromatography using silica gel (200-425 mesh) and ethyl acetate : hexanes 1:1, 3:1, and ethyl acetate, followed by concentration of the ethyl acetate fractions by rotary evaporation gave the pure product as a pale brown solid. Yield 0.22 g (22.5%); m.p. 95-98˚C; ^{1}H NMR (DMSO-d_6, 400 MHz) δ 2.54 (s, 3H), 5.52 (s, 2H), 7.08 (s, 1H), 7.16 (m, 2H), 7.25 (d, 2H, J = 8.4 Hz), 7.49 (m, 1H), 7.56 (m, 1H), 7.60 (d, 2H, J = 8.8 Hz), 7.69 (s, 1H), 8.20 (s, 1H).

8.2.2 General procedure for syntheses of binary co-crystals

4-[(Benzimidazol-1-yl)methyl]-imidazol-1-ylbenzene and either a carboxylic acid, oxime, carboxamide, or *bis*-phenol were combined in a 1:1 molar ratio and dissolved in a minimum amount of absolute ethanol. Amorphous solids were obtained after about two weeks of slow evaporation of the solvent, and examined by IR spectroscopy.

8.2.3 General procedure for syntheses of ternary co-crystals

4-[(2-Methylbenzimidazol-1-yl)methyl]-imidazol-1-ylbenzene was added to ethanolic solutions each containing two different carboxylic acids in 1:1:1 stoichiometries, and the resulting solutions allowed to evaporate under ambient conditions. Amorphous solids were afforded after about two weeks, and characterized by IR spectroscopy.

8.2.4 Infrared spectroscopy of binary and ternary co-crystals

All samples were prepared for IR analysis as KBr discs. IR spectroscopy of co-crystals was performed using a Protégé™ 460 E.S.P.™ FT-IR spectrometer,[8] and the data analyzed with the Nicolet OMNIC® software[8] between 4000 and 400 cm^{-1}.

8.3 Results

Table 8.1 summarizes the O–H···N hydrogen-bond IR bands of binary and ternary co-crystallization experiments carried out using 4-[(benzimidazol-1-yl)methyl]-imidazol-1-ylbenzene and various co-crystallizing agents. Table 8.2 incorporates the O–H···N hydrogen-bond IR frequencies of ternary co-crystallization experiments with 4-[(2-methylbenzimidazol-1-yl)methyl]-imidazol-1-ylbenzene and two different co-crystallizing agents.

Table 8.1 IR data for binary and ternary co-crystallization experiments carried out using 4-[(benzimidazol-1-yl)methyl]-imidazol-1-ylbenzene and several co-crystallizing agents.

Experiment	Compound A	Compound B	$\nu_{O-H\cdots N}$ (cm^{-1})
1	3,5-dinitrobenzoic acid[9]	–	–
2	4-nitrobenzoic acid	–	2578, 1942
3	2,3-dimethylbenzoic acid	–	2511, 1942
4	succinic acid	–	2589, 1918
5	4-bromophenyl-acetyloxime	–	–
6	3,5-dinitrobenzamide[10]	–	–
7	resorcinol	–	–
8	3,5-dinitrobenzoic acid	4-nitrobenzoic acid	2444, 1918
9	3,5-dinitrobenzoic acid	3-*N*,*N*-dimethylamino-benzoic acid	2499, 1918
10	3-nitrobenzoic acid	4-cyanobenzoic acid	2509, 1918

Table 8.2 IR data for ternary co-crystallization experiments with 4-[(2-methylbenzimidazol-1-yl)methyl]-imidazol-1-ylbenzene and various co-crystallizing agents.

Experiment	Compound A	Compound B	$\nu_{O-H\cdots N}$ (cm^{-1})
11	3,5-dinitrobenzoic acid	4-cyanobenzoic acid	2427, 1918
12	4-nitrobenzoic acid	4-cyanobenzoic acid	2444, 1942
13	4-nitrobenzoic acid	3-*N*,*N*-dimethylaminobenzoic acid	2443, 1918
14	4-nitrobenzoic acid	3-hydroxycinnamic acid	2441, 1902
15	4-cyanobenzoic acid	3-*N*,*N*-dimethylaminobenzoic acid	2450, 1932
16	4-cyanobenzoic acid	3,5-dimethylbenzoic acid	2443, 1918
17	4-cyanobenzoic acid	4-chlorobenzoic acid	2473, 1932
18	2-fluorobenzoic acid	4-hydroxy-3-methoxycinnamic acid	2583, 1918
19	2-fluorobenzoic acid	3-*N*,*N*-dimethylaminobenzoic acid	2484, 1918
20	3-*N*,*N*-dimethylaminobenzoic acid	4-bromophenyl-acetyloxime	–

Table 8.2 (continued) IR data for ternary co-crystallization experiments with 4-[(2-methylbenzimidazol-1-yl)methyl]-imidazol-1-ylbenzene and various co-crystallizing agents.

Experiment	Compound A	Compound B	$\nu_{O-H\cdots N}$ (cm^{-1})
21	3,5-dinitrobenzoic acid	4-chlorobenzoic acid	–
22	3,5-dinitrobenzoic acid	4-nitrobenzoic acid	2491, 1918
23	3,5-dinitrobenzoic acid	3-*N*,*N*-dimethylaminobenzoic acid	2613, 1918
24	3,5-dinitrobenzoic acid	4-*N*,*N*-dimethylaminobenzoic acid	–
25	4-nitrobenzoic acid	4-*N*,*N*-dimethylaminobenzoic acid	–
26	4-cyanobenzoic acid	4-*N*,*N*-dimethylaminobenzoic acid	2560, 1918
27	3,5-dinitrobenzoic acid	3-iodobenzoic acid	2591, 1918
28	3,5-dinitrobenzoic acid	3-cyanobenzoic acid	2527, 1918
29	4-iodobenzoic acid	pentamethylbenzoic acid	2492, 1942
30	3,5-dinitrobenzoic acid	pentamethylbenzoic acid	2530, 1918
31	4-nitrobenzoic acid	pentamethylbenzoic acid	2478, 1942
32	4-cyanobenzoic acid	pentamethylbenzoic acid	2474, 1942
33	3,5-dinitrobenzoic acid	2,3-dimethylbenzoic acid	–
34	4-nitrobenzoic acid	2,3-dimethylbenzoic acid	2512, 1900
35	4-cyanobenzoic acid	2,3-dimethylbenzoic acid	2468, 1942
36	3-nitrobenzoic acid	4-cyanobenzoic acid	2498, 1942
37	2-nitrobenzoic acid	4-cyanobenzoic acid	2490, 1942
38	3,5-dinitrobenzoic acid	3-nitrobenzoic acid	2499, 1918

8.4 Discussion

IR analyses of both binary and ternary co-crystallization experiments involving both SR's and various co-crystallizing agents did provide an indication of co-crystal formation *via* the presence of characteristic broad O–H···N stretches between 2613-2427 cm^{-1} and

1942-1900 cm^{-1}. These bands fall within the range of typical values addressed in previous studies (2600-2500 cm^{-1} and ca. 1900 cm^{-1}).[3,4,5] These bands do not allow us to distinguish between binary and ternary co-crystals, since the differences in stretching frequencies of the two distinct heteromeric O–H···N interactions are not expected to be significant. We can state, however, that in IR spectra of ternary co-crystallization experiments displaying these bands, at least a binary co-crystal had formed. In the case of binary co-crystallization experiments, the presence of O–H···N stretches in their IR spectra directly points to the formation of the desired co-crystal.

The IR spectrum of ternary co-crystallization experiment **29** (also see Table 8.2), comprising 4-[(2-methylbenzimidazol-1-yl)methyl]-imidazol-1-ylbenzene, 4-iodobenzoic acid, and pentamethylbenzoic acid, is a typical example of an IR spectrum containing the two O–H···N stretches indicative of co-crystal formation, Figure 8.1.

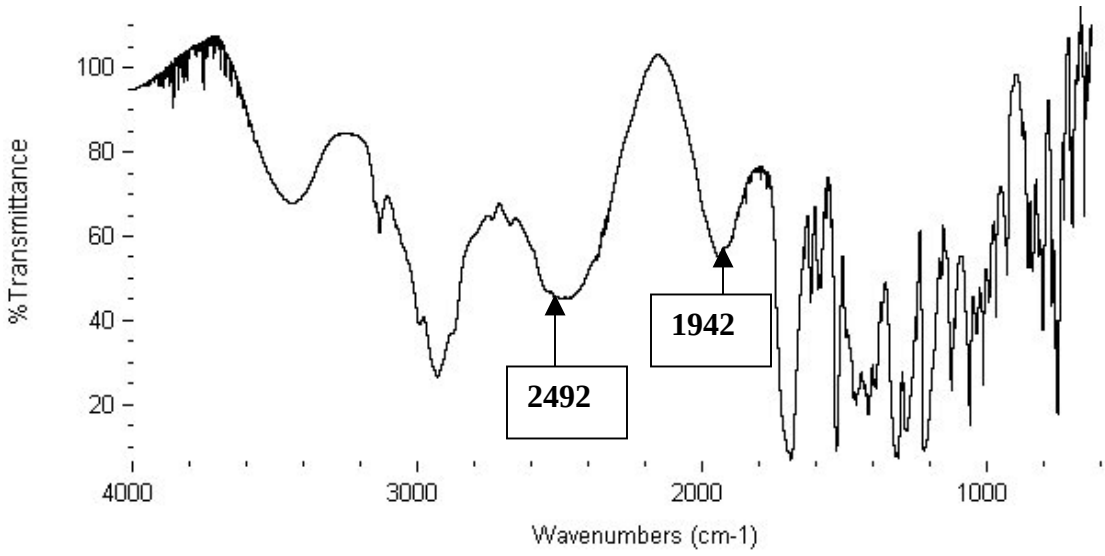

Figure 8.1 IR spectrum of a ternary co-crystallization attempt indicative of co-crystal formation involving 4-[(2-methylbenzimidazol-1-yl)methyl]-imidazol-1-ylbenzene, 4-iodobenzoic acid, and pentamethylbenzoic acid, **29**, pointing out to the two broad O–H···N bands at 2492 cm^{-1} and 1942 cm^{-1}.

Having established co-crystal formation by IR spectroscopy, the supramolecular yield of 4-[(benzimidazol-1-yl)methyl]-imidazol-1-ylbenzene was determined. IR spectra containing the SR 4-[(benzimidazol-1-yl)methyl]-imidazol-1-ylbenzene (Table 8.1) shows successful co-crystal formation in six out of the total ten attempts, equating to a

60% supramolecular yield. This yield includes attempts with 4-bromophenylacetyloxime, **5**; 3,5-dinitrobenzamide, **6**; and resorcinol, **7**. None of these compounds formed co-crystals, which may be the reason why they are not popular choices as hydrogen-bond donors for *N*-heterocycles. On the other hand, the use of carboxylic acids gave rise to all six co-crystals, which emphasizes why such supramolecular synthons have become successful in organic crystal engineering. Similar results were obtained in Chapter 3, whereby *bis*-imidazol-1-yl/benzimidazol-1-yl SR's, given a choice for co-crystal formation with carboxylic acids, oximes, or carboxamides, showed a clear preference for binary co-crystal formation with carboxylic acids.

Attempts at forming binary and ternary crystalline samples suitable for X-ray crystallography with 4-[(benzimidazol-1-yl)methyl]-imidazol-1-ylbenzene and 4-[(2-methylbenzimidazol-1-yl)methyl]-imidazol-1-ylbenzene, each with several co-crystallizing agents, proved futile. It is not likely that the failure to produce single crystals is due to the solubility of the SR's, since they are comparatively soluble to the pyridyl/benzimidazol-1-yl SR's. However, the pK_a differences of the heterocyclic moieties in each SR may not be sufficient for them to display the intended selectivity (see Schemes 8.1a and 8.1b). It is possible, therefore, that a mixture of products for both binary and ternary (three and eight possible combinations respectively) co-crystallizations was obtained, Schemes 8.2 and 8.3 respectively.

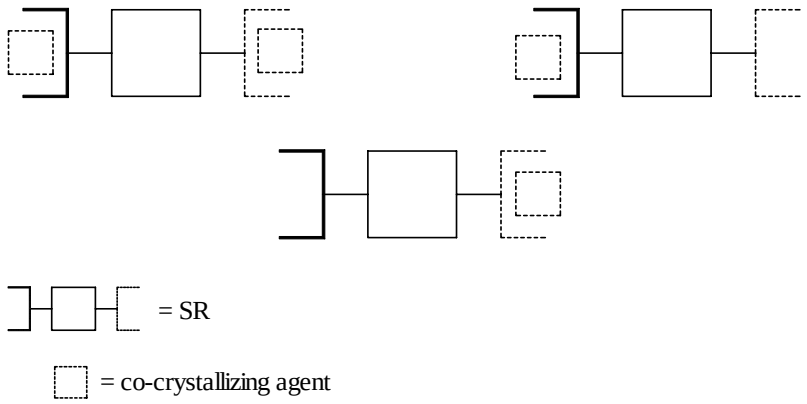

Scheme 8.2 Possible combinations in binary experiments involving imidazol-1-yl-benzimidazol-1-yl SR's and co-crystallizing agents.

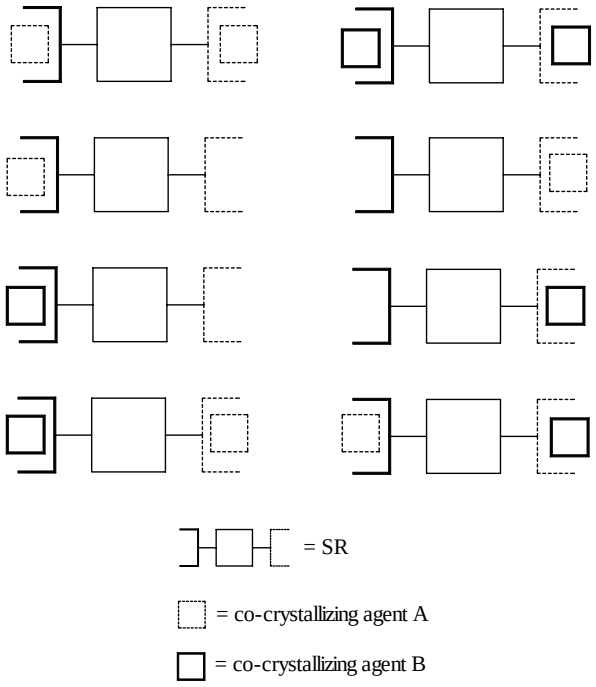

Scheme 8.3 Possible combinations in ternary experiments involving imidazol-1-yl-benzimidazol-1-yl SR's and co-crystallizing agents.

The possible presence of these impurities could prevent the formation of suitable crystals and, as a result, the structural selectivity and specificity of each SR for the co-crystallizing partner(s) remains unknown.

We attempted to employ other means of characterization such as TLC and powder XRD in order to obtain useful information about the compositions of the co-crystallization experiments, but they could not be used due to the amorphous and/or oily nature of these products. TLC could not provide accurate information about the number of components present in these solids, while powder XRD analysis could not distinguish between the formations of binary or ternary compounds.

8.5 Conclusions

The supramolecular reactions between two asymmetric imidazol-1-yl/benzimidazol-1-yl-based SR's and a variety of hydrogen-bond donors were determined by IR spectroscopy. This study provides an alternative yet useful approach to understanding the solid-state behavior of the various components, and may become a reliable screening

method for determining co-crystal formation when presented with a multitude of individual supramolecular reactions.

Although the two SR's employed in this study did not produce crystalline samples, and did not allow us to explore their structural selectivities and specificities for the donor compounds involved, they can still be fine-tuned such that a greater difference between the two acceptor sites is achieved.

References

[1] Aakeröy, C. B.; Desper, J.; Urbina, J. F. *Chem. Commun.* **2005**, ASAP article.

[2] The corresponding pK_a values were calculated using ACD/Solaris v4.76; Advanced Chemistry Development, Inc.: Toronto, ON, Canada, www.acdlabs.com, 1994-2005.

[3] IR studies of the carboxylic acid···pyridine interaction have been carried out in both solid and liquid states. Examples include: (a) Johnson, S. L.; Rumon, K. A. *J. Phys. Chem.* **1965**, *69*, 74. (b) Drichko, N. V.; Yu. Kerenskaia, G.; Schreiber, V. M. *J. Mol. Struct.* **1999**, *477*, 127. (c) Langner, R.; Zundel, G. *J. Chem. Soc., Faraday Trans.* **1995**, *91*, 3831. (d) Lindemann, R.; Zundel, G. *J. Chem. Soc., Faraday Trans. 2* **1977**, *73*, 788.

[4] Trivedi, D. R.; Ballabh, A.; Dastidar, P. *CrystEngComm* **2003**, *5*, 358.

[5] (a) Aakeröy, C. B.; Desper, J.; Leonard, B.; Urbina, J. F. *Cryst. Growth Des.* **2005**, DOI: 10.1021/cg049682i. (b) Aakeröy, C. B.; Desper, J.; Elisabeth, E.; Helfrich, B. A.; Levin, B.; Urbina, J. F. *Zeit. Kristallogr.* **2005**, *220*, 325.

[6] Although rare, there are still examples of co-crystals formed through homomeric synthons, instead of the intended heteromeric interactions: (a) Sharma, C. V. K.; Panneerselvam, K.; Pilati, T.; Desiraju, G. R. *J. Chem. Soc., Perkin Trans. 2* **1993**, 2209. (b) Aakeröy, C. B.; Desper, J.; Helfrich, B. A. *CrystEngComm* **2004**, *6*, 19.

[7] (a) Antilla, J. C.; Baskin, J. M.; Barder, T. E.; Buchwald, S. L. *J. Org. Chem.* **2004**, *69*, 5578. (b) Klapars, A.; Antilla, J. C.; Huang, X.; Buchwald, S. L. *J. Am. Chem. Soc.* **2001**, *123*, 7727.

[8] Nicolet Instrument Corporation: Madison, WI 53711, 1997.

[9] Asymmetric (1534 cm^{-1}) and symmetric (1460 cm^{-1}) CO_2 stretches in the IR spectrum suggest the formation of a salt. Lin-Vien, D.; Colthup, N. B.; Fateley, W. G.; Grasselli, J. G. *The Handbook of Infrared and Raman Characteristic Frequencies of Organic Molecules*; Academic Press, Inc.: San Diego, CA, 1991.

[10] No broad N–H stretching bands corresponding to hydrogen-bonded N–H···N(pyridine) were observed at 3234-3374 cm^{-1} in co-crystallization **6** involving 3,5-dinitrobenzamide. Huang, B.; Parquette, J. R. *Org. Lett.* **2000**, *2*, 239.

Chapter 9

The quest for quaternary co-crystals

9.1 Introduction

In Chapter 7 it was demonstrated that SR's containing two distinct heterocyclic moieties can give rise to ternary co-crystals with predictable connectivities when combined with two different monocarboxylic acids.[1] The stronger carboxylic acid interacts with the more basic site while the weaker acid engages in hydrogen bonding with the less basic hydrogen-bond acceptor and, thus, follows the best donor-best acceptor, second best donor-second best acceptor guidelines. With this success, we reasoned that our hierarchical approach could result in a even higher level of complexity by designing a SR containing *three* different hydrogen-bond acceptor sites with the goal of making quaternary co-crystals, through a combination of heterocycles utilized in Chapters 7 and 8 (pyridine, benzimidazole, and imidazole), Scheme 9.1.

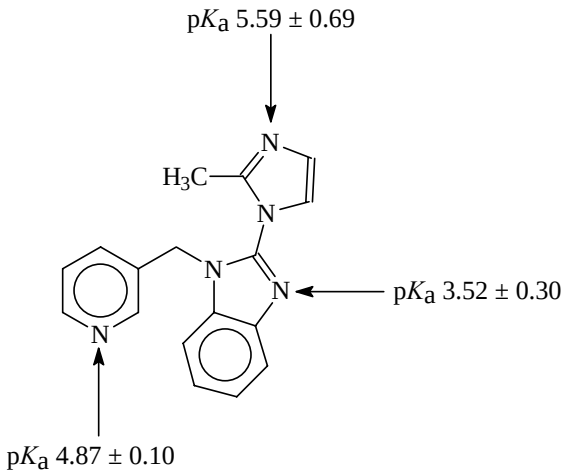

Scheme 9.1 Proposed strategy for quaternary supermolecules based upon an asymmetric SR, 3-[2-(2-methylimidazol-1-yl)benzimidazol-1-yl]-methylpyridine.

The basicities of these binding sites are in the order 2-methylimidazol-1-yl > pyridyl > benzimidazol-1-yl.[2] This SR is capable of forming co-crystals, since the binding sites possess reasonably different basicities, and the basicity of each heterocycle can be independently tuned through various substituents.

It was shown in previous chapters (i.e. Chapters 3, 4, and 7) that each heterocyclic moiety present in this SR is readily able to form co-crystals with carboxylic acids through reliable and robust heteromeric O–H···N hydrogen bonds.[1,3] This SR may also have the added benefit of good solubility in an array of polar solvents through a bridging methylene group, and this attribute is an important requirement for possible co-crystal formation.

A helpful starting point in understanding the hierarchical nature of intermolecular forces possible in this SR is to form binary co-crystals, since in Chapter 7 it was observed in 1:1 co-crystals that a single carboxylic acid, when given the choice of two different binding sites, preferentially hydrogen-bonds to the best acceptor. In this chapter, therefore, we will first attempt to generate binary co-crystals in order to begin exploring the structural selectivity and specificity of this SR, and consequently carry out co-crystallization experiments involving the SR and three different carboxylic acids with the ultimate goal of producing quaternary co-crystals with predictable connectivities.

9.2 Experimental

9.2.1 Synthesis

All starting materials were obtained from Aldrich and used without further purification. The synthesis of 3-(2-chlorobenzimidazol-1-yl)methylpyridine is reported in Chapter 7. Melting points were determined on a Fisher-Johns melting point apparatus and are uncorrected.

9.2.1.1 Synthesis of 3-[2-(2-methylimidazol-1-yl)benzimidazol-1-yl]-methylpyridine

2-Methylimidazole (2.02 g, 24.6 mmol) was dissolved in 60 mL of anhydrous DMF with stirring in a 500 mL three-necked flask under a N_2 atmosphere. To the clear, colorless solution was added NaH (1.18 g, 49.2 mmol) inside a glove bag under a N_2 atmosphere whereupon effervescence was observed. Once fizzing had subsided, the white cloudy suspension was heated and stirred under reflux for 1 h under a N_2 atmosphere. A solution containing 3-(2-chlorobenzimidazol-1-yl)methylpyridine (6.00 g, 24.6 mmol) in 120 mL of anhydrous DMF was added dropwise to the dark brown mixture using a dropping funnel, and the resulting mixture turned dark yellow-brown. This mixture was then

heated and stirred under reflux under a N_2 atmosphere, and the reaction progress followed by TLC. After 48 h, the deep brown reaction mixture was cooled to room temperature, the NaCl that formed during the reaction filtered *via* vacuum filtration, and the clear dark brown filtrate concentrated by rotary evaporation to obtain the crude product as a thick brown syrup. The crude product was purified by column chromatography using silica gel (200-425 mesh) and hexanes : ethyl acetate 5:1, 3:1, and 1:1, followed by ethyl acetate as eluents. Rotary evaporation of the ethyl acetate fractions afforded the desired product as a pale yellow microcrystalline solid. This solid was then washed with hexanes : ethyl acetate 3:2 (75 mL : 50 mL) with heat and the off-white solid isolated via vacuum filtration. The off-white solid was further washed with small portions of hexanes, dried, and collected to give the pure product. Slow evaporation of a 1 mL ethyl acetate solution containing 0.03 g of the pure product yielded colorless blocks after 2 days. Yield 4.84 g (68.1%); m.p. 115-117˚C; ^{1}H NMR (DMSO-d_6, 400 MHz) δ 2.00 (s, 3H), 5.41 (s, 2H), 7.04 (d, 1H, J = 1.6 Hz), 7.28 (dd, 2H, J_1 = 3.4 Hz, J_2 = 1.6 Hz), 7.38 (m, 2H), 7.59 (d, 1H, J = 1.2 Hz), 7.76 (d, 1H, J = 7.6 Hz), 7.81 (d, 1H, J = 8 Hz), 8.18 (s, 1H), 8.46 (t, 1H, J = 3 Hz).

9.2.2 Syntheses of co-crystals

9.2.2.1 Synthesis of 3-[2-(2-methylimidazol-1-yl)benzimidazol-1-yl]-methylpyridine 4-nitrobenzoic acid, **56**

4-Nitrobenzoic acid (0.012 g, 0.069 mmol) was dissolved in 2 mL of absolute ethanol. To this solution was added an ethanolic solution (1 mL) containing 3-[2-(2-methylimidazol-1-yl)benzimidazol-1-yl]-methylpyridine (0.020 g, 0.069 mmol), and the resulting mixture allowed to stand under ambient conditions. Slow evaporation of the solvent produced colorless plates, **56**, after 12 days. M.p. 163-166˚C.

9.2.3 Infrared spectroscopy of co-crystals

All samples were prepared for IR analysis as KBr discs. IR spectroscopy of co-crystals was performed using a Protégé™ 460 E.S.P.™ FT-IR spectrometer,[4] and the data analyzed with the Nicolet OMNIC® software[4] between 4000 and 400 cm^{-1}.

9.2.4 X-ray crystallography

X-ray data were collected on a Bruker SMART 1000 four-circle CCD diffractometer using a fine-focus molybdenum Kα tube. Data were collected using SMART.[5] Initial cell constants were found by small widely separated "matrix" runs. Preliminary Laué symmetry was determined from axial images. Generally, an entire hemisphere of reciprocal space was collected regardless of Laué symmetry. Scan speed and scan width were chosen based on scattering power and peak rocking curves. Unless otherwise noted, data were collected at low temperatures, using a scan width appropriate for the crystal's mosaic spread.

Unit cell constants and orientation matrix were improved by least-squares refinement of reflections thresholded from the entire dataset. Integration was performed with SAINT,[6] using this improved unit cell as a starting point. Precise unit cell constants were calculated in SAINT from the final merged dataset. Lorenz and polarization corrections were applied. Laué symmetry, space group, and unit cell contents were found with XPREP.

Data were reduced with SHELXTL.[7] The structure was solved by direct methods without incident. In general, hydrogens were assigned to idealized positions and were allowed to ride. Where possible, the coordinates of hydrogen-bonding hydrogens were allowed to refine. Heavy atoms were refined with anisotropic thermal parameters.

9.3 Results

Crystallographic data for **56** are given in Table A56, the hydrogen-bond geometries in Table 9.1, and the thermal ellipsoid plot (50% probability level) and labeling scheme shown in Figure 9.1. IR data for **56** and a few quaternary co-crystallization reactions are displayed in Table 9.2.

Table 9.1 Hydrogen-bond geometries for **56**.

Compound	D-H A	D-H/Å	H...A/Å	D...A/Å	<(DHA)/°	generator for A
56	O41 H41 N31	0.95(3)	1.66(4)	2.606(3)	176(3)	–
	O51 H51 N23	0.98(3)	1.74(3)	2.709(3)	170(3)	–

Table 9.2 IR data for products from quaternary co-crystallization reactions involving 3-[2-(2-methylimidazol-1-yl)benzimidazol-1-yl]-methylpyridine and carboxylic acids.

Compound	Acid A	Acid B	Acid C	$\nu_{O-H\cdots N}$ (cm^{-1})
56	4-nitrobenzoic acid	–	–	2456, 1889
–	3,5-dinitrobenzoic acid	4-nitrobenzoic acid	4-cyanobenzoic acid	2460, 1904
–	4-nitrobenzoic acid	4-cyanobenzoic acid	3-hydroxybenzoic acid	2453, 1905

9.3.1 Crystal structure of 3-[2-(2-methylimidazol-1-yl)benzimidazol-1-yl]-methylpyridine 4-nitrobenzoic acid, **56**

The crystal structure of **56** shows a 1:2 co-crystal consisting of 3-[2-(2-methylimidazol-1-yl)benzimidazol-1-yl]-methylpyridine and 4-nitrobenzoic acid respectively, Figure 9.1. One 4-nitrobenzoic acid molecule interacts with the most basic site, the 2-methylimidazol-1-yl nitrogen atom, *via* an O–H···N hydrogen bond (O51···N23, 2.709(3) Å), while a second carboxylic acid forms an O–H···N hydrogen bond with the second-best acceptor, the pyridyl moiety (O41···N31, 2.606(3) Å). The benzimidazol-1-yl nitrogen atom, however, is not involved in any significant interactions. The two carboxylic acids are arranged in a parallel manner, and are separated by about 3.6 Å.

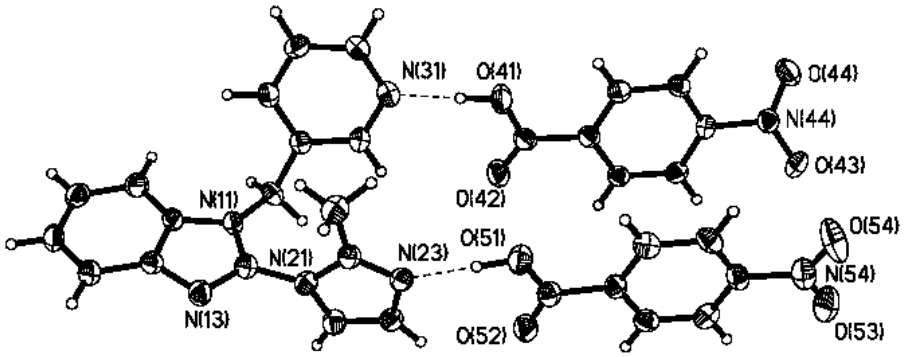

Figure 9.1 Binary co-crystal in **56**.

9.4 Discussion

The SR 3-[2-(2-methylimidazol-1-yl)benzimidazol-1-yl]-methylpyridine was prepared according to a two-step procedure in good yield, and displays good solubility in a range of polar solvents. Its solubility was compatible with those of most aromatic carboxylic acids used in binary and quaternary co-crystallization experiments, and as such provided an opportunity for co-crystal formation.

A 1:2 co-crystal was obtained in **56** when 1:1 molar equivalents of the SR and 4-nitrobenzoic acid, respectively, were combined. Even though there is only one data point available to date, the crystal structure of **56**, however, provides an encouraging result in that the two carboxylic acids showed preference for the best and second-best hydrogen-bond acceptors (the 2-methylimidazol-1-yl and pyridyl moieties respectively) over the other two possible binding options (a 33% probability). A hierarchy of hydrogen bonds is therefore observed in the crystal structure.

Co-crystallization reactions were subsequently carried out with the aim of producing quaternary supermolecules. In each case, three carboxylic acids and the SR were combined in a 1:1:1:1 ratio. Although no structural information has been obtained yet from the crystals produced (in most cases), TLC[8] and IR analyses were performed on individual crystallites of a few reactions in an attempt to determine the number of components present as well as possible co-crystal formation. The IR data for the two quaternary co-crystallization reactions in Table 9.2 shows the two broad O–H···N bands at around 2460 and 1900 cm^{-1}, but this information does not indicate whether a binary, ternary or quaternary co-crystal had formed.

9.5 Conclusions and future work

We have shown that an asymmetric tritopic SR, 3-[2-(2-methylimidazol-1-yl)benzimidazol-1-yl]-methylpyridine, is capable of forming a 1:2 binary co-crystal with 4-nitrobenzoic acid, and also that the two acids in this crystal structure form hydrogen bonds according to the proposed supramolecular assembly guidelines. It is therefore possible that this SR can act as a central hub for the formation of quaternary co-crystals with structural selectivity and specificity.

A few possible candidates as SR's for quaternary supermolecules may be prepared through the use of a combination of heterocycles possessing independently tunable binding sites, Scheme 9.2 and Table 9.3.

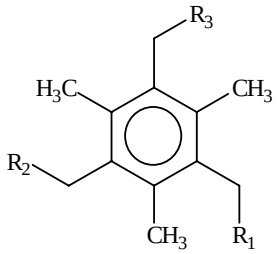

Scheme 9.2 A few possible SR's for the directed assembly of quaternary supermolecules.

Table 9.3 Calculated pK_a values[2] of a few possible SR's for quaternary supermolecules.

SR	pK_a of R_1	pK_a of R_2	pK_a of R_3
1	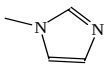 imidazol-1-yl, 6.77 ± 0.12	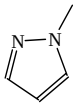 pyrazol-1-yl, 1.78 ± 0.19	 benzimidazol-1-yl, 5.53 ± 0.12
2	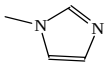 imidazol-1-yl, 6.76 ± 0.12	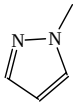 pyrazol-1-yl, 1.75 ± 0.19	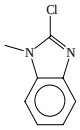 2-chlorobenzimidazol-1-yl, 3.86 ± 0.34
3	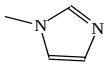 imidazol-1-yl, 6.77 ± 0.12	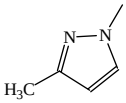 3-methylpyrazol-1-yl, 2.29 ± 0.50	 benzimidazol-1-yl, 5.54 ± 0.30
4	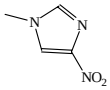 4-nitroimidazol-1-yl, 0.02 ± 0.61	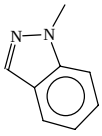 indazol-1-yl, 1.10 ± 0.40	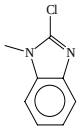 2-chlorobenzimidazol-1-yl, 3.87 ± 0.34
5	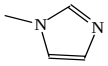 imidazol-1-yl, 6.72 ± 0.12	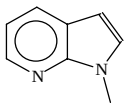 7-azaindol-1-yl, 5.10 ± 0.30	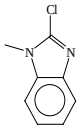 2-chlorobenzimidazol-1-yl, 3.83 ± 0.34

Much work lies ahead in the quest for quaternary and higher-order supermolecules, which can only be achieved through a modular, systematic, and transferable non-covalent synthetic approach. We are currently exploring the limits and limitations of our supramolecular strategy by designing and preparing a library of SR's that contain different binding sites.

References

[1] Aakeröy, C. B.; Desper, J.; Urbina, J. F. *Chem. Commun*. **2005**, ASAP.

[2] The calculations were performed using ACD/Solaris v4.76; Advanced Chemistry Development, Inc.: Toronto, ON, Canada, www.acdlabs.com, 1994–2005.

[3] (a) Aakeröy, C. B.; Desper, J.; Leonard, B.; Urbina, J. F. *Cryst. Growth Des*. **2005**, DOI: 10.1021/cg049682i. (b) Aakeröy, C. B.; Desper, J.; Urbina, J. F. *Cryst. Growth Des*. **2005**, DOI: 10.1021/cg049579t. (c) Aakeröy, C. B.; Desper, J.; Elisabeth, E.; Helfrich, B. A.; Levin, B.; Urbina, J. F. *Zeit. Kristallogr*. **2005**, *220*, 325.

[4] Nicolet Instrument Corporation: Madison, WI 53711, 1997.

[5] SMART v5.060; Bruker Analytical X-ray Systems: Madison, WI, 1997–1999.

[6] SAINT v6.02; Bruker Analytical X-ray Systems: Madison, WI, 1997–1999.

[7] SHELXTL v5.10; Bruker Analytical X-ray Systems: Madison, WI, 1997.

[8] According to TLC analysis, it was difficult to determine how many carboxylic acids were present in these co-crystallization reactions, since the spots corresponding to the acids streaked on the TLC plates.

APPENDIX 1

^{1}H NMR SPECTRA

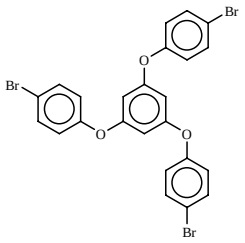
Br
O
Br
O
O
Br

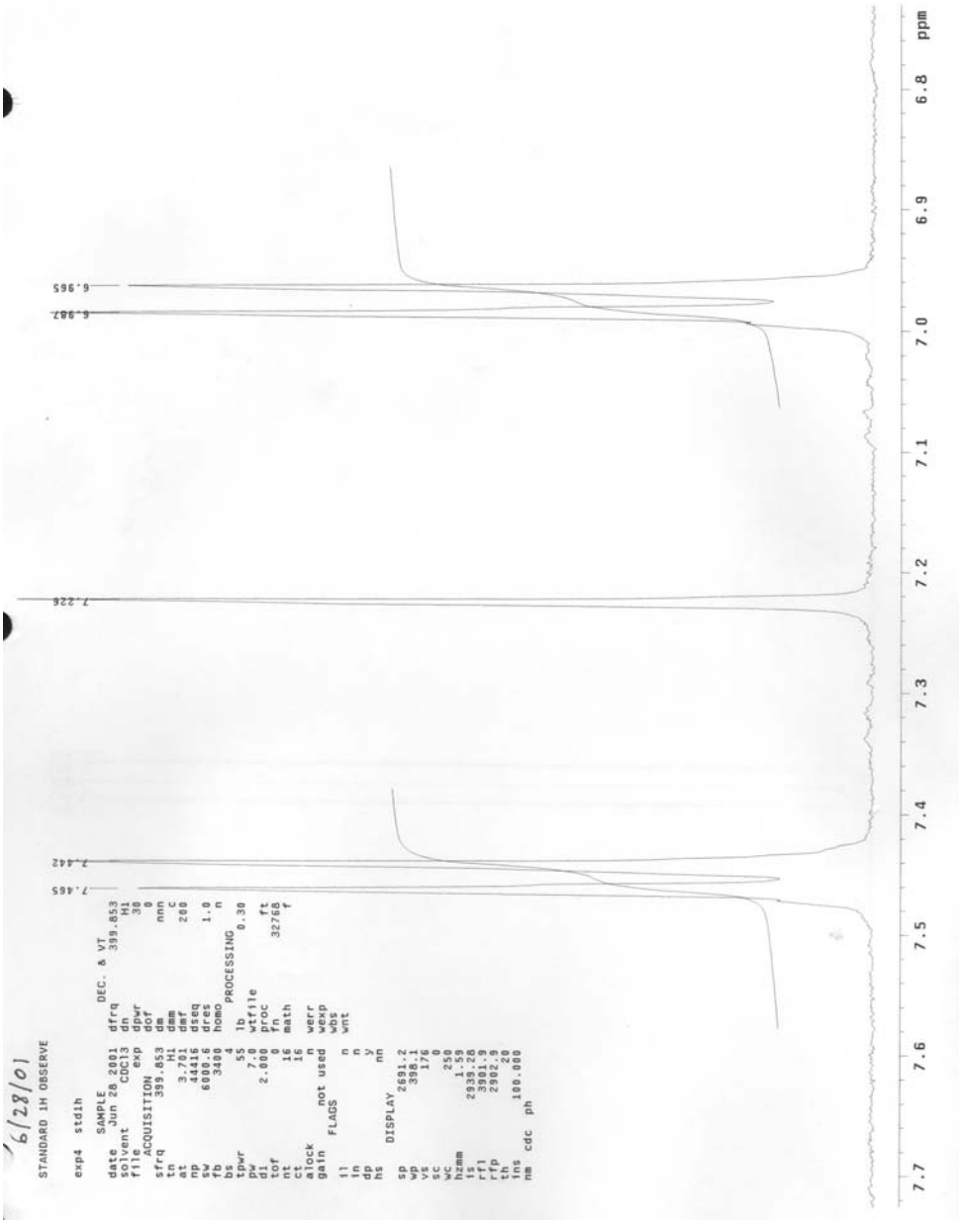
6/28/01
STANDARD 1H OBSERVE
exp4 std1h
SAMPLE
date Jun 28 2001
solvent CDCl3
file exp
ACQUISITION
sfrq 399.853
tn H1
at 3.701
np 44416
sw 6000.6
fb 3400
bs 4
tpwr 55
pw 7.0
d1 2.000
nt 16
ct 16
alock n
gain not used
ll n
in n
dp y
hs nn
DISPLAY
sp 2691.2
wp 3981.1
vp 176
sc 0
wc 250
hzmm 1.59
is 2939.28
rfl 3981.9
rfp 2902.9
th 20
ins 100.000
nm cdc ph
DEC. & VT
dfrq 399.853
dn H1
dpwr 30
dof 0
dm nnn
dmm c
dmf 200
dseq
dres 1.0
homo n
PROCESSING
lb 0.30
wtfile
proc ft
fn 32768
math f
werr
wexp
wbs
wnt
7.465
7.442
7.226
6.985
6.982
7.7
7.6
7.5
7.4
7.3
7.2
7.1
7.0
6.9
6.8
ppm

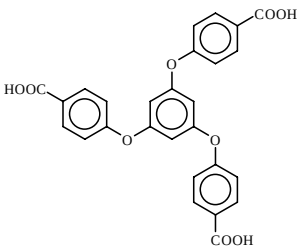
COOH
HOOC
O
O
O
COOH

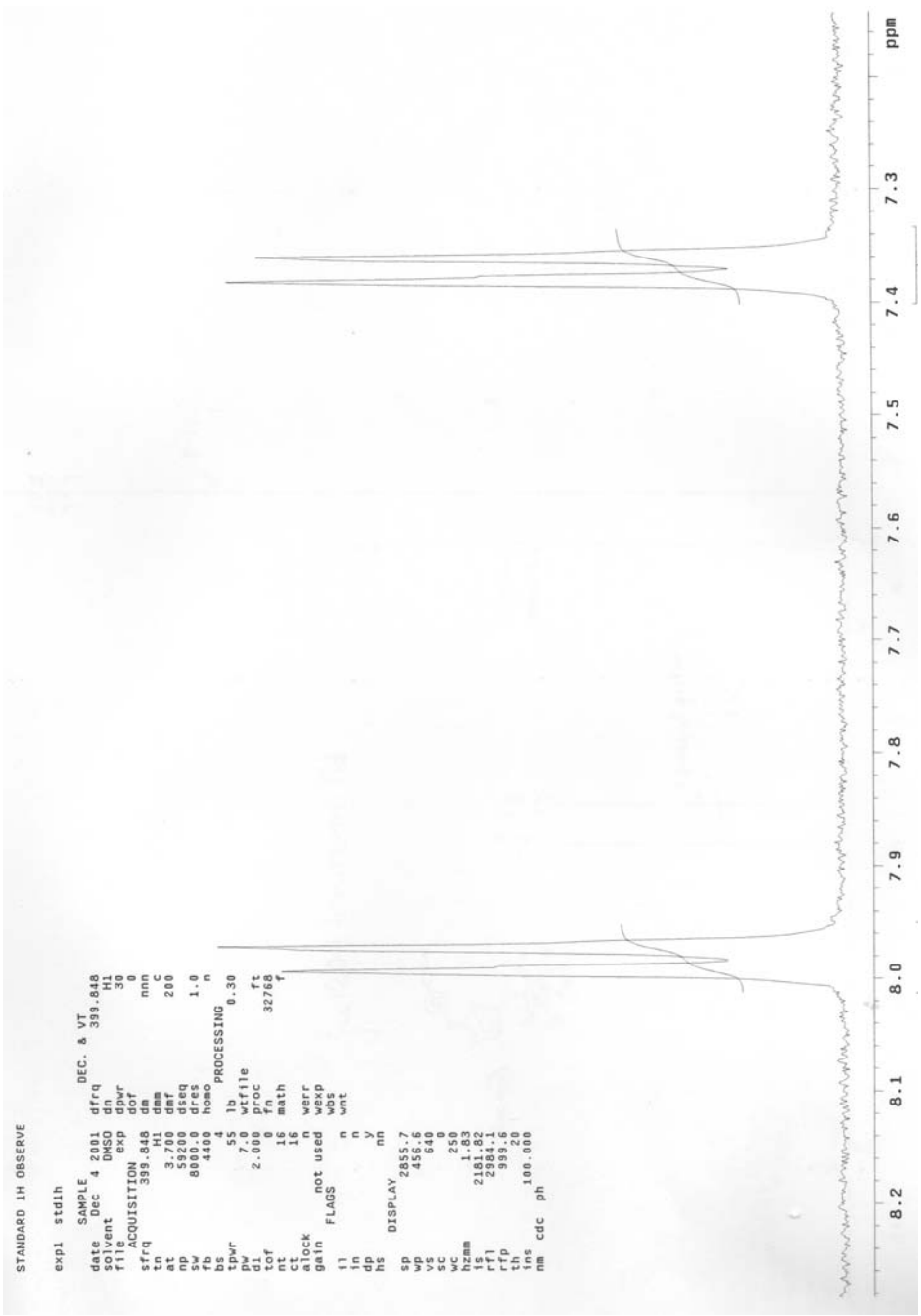
STANDARD 1H OBSERVE
exp1 stdih
DEC. & VT
SAMPLE
date Dec 4 2001 dfrq 399.848
solvent DMSO dn H1
file exp dpwr 30
ACQUISITION dof 0
sfrq 399.848 dmm nnn
tn H1 dmm C
at 3.700 dmf 200
np 59200 dseq
sw 8000.0 dres 1.0
fb 4400 homo n
PROCESSING
bs 4 lb 0.30
tpwr 55 wtfile
pw 7.0 proc ft
dl 2.000 fn 32768
nt 16 math f
ct 16
alock n werr
gain not used wexp
FLAGS wbs
il n wnt
in n
dp y
hs nn
DISPLAY
sp 2855.7
wp 456.6
vs 640
sc 0
wc 250
hzmm 1.83
is 2181.82
rfl 2984.1
rfp 999.6
th 20
ins 100.000
nm cdc ph
8.2
8.1
8.0
7.9
7.8
7.7
7.6
7.5
7.4
7.3
ppm

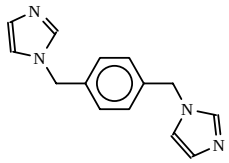

STANDARD 1H OBSERVE

exp1 std1h

	SAMPLE		DEC. & VT
date	Jun 22 2002	dfrq	399.842
solvent	DMSO	dn	H1
file	/export/home/~	dpwr	30
chem/rtmr/aakerov/JO~		dof	0
aquin/2003/ju0621/~		dm	nnn
midazole/ligand/pure~		dmm	c
	fld	dmf	200
	ACQUISITION		dseq
sfrq	399.842	dres	1.0
tn	H1	homo	n
at	3.701		PROCESSING
np	44416	lb	0.30
sw	6000.6	wtfile	
fb	3400	proc	ft
bs	4	trf	32768
tpwr	55	math	f
pw	7.0		
d1	2.000	werr	
tof	0	wexp	
nt	16	wbs	
ct	16	wnt	
alock	n		
gain	not used		
	FLAGS		
ii	n		
in	n		
dp	y		
hs	nn		
	DISPLAY		
sp	-992.9		
wp	6000.6		
vs	157		
sc	0		
wc	250		
hzmm	24.00		
is	106.94		
rfl	1992.5		
rfp	999.6		
th	20		
ins	100.000		
nm	cdc	ph	

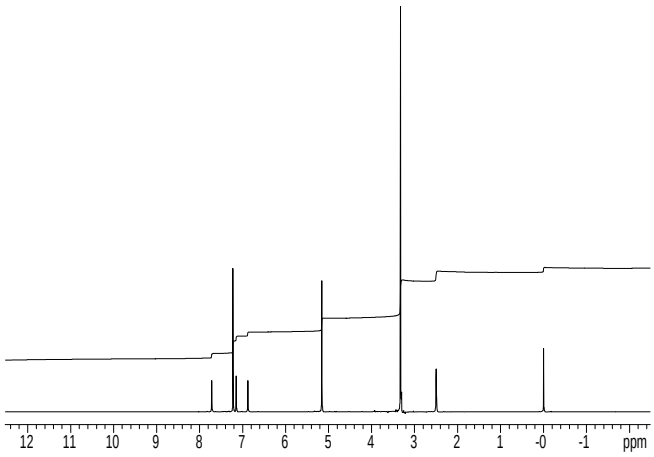

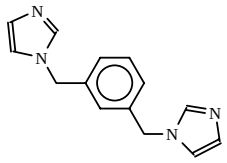

STANDARD 1H OBSERVE

exp1 std1h

SAMPLE DEC. & VT
date Sep 18 2003 dfrq 399.822
solvent DMSO dn H1
file /export/home/~ dpwr 30
chemrlmr/aakerov/JG~ dof 0
aquin/2003/ju09180~ dm nnn
5-13bxpute.fid dmm c
ACQUISITION dmf 200
sfrq 399.822 dseq
tn H1 dres 1.0
at 3.701 homo n
np 44416 PROCESSING
sw 6000.6 wtfile
fb 3400 proc ft
bs 4 fn 32768
tpwr 55 math f
pw 19.8
d1 1.000 werr
tof 0 wexp
nt 4 wbs
ct 4 wnt
alock n
gain 30
FLAGS
il n
in n
dp y
hs nn
DISPLAY
sp -981.6
wp 6000.6
vs 160
sc 0
wc 250
hzmm 24.00
is 2358.04
rfl 1981.2
rfp 999.6
th 20
ins 100.000
nm cdc ph

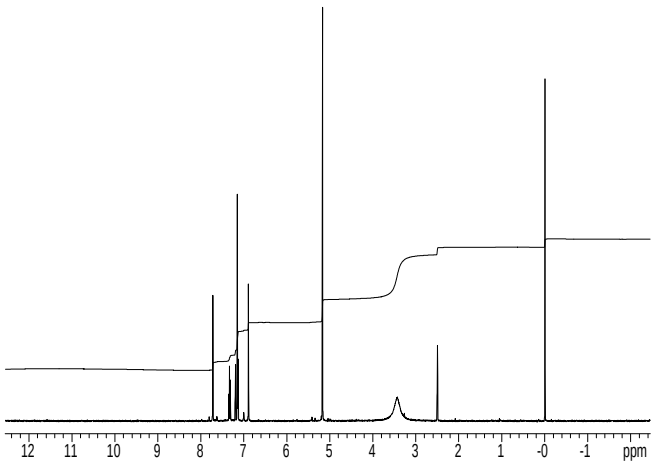

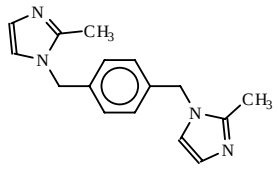

STANDARD 1H OBSERVE

exp1 std1h

SAMPLE		DEC. & VT	
date	Sep 19 2003	dfrq	399.822
solvent	DMSO	dn	H1
file	/export/home/~ dpwr		30
chemmm/aakerov/JJ~ dof			0
aquin/2003/ju09190~ dm			nnn
3-2Mebixpure.fid		dmm	c
ACQUISITION		dmf	200
sfrq	399.822	dseq	
tn	H1	dres	1.0
at	3.701	homo	n
np	44416	PROCESSING	
sw	6000.6	wtfile	
fb	3400	proc	ft
bs	4	fn	32768
tpwr	55	math	f
pw	19.8		
d1	1.000	werr	
tof	0	wexp	
nt	4	wbs	
ct	4	wnt	
alock	n		
gain	30		
FLAGS			
il	n		
in	n		
dp	y		
hs	nn		
DISPLAY			
sp	-981.6		
wp	6000.6		
vs	117		
sc	0		
wc	250		
hzmm	24.00		
is	2026.96		
rfl	1981.2		
rfp	999.6		
th	20		
ins	100.000		
nm	cdc	ph	

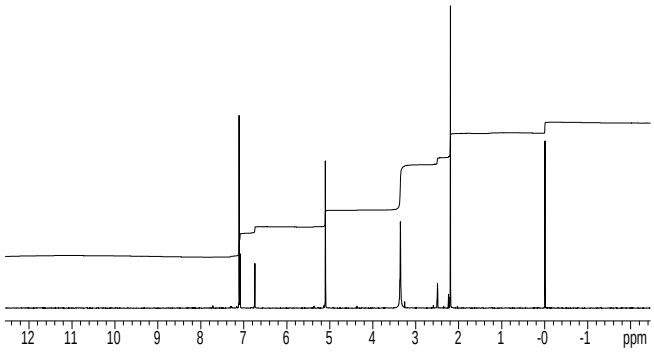

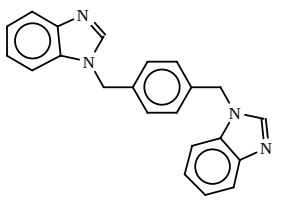

STANDARD 1H OBSERVE

exp1 std1h

SAMPLE DEC. & VT
date Aug 27 2002 dfrq 199.980
solvent DMSO dn H1
file /export/home/~ dof 0
chemnmr/Gemini Dat~ dm nnn
a/Aakeroy/ju0827-b~ dmm c
is-benzimidazoleps~ dmf 200
re.fid PROCESSING
ACQUISITION wtfile
sfrq 199.980 proc ft
tn H1 fn not used
at 1.994
np 11968 werr
sw 3000.3 wexp
fb 1500 wbs
bs 16 wnt
pw 7.0
d1 2.000
tof 0
nt 16
ct 16
alock n
gain not used
FLAGS
ii n
in n
dp y
DISPLAY
sp -496.0
wp 3000.3
vs 142
sc 0
wc 250
hzmm 12.00
is 3503.72
rfl 995.9
rfp 499.9
th 20
ins 100.000
nm cdc ph

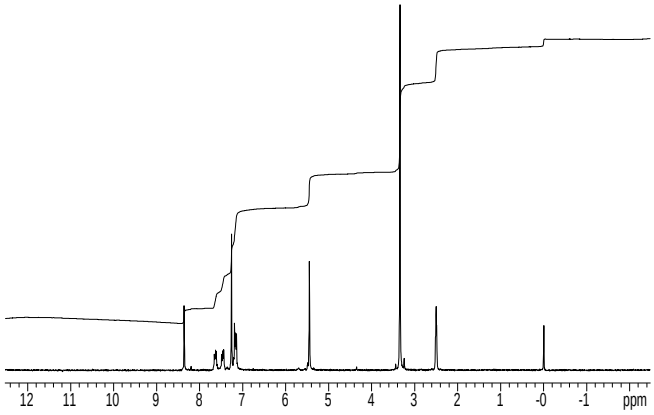

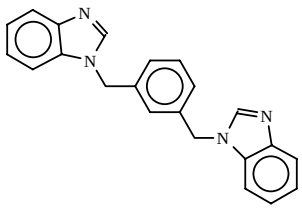

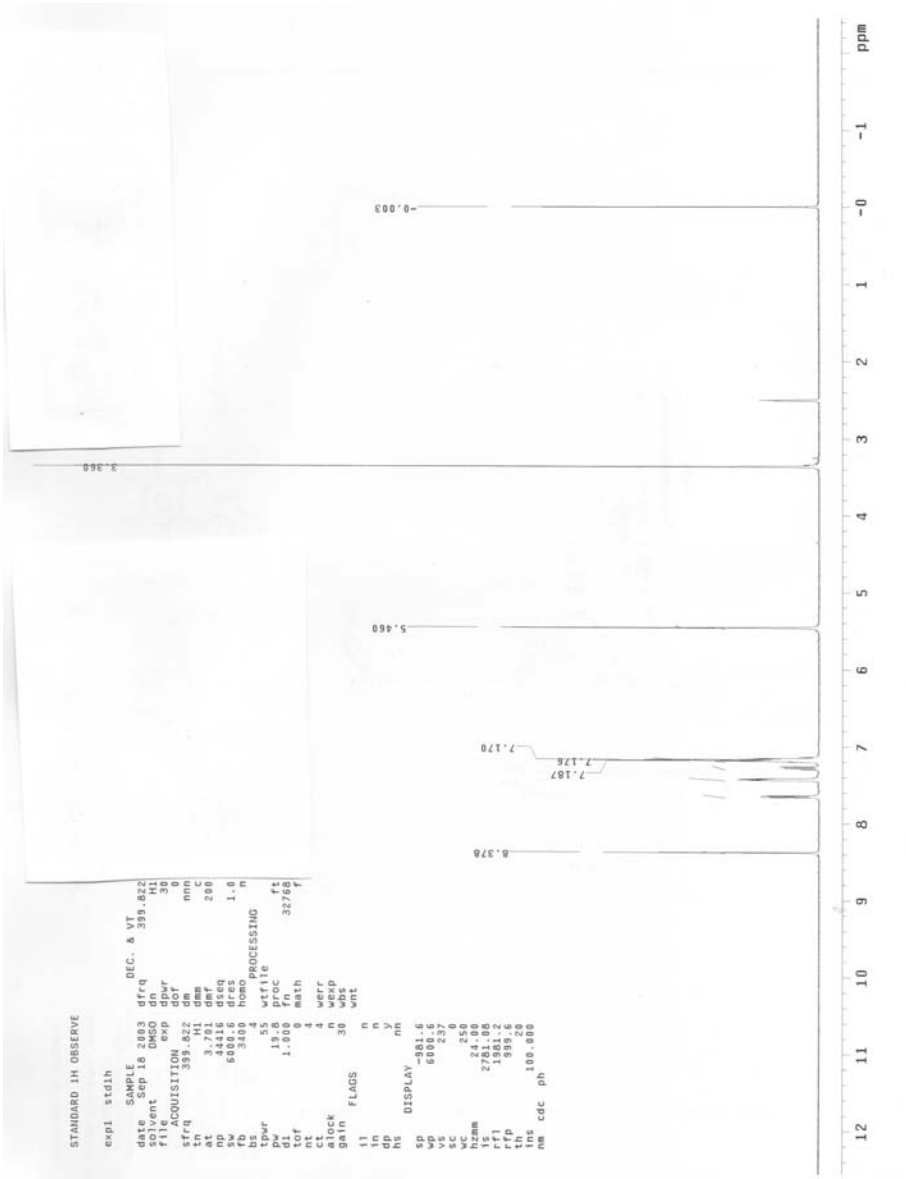
STANDARD 1H OBSERVE
expl stdih
SAMPLE DEC. & VT
date Sep 18 2003 dfrq 399.822
solvent DMSO dn H1
file exp dpwr 30
ACQUISITION dof 0
sfrq 399.822 dm nnn
tn H1 dmm c
at 3.701 dmf 200
np 4416 dres
sw 6001.6 homo 1.0
fb 3400 PROCESSING n
bs 4
tpwr 55 wtfile
pw 10.8 proc ft
d1 1.000 fn 32768
tof 0 math f
nt 4 werr
ct 0 wexp
alock n wbs
gain 30 wnt
FLAGS
il n
in n
dp y
hs nn
DISPLAY
sp -881.6
wp 6000.6
vs 237
sc 0
wc 250
hzcm 24.00
hz/cm 2781.108
fl 1981.72
flp 999.6
th 20
ins 100.000
nm cdc ph
8.376
7.187
7.176
7.170
5.460
3.360
0.003
ppm

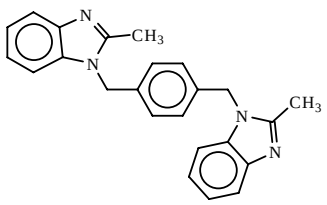

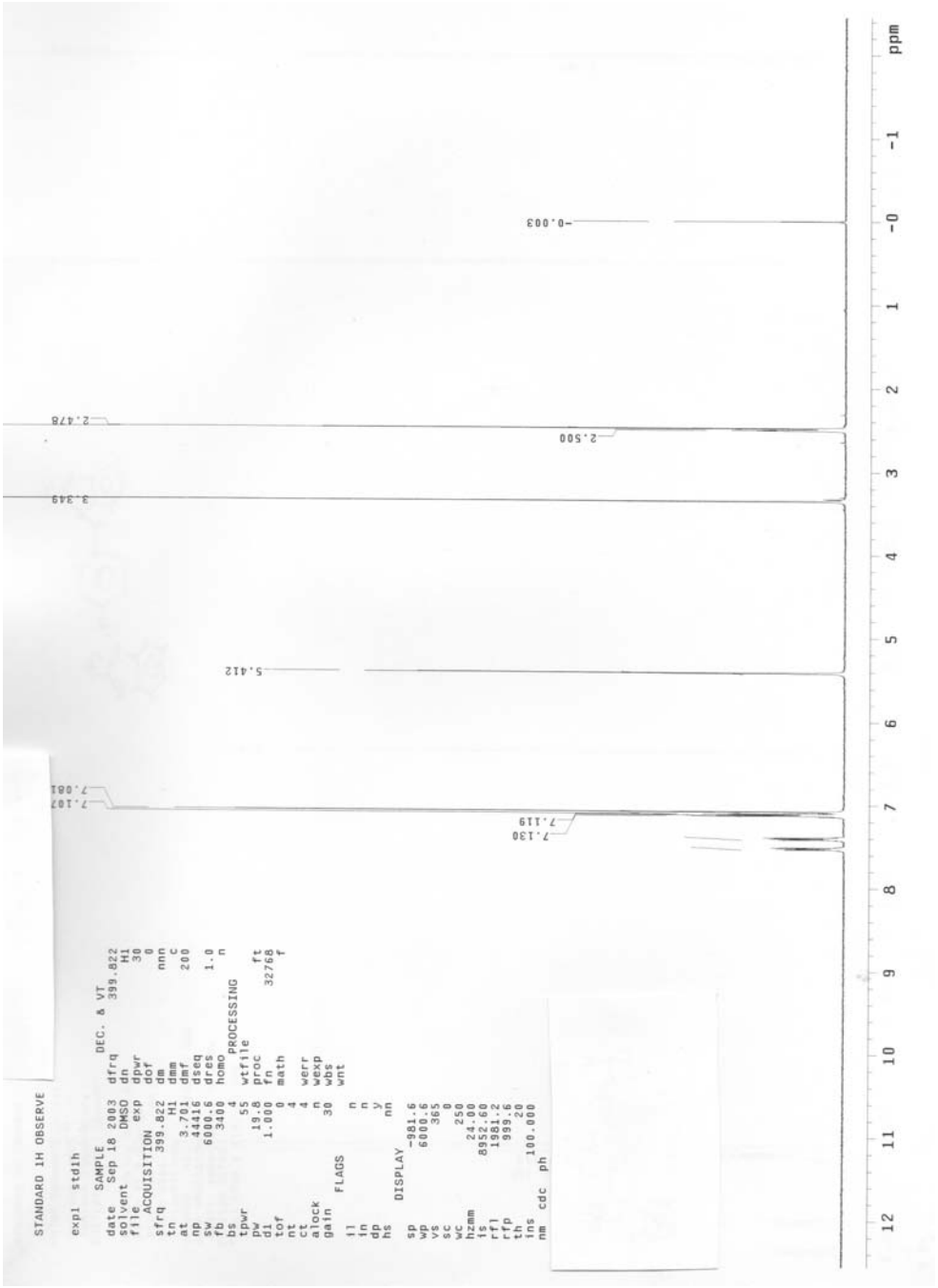
STANDARD 1H OBSERVE
expl stdih
SAMPLE DEC. & VT
date Sep 18 2003 dfrq 399.822
solvent DMSO dn H1
file exp dpwr 30
ACQUISITION dof 0
sfrq 399.822 dm nnn
tn H1 dmm c
at 3.701 dmf 200
np 44416 dseq
sw 6009.6 dres 1.0
fb 3400 homo n
bs 4 PROCESSING
tpwr 55 wtfile
pw 19.8 proc ft
d1 1.000 fn 32768
tof 0 math f
nt 4
ct 4 werr
alock n wexp
gain 30 wbs
FLAGS wnt
il n
in n
dp y
hs nn
DISPLAY
sp -981.6
wp 6000.6
vs 365
sc 0
wc 250
hzmm 24.00
is 8952.60
rfl 1981.2
rfp 999.6
th 20
ins 100.000
nm cdc ph
7.182
7.061
5.412
7.119
7.130
3.349
2.478
2.500
0.003
ppm

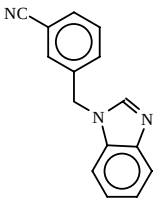

STANDARD 1H OBSERVE

exp1 std1h

SAMPLE		DEC. & VT	
date	Sep 29 2003	dfrq	399.822
solvent	DMSO	dn	H1
file	/export/home/~	dpwr	30
chemrinm/aakerov/Jo~		dof	0
aquin/2003/ju09290~		dm	nnn
3-3CNbenzylbenzim~		dmm	c
dpure.fid		dmf	200
ACQUISITION		dseq	
sfrq	399.822	dres	1.0
tn	H1	homo	n
at	3.701	PROCESSING	
np	44416	wtfile	
sw	6000.6	proc	ft
fb	9400	fn	32768
bs	4	math	f
tpwr	55		
pw	19.8	werr	
d1	1.000	wexp	
tof	0	wbs	
nt	4	wnt	
ct	4		
alock	n		
gain	30		
FLAGS			
il	n		
in	n		
dp	y		
hs	nn		
DISPLAY			
sp	-980.1		
wp	6000.6		
vs	718		
sc	0		
wc	250		
hzmm	24.00		
is	5087.92		
rfl	1979.7		
rfp	999.6		
th	20		
ins	100.000		

nm cdc ph

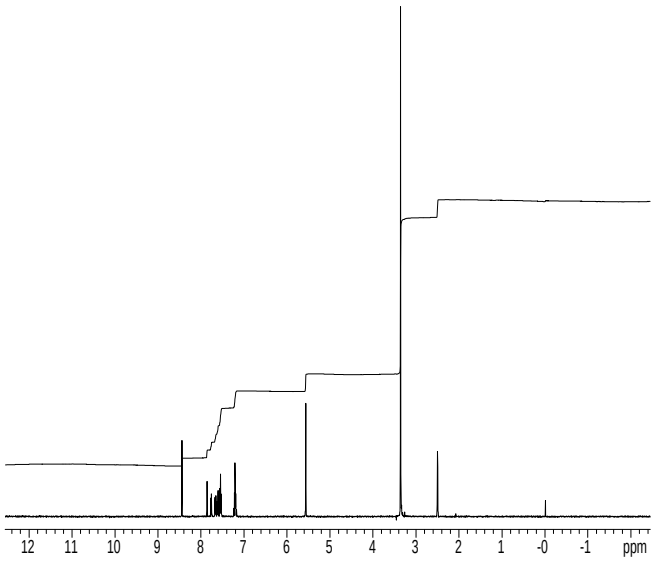

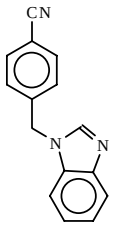

STANDARD 1H OBSERVE

exp1 std1h

SAMPLE DEC. & VT
date Sep 8 2003 dfrq 399.822
solvent DMSO dn H1
file /export/home/~ dpwr 30
chemnmr/aakeroy/0~ dof 0
aquin/2003/ju09080~ dm nnn
3-4CN1Hbenzylbenzi~ dmm c
mid.tid dmf 200
ACQUISITION dseq
sfrq 399.822 dres 1.0
tn H1 homo n
at 3.701 PROCESSING
np 44416 wtfile
sw 6000.6 proc ft
fb 3400 fn 32768
bs 4 math f
tpwr 55
pw 19.8 werr
d1 1.000 wexp
tof 0 wbs
nt 4 wnt
ct 4
alock n
gain 30
FLAGS
ii n
in n
dp y
hs nn
DISPLAY
sp -981.6
wp 6000.6
vs 693
sc 0
wc 250
hzmm 24.00
is 3673.37
rfl 1981.2
rfp 999.6
th 20
ins 100.000
nm cdc ph

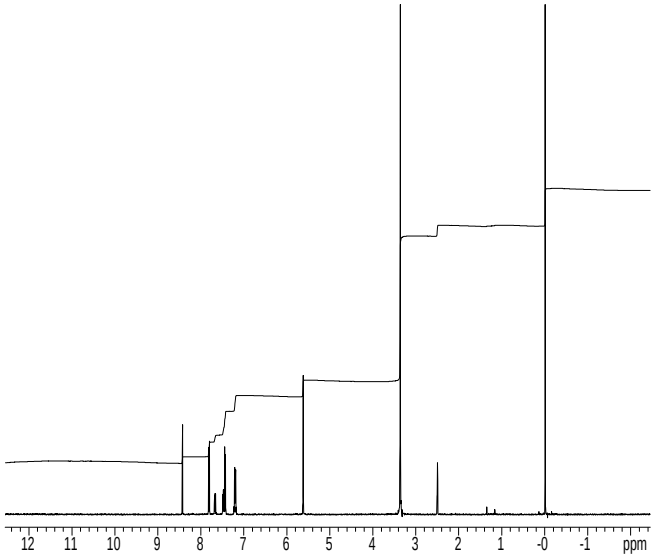

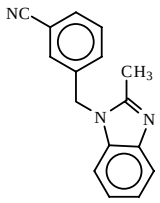

STANDARD 1H OBSERVE

exp1 std1h

SAMPLE DEC. & VT
date Sep 29 2003 dfrq 399.823
solvent CD3CN dn H1
file /export/home/~ dpwr 30
chemrinm/aakerov/Jo~ dof 0
aquin/2003/ju06290~ dm nnn
3-3CNbenzyl2Mebenz~ dmm c
imidcrude.fid dmf 200
ACQUISITION dseq
sfrq 399.823 dres 1.0
tn H1 homo n
at 3.701 PROCESSING
np 44416 wtfile
sw 6000.6 proc ft
fb 9400 fn 32768
bs 4 math f
tpwr 55
pw 19.8 werr
d1 1.000 wexp
tof 0 wbs
nt 4 wnt
ct 4
alock n
gain 30
FLAGS
il n
in n
dp y
hs nn
DISPLAY
sp -996.7
wp 6000.6
vs 232
sc 0
wc 250
hzmm 24.00
is 2307.28
rfl 1772.4
rfp 775.7
th 20
ins 100.000
nm cdc ph

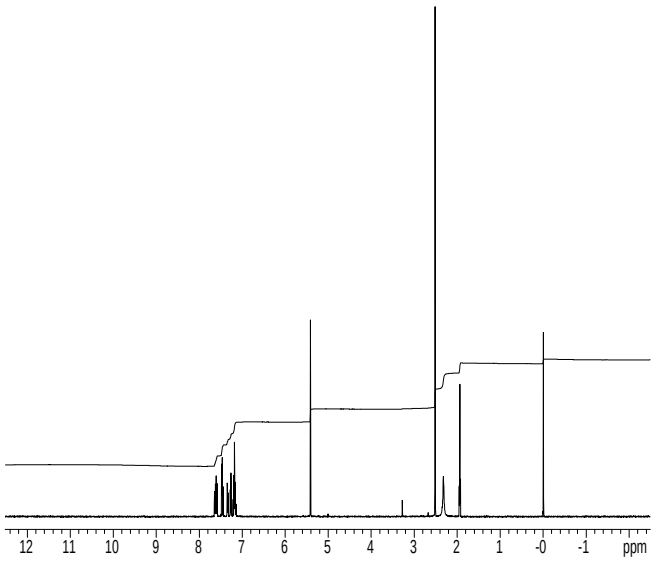

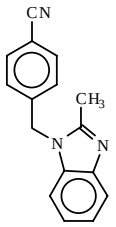

STANDARD 1H OBSERVE

exp1 std1h

SAMPLE DEC. & VT
date Sep 8 2003 dfrq 399.823
solvent CD3CN dn H1
file /export/home/~ dpwr 30
chemnmr/aakerov/Ak~ dof 0
aquin/2003/ju09080~ dm nnn
3-4CN2Mebenzylbenz~ dmm c
imid.hd dmf 200
ACQUISITION dseq
sfrq 399.823 dres 1.0
tn H1 homo n
at 3.701 PROCESSING
np 44416 wtfile
sw 6000.6 proc ft
fb 3400 fn 32768
bs 4 math f
tpwr 55
pw 19.8 werr
d1 1.000 wexp
tof 0 wbs
nt 4 wnt
ct 4
alock n
gain 30
FLAGS
il n
in n
dp y
hs nn
DISPLAY
sp -927.5
wp 6000.6
vs 226
sc 0
wc 250
hzmm 24.00
is 3935.69
rfl 1773.1
rfp 775.7
th 20
ins 100.000
nm cdc ph

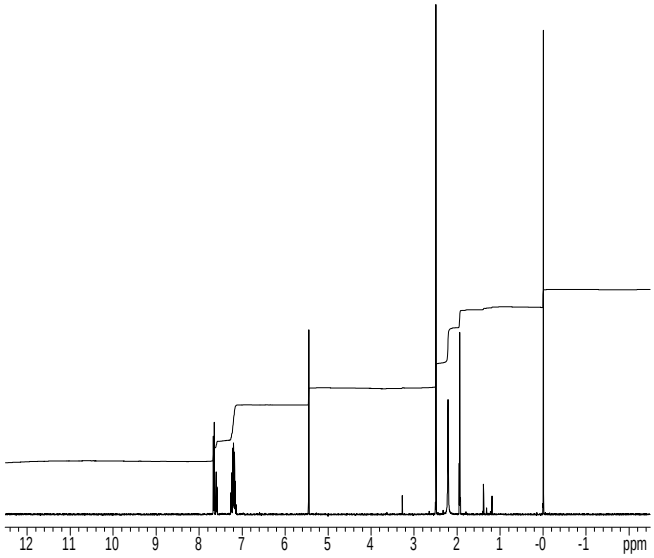

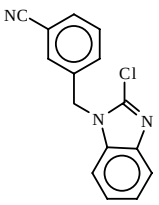

STANDARD 1H OBSERVE

exp1 std1h

SAMPLE		DEC. & VT	
date	May 27 2003	dfrq	399.822
solvent	DMSO	dn	H1
file	/export/home/~	dpwr	45
chemnmr/aakeroy/J6~		dof	0
aquin/2003/jo5270~		dm	nnn
3-3CNbenzyl2Clbenz~		dmm	c
imidpure.fid		dmf	6100
ACQUISITION		dseq	
sfrq	399.822	dres	1.0
tn	H1	homo	n
at	3.701	PROCESSING	
np	44416	wtfile	
sw	6000.6	proc	ft
fb	3400	fn	32768
bs	4	math	f
tpwr	55		
pw	20.0	werr	
d1	1.000	wexp	
tof	0	wbs	
nt	4	wnt	
ct	4		
alock	n		
gain	not used		
FLAGS			
ii	n		
in	n		
dp	y		
hs	nn		
DISPLAY			
sp	-982.3		
wp	6000.6		
vs	155		
sc	0		
wc	250		
hzmm	24.00		
is	149.96		
rfl	1981.9		
rfp	999.6		
th	20		
ins	100.000		
nm	cdc	ph	

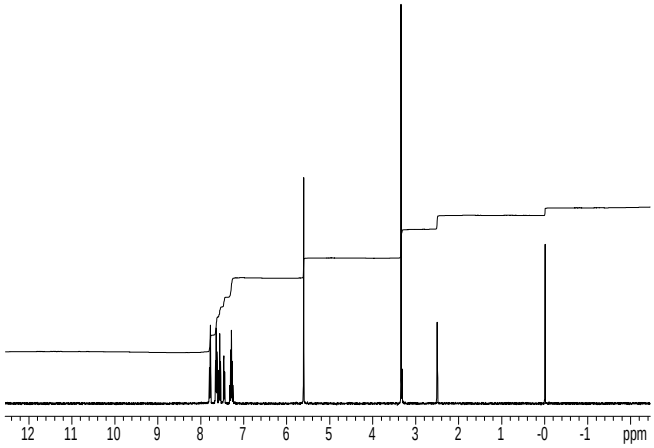

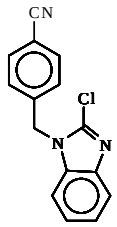

STANDARD 1H OBSERVE

exp1 std1h

SAMPLE DEC. & VT
date Sep 11 2003 dfrq 399.822
solvent DMSO dn H1
file /export/home/~ dpwr 30
chemnmr/aakeroy/Ut~ dof 0
aquin/2003/ju09110~ dm nnn
3-4CNbenzyl2Clbenz~ dmm c
imidpure.fid dmf 200
ACQUISITION dseq
sfrq 399.822 dres 1.0
tn H1 homo n
at 3.701 PROCESSING
np 44416 wtfile
sw 6000.6 proc ft
fb 3400 fn 32768
bs 4 math f
tpwr 55
pw 19.8 werr
d1 1.000 wexp
tof 0 wbs
nt 4 wnt
ct 4
alock n
gain 30
FLAGS
ii n
in n
dp y
hs nn
DISPLAY
sp -982.0
wp 6000.6
vs 389
sc 0
wc 250
hzmm 24.00
is 4192.52
rfl 1981.5
rfp 999.6
th 20
ins 100.000
nm cdc ph

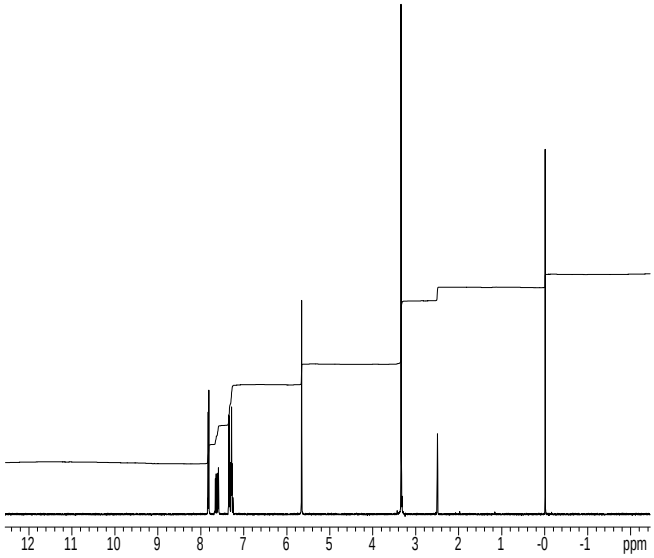

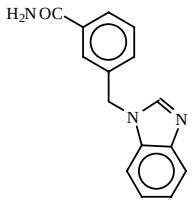

STANDARD 1H OBSERVE

exp1 std1h

SAMPLE		DEC. & VT	
date	May 5 2005	dfrq	399.796
solvent	DMSO	dn	H1
file	exp	dpwr	30
ACQUISITION		dof	0
sfrq	399.796	dm	nnn
tn	H1	dmm	c
at	3.701	dmf	200
np	44416	dseq	
sw	6000.6	dres	1.0
fb	3400	homo	n
bs	4	PROCESSING	
tpwr	55	wtfile	
pw	6.0	proc	ft
d1	1.000	fn	32768
tof	0	math	f
nt	4		
ct	4	werr	
alock	n	wexp	
gain	not used	wbs	
FLAGS		wnt	
ii	n		
in	n		
dp	y		
hs	nn		
DISPLAY			
sp	-992.7		
wp	6000.6		
vs	153		
sc	0		
wc	250		
hzmm	24.00		
is	168.92		
rfl	1992.1		
rfp	999.5		
th	20		
ins	100.000		
nm	cdc	ph	

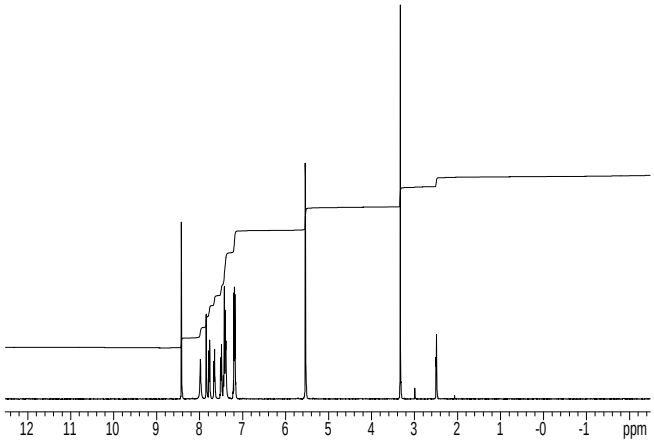

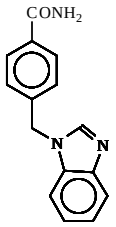

STANDARD 1H OBSERVE

exp1 std1h

```
    SAMPLE          DEC. & VT
date  Oct  8 2003 dfrq      399.822
solvent     DMSO  dn           H1
file /export/home/~ dpwr        30
chemnmr/aakerov/Jo~ dof          0
acqim/2003/lu10080~ dm           nnn
3-4amidebenzylbenz~ dmm          c
    imidpure.fid  dmf          200
  ACQUISITION     dseq
sfrq     399.822  dres        1.0
tn          H1  homo          n
at        3.701    PROCESSING
np        44416  wtfile
sw        6000.6  proc          ft
fb        3400  fn          32768
bs           4  math          f
tpwr        55
pw        19.8  werr
d1        1.000  wexp
tof          0  wbs
nt           4  wnt
ct           4
alock        n
gain        30
    FLAGS
ii           n
in           n
dp           y
hs          nn
   DISPLAY
sp       -980.1
wp        6000.6
vs           769
sc             0
wc           250
hzmm       24.00
is        4172.91
rfl       1979.7
rfp        999.6
th            20
ins     100.000
nm  cdc  ph
```

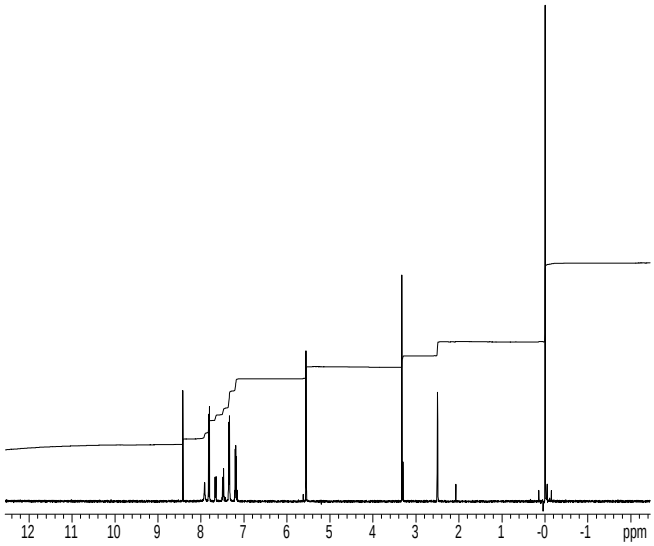

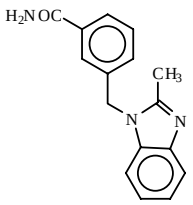

STANDARD 1H OBSERVE

exp1 std1h

SAMPLE		DEC. & VT	
date	Oct 8 2003	dfrq	399.822
solvent	DMSO	dn	H1
file	/export/home/~	dpwr	30
chemrinnr/aakeroy/Jo~		dof	0
aquin/2003/ju10080~		dm	nnn
3-Samidebenzy(2Meb~		dmm	c
enzimidpure.fid		dmf	200
ACQUISITION		dseq	
sfrq	399.822	dres	1.0
tn	H1	homo	n
at	3.701	PROCESSING	
np	44416	wtfile	
sw	6000.6	proc	ft
fb	9400	fn	32768
bs	4	math	f
tpwr	55		
pw	19.8	werr	
d1	1.000	wexp	
tof	0	wbs	
nt	4	wnt	
ct	4		
alock	n		
gain	30		
FLAGS			
il	n		
in	n		
dp	y		
hs	nn		
DISPLAY			
sp	-980.1		
wp	6000.6		
vs	253		
sc	0		
wc	250		
hzmm	24.00		
is	5044.96		
rfl	1979.7		
rfp	999.6		
th	20		
ins	100.000		
nm cdc ph			

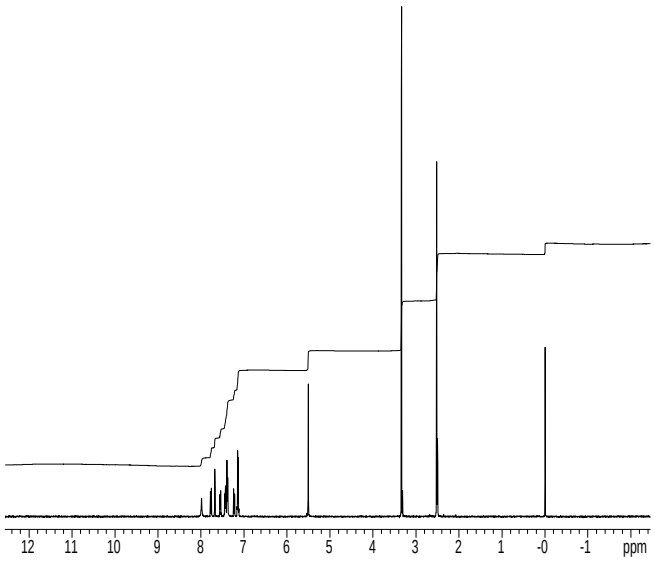

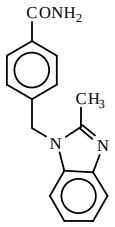

STANDARD 1H OBSERVE

exp1 std1h

SAMPLE DEC. & VT
date Oct 6 2003 dfrq 399.822
solvent DMSO dn H1
file /export/home/~ dpwr 30
chemnmr/aakeroy/Uc~ dof 0
aquin/2003/ju10060~ dm nnn
3-4amidebenzyl2Meb~ dmm c
enzimidpure.fid dmf 200
ACQUISITION dseq
sfrq 399.822 dres 1.0
tn H1 homo n
at 3.701 PROCESSING
np 44416 wtfile
sw 6000.6 proc ft
fb 3400 fn 32768
bs 4 math f
tpwr 55
pw 19.8 werr
d1 1.000 wexp
tof 0 wbs
nt 4 wnt
ct 4
alock n
gain 30
FLAGS
ii n
in n
dp y
hs nn
DISPLAY
sp -980.1
wp 6000.6
vs 394
sc 0
wc 250
hzmm 24.00
is 4723.57
rfl 1979.7
rfp 999.6
th 20
ins 100.000
nm cdc ph

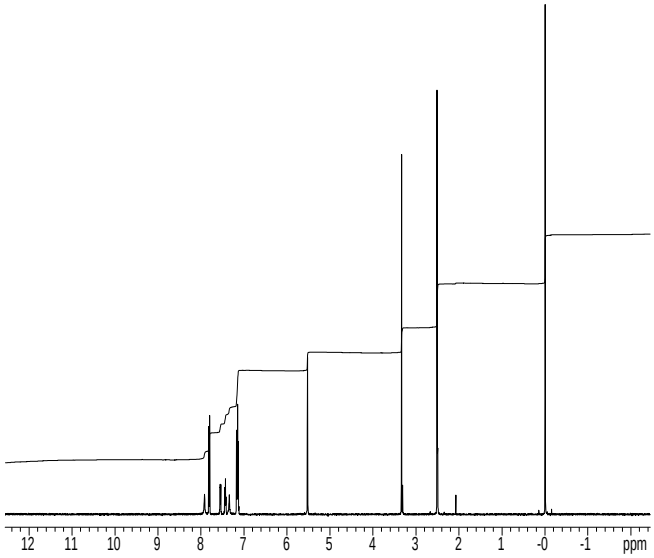

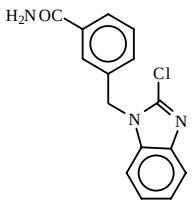

STANDARD 1H OBSERVE

exp1 std1h

	SAMPLE		DEC. & VT
date	Oct 6 2003	dfrq	399.822
solvent	DMSO	dn	H1
file	/export/home/~	dpwr	30
chemnmr/aakeroy/Jo~		dof	0
aquin/2003/ju10060~		dm	nnn
3-3amidebenzyl2Clb~		dmm	c
enzoimidoure.fid		dmf	200
	ACQUISITION	dseq	
sfrq	399.822	dres	1.0
tn	H1	homo	n
at	3.701		PROCESSING
np	44416	wtfile	
sw	6000.6	proc	ft
fb	3400	fn	32768
bs	4	math	f
tpwr	55		
pw	19.8	werr	
d1	1.000	wexp	
tof	0	wbs	
nt	4	wnt	
ct	4		
alock	n		
gain	30		
	FLAGS		
il	n		
in	n		
dp	y		
hs	nn		
	DISPLAY		
sp	-980.5		
wp	6000.6		
vs	733		
sc	0		
wc	250		
hzmm	24.00		
is	6664.45		
rfl	1980.1		
rfp	999.6		
th	20		
ins	100.000		
nm	cdc	ph	

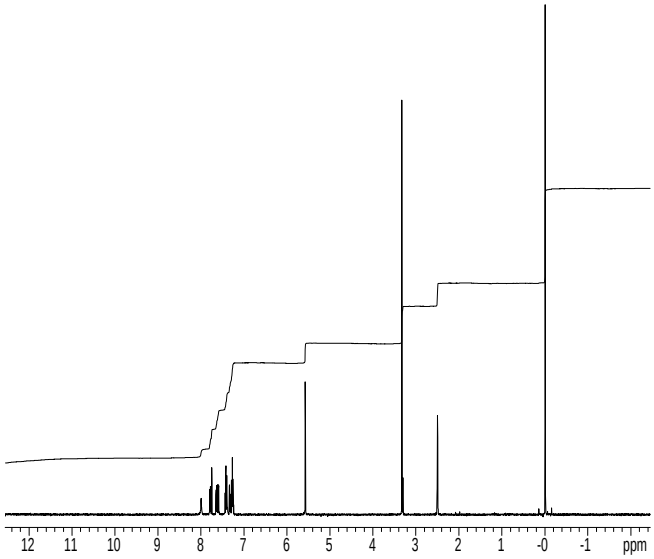

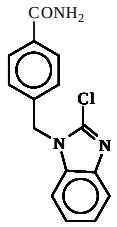

STANDARD 1H OBSERVE

exp1 std1h

SAMPLE DEC. & VT
date Oct 5 2003 dfrq 399.822
solvent DMSO dn H1
file /export/home/~ dpwr 30
chemnmr/aakeroy/Uc~ dof 0
aquin/2003/ju10050~ dm nnn
3-4amidebenzyl2Clb~ dmm c
enzimidpure.fid dmf 200
ACQUISITION dseq
sfrq 399.822 dres 1.0
tn H1 homo n
at 3.701 PROCESSING
np 44416 wtfile
sw 6000.6 proc ft
fb 3400 fn 32768
bs 4 math f
tpwr 55
pw 19.8 werr
d1 1.000 wexp
tof 0 wbs
nt 4 wnt
ct 4
alock n
gain 30
FLAGS
ii n
in n
dp y
hs nn
DISPLAY
sp -980.5
wp 6000.6
vs 845
sc 0
wc 250
hzmm 24.00
is 3633.90
rfl 1980.1
rfp 999.6
th 20
ins 100.000
nm cdc ph

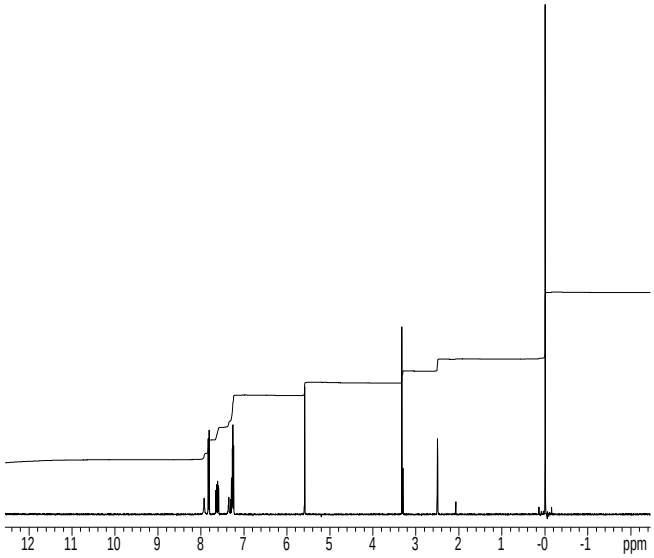

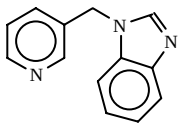

STANDARD 1H OBSERVE

exp1 std1h

SAMPLE		DEC. & VT	
date	Mar 8 2004	dfrq	399.816
solvent	DMSO	dn	H1
file	/export/home/~	dpwr	30
chemnmr/aakeroy/Jo~		dof	0
acqun/2004/ju03080~		dm	nnn
4-3benzimidazol1yl~		dmm	c
methylpyridnepure~		dmf	200
	fid	dseq	
ACQUISITION		dres	1.0
sfrq	399.816	homo	n
tn	H1	PROCESSING	
at	3.701	wtfile	
np	44416	proc	ft
sw	6000.6	fn	32768
fb	3400	math	f
bs	4		
tpwr	55	werr	
pw	19.8	wexp	
d1	1.000	wbs	
tof	0	wnt	
nt	4		
ct	4		
alock	n		
gain	30		
FLAGS			
ii	n		
in	n		
dp	y		
hs	nn		
DISPLAY			
sp	-987.1		
wp	6000.6		
vs	148		
sc	0		
wc	250		
hzmm	24.00		
is	6261.62		
rfl	1986.6		
rfp	999.5		
th	20		
ins	100.000		
nm	cdc	ph	

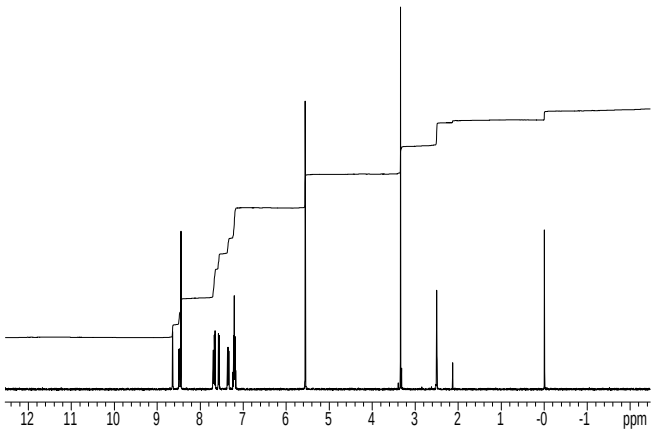

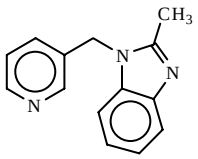

STANDARD 1H OBSERVE

exp1 std1h

	SAMPLE		DEC. & VT
date	Aug 17 2004	dfrq	399.809
solvent	cd3od	dn	H1
file /export/home/~		dpwr	30
chemnmr/aakeroy/Jo~		dof	0
aquin/2004/joaquin~		dm	nnn
	17Aug04.fid	dmm	c
	ACQUISITION	dmf	200
sfrq	399.809	dseq	
tn	H1	dres	1.0
at	3.701	homo	n
np	44416		PROCESSING
sw	6000.6	wtfile	
fb	3400	proc	ft
bs	4	fn	32768
tpwr	55	math	f
pw	6.0		
d1	1.000	werr	
tof	0	wexp	
nt	256	wbs	
ct	256	wnt	
alock	n		
gain	40		
	FLAGS		
il	n		
in	n		
dp	y		
hs	nn		
	DISPLAY		
sp	-1000.9		
wp	6000.6		
vs	418		
sc	0		
wc	250		
hzmm	24.00		
is	364.41		
rfl	1000.9		
rfp	0		
th	20		
ins	100.000		
nm	cdc	ph	

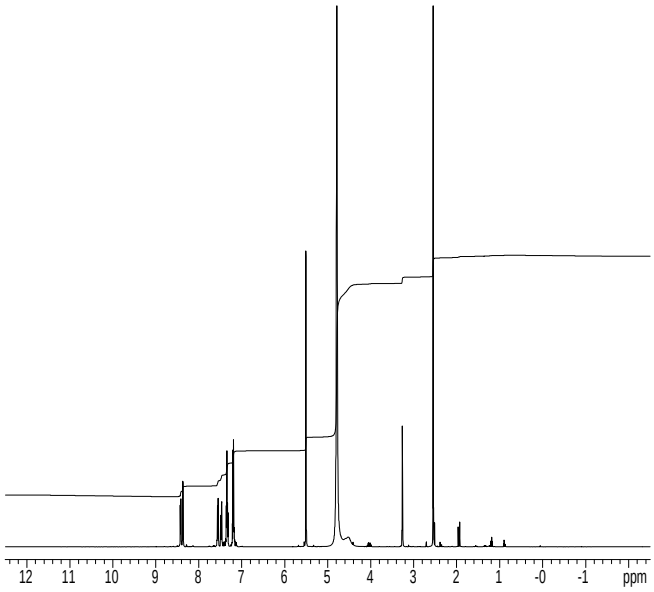

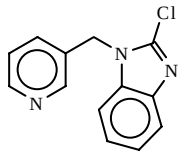

STANDARD 1H OBSERVE

exp1 std1h

SAMPLE		DEC. & VT	
date	Oct 27 2004	dfrq	399.809
solvent	DMSO	dn	H1
file	/export/home/~	dpwr	30
chemnmr/aakeroy/Jo~		dof	0
aquin/2004/ju10270~		dm	nnn
4-32Cbenzimidazol~		dmm	c
1ylmethylpyridinep~		dmf	200
	ure.fid	dseq	
ACQUISITION		dres	1.0
sfrq	399.809	homo	n
tn	H1	PROCESSING	
at	3.701	wtfile	
np	44416	proc	ft
sw	6000.6	fn	32768
fb	3400	math	f
bs	4		
tpwr	55	werr	
pw	19.8	wexp	
d1	1.000	wbs	
tof	0	wnt	
nt	4		
ct	4		
alock	n		
gain	not used		
FLAGS			
ii	n		
in	n		
dp	y		
hs	nn		
DISPLAY			
sp	-980.9		
wp	6000.6		
vs	186		
sc	0		
wc	250		
hzmm	24.00		
is	358.90		
rfl	1980.4		
rfp	999.5		
th	20		
ins	100.000		
nm	cdc	ph	

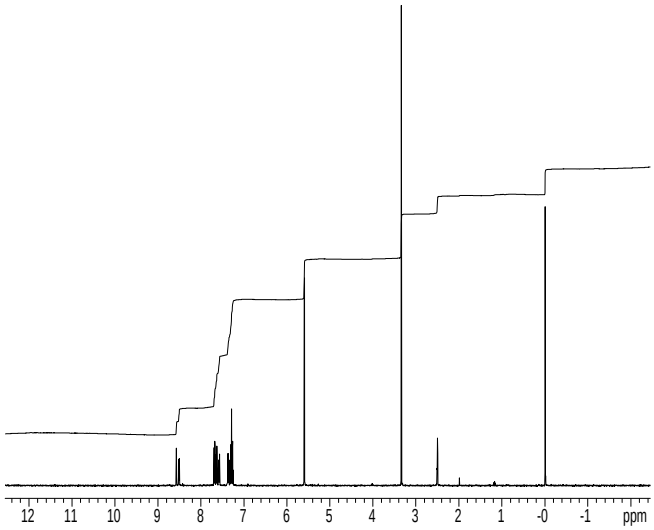

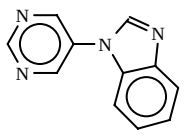

STANDARD 1H OBSERVE

exp1 std1h

SAMPLE		DEC. & VT	
date	Jan 19 2004	dfrq	399.816
solvent	DMSO	dn	H1
file	/export/home/~dpwr		30
chemnmr/aakeroy/Jo~		dof	0
aquin/2004/ju01190~		dm	nnn
4-5benzimidazol1yl~		dmm	c
pyrimidinepure.fid'		dmf	200
ACQUISITION		dseq	
sfrq	399.816	dres	1.0
tn	H1	homo	n
at	3.701	PROCESSING	
np	44416	wtfile	
sw	6000.6	proc	ft
fb	3400	fn	32768
bs	4	math	f
tpwr	55		
pw	19.8	werr	
d1	1.000	wexp	
tof	0	wbs	
nt	4	wnt	
ct	4		
alock	n		
gain	30		
FLAGS			
ii	n		
in	n		
dp	y		
hs	nn		
DISPLAY			
sp	-987.8		
wp	6000.6		
vs	80		
sc	0		
wc	250		
hzmm	24.00		
is	10360.78		
rfl	1987.4		
rfp	999.5		
th	20		
ins	100.000		
nm	cdc	ph	

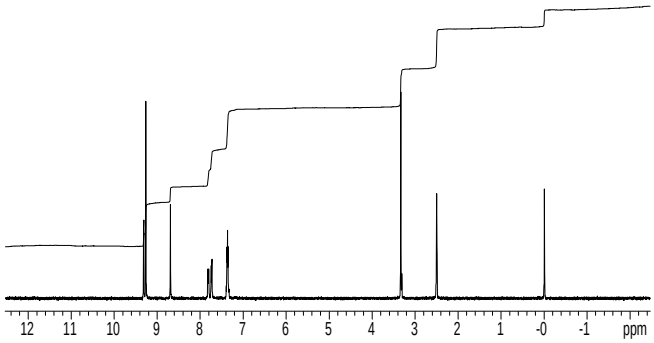

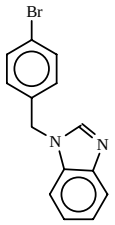

STANDARD 1H OBSERVE

exp1 std1h

	SAMPLE		DEC. & VT
date	Mar 4 2003	dfrq	399.822
solvent	DMSO	dn	H1
file	/export/home/~	dpwr	45
chemnmr/aakerov/Jo~		dof	0
aquin/2003/n/c004~		dm	nnn
4br-benzimid.fid		dmm	c
	ACQUISITION	dmf	6100
sfrq	399.822	dseq	
tn	H1	dres	1.0
at	3.701	homo	n
np	44416	PROCESSING	
sw	6000.6	wtfile	
fb	3400	proc	ft
bs	4	fn	32768
tpwr	55	math	f
pw	20.0		
d1	1.000	werr	
tof	0	wexp	
nt	4	wbs	
ct	4	wnt	
alock	n		
gain	48		
	FLAGS		
il	n		
in	n		
dp	y		
hs	nn		
	DISPLAY		
sp	-980.5		
wp	6000.6		
vs	166		
sc	0		
wc	250		
hzmm	24.00		
is	1340.24		
rfl	1980.1		
rfp	999.6		
th	20		
ins	100.000		
nm	cdc	ph	

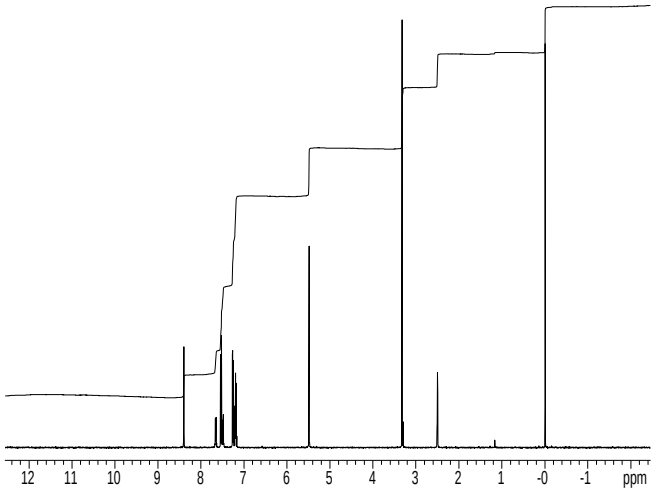

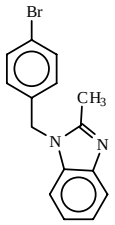

STANDARD 1H OBSERVE

exp1 std1h

SAMPLE DEC. & VT
date Apr 2 2003 dfrq 399.822
solvent DMSO dn H1
file /export/home/~ dpwr 45
chemr/nmr/aakerov/Jd~ dof 0
acqim/2003/Ju04020~ dm nnn
3-4Br2Mebenzimid.f~ dmm c
id dmf 6100
ACQUISITION dseq
sfrq 399.822 dres 1.0
tn H1 homo n
at 3.701 PROCESSING
np 44416 wtfile
sw 6000.6 proc ft
fb 3400 fn 32768
bs 4 math f
tpwr 55
pw 20.0 werr
d1 1.000 wexp
tof 0 wbs
nt 4 wnt
ct 4
alock n
gain not used
FLAGS
ii n
in n
dp y
hs nn
DISPLAY
sp -983.4
wp 6000.6
vs 178
sc 0
wc 250
hzmm 24.00
is 332.50
rfl 1983.0
rfp 999.6
th 20
ins 100.000
nm cdc ph

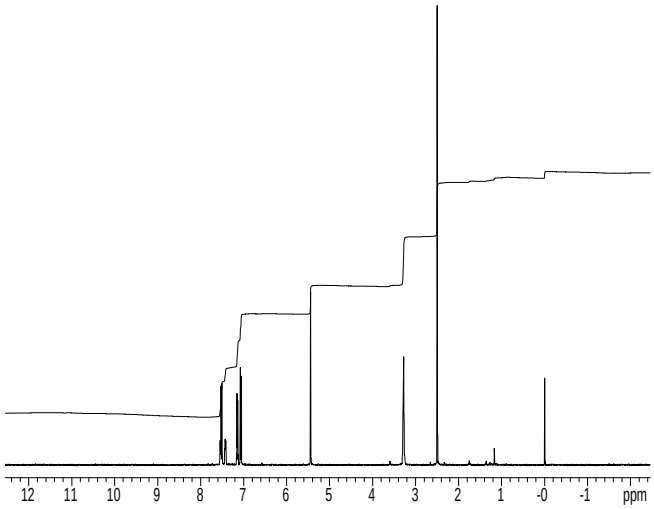

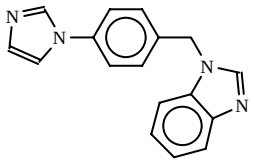

STANDARD 1H OBSERVE

exp1 std1h

SAMPLE		DEC. & VT	
date	Mar 20 2004	dfrq	399.816
solvent	DMSO	dn	H1
file	/export/home/~	dpwr	30
chemnmr/aakeroy/Jo~		dof	0
aquin/2004/ju04010~		dm	nnn
5-imidbenzylbenzim~		dmm	c
	std2.fid	dmf	200
ACQUISITION		dseq	
sfrq	399.816	dres	1.0
tn	H1	homo	n
at	3.701	PROCESSING	
np	44416	lb	0.50
sw	6000.6	wtfile	
fb	3400	proc	ft
bs	4	fn	32768
tpwr	55	math	f
pw	19.8		
d1	1.000	werr	
tof	0	wexp	
nt	4	wbs	
ct	4	wnt	
alock	n		
gain	30		
FLAGS			
il	n		
in	n		
dp	y		
hs	nn		
DISPLAY			
sp	-987.5		
wp	6000.6		
vs	106		
sc	0		
wc	250		
hzmm	24.00		
is	3817.24		
rfl	1987.0		
rfp	999.5		
th	20		
ins	100.000		
nm	cdc	ph	

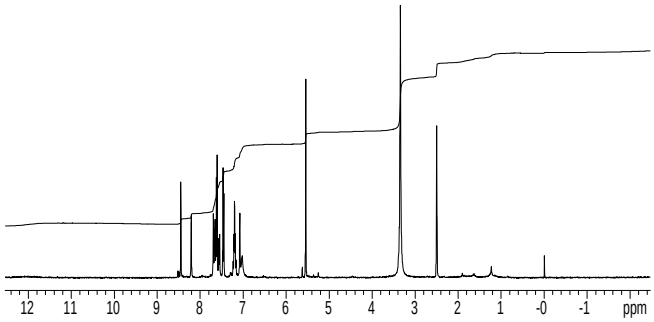

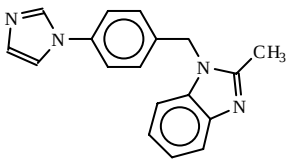

STANDARD 1H OBSERVE

exp1 std1h

	SAMPLE		DEC. & VT
date	Apr 1 2005	dfrq	399.803
solvent	DMSO	dn	H1
file	/export/home/~	dpwr	30
chemrlmr/aakeroy/Jd~		dof	0
aquin/2005/ju04010~		dm	nnn
5-imidbenzyl2Meben~		dmm	c
	zimod.fid	dmf	200
	ACQUISITION	dseq	
sfrq	399.803	dres	1.0
tn	H1	homo	n
at	3.701	PROCESSING	
np	44416	wtfile	
sw	6000.6	proc	ft
fb	3400	fn	32768
bs	4	math	f
tpwr	55		
pw	19.8	werr	
d1	1.000	wexp	
tof	0	wbs	
nt	32	wnt	
ct	32		
alock	n		
gain	not used		
	FLAGS		
il	n		
in	n		
dp	y		
hs	nn		
	DISPLAY		
sp	-986.8		
wp	6000.6		
vs	162		
sc	0		
wc	250		
hzmm	24.00		
is	333.60		
rfl	1986.3		
rfp	999.5		
th	20		
ins	100.000		
nm	cdc	ph	

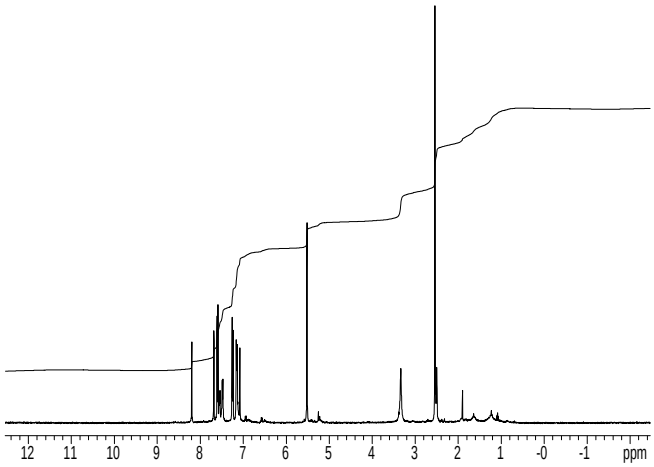

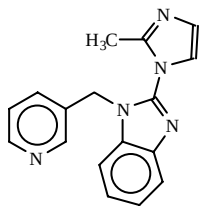

STANDARD 1H OBSERVE

exp1 std1h

SAMPLE DEC. & VT
date Mar 16 2005 dfrq 399.803
solvent DMSO dn H1
file /export/home/~ dpwr 30
chemnmr/aakerov/J6~ dof 0
aquin/2005/u03180~ dm nnn
5-quaternary2Meimi~ dmm c
dpurelargesc.fid dmf 200
ACQUISITION dseq
sfrq 399.803 dres 1.0
tn H1 homo n
at 3.701 PROCESSING
np 44416 wtfile
sw 6000.6 proc ft
fb 9400 fn 32768
bs 4 math f
tpwr 55
pw 6.0 werr
d1 1.000 wexp
tof 0 wbs
nt 4 wnt
ct 4
alock n
gain not used
FLAGS
ii n
in n
dp y
hs nn
DISPLAY
sp -986.4
wp 6000.6
vs 151
sc 0
wc 250
hzmm 24.00
is 214.44
rfl 1985.9
rfp 999.5
th 20
ins 100.000
nm cdc ph

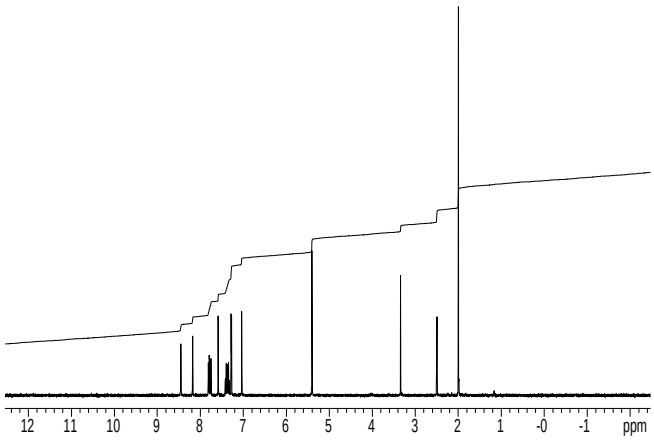

APPENDIX 2

LIST OF CRYSTALLOGRAPHIC TABLES

Table A1. Crystal data and structure refinement for **1**.

Empirical formula	C78 H54 N12 O18	
Formula weight	1447.33	
Temperature	203(2) K	
Wavelength	0.71073 Å	
Crystal system	Triclinic	
Space group	P-1	
Unit cell dimensions	a = 9.1053(3) Å	α= 93.474(3)°.
	b = 10.2214(4) Å	β= 91.530(2)°.
	c = 19.8293(7) Å	γ = 115.155(2)°.
Volume	1664.58(10) $Å^3$	
Z	1	
Density (calculated)	1.444 g/cm^3	
Absorption coefficient	0.105 mm^{-1}	
F(000)	750	
Crystal size	0.40 x 0.30 x 0.05 mm^3	
Theta range for data collection	2.06 to 28.27°.	
Index ranges	-11<=h<=11, -13<=k<=13, -24<=l<=26	
Reflections collected	12493	
Independent reflections	7441 [R(int) = 0.0412]	
Completeness to theta = 28.27°	90.1 %	
Absorption correction	None	
Refinement method	Full-matrix least-squares on F^2	
Data / restraints / parameters	7441 / 0 / 497	
Goodness-of-fit on F^2	0.883	
Final R indices [I>2sigma(I)]	R1 = 0.0522, wR2 = 0.1152	
R indices (all data)	R1 = 0.1087, wR2 = 0.1352	
Extinction coefficient	0.0194(15)	
Largest diff. peak and hole	0.360 and -0.293 $e.Å^{-3}$	

Table A2. Crystal data and structure refinement for **2**.

Empirical formula	C78 H54 N12 O18.30	
Formula weight	1452.13	
Temperature	203(2) K	
Wavelength	0.71073 Å	
Crystal system	Triclinic	
Space group	P-1	
Unit cell dimensions	a = 9.1469(18) Å	α= 93.606(4)°.
	b = 10.239(2) Å	β= 91.498(4)°.
	c = 19.880(4) Å	γ = 115.046(4)°.
Volume	1680.6(6) $Å^3$	
Z	1	
Density (calculated)	1.435 g/cm^3	
Absorption coefficient	0.105 mm^{-1}	
F(000)	752	
Crystal size	0.5 x 0.4 x 0.05 mm^3	
Theta range for data collection	1.03 to 27.48°.	
Index ranges	-11<=h<=11, -13<=k<=13, -25<=l<=25	
Reflections collected	11565	
Independent reflections	7336 [R(int) = 0.0209]	
Completeness to theta = 27.48°	95.1 %	
Absorption correction	None	
Refinement method	Full-matrix least-squares on F^2	
Data / restraints / parameters	7336 / 0 / 500	
Goodness-of-fit on F^2	0.918	
Final R indices [I>2sigma(I)]	R1 = 0.0472, wR2 = 0.1098	
R indices (all data)	R1 = 0.0991, wR2 = 0.1373	
Largest diff. peak and hole	0.240 and -0.238 $e.Å^{-3}$	

Table A3. Crystal data and structure refinement for **3**.

Empirical formula	C84 H60 N12 O18	
Formula weight	1525.44	
Temperature	203(2) K	
Wavelength	0.71073 Å	
Crystal system	Triclinic	
Space group	P-1	
Unit cell dimensions	a = 7.5039(15) Å	α= 107.274(3)°.
	b = 14.003(3) Å	β= 94.192(4)°.
	c = 18.931(4) Å	γ = 101.419(4)°.
Volume	1843.3(7) Å^3	
Z	1	
Density (calculated)	1.374 g/cm^3	
Absorption coefficient	0.099 mm^{-1}	
F(000)	792	
Crystal size	0.30 x 0.20 x 0.20 mm^3	
Theta range for data collection	1.57 to 23.85°.	
Index ranges	-8<=h<=7, -15<=k<=15, -21<=l<=21	
Reflections collected	8307	
Independent reflections	5593 [R(int) = 0.0254]	
Completeness to theta = 23.85°	98.1 %	
Absorption correction	None	
Refinement method	Full-matrix least-squares on F^2	
Data / restraints / parameters	5593 / 0 / 523	
Goodness-of-fit on F^2	0.870	
Final R indices [I>2sigma(I)]	R1 = 0.0502, wR2 = 0.1131	
R indices (all data)	R1 = 0.1119, wR2 = 0.1354	
Largest diff. peak and hole	0.556 and -0.340 e.Å^{-3}	

Table A4. Crystal data and structure refinement for **4**.

Empirical formula	C84 H66 N12 O18	
Formula weight	1531.49	
Temperature	203(2) K	
Wavelength	0.71073 Å	
Crystal system	Triclinic	
Space group	P-1	
Unit cell dimensions	a = 7.5699(16) Å	α= 106.044(4)°.
	b = 13.952(3) Å	β= 94.194(6)°.
	c = 19.020(4) Å	γ = 101.069(5)°.
Volume	1877.5(7) $Å^3$	
Z	1	
Density (calculated)	1.354 g/cm^3	
Absorption coefficient	0.097 mm^{-1}	
F(000)	798	
Crystal size	0.05 x 0.20 x 0.40 mm^3	
Theta range for data collection	1.56 to 27.48°.	
Index ranges	-9<=h<=9, -18<=k<=17, -24<=l<=24	
Reflections collected	14505	
Independent reflections	8216 [R(int) = 0.0622]	
Completeness to theta = 27.48°	95.5 %	
Absorption correction	None	
Refinement method	Full-matrix least-squares on F^2	
Data / restraints / parameters	8216 / 0 / 524	
Goodness-of-fit on F^2	0.860	
Final R indices [I>2sigma(I)]	R1 = 0.0592, wR2 = 0.1391	
R indices (all data)	R1 = 0.1321, wR2 = 0.1678	
Extinction coefficient	0.036(2)	
Largest diff. peak and hole	0.389 and -0.340 $e.Å^{-3}$	

Table A5. Crystal data and structure refinement for **5**.

Empirical formula	C74 H58 N10 O18	
Formula weight	1375.30	
Temperature	203(2) K	
Wavelength	0.71073 Å	
Crystal system	Triclinic	
Space group	P-1	
Unit cell dimensions	a = 7.5781(17) Å	α= 92.884(4)°.
	b = 9.419(2) Å	β= 92.293(6)°.
	c = 23.145(5) Å	γ = 105.501(4)°.
Volume	1587.4(6) $Å^3$	
Z	1	
Density (calculated)	1.439 g/cm^3	
Absorption coefficient	0.105 mm^{-1}	
F(000)	716	
Crystal size	0.28 x 0.12 x 0.08 mm^3	
Theta range for data collection	1.76 to 27.47°.	
Index ranges	-9<=h<=9, -12<=k<=11, -26<=l<=29	
Reflections collected	10469	
Independent reflections	6717 [R(int) = 0.0775]	
Completeness to theta = 27.47°	92.5 %	
Absorption correction	None	
Refinement method	Full-matrix least-squares on F^2	
Data / restraints / parameters	6717 / 0 / 470	
Goodness-of-fit on F^2	1.000	
Final R indices [I>2sigma(I)]	R1 = 0.0810, wR2 = 0.1628	
R indices (all data)	R1 = 0.1922, wR2 = 0.1838	
Extinction coefficient	0.0171(15)	
Largest diff. peak and hole	0.292 and -0.315 $e.Å^{-3}$	

Table A6. Crystal data and structure refinement for **6**.

Empirical formula	C66 H56 N10 O20	
Formula weight	1309.21	
Temperature	203(2) K	
Wavelength	0.71073 Å	
Crystal system	Triclinic	
Space group	P-1	
Unit cell dimensions	a = 7.2958(6) Å	α= 85.884(2)°.
	b = 9.3808(7) Å	β= 86.036(2)°.
	c = 22.8854(17) Å	γ = 77.521(2)°.
Volume	1523.0(2) $Å^3$	
Z	1	
Density (calculated)	1.427 g/cm^3	
Absorption coefficient	0.108 mm^{-1}	
F(000)	682	
Crystal size	0.40 x 0.40 x 0.25 mm^3	
Theta range for data collection	1.79 to 27.48°.	
Index ranges	-8<=h<=9, -11<=k<=10, -29<=l<=29	
Reflections collected	11376	
Independent reflections	6701 [R(int) = 0.0322]	
Completeness to theta = 27.48°	95.6 %	
Absorption correction	None	
Refinement method	Full-matrix least-squares on F^2	
Data / restraints / parameters	6701 / 0 / 443	
Goodness-of-fit on F^2	1.084	
Final R indices [I>2sigma(I)]	R1 = 0.0445, wR2 = 0.1300	
R indices (all data)	R1 = 0.0577, wR2 = 0.1391	
Extinction coefficient	0.047(3)	
Largest diff. peak and hole	0.359 and -0.243 $e.Å^{-3}$	

Table A7. Crystal data and structure refinement for **7**.

Empirical formula	C22 H18 N4	
Formula weight	338.40	
Temperature	203(2) K	
Wavelength	0.71073 Å	
Crystal system	Monoclinic	
Space group	C2/c	
Unit cell dimensions	a = 14.7435(5) Å	α= 90°.
	b = 18.5337(5) Å	β= 101.685(2)°.
	c = 12.6624(4) Å	γ = 90°.
Volume	3388.31(18) $Å^3$	
Z	8	
Density (calculated)	1.327 Mg/m^3	
Absorption coefficient	0.081 mm^{-1}	
F(000)	1424	
Crystal size	0.35 x 0.30 x 0.20 mm^3	
Theta range for data collection	1.79 to 28.29°.	
Index ranges	-18<=h<=17, -23<=k<=23, -16<=l<=15	
Reflections collected	12807	
Independent reflections	3982 [R(int) = 0.0543]	
Completeness to theta = 28.29°	94.4 %	
Absorption correction	None	
Refinement method	Full-matrix least-squares on F^2	
Data / restraints / parameters	3982 / 0 / 236	
Goodness-of-fit on F^2	0.969	
Final R indices [I>2sigma(I)]	R1 = 0.0423, wR2 = 0.1013	
R indices (all data)	R1 = 0.0688, wR2 = 0.1152	
Extinction coefficient	0.0141(9)	
Largest diff. peak and hole	0.224 and -0.228 $e.Å^{-3}$	

Table A8. Crystal data and structure refinement for **8**.

Empirical formula	$C_{22.80}H_{22}N_4O_{1.40}$	
Formula weight	374.44	
Temperature	203(2) K	
Wavelength	0.71073 Å	
Crystal system	Monoclinic	
Space group	C2/c	
Unit cell dimensions	a = 21.0283(12) Å	α= 90°.
	b = 10.3074(6) Å	β= 113.199(4)°.
	c = 18.9978(11) Å	γ = 90°.
Volume	3784.8(4) $Å^3$	
Z	8	
Density (calculated)	1.314 g/cm^3	
Absorption coefficient	0.085 mm^{-1}	
F(000)	1584	
Crystal size	0.35 x 0.30 x 0.25 mm^3	
Theta range for data collection	2.11 to 28.30°.	
Index ranges	-27<=h<=27, -13<=k<=13, -25<=l<=25	
Reflections collected	13677	
Independent reflections	4412 [R(int) = 0.0651]	
Completeness to theta = 28.30°	93.5 %	
Absorption correction	None	
Refinement method	Full-matrix least-squares on F^2	
Data / restraints / parameters	4412 / 6 / 279	
Goodness-of-fit on F^2	0.955	
Final R indices [I>2sigma(I)]	R1 = 0.0576, wR2 = 0.1488	
R indices (all data)	R1 = 0.1032, wR2 = 0.1708	
Extinction coefficient	0.0106(9)	
Largest diff. peak and hole	0.522 and -0.217 $e.Å^{-3}$	

Table A9. Crystal data and structure refinement for **9**.

Empirical formula	C24 H22 N4	
Formula weight	366.46	
Temperature	203(2) K	
Wavelength	0.71073 Å	
Crystal system	Monoclinic	
Space group	C2/c	
Unit cell dimensions	a = 29.5856(12) Å	α= 90°.
	b = 5.3536(2) Å	β= 113.442(2)°.
	c = 12.7407(6) Å	γ = 90°.
Volume	1851.43(13) $Å^3$	
Z	4	
Density (calculated)	1.315 g/cm^3	
Absorption coefficient	0.080 mm^{-1}	
F(000)	776	
Crystal size	0.45 x 0.45 x 0.10 mm^3	
Theta range for data collection	1.50 to 28.27°.	
Index ranges	-37<=h<=38, -7<=k<=7, -16<=l<=16	
Reflections collected	6700	
Independent reflections	2158 [R(int) = 0.0605]	
Completeness to theta = 28.27°	94.3 %	
Absorption correction	None	
Refinement method	Full-matrix least-squares on F^2	
Data / restraints / parameters	2158 / 0 / 128	
Goodness-of-fit on F^2	1.043	
Final R indices [I>2sigma(I)]	R1 = 0.0430, wR2 = 0.1112	
R indices (all data)	R1 = 0.0578, wR2 = 0.1218	
Extinction coefficient	0.032(3)	
Largest diff. peak and hole	0.216 and -0.167 $e.Å^{-3}$	

Table A10. Crystal data and structure refinement for **10**.

Empirical formula	C20 H22 N4 O4	
Formula weight	382.42	
Temperature	203(2) K	
Wavelength	0.71073 Å	
Crystal system	Monoclinic	
Space group	P2(1)/n	
Unit cell dimensions	a = 6.3599(9) Å	α= 90°.
	b = 9.7320(14) Å	β= 94.874(3)°.
	c = 15.357(2) Å	γ = 90°.
Volume	947.1(2) $Å^3$	
Z	2	
Density (calculated)	1.341 g/cm^3	
Absorption coefficient	0.095 mm^{-1}	
F(000)	404	
Crystal size	0.40 x 0.30 x 0.20 mm^3	
Theta range for data collection	2.48 to 28.23°.	
Index ranges	-8<=h<=8, -12<=k<=12, -20<=l<=20	
Reflections collected	6970	
Independent reflections	2200 [R(int) = 0.0431]	
Completeness to theta = 28.23°	93.7 %	
Absorption correction	None	
Refinement method	Full-matrix least-squares on F^2	
Data / restraints / parameters	2200 / 0 / 133	
Goodness-of-fit on F^2	1.073	
Final R indices [I>2sigma(I)]	R1 = 0.0534, wR2 = 0.1219	
R indices (all data)	R1 = 0.0709, wR2 = 0.1332	
Largest diff. peak and hole	0.259 and -0.510 $e.Å^{-3}$	

Table A11. Crystal data and structure refinement for **11**.

Empirical formula	C18 H18 N4 O4	
Formula weight	354.36	
Temperature	203(2) K	
Wavelength	0.71073 Å	
Crystal system	Monoclinic	
Space group	P2(1)/n	
Unit cell dimensions	a = 5.2226(6) Å	α= 90°.
	b = 13.2875(15) Å	β= 93.256(2)°.
	c = 12.1453(15) Å	γ = 90°.
Volume	841.47(17) $Å^3$	
Z	2	
Density (calculated)	1.399 g/cm^3	
Absorption coefficient	0.101 mm^{-1}	
F(000)	372	
Crystal size	0.45 x 0.40 x 0.30 mm^3	
Theta range for data collection	2.27 to 28.26°.	
Index ranges	-6<=h<=6, -17<=k<=17, -16<=l<=15	
Reflections collected	6268	
Independent reflections	1954 [R(int) = 0.0367]	
Completeness to theta = 28.26°	94.6 %	
Absorption correction	None	
Refinement method	Full-matrix least-squares on F^2	
Data / restraints / parameters	1954 / 0 / 124	
Goodness-of-fit on F^2	1.102	
Final R indices [I>2sigma(I)]	R1 = 0.0484, wR2 = 0.1153	
R indices (all data)	R1 = 0.0575, wR2 = 0.1228	
Largest diff. peak and hole	0.243 and -0.437 $e.Å^{-3}$	

Table A12. Crystal data and structure refinement for **12**.

Empirical formula	C18 H20 N4 O4	
Formula weight	356.38	
Temperature	203(2) K	
Wavelength	0.71073 Å	
Crystal system	Monoclinic	
Space group	P2(1)/n	
Unit cell dimensions	a = 5.0725(7) Å	α= 90°.
	b = 13.7671(18) Å	β= 91.248(3)°.
	c = 12.1951(17) Å	γ = 90°.
Volume	851.4(2) $Å^3$	
Z	2	
Density (calculated)	1.390 Mg/m^3	
Absorption coefficient	0.101 mm^{-1}	
F(000)	376	
Crystal size	0.40 x 0.40 x 0.25 mm^3	
Theta range for data collection	2.23 to 28.19°.	
Index ranges	-6<=h<=6, -17<=k<=17, -15<=l<=15	
Reflections collected	6042	
Independent reflections	1917 [R(int) = 0.0370]	
Completeness to theta = 28.19°	91.4 %	
Absorption correction	None	
Refinement method	Full-matrix least-squares on F^2	
Data / restraints / parameters	1917 / 0 / 125	
Goodness-of-fit on F^2	1.093	
Final R indices [I>2sigma(I)]	R1 = 0.0397, wR2 = 0.1037	
R indices (all data)	R1 = 0.0468, wR2 = 0.1083	
Extinction coefficient	0.089(8)	
Largest diff. peak and hole	0.305 and -0.187 $e.Å^{-3}$	

Table A13. Crystal data and structure refinement for **13**.

Empirical formula	C22 H20 N4 O4	
Formula weight	404.42	
Temperature	203(2) K	
Wavelength	0.71073 Å	
Crystal system	Monoclinic	
Space group	C2/c	
Unit cell dimensions	a = 28.229(4) Å	α= 90°.
	b = 6.9743(10) Å	β= 111.248(3)°.
	c = 10.8784(15) Å	γ = 90°.
Volume	1996.1(5) $Å^3$	
Z	4	
Density (calculated)	1.346 g/cm^3	
Absorption coefficient	0.095 mm^{-1}	
F(000)	848	
Crystal size	0.40 x 0.40 x 0.40 mm^3	
Theta range for data collection	1.55 to 28.28°.	
Index ranges	-35<=h<=37, -8<=k<=8, -14<=l<=14	
Reflections collected	7250	
Independent reflections	2307 [R(int) = 0.0656]	
Completeness to theta = 28.28°	92.8 %	
Absorption correction	None	
Refinement method	Full-matrix least-squares on F^2	
Data / restraints / parameters	2307 / 0 / 144	
Goodness-of-fit on F^2	1.045	
Final R indices [I>2sigma(I)]	R1 = 0.0479, wR2 = 0.1100	
R indices (all data)	R1 = 0.0722, wR2 = 0.1237	
Extinction coefficient	0.0343(16)	
Largest diff. peak and hole	0.213 and -0.213 $e.Å^{-3}$	

Table A14. Crystal data and structure refinement for **14**.

Empirical formula	C26 H22 N4 O4	
Formula weight	454.48	
Temperature	203(2) K	
Wavelength	0.71073 Å	
Crystal system	Monoclinic	
Space group	C2/c	
Unit cell dimensions	a = 19.6454(17) Å	α= 90°.
	b = 11.7257(11) Å	β= 108.704(2)°.
	c = 10.0116(8) Å	γ = 90°.
Volume	2184.4(3) $Å^3$	
Z	4	
Density (calculated)	1.382 g/cm^3	
Absorption coefficient	0.095 mm^{-1}	
F(000)	952	
Crystal size	0.40 x 0.20 x 0.05 mm^3	
Theta range for data collection	2.05 to 28.18°.	
Index ranges	-23<=h<=25, -15<=k<=14, -13<=l<=13	
Reflections collected	7892	
Independent reflections	2515 [R(int) = 0.0423]	
Completeness to theta = 28.18°	93.4 %	
Absorption correction	None	
Refinement method	Full-matrix least-squares on F^2	
Data / restraints / parameters	2515 / 0 / 161	
Goodness-of-fit on F^2	1.023	
Final R indices [I>2sigma(I)]	R1 = 0.0439, wR2 = 0.1158	
R indices (all data)	R1 = 0.0592, wR2 = 0.1265	
Extinction coefficient	0.0107(16)	
Largest diff. peak and hole	0.275 and -0.210 $e.Å^{-3}$	

Table A15. Crystal data and structure refinement for **15**.

Empirical formula	C25 H22 N4 O4	
Formula weight	442.47	
Temperature	203(2) K	
Wavelength	0.71073 Å	
Crystal system	Triclinic	
Space group	P-1	
Unit cell dimensions	a = 7.9999(12) Å	α= 75.050(3)°.
	b = 12.0030(17) Å	β= 73.567(3)°.
	c = 12.1462(17) Å	γ = 75.081(3)°.
Volume	1059.2(3) $Å^3$	
Z	2	
Density (calculated)	1.387 g/cm^3	
Absorption coefficient	0.096 mm^{-1}	
F(000)	464	
Crystal size	0.50 x 0.45 x 0.45 mm^3	
Theta range for data collection	1.78 to 27.87°.	
Index ranges	-10<=h<=10, -15<=k<=15, -15<=l<=15	
Reflections collected	7558	
Independent reflections	4633 [R(int) = 0.0309]	
Completeness to theta = 27.87°	91.6 %	
Absorption correction	None	
Refinement method	Full-matrix least-squares on F^2	
Data / restraints / parameters	4633 / 0 / 318	
Goodness-of-fit on F^2	1.094	
Final R indices [I>2sigma(I)]	R1 = 0.0559, wR2 = 0.1645	
R indices (all data)	R1 = 0.0671, wR2 = 0.1705	
Extinction coefficient	0.086(7)	
Largest diff. peak and hole	0.446 and -0.258 $e.Å^{-3}$	

Table A16. Crystal data and structure refinement for **16**.

Empirical formula	C31 H26.50 N4 O4.50	
Formula weight	527.06	
Temperature	203(2) K	
Wavelength	0.71073 Å	
Crystal system	Triclinic	
Space group	P-1	
Unit cell dimensions	a = 7.2994(5) Å	α= 81.721(2)°.
	b = 12.8648(10) Å	β= 89.530(2)°.
	c = 14.6528(11) Å	γ = 74.090(2)°.
Volume	1308.77(17) $Å^3$	
Z	2	
Density (calculated)	1.337 g/cm^3	
Absorption coefficient	0.091 mm^{-1}	
F(000)	553	
Crystal size	0.50 x 0.45 x 0.45 mm^3	
Theta range for data collection	1.41 to 27.10°.	
Index ranges	-8<=h<=9, -16<=k<=15, -17<=l<=18	
Reflections collected	8877	
Independent reflections	5333 [R(int) = 0.0330]	
Completeness to theta = 27.10°	92.3 %	
Absorption correction	None	
Refinement method	Full-matrix least-squares on F^2	
Data / restraints / parameters	5333 / 6 / 372	
Goodness-of-fit on F^2	1.056	
Final R indices [I>2sigma(I)]	R1 = 0.0487, wR2 = 0.1334	
R indices (all data)	R1 = 0.0594, wR2 = 0.1425	
Extinction coefficient	0.107(7)	
Largest diff. peak and hole	0.380 and -0.511 $e.Å^{-3}$	

Table A17. Crystal data and structure refinement for **17**.

Empirical formula	C31 H27.50 N5 O4.50	
Formula weight	542.08	
Temperature	203(2) K	
Wavelength	0.71073 Å	
Crystal system	Triclinic	
Space group	P-1	
Unit cell dimensions	a = 7.5488(4) Å	α= 97.729(3)°.
	b = 12.6754(6) Å	β= 91.058(4)°.
	c = 14.4453(8) Å	γ = 105.310(3)°.
Volume	1318.91(12) $Å^3$	
Z	2	
Density (calculated)	1.365 g/cm^3	
Absorption coefficient	0.094 mm^{-1}	
F(000)	569	
Crystal size	0.45 x 0.45 x 0.15 mm^3	
Theta range for data collection	1.42 to 28.31°.	
Index ranges	-10<=h<=10, -16<=k<=16, -18<=l<=18	
Reflections collected	10106	
Independent reflections	5914 [R(int) = 0.0450]	
Completeness to theta = 28.31°	90.3 %	
Absorption correction	None	
Refinement method	Full-matrix least-squares on F^2	
Data / restraints / parameters	5914 / 6 / 390	
Goodness-of-fit on F^2	1.030	
Final R indices [I>2sigma(I)]	R1 = 0.0460, wR2 = 0.1143	
R indices (all data)	R1 = 0.0657, wR2 = 0.1264	
Extinction coefficient	0.072(5)	
Largest diff. peak and hole	0.320 and -0.233 $e.Å^{-3}$	

Table A18. Crystal data and structure refinement for **18**.

Empirical formula	C25 H22 N4 O4	
Formula weight	442.47	
Temperature	203(2) K	
Wavelength	0.71073 Å	
Crystal system	Monoclinic	
Space group	P2(1)/n	
Unit cell dimensions	a = 14.7902(15) Å	α= 90°.
	b = 8.5534(7) Å	β= 95.463(6)°.
	c = 17.1781(15) Å	γ = 90°.
Volume	2163.3(3) $Å^3$	
Z	4	
Density (calculated)	1.359 g/cm^3	
Absorption coefficient	0.094 mm^{-1}	
F(000)	928	
Crystal size	0.40 x 0.30 x 0.20 mm^3	
Theta range for data collection	1.74 to 28.31°.	
Index ranges	-19<=h<=19, -11<=k<=10, -21<=l<=22	
Reflections collected	15583	
Independent reflections	5039 [R(int) = 0.0377]	
Completeness to theta = 28.31°	93.5 %	
Absorption correction	None	
Refinement method	Full-matrix least-squares on F^2	
Data / restraints / parameters	5039 / 0 / 305	
Goodness-of-fit on F^2	1.017	
Final R indices [I>2sigma(I)]	R1 = 0.0428, wR2 = 0.1086	
R indices (all data)	R1 = 0.0629, wR2 = 0.1179	
Extinction coefficient	0.0208(17)	
Largest diff. peak and hole	0.281 and -0.223 $e.Å^{-3}$	

Table A19. Crystal data and structure refinement for **19**.

Empirical formula	C30 H30 N4 O4	
Formula weight	510.58	
Temperature	203(2) K	
Wavelength	0.71073 Å	
Crystal system	Triclinic	
Space group	P-1	
Unit cell dimensions	a = 8.3455(19) Å	α= 77.825(14)°.
	b = 9.0921(19) Å	β= 75.061(15)°.
	c = 9.858(2) Å	γ = 66.352(9)°.
Volume	657.1(3) $Å^3$	
Z	1	
Density (calculated)	1.290 g/cm^3	
Absorption coefficient	0.087 mm^{-1}	
F(000)	270	
Crystal size	0.40 x 0.20 x 0.10 mm^3	
Theta range for data collection	2.15 to 28.23°.	
Index ranges	-9<=h<=10, -10<=k<=11, -13<=l<=12	
Reflections collected	4931	
Independent reflections	2969 [R(int) = 0.0393]	
Completeness to theta = 28.23°	91.5 %	
Absorption correction	None	
Refinement method	Full-matrix least-squares on F^2	
Data / restraints / parameters	2969 / 3 / 183	
Goodness-of-fit on F^2	0.891	
Final R indices [I>2sigma(I)]	R1 = 0.0467, wR2 = 0.0956	
R indices (all data)	R1 = 0.0990, wR2 = 0.1132	
Extinction coefficient	0.076(6)	
Largest diff. peak and hole	0.209 and -0.291 $e.Å^{-3}$	

Table A20. Crystal data and structure refinement for **20**.

Empirical formula	C30 H32 N4 O4	
Formula weight	512.60	
Temperature	203(2) K	
Wavelength	0.71073 Å	
Crystal system	Triclinic	
Space group	P-1	
Unit cell dimensions	a = 8.4774(18) Å	α= 78.057(14)°.
	b = 9.306(2) Å	β= 67.175(12)°.
	c = 9.4594(18) Å	γ = 74.613(15)°.
Volume	658.6(2) $Å^3$	
Z	1	
Density (calculated)	1.292 g/cm^3	
Absorption coefficient	0.087 mm^{-1}	
F(000)	272	
Crystal size	0.40 x 0.40 x 0.10 mm^3	
Theta range for data collection	2.29 to 27.48°.	
Index ranges	-10<=h<=10, -12<=k<=11, -11<=l<=12	
Reflections collected	4637	
Independent reflections	2856 [R(int) = 0.0442]	
Completeness to theta = 27.48°	95.1 %	
Absorption correction	None	
Refinement method	Full-matrix least-squares on F^2	
Data / restraints / parameters	2856 / 0 / 175	
Goodness-of-fit on F^2	0.939	
Final R indices [I>2sigma(I)]	R1 = 0.0529, wR2 = 0.1176	
R indices (all data)	R1 = 0.0836, wR2 = 0.1296	
Largest diff. peak and hole	0.221 and -0.428 e.$Å^{-3}$	

Table A21. Crystal data and structure refinement for **21**.

Empirical formula	C15 H13 N3 O	
Formula weight	251.28	
Temperature	203(2) K	
Wavelength	0.71073 Å	
Crystal system	Triclinic	
Space group	P-1	
Unit cell dimensions	a = 9.2133(11) Å	α= 104.058(9)°.
	b = 11.6848(13) Å	β= 98.623(8)°.
	c = 12.1071(15) Å	γ = 94.900(7)°.
Volume	1239.9(3) $Å^3$	
Z	4	
Density (calculated)	1.346 g/cm^3	
Absorption coefficient	0.088 mm^{-1}	
F(000)	528	
Crystal size	0.40 x 0.35 x 0.10 mm^3	
Theta range for data collection	2.25 to 27.87°.	
Index ranges	-11<=h<=12, -15<=k<=15, -15<=l<=15	
Reflections collected	8487	
Independent reflections	5341 [R(int) = 0.0514]	
Completeness to theta = 27.87°	90.4 %	
Absorption correction	None	
Refinement method	Full-matrix least-squares on F^2	
Data / restraints / parameters	5341 / 0 / 356	
Goodness-of-fit on F^2	0.988	
Final R indices [I>2sigma(I)]	R1 = 0.0510, wR2 = 0.1208	
R indices (all data)	R1 = 0.0894, wR2 = 0.1409	
Extinction coefficient	0.015(2)	
Largest diff. peak and hole	0.286 and -0.247 $e.Å^{-3}$	

Table A22. Crystal data and structure refinement for **22**.

Empirical formula	C16 H15 N3 O	
Formula weight	265.31	
Temperature	203(2) K	
Wavelength	0.71073 Å	
Crystal system	Triclinic	
Space group	P-1	
Unit cell dimensions	a = 8.7022(19) Å	α= 93.162(17)°.
	b = 12.118(3) Å	β= 106.515(12)°.
	c = 13.920(3) Å	γ = 110.538(15)°.
Volume	1298.1(5) $Å^3$	
Z	4	
Density (calculated)	1.358 g/cm^3	
Absorption coefficient	0.088 mm^{-1}	
F(000)	560	
Crystal size	0.40 x 0.35 x 0.10 mm^3	
Theta range for data collection	2.18 to 27.47°.	
Index ranges	-10<=h<=9, -15<=k<=15, -16<=l<=17	
Reflections collected	7988	
Independent reflections	5294 [R(int) = 0.0483]	
Completeness to theta = 27.47°	88.9 %	
Absorption correction	None	
Refinement method	Full-matrix least-squares on F^2	
Data / restraints / parameters	5294 / 0 / 373	
Goodness-of-fit on F^2	0.899	
Final R indices [I>2sigma(I)]	R1 = 0.0660, wR2 = 0.1607	
R indices (all data)	R1 = 0.1232, wR2 = 0.1845	
Largest diff. peak and hole	0.482 and -0.445 $e.Å^{-3}$	

Table A23. Crystal data and structure refinement for **23**.

Empirical formula	C16 H15 N3 O	
Formula weight	265.31	
Temperature	203(2) K	
Wavelength	0.71073 Å	
Crystal system	Monoclinic	
Space group	P2(1)/c	
Unit cell dimensions	a = 9.9852(13) Å	α= 90°.
	b = 15.912(2) Å	β= 93.480(9)°.
	c = 8.3680(13) Å	γ = 90°.
Volume	1327.1(3) $Å^3$	
Z	4	
Density (calculated)	1.328 g/cm^3	
Absorption coefficient	0.086 mm^{-1}	
F(000)	560	
Crystal size	0.40 x 0.10 x 0.10 mm^3	
Theta range for data collection	2.41 to 28.58°.	
Index ranges	-13<=h<=13, -20<=k<=20, -11<=l<=10	
Reflections collected	9462	
Independent reflections	3155 [R(int) = 0.1088]	
Completeness to theta = 28.58°	92.8 %	
Absorption correction	None	
Refinement method	Full-matrix least-squares on F^2	
Data / restraints / parameters	3155 / 0 / 188	
Goodness-of-fit on F^2	0.895	
Final R indices [I>2sigma(I)]	R1 = 0.0514, wR2 = 0.1119	
R indices (all data)	R1 = 0.1462, wR2 = 0.1480	
Extinction coefficient	0.062(5)	
Largest diff. peak and hole	0.226 and -0.212 $e.Å^{-3}$	

Table A24. Crystal data and structure refinement for **24**.

Empirical formula	C15 H12 Cl N3 O	
Formula weight	285.73	
Temperature	203(2) K	
Wavelength	0.71073 Å	
Crystal system	Triclinic	
Space group	P-1	
Unit cell dimensions	a = 8.8067(7) Å	α= 74.800(4)°.
	b = 11.8803(12) Å	β= 72.485(5)°.
	c = 14.0856(15) Å	γ = 68.786(4)°.
Volume	1290.5(2) $Å^3$	
Z	4	
Density (calculated)	1.471 g/cm^3	
Absorption coefficient	0.294 mm^{-1}	
F(000)	592	
Crystal size	0.20 x 0.40 x 0.40 mm^3	
Theta range for data collection	2.21 to 28.25°.	
Index ranges	-11<=h<=11, -15<=k<=15, -17<=l<=18	
Reflections collected	9203	
Independent reflections	5752 [R(int) = 0.0485]	
Completeness to theta = 28.25°	90.1 %	
Absorption correction	None	
Refinement method	Full-matrix least-squares on F^2	
Data / restraints / parameters	5752 / 0 / 373	
Goodness-of-fit on F^2	1.007	
Final R indices [I>2sigma(I)]	R1 = 0.0438, wR2 = 0.1209	
R indices (all data)	R1 = 0.0653, wR2 = 0.1305	
Largest diff. peak and hole	0.221 and -0.389 $e.Å^{-3}$	

Table A25. Crystal data and structure refinement for **25**.

Empirical formula	C15 H14 Cl N3 O2	
Formula weight	303.74	
Temperature	203(2) K	
Wavelength	0.71073 Å	
Crystal system	Orthorhombic	
Space group	P2(1)2(1)2(1)	
Unit cell dimensions	a = 6.0212(10) Å	α= 90°.
	b = 12.4652(19) Å	β= 90°.
	c = 19.166(3) Å	γ = 90°.
Volume	1438.5(4) $Å^3$	
Z	4	
Density (calculated)	1.402 g/cm^3	
Absorption coefficient	0.273 mm^{-1}	
F(000)	632	
Crystal size	0.40 x 0.25 x 0.10 mm^3	
Theta range for data collection	2.68 to 28.33°.	
Index ranges	-7<=h<=7, -15<=k<=16, -25<=l<=16	
Reflections collected	6885	
Independent reflections	3255 [R(int) = 0.0484]	
Completeness to theta = 28.33°	94.4 %	
Absorption correction	None	
Refinement method	Full-matrix least-squares on F^2	
Data / restraints / parameters	3255 / 0 / 204	
Goodness-of-fit on F^2	0.937	
Final R indices [I>2sigma(I)]	R1 = 0.0382, wR2 = 0.0755	
R indices (all data)	R1 = 0.0602, wR2 = 0.0821	
Absolute structure parameter	0.28(7)	
Extinction coefficient	0.044(2)	
Largest diff. peak and hole	0.225 and -0.201 $e.Å^{-3}$	

Table A26. Crystal data and structure refinement for **26**.

Empirical formula	C22 H18 N4 O5	
Formula weight	418.40	
Temperature	203(2) K	
Wavelength	0.71073 Å	
Crystal system	Triclinic	
Space group	P-1	
Unit cell dimensions	a = 7.5178(9) Å	α= 105.516(6)°.
	b = 9.1850(11) Å	β= 100.600(7)°.
	c = 15.0850(15) Å	γ = 100.339(8)°.
Volume	957.36(19) $Å^3$	
Z	2	
Density (calculated)	1.451 g/cm^3	
Absorption coefficient	0.106 mm^{-1}	
F(000)	436	
Crystal size	0.30 x 0.25 x 0.20 mm^3	
Theta range for data collection	2.36 to 28.25°.	
Index ranges	-9<=h<=10, -12<=k<=12, -17<=l<=19	
Reflections collected	7257	
Independent reflections	4292 [R(int) = 0.0629]	
Completeness to theta = 28.25°	90.9 %	
Absorption correction	None	
Refinement method	Full-matrix least-squares on F^2	
Data / restraints / parameters	4292 / 0 / 290	
Goodness-of-fit on F^2	0.977	
Final R indices [I>2sigma(I)]	R1 = 0.0529, wR2 = 0.1338	
R indices (all data)	R1 = 0.0794, wR2 = 0.1513	
Extinction coefficient	0.031(5)	
Largest diff. peak and hole	0.371 and -0.325 $e.Å^{-3}$	

Table A27. Crystal data and structure refinement for **27**.

Empirical formula	C30 H25 N5 O9	
Formula weight	599.55	
Temperature	173(2) K	
Wavelength	0.71073 Å	
Crystal system	Triclinic	
Space group	P-1	
Unit cell dimensions	a = 7.5292(5) Å	α= 81.865(4)°.
	b = 11.0980(8) Å	β= 77.854(3)°.
	c = 17.2512(11) Å	γ = 74.581(4)°.
Volume	1352.89(16) $Å^3$	
Z	2	
Density (calculated)	1.472 g/cm^3	
Absorption coefficient	0.111 mm^{-1}	
F(000)	624	
Crystal size	0.40 x 0.35 x 0.05 mm^3	
Theta range for data collection	2.43 to 28.27°.	
Index ranges	-9<=h<=9, -14<=k<=14, -22<=l<=22	
Reflections collected	10285	
Independent reflections	6089 [R(int) = 0.0677]	
Completeness to theta = 28.27°	91.2 %	
Absorption correction	None	
Refinement method	Full-matrix least-squares on F^2	
Data / restraints / parameters	6089 / 0 / 410	
Goodness-of-fit on F^2	0.837	
Final R indices [I>2sigma(I)]	R1 = 0.0491, wR2 = 0.1016	
R indices (all data)	R1 = 0.1211, wR2 = 0.1269	
Extinction coefficient	0.0140(13)	
Largest diff. peak and hole	0.339 and -0.272 $e.Å^{-3}$	

Table A28. Crystal data and structure refinement for **28**.

Empirical formula	C30 H24 Cl2 N4 O7	
Formula weight	623.43	
Temperature	173(2) K	
Wavelength	0.71073 Å	
Crystal system	Monoclinic	
Space group	P2(1)/c	
Unit cell dimensions	a = 21.633(2) Å	α= 90°.
	b = 9.6239(10) Å	β= 98.655(6)°.
	c = 13.3888(14) Å	γ = 90°.
Volume	2755.8(5) $Å^3$	
Z	4	
Density (calculated)	1.503 g/cm^3	
Absorption coefficient	0.293 mm^{-1}	
F(000)	1288	
Crystal size	0.40 x 0.40 x 0.15 mm^3	
Theta range for data collection	1.90 to 28.28°.	
Index ranges	-27<=h<=28, -12<=k<=12, -17<=l<=15	
Reflections collected	19818	
Independent reflections	6399 [R(int) = 0.0957]	
Completeness to theta = 28.28°	93.7 %	
Absorption correction	None	
Refinement method	Full-matrix least-squares on F^2	
Data / restraints / parameters	6399 / 0 / 401	
Goodness-of-fit on F^2	0.942	
Final R indices [I>2sigma(I)]	R1 = 0.0496, wR2 = 0.1221	
R indices (all data)	R1 = 0.0743, wR2 = 0.1368	
Extinction coefficient	0.0102(10)	
Largest diff. peak and hole	0.386 and -0.334 $e.Å^{-3}$	

Table A29. Crystal data and structure refinement for **29**.

Empirical formula	C32 H30 Ag B F4 N6 O5.40	
Formula weight	779.70	
Temperature	163(2) K	
Wavelength	0.71073 Å	
Crystal system	Monoclinic	
Space group	C2/c	
Unit cell dimensions	a = 40.141(3) Å	α= 90°.
	b = 4.9633(5) Å	β= 96.855(6)°.
	c = 18.6857(19) Å	γ = 90°.
Volume	3696.1(6) $Å^3$	
Z	4	
Density (calculated)	1.401 g/cm^3	
Absorption coefficient	0.612 mm^{-1}	
F(000)	1581	
Crystal size	0.46 x 0.16 x 0.14 mm^3	
Theta range for data collection	2.04 to 28.23°.	
Index ranges	-51<=h<=47, -6<=k<=6, -24<=l<=24	
Reflections collected	12547	
Independent reflections	4292 [R(int) = 0.0324]	
Completeness to theta = 28.23°	93.6 %	
Absorption correction	Semi-empirical from equivalents	
Max. and min. transmission	1.000 and 0.577	
Refinement method	Full-matrix least-squares on F^2	
Data / restraints / parameters	4292 / 20 / 261	
Goodness-of-fit on F^2	1.292	
Final R indices [I>2sigma(I)]	R1 = 0.0574, wR2 = 0.1715	
R indices (all data)	R1 = 0.0835, wR2 = 0.1863	
Largest diff. peak and hole	1.532 and -0.819 $e.Å^{-3}$	

Table A30. Crystal data and structure refinement for **30**.

Empirical formula	C32 H30 Ag B F4 N6 O2	
Formula weight	725.30	
Temperature	203(2) K	
Wavelength	0.71073 Å	
Crystal system	Triclinic	
Space group	P-1	
Unit cell dimensions	a = 11.666(2) Å	α= 109.136(13)°.
	b = 12.237(2) Å	β= 114.266(8)°.
	c = 13.013(2) Å	γ = 92.310(14)°.
Volume	1566.6(5) $Å^3$	
Z	2	
Density (calculated)	1.538 g/cm^3	
Absorption coefficient	0.708 mm^{-1}	
F(000)	736	
Crystal size	0.46 x 0.20 x 0.10 mm^3	
Theta range for data collection	1.80 to 27.48°.	
Index ranges	-14<=h<=15, -14<=k<=15, -16<=l<=16	
Reflections collected	11253	
Independent reflections	6860 [R(int) = 0.0408]	
Completeness to theta = 27.48°	95.5 %	
Absorption correction	None	
Refinement method	Full-matrix least-squares on F^2	
Data / restraints / parameters	6860 / 20 / 448	
Goodness-of-fit on F^2	0.918	
Final R indices [I>2sigma(I)]	R1 = 0.0385, wR2 = 0.0844	
R indices (all data)	R1 = 0.0634, wR2 = 0.0929	
Largest diff. peak and hole	0.398 and -0.944 $e.Å^{-3}$	

Table A31. Crystal data and structure refinement for **31**.

Empirical formula	C33 H34 Ag As F6 N6 O3	
Formula weight	859.45	
Temperature	100(2) K	
Wavelength	0.71073 Å	
Crystal system	Monoclinic	
Space group	P2(1)/c	
Unit cell dimensions	a = 7.3084(4) Å	α= 90°.
	b = 18.5828(11) Å	β= 96.8060(10)°.
	c = 25.1620(15) Å	γ = 90°.
Volume	3393.2(3) $Å^3$	
Z	4	
Density (calculated)	1.682 g/cm^3	
Absorption coefficient	1.639 mm^{-1}	
F(000)	1728	
Crystal size	0.10 x 0.15 x 0.26 mm^3	
Theta range for data collection	1.96 to 30.02°.	
Index ranges	-10<=h<=10, -24<=k<=26, -35<=l<=34	
Reflections collected	38915	
Independent reflections	9874 [R(int) = 0.0316]	
Completeness to theta = 30.02°	99.5 %	
Absorption correction	Semi-empirical from equivalents	
Max. and min. transmission	1.000 and 0.791	
Refinement method	Full-matrix least-squares on F^2	
Data / restraints / parameters	9874 / 25 / 486	
Goodness-of-fit on F^2	1.079	
Final R indices [I>2sigma(I)]	R1 = 0.0382, wR2 = 0.1073	
R indices (all data)	R1 = 0.0472, wR2 = 0.1133	
Largest diff. peak and hole	1.379 and -0.840 $e.Å^{-3}$	

Table A32. Crystal data and structure refinement for **32**.

Empirical formula	C32.50 H32 Ag As F6 N6 O2.50	
Formula weight	843.43	
Temperature	203(2) K	
Wavelength	0.71073 Å	
Crystal system	Triclinic	
Space group	P-1	
Unit cell dimensions	a = 11.8443(8) Å	α= 66.333(3)°.
	b = 12.1157(7) Å	β= 69.670(3)°.
	c = 13.3329(8) Å	γ = 87.960(3)°.
Volume	1631.16(17) $Å^3$	
Z	2	
Density (calculated)	1.717 g/cm^3	
Absorption coefficient	1.702 mm^{-1}	
F(000)	846	
Crystal size	0.35 x 0.25 x 0.20 mm^3	
Theta range for data collection	1.85 to 27.88°.	
Index ranges	-15<=h<=14, -15<=k<=15, -16<=l<=17	
Reflections collected	11734	
Independent reflections	7133 [R(int) = 0.0330]	
Completeness to theta = 27.88°	91.8 %	
Absorption correction	Semi-empirical from equivalents	
Max. and min. transmission	1.000 and 0.639	
Refinement method	Full-matrix least-squares on F^2	
Data / restraints / parameters	7133 / 4 / 458	
Goodness-of-fit on F^2	1.043	
Final R indices [I>2sigma(I)]	R1 = 0.0481, wR2 = 0.1286	
R indices (all data)	R1 = 0.0590, wR2 = 0.1361	
Largest diff. peak and hole	0.682 and -1.195 $e.Å^{-3}$	

Table A33. Crystal data and structure refinement for **33**.

Empirical formula	C32 H30 Ag F6 N6 O5 Sb	
Formula weight	922.24	
Temperature	100(2) K	
Wavelength	0.71073 Å	
Crystal system	Monoclinic	
Space group	P2(1)/c	
Unit cell dimensions	a = 7.5069(5) Å	α= 90°.
	b = 18.6924(12) Å	β= 98.4920(10)°.
	c = 24.9808(17) Å	γ = 90°.
Volume	3466.9(4) $Å^3$	
Z	4	
Density (calculated)	1.767 g/cm^3	
Absorption coefficient	1.426 mm^{-1}	
F(000)	1824	
Crystal size	0.40 x 0.29 x 0.20 mm^3	
Theta range for data collection	1.98 to 30.01°.	
Index ranges	-10<=h<=10, -26<=k<=26, -34<=l<=35	
Reflections collected	39338	
Independent reflections	10098 [R(int) = 0.0361]	
Completeness to theta = 30.01°	99.6 %	
Absorption correction	Semi-empirical from equivalents	
Max. and min. transmission	1.000 and 0.768	
Refinement method	Full-matrix least-squares on F^2	
Data / restraints / parameters	10098 / 21 / 488	
Goodness-of-fit on F^2	1.427	
Final R indices [I>2sigma(I)]	R1 = 0.0623, wR2 = 0.1714	
R indices (all data)	R1 = 0.0731, wR2 = 0.1773	
Largest diff. peak and hole	2.298 and -0.971 $e.Å^{-3}$	

Table A34. Crystal data and structure refinement for **34**.

Empirical formula	C32 H30 Ag F6 N6 O2 Sb	
Formula weight	874.24	
Temperature	100(2) K	
Wavelength	0.71073 Å	
Crystal system	Triclinic	
Space group	P-1	
Unit cell dimensions	a = 9.2644(4) Å	α= 74.5580(10)°.
	b = 13.2045(6) Å	β= 81.7510(10)°.
	c = 14.2022(6) Å	γ = 72.2750(10)°.
Volume	1591.47(12) $Å^3$	
Z	2	
Density (calculated)	1.824 g/cm^3	
Absorption coefficient	1.540 mm^{-1}	
F(000)	864	
Crystal size	0.34 x 0.22 x 0.08 mm^3	
Theta range for data collection	1.96 to 30.01°.	
Index ranges	-12<=h<=13, -18<=k<=18, -19<=l<=19	
Reflections collected	18528	
Independent reflections	9123 [R(int) = 0.0216]	
Completeness to theta = 30.01°	98.2 %	
Absorption correction	Semi-empirical from equivalents	
Max. and min. transmission	1.000 and 0.796	
Refinement method	Full-matrix least-squares on F^2	
Data / restraints / parameters	9123 / 0 / 445	
Goodness-of-fit on F^2	1.017	
Final R indices [I>2sigma(I)]	R1 = 0.0313, wR2 = 0.0775	
R indices (all data)	R1 = 0.0366, wR2 = 0.0806	
Largest diff. peak and hole	1.242 and -0.497 $e.Å^{-3}$	

Table A35. Crystal data and structure refinement for **35**.

Empirical formula	C44 H50 Cu2 N4 O8.20	
Formula weight	893.16	
Temperature	203(2) K	
Wavelength	0.71073 Å	
Crystal system	Triclinic	
Space group	P-1	
Unit cell dimensions	a = 8.3782(5) Å	α= 91.000(3)°.
	b = 9.4085(5) Å	β= 101.071(2)°.
	c = 13.7176(8) Å	γ = 104.723(3)°.
Volume	1023.84(10) $Å^3$	
Z	1	
Density (calculated)	1.449 g/cm^3	
Absorption coefficient	1.098 mm^{-1}	
F(000)	466	
Crystal size	0.30 x 0.30 x 0.15 mm^3	
Theta range for data collection	1.52 to 27.47°.	
Index ranges	-10<=h<=10, -12<=k<=12, -17<=l<=15	
Reflections collected	7172	
Independent reflections	4437 [R(int) = 0.0457]	
Completeness to theta = 27.47°	94.7 %	
Absorption correction	None	
Refinement method	Full-matrix least-squares on F^2	
Data / restraints / parameters	4437 / 0 / 267	
Goodness-of-fit on F^2	1.052	
Final R indices [I>2sigma(I)]	R1 = 0.0403, wR2 = 0.1082	
R indices (all data)	R1 = 0.0511, wR2 = 0.1148	
Extinction coefficient	0.015(2)	
Largest diff. peak and hole	0.415 and -0.601 $e.Å^{-3}$	

Table A36. Crystal data and structure refinement for **36**.

Empirical formula	C24 H16 Cu F12 N4 O4	
Formula weight	715.95	
Temperature	203(2) K	
Wavelength	0.71073 Å	
Crystal system	Monoclinic	
Space group	P2(1)/c	
Unit cell dimensions	a = 8.486(4) Å	α= 90°.
	b = 12.203(6) Å	β= 102.63(3)°.
	c = 13.094(5) Å	γ = 90°.
Volume	1323.0(10) $Å^3$	
Z	2	
Density (calculated)	1.797 g/cm^3	
Absorption coefficient	0.951 mm^{-1}	
F(000)	714	
Crystal size	0.40 x 0.10 x 0.10 mm^3	
Theta range for data collection	2.31 to 28.21°.	
Index ranges	-11<=h<=11, -16<=k<=15, -16<=l<=16	
Reflections collected	8786	
Independent reflections	3045 [R(int) = 0.0912]	
Completeness to theta = 28.21°	93.2 %	
Absorption correction	None	
Refinement method	Full-matrix least-squares on F^2	
Data / restraints / parameters	3045 / 0 / 205	
Goodness-of-fit on F^2	0.907	
Final R indices [I>2sigma(I)]	R1 = 0.0435, wR2 = 0.0927	
R indices (all data)	R1 = 0.0793, wR2 = 0.1054	
Largest diff. peak and hole	0.355 and -0.835 $e.Å^{-3}$	

Table A37. Crystal data and structure refinement for **37**.

Empirical formula	C54 H44 Cu N4 O4	
Formula weight	876.47	
Temperature	173(2) K	
Wavelength	0.71073 Å	
Crystal system	Triclinic	
Space group	P-1	
Unit cell dimensions	a = 9.8140(7) Å	α= 112.687(5)°.
	b = 10.8479(9) Å	β= 90.197(4)°.
	c = 11.0899(9) Å	γ = 95.503(6)°.
Volume	1083.22(15) $Å^3$	
Z	1	
Density (calculated)	1.344 g/cm^3	
Absorption coefficient	0.557 mm^{-1}	
F(000)	457	
Crystal size	0.35 x 0.25 x 0.05 mm^3	
Theta range for data collection	2.23 to 27.48°.	
Index ranges	-12<=h<=12, -14<=k<=12, -13<=l<=13	
Reflections collected	7706	
Independent reflections	4718 [R(int) = 0.0507]	
Completeness to theta = 27.48°	95.1 %	
Absorption correction	None	
Refinement method	Full-matrix least-squares on F^2	
Data / restraints / parameters	4718 / 0 / 286	
Goodness-of-fit on F^2	0.857	
Final R indices [I>2sigma(I)]	R1 = 0.0428, wR2 = 0.0879	
R indices (all data)	R1 = 0.0837, wR2 = 0.0984	
Largest diff. peak and hole	0.381 and -0.553 $e.Å^{-3}$	

Table A38. Crystal data and structure refinement for **38**.

Empirical formula	C70 H68 Co N6 O8	
Formula weight	1180.23	
Temperature	203(2) K	
Wavelength	0.71073 Å	
Crystal system	Triclinic	
Space group	P-1	
Unit cell dimensions	a = 8.9670(6) Å	α= 75.533(3)°.
	b = 11.2006(7) Å	β= 80.377(4)°.
	c = 15.3238(9) Å	γ = 79.221(4)°.
Volume	1452.18(16) $Å^3$	
Z	1	
Density (calculated)	1.350 g/cm^3	
Absorption coefficient	0.360 mm^{-1}	
F(000)	621	
Crystal size	0.40 x 0.18 x 0.12 mm^3	
Theta range for data collection	1.38 to 27.48°.	
Index ranges	-11<=h<=10, -14<=k<=14, -19<=l<=19	
Reflections collected	10224	
Independent reflections	6254 [R(int) = 0.0877]	
Completeness to theta = 27.48°	93.8 %	
Absorption correction	Numerical	
Max. and min. transmission	0.942 and 0.915	
Refinement method	Full-matrix least-squares on F^2	
Data / restraints / parameters	6254 / 20 / 380	
Goodness-of-fit on F^2	1.334	
Final R indices [I>2sigma(I)]	R1 = 0.0746, wR2 = 0.2005	
R indices (all data)	R1 = 0.0930, wR2 = 0.2109	
Largest diff. peak and hole	0.439 and -0.666 $e.Å^{-3}$	

Table A39. Crystal data and structure refinement for **39**.

Empirical formula	C70 H68 N6 Ni O8	
Formula weight	1180.01	
Temperature	203(2) K	
Wavelength	0.71073 Å	
Crystal system	Triclinic	
Space group	P-1	
Unit cell dimensions	a = 8.9948(19) Å	α= 75.737(9)°.
	b = 11.185(2) Å	β= 79.844(13)°.
	c = 15.409(3) Å	γ = 78.971(16)°.
Volume	1461.1(5) $Å^3$	
Z	1	
Density (calculated)	1.341 g/cm^3	
Absorption coefficient	0.397 mm^{-1}	
F(000)	622	
Crystal size	0.40 x 0.25 x 0.15 mm^3	
Theta range for data collection	1.38 to 27.40°.	
Index ranges	-11<=h<=11, -13<=k<=14, -19<=l<=19	
Reflections collected	9284	
Independent reflections	6080 [R(int) = 0.0576]	
Completeness to theta = 27.40°	91.3 %	
Absorption correction	Semi-empirical from equivalents	
Max. and min. transmission	1.000 and 0.481	
Refinement method	Full-matrix least-squares on F^2	
Data / restraints / parameters	6080 / 20 / 380	
Goodness-of-fit on F^2	1.042	
Final R indices [I>2sigma(I)]	R1 = 0.0829, wR2 = 0.2003	
R indices (all data)	R1 = 0.1359, wR2 = 0.2274	
Largest diff. peak and hole	0.991 and -1.080 $e.Å^{-3}$	

Table A40. Crystal data and structure refinement for **40**.

Empirical formula	C13 H13 N3 O	
Formula weight	227.26	
Temperature	100(2) K	
Wavelength	0.71073 Å	
Crystal system	Monoclinic	
Space group	C2/c	
Unit cell dimensions	a = 16.9569(10) Å	α= 90°.
	b = 13.4777(8) Å	β= 119.4630(10)°.
	c = 11.3934(7) Å	γ = 90°.
Volume	2267.1(2) $Å^3$	
Z	8	
Density (calculated)	1.332 g/cm^3	
Absorption coefficient	0.088 mm^{-1}	
F(000)	960	
Crystal size	0.08 x 0.20 x 0.35 mm^3	
Theta range for data collection	2.05 to 30.01°.	
Index ranges	-23<=h<=23, -18<=k<=18, -16<=l<=16	
Reflections collected	12901	
Independent reflections	3298 [R(int) = 0.0280]	
Completeness to theta = 30.01°	99.5 %	
Absorption correction	Semi-empirical from equivalents	
Max. and min. transmission	1.000 and 0.810	
Refinement method	Full-matrix least-squares on F^2	
Data / restraints / parameters	3298 / 0 / 165	
Goodness-of-fit on F^2	1.214	
Final R indices [I>2sigma(I)]	R1 = 0.0494, wR2 = 0.1285	
R indices (all data)	R1 = 0.0558, wR2 = 0.1330	
Largest diff. peak and hole	0.525 and -0.225 $e.Å^{-3}$	

Table A41. Crystal data and structure refinement for **41**.

Empirical formula	C13 H12 Cl N3 O	
Formula weight	261.71	
Temperature	173(2) K	
Wavelength	0.71073 Å	
Crystal system	Monoclinic	
Space group	P2(1)/n	
Unit cell dimensions	a = 9.659(2) Å	α= 90°.
	b = 11.329(2) Å	β= 113.523(10)°.
	c = 11.948(2) Å	γ = 90°.
Volume	1198.9(4) $Å^3$	
Z	4	
Density (calculated)	1.450 Mg/m^3	
Absorption coefficient	0.309 mm^{-1}	
F(000)	544	
Crystal size	0.35 x 0.25 x 0.20 mm^3	
Theta range for data collection	2.31 to 28.26°.	
Index ranges	-12<=h<=12, -14<=k<=14, -15<=l<=15	
Reflections collected	8552	
Independent reflections	2784 [R(int) = 0.0650]	
Completeness to theta = 28.26°	94.2 %	
Absorption correction	None	
Refinement method	Full-matrix least-squares on F^2	
Data / restraints / parameters	2784 / 0 / 170	
Goodness-of-fit on F^2	1.063	
Final R indices [I>2sigma(I)]	R1 = 0.0397, wR2 = 0.0995	
R indices (all data)	R1 = 0.0496, wR2 = 0.1057	
Extinction coefficient	0.053(5)	
Largest diff. peak and hole	0.346 and -0.236 $e.Å^{-3}$	

Table A42. Crystal data and structure refinement for **42**.

Empirical formula	C27 H21 N5 O8	
Formula weight	543.49	
Temperature	100(2) K	
Wavelength	0.71073 Å	
Crystal system	Triclinic	
Space group	P-1	
Unit cell dimensions	a = 8.6633(4) Å	α= 87.5430(10)°.
	b = 11.0661(6) Å	β= 80.3330(10)°.
	c = 12.9218(7) Å	γ = 84.1120(10)°.
Volume	1214.35(11) $Å^3$	
Z	2	
Density (calculated)	1.486 g/cm^3	
Absorption coefficient	0.112 mm^{-1}	
F(000)	564	
Crystal size	0.30 x 0.28 x 0.27 mm^3	
Theta range for data collection	1.85 to 30.00°.	
Index ranges	-12<=h<=12, -15<=k<=15, -18<=l<=18	
Reflections collected	14130	
Independent reflections	6969 [R(int) = 0.0208]	
Completeness to theta = 30.00°	98.3 %	
Absorption correction	Semi-empirical from equivalents	
Max. and min. transmission	1.000 and 0.810	
Refinement method	Full-matrix least-squares on F^2	
Data / restraints / parameters	6969 / 0 / 367	
Goodness-of-fit on F^2	1.031	
Final R indices [I>2sigma(I)]	R1 = 0.0455, wR2 = 0.1268	
R indices (all data)	R1 = 0.0516, wR2 = 0.1332	
Largest diff. peak and hole	0.505 and -0.404 $e.Å^{-3}$	

Table A43. Crystal data and structure refinement for **43**.

Empirical formula	C22 H21 N3 O2	
Formula weight	359.42	
Temperature	100(2) K	
Wavelength	0.71073 Å	
Crystal system	Triclinic	
Space group	P-1	
Unit cell dimensions	a = 9.6581(12) Å	α= 84.007(2)°.
	b = 9.9523(12) Å	β= 65.713(2)°.
	c = 10.7006(13) Å	γ = 73.066(2)°.
Volume	896.73(19) $Å^3$	
Z	2	
Density (calculated)	1.331 g/cm^3	
Absorption coefficient	0.087 mm^{-1}	
F(000)	380	
Crystal size	0.36 x 0.24 x 0.24 mm^3	
Theta range for data collection	2.09 to 30.00°.	
Index ranges	-13<=h<=13, -13<=k<=13, -14<=l<=15	
Reflections collected	10393	
Independent reflections	5127 [R(int) = 0.0187]	
Completeness to theta = 30.00°	98.1 %	
Absorption correction	Semi-empirical from equivalents	
Max. and min. transmission	1.000 and 0.849	
Refinement method	Full-matrix least-squares on F^2	
Data / restraints / parameters	5127 / 0 / 247	
Goodness-of-fit on F^2	1.025	
Final R indices [I>2sigma(I)]	R1 = 0.0473, wR2 = 0.1245	
R indices (all data)	R1 = 0.0519, wR2 = 0.1286	
Largest diff. peak and hole	0.462 and -0.305 $e.Å^{-3}$	

Table A44. Crystal data and structure refinement for **44**.

Empirical formula	C23 H24 N4 O2	
Formula weight	388.46	
Temperature	173(2) K	
Wavelength	0.71073 Å	
Crystal system	Triclinic	
Space group	P-1	
Unit cell dimensions	a = 9.6685(9) Å	α= 91.689(5)°.
	b = 10.7168(9) Å	β= 109.241(5)°.
	c = 11.6225(9) Å	γ = 115.952(4)°.
Volume	1000.72(15) $Å^3$	
Z	2	
Density (calculated)	1.289 Mg/m^3	
Absorption coefficient	0.085 mm^{-1}	
F(000)	412	
Crystal size	0.35 x 0.25 x 0.15 mm^3	
Theta range for data collection	1.90 to 27.86°.	
Index ranges	-12<=h<=12, -14<=k<=13, -15<=l<=15	
Reflections collected	7150	
Independent reflections	4346 [R(int) = 0.0676]	
Completeness to theta = 27.86°	91.2 %	
Absorption correction	None	
Refinement method	Full-matrix least-squares on F^2	
Data / restraints / parameters	4346 / 0 / 266	
Goodness-of-fit on F^2	1.047	
Final R indices [I>2sigma(I)]	R1 = 0.0681, wR2 = 0.1684	
R indices (all data)	R1 = 0.0934, wR2 = 0.1840	
Extinction coefficient	0.059(8)	
Largest diff. peak and hole	0.402 and -0.343 $e.Å^{-3}$	

Table A45. Crystal data and structure refinement for **45**.

Empirical formula	C28 H21 N7 O12	
Formula weight	647.52	
Temperature	173(2) K	
Wavelength	0.71073 Å	
Crystal system	Monoclinic	
Space group	P2(1)/c	
Unit cell dimensions	a = 23.5249(17) Å	α= 90°.
	b = 5.7765(4) Å	β= 99.351(5)°.
	c = 20.5203(14) Å	γ = 90°.
Volume	2751.5(3) $Å^3$	
Z	4	
Density (calculated)	1.563 Mg/m^3	
Absorption coefficient	0.125 mm^{-1}	
F(000)	1336	
Crystal size	0.35 x 0.25 x 0.12 mm^3	
Theta range for data collection	1.75 to 28.29°.	
Index ranges	-31<=h<=31, -7<=k<=6, -26<=l<=24	
Reflections collected	19500	
Independent reflections	6433 [R(int) = 0.0776]	
Completeness to theta = 28.29°	94.0 %	
Absorption correction	None	
Refinement method	Full-matrix least-squares on F^2	
Data / restraints / parameters	6433 / 0 / 431	
Goodness-of-fit on F^2	1.004	
Final R indices [I>2sigma(I)]	R1 = 0.0485, wR2 = 0.1150	
R indices (all data)	R1 = 0.0782, wR2 = 0.1282	
Extinction coefficient	0.0117(10)	
Largest diff. peak and hole	0.275 and -0.269 $e.Å^{-3}$	

Table A46. Crystal data and structure refinement for **46**.

Empirical formula	C37 H43 N3 O4	
Formula weight	593.74	
Temperature	100(2) K	
Wavelength	0.71073 Å	
Crystal system	Triclinic	
Space group	P-1	
Unit cell dimensions	a = 8.5326(7) Å	α= 93.446(2)°.
	b = 11.1399(9) Å	β= 98.810(2)°.
	c = 17.5311(14) Å	γ = 103.366(2)°.
Volume	1594.2(2) $Å^3$	
Z	2	
Density (calculated)	1.237 g/cm^3	
Absorption coefficient	0.080 mm^{-1}	
F(000)	636	
Crystal size	0.44 x 0.40 x 0.36 mm^3	
Theta range for data collection	1.89 to 30.01°.	
Index ranges	-11<=h<=11, -15<=k<=15, -24<=l<=24	
Reflections collected	17348	
Independent reflections	9077 [R(int) = 0.0188]	
Completeness to theta = 30.01°	97.6 %	
Absorption correction	Semi-empirical from equivalents	
Max. and min. transmission	1.000 and 0.825	
Refinement method	Full-matrix least-squares on F^2	
Data / restraints / parameters	9077 / 0 / 403	
Goodness-of-fit on F^2	1.047	
Final R indices [I>2sigma(I)]	R1 = 0.0514, wR2 = 0.1448	
R indices (all data)	R1 = 0.0571, wR2 = 0.1505	
Largest diff. peak and hole	0.571 and -0.349 $e.Å^{-3}$	

Table A47. Crystal data and structure refinement for **47**.

Empirical formula	C27 H19 N7 O12	
Formula weight	633.49	
Temperature	100(2) K	
Wavelength	0.71073 Å	
Crystal system	Monoclinic	
Space group	P2(1)/c	
Unit cell dimensions	a = 23.6268(12) Å	α= 90°.
	b = 7.4221(4) Å	β= 107.4780(10)°.
	c = 16.1594(8) Å	γ = 90°.
Volume	2702.9(2) $Å^3$	
Z	4	
Density (calculated)	1.557 g/cm^3	
Absorption coefficient	0.126 mm^{-1}	
F(000)	1304	
Crystal size	0.11 x 0.23 x 0.36 mm^3	
Theta range for data collection	2.52 to 30.02°.	
Index ranges	-33<=h<=33, -10<=k<=10, -22<=l<=22	
Reflections collected	29845	
Independent reflections	7875 [R(int) = 0.0298]	
Completeness to theta = 30.02°	99.7 %	
Absorption correction	Semi-empirical from equivalents	
Max. and min. transmission	1.000 and 0.754	
Refinement method	Full-matrix least-squares on F^2	
Data / restraints / parameters	7875 / 0 / 421	
Goodness-of-fit on F^2	1.173	
Final R indices [I>2sigma(I)]	R1 = 0.0606, wR2 = 0.1518	
R indices (all data)	R1 = 0.0704, wR2 = 0.1575	
Largest diff. peak and hole	0.588 and -0.368 $e.Å^{-3}$	

Table A48. Crystal data and structure refinement for **48**.

Empirical formula	C28 H25 N5 O9	
Formula weight	575.53	
Temperature	173(2) K	
Wavelength	0.71073 Å	
Crystal system	Triclinic	
Space group	P-1	
Unit cell dimensions	a = 9.627(3) Å	α= 81.802(14)°.
	b = 10.053(3) Å	β= 81.015(19)°.
	c = 14.062(4) Å	γ = 74.507(18)°.
Volume	1288.0(6) $Å^3$	
Z	2	
Density (calculated)	1.484 g/cm^3	
Absorption coefficient	0.113 mm^{-1}	
F(000)	600	
Crystal size	0.40 x 0.30 x 0.05 mm^3	
Theta range for data collection	1.47 to 28.36°.	
Index ranges	-12<=h<=12, -11<=k<=12, -18<=l<=18	
Reflections collected	9617	
Independent reflections	5768 [R(int) = 0.0833]	
Completeness to theta = 28.36°	89.5 %	
Absorption correction	None	
Refinement method	Full-matrix least-squares on F^2	
Data / restraints / parameters	5768 / 0 / 392	
Goodness-of-fit on F^2	0.887	
Final R indices [I>2sigma(I)]	R1 = 0.0652, wR2 = 0.1516	
R indices (all data)	R1 = 0.1113, wR2 = 0.1722	
Extinction coefficient	0.017(3)	
Largest diff. peak and hole	0.467 and -0.397 $e.Å^{-3}$	

Table A49. Crystal data and structure refinement for **49**.

Empirical formula	C18 H12 N6 O6	
Formula weight	408.34	
Temperature	173(2) K	
Wavelength	0.71073 Å	
Crystal system	Triclinic	
Space group	P-1	
Unit cell dimensions	a = 7.5160(5) Å	α= 76.258(3)°.
	b = 9.1032(5) Å	β= 88.904(4)°.
	c = 12.9495(8) Å	γ = 82.037(4)°.
Volume	852.25(9) $Å^3$	
Z	2	
Density (calculated)	1.591 g/cm^3	
Absorption coefficient	0.124 mm^{-1}	
F(000)	420	
Crystal size	0.40 x 0.15 x 0.15 mm^3	
Theta range for data collection	2.33 to 27.85°.	
Index ranges	-9<=h<=9, -11<=k<=11, -16<=l<=14	
Reflections collected	6230	
Independent reflections	3758 [R(int) = 0.0483]	
Completeness to theta = 27.85°	92.7 %	
Absorption correction	None	
Refinement method	Full-matrix least-squares on F^2	
Data / restraints / parameters	3758 / 0 / 275	
Goodness-of-fit on F^2	1.091	
Final R indices [I>2sigma(I)]	R1 = 0.0470, wR2 = 0.1284	
R indices (all data)	R1 = 0.0557, wR2 = 0.1372	
Largest diff. peak and hole	0.261 and -0.398 $e.Å^{-3}$	

Table A50. Crystal data and structure refinement for **50**.

Empirical formula	C25 H18 N6 O8	
Formula weight	530.45	
Temperature	100(2) K	
Wavelength	0.71073 Å	
Crystal system	Triclinic	
Space group	P-1	
Unit cell dimensions	a = 6.3823(3) Å	α= 96.4250(10)°.
	b = 8.5498(4) Å	β= 91.8040(10)°.
	c = 21.4246(9) Å	γ = 98.6340(10)°.
Volume	1147.19(9) $Å^3$	
Z	2	
Density (calculated)	1.536 g/cm^3	
Absorption coefficient	0.118 mm^{-1}	
F(000)	548	
Crystal size	0.40 x 0.34 x 0.21 mm^3	
Theta range for data collection	1.92 to 30.02°.	
Index ranges	-8<=h<=8, -12<=k<=12, -28<=l<=30	
Reflections collected	13277	
Independent reflections	6547 [R(int) = 0.0178]	
Completeness to theta = 30.02°	98.1 %	
Absorption correction	Semi-empirical from equivalents	
Max. and min. transmission	1.000 and 0.853	
Refinement method	Full-matrix least-squares on F^2	
Data / restraints / parameters	6547 / 0 / 358	
Goodness-of-fit on F^2	1.063	
Final R indices [I>2sigma(I)]	R1 = 0.0417, wR2 = 0.1166	
R indices (all data)	R1 = 0.0461, wR2 = 0.1203	
Largest diff. peak and hole	0.498 and -0.300 $e.Å^{-3}$	

Table A51. Crystal data and structure refinement for **51**.

Empirical formula	C27 H20 N6 O10	
Formula weight	588.49	
Temperature	100(2) K	
Wavelength	0.71073 Å	
Crystal system	Triclinic	
Space group	P-1	
Unit cell dimensions	a = 7.7602(11) Å	α= 82.064(3)°.
	b = 15.269(2) Å	β= 81.610(3)°.
	c = 22.456(3) Å	γ = 78.915(3)°.
Volume	2566.7(6) $Å^3$	
Z	4	
Density (calculated)	1.523 g/cm^3	
Absorption coefficient	0.119 mm^{-1}	
F(000)	1216	
Crystal size	0.37 x 0.21 x 0.06 mm^3	
Theta range for data collection	1.56 to 30.14°.	
Index ranges	-10<=h<=10, -21<=k<=21, -31<=l<=31	
Reflections collected	30029	
Independent reflections	14779 [R(int) = 0.0932]	
Completeness to theta = 30.14°	97.7 %	
Absorption correction	None	
Refinement method	Full-matrix least-squares on F^2	
Data / restraints / parameters	14779 / 3 / 796	
Goodness-of-fit on F^2	0.886	
Final R indices [I>2sigma(I)]	R1 = 0.0544, wR2 = 0.0980	
R indices (all data)	R1 = 0.0911, wR2 = 0.1090	
Largest diff. peak and hole	0.341 and -0.379 $e.Å^{-3}$	

Table A52. Crystal data and structure refinement for **52**.

Empirical formula	C29 H26 N6 O8	
Formula weight	586.56	
Temperature	203(2) K	
Wavelength	0.71073 Å	
Crystal system	Triclinic	
Space group	P-1	
Unit cell dimensions	a = 8.1324(7) Å	α= 95.489(4)°.
	b = 10.8110(9) Å	β= 90.318(5)°.
	c = 15.3761(13) Å	γ = 91.503(5)°.
Volume	1345.2(2) $Å^3$	
Z	2	
Density (calculated)	1.448 g/cm^3	
Absorption coefficient	0.108 mm^{-1}	
F(000)	612	
Crystal size	0.35 x 0.35 x 0.15 mm^3	
Theta range for data collection	1.33 to 27.51°.	
Index ranges	-10<=h<=10, -14<=k<=13, -17<=l<=19	
Reflections collected	9845	
Independent reflections	5871 [R(int) = 0.0691]	
Completeness to theta = 27.51°	94.8 %	
Absorption correction	None	
Refinement method	Full-matrix least-squares on F^2	
Data / restraints / parameters	5871 / 0 / 394	
Goodness-of-fit on F^2	0.974	
Final R indices [I>2sigma(I)]	R1 = 0.0628, wR2 = 0.1587	
R indices (all data)	R1 = 0.1044, wR2 = 0.1840	
Largest diff. peak and hole	0.305 and -0.322 $e.Å^{-3}$	

Table A53. Crystal data and structure refinement for **53**.

Empirical formula	C28 H20 N6 O8	
Formula weight	568.50	
Temperature	203(2) K	
Wavelength	0.71073 Å	
Crystal system	Triclinic	
Space group	P-1	
Unit cell dimensions	a = 7.7854(5) Å	α= 80.936(3)°.
	b = 15.4355(10) Å	β= 82.691(5)°.
	c = 22.0882(13) Å	γ = 81.375(5)°.
Volume	2577.0(3) $Å^3$	
Z	4	
Density (calculated)	1.465 g/cm^3	
Absorption coefficient	0.111 mm^{-1}	
F(000)	1176	
Crystal size	0.40 x 0.30 x 0.20 mm^3	
Theta range for data collection	1.35 to 27.49°.	
Index ranges	-10<=h<=10, -18<=k<=19, -28<=l<=26	
Reflections collected	17386	
Independent reflections	10885 [R(int) = 0.0969]	
Completeness to theta = 27.49°	92.1 %	
Absorption correction	None	
Refinement method	Full-matrix least-squares on F^2	
Data / restraints / parameters	10885 / 0 / 769	
Goodness-of-fit on F^2	0.805	
Final R indices [I>2sigma(I)]	R1 = 0.0562, wR2 = 0.1164	
R indices (all data)	R1 = 0.1248, wR2 = 0.1347	
Largest diff. peak and hole	0.303 and -0.331 $e.Å^{-3}$	

Table A54. Crystal data and structure refinement for **54**.

Empirical formula	C28 H22 N6 O10	
Formula weight	602.52	
Temperature	173(2) K	
Wavelength	0.71073 Å	
Crystal system	Monoclinic	
Space group	P2(1)/c	
Unit cell dimensions	a = 7.7318(8) Å	α= 90°.
	b = 7.0062(7) Å	β= 91.012(6)°.
	c = 49.395(5) Å	γ = 90°.
Volume	2675.3(5) $Å^3$	
Z	4	
Density (calculated)	1.496 g/cm^3	
Absorption coefficient	0.116 mm^{-1}	
F(000)	1248	
Crystal size	0.35 x 0.35 x 0.10 mm^3	
Theta range for data collection	1.65 to 28.26°.	
Index ranges	-10<=h<=9, -9<=k<=8, -65<=l<=64	
Reflections collected	18644	
Independent reflections	6183 [R(int) = 0.1180]	
Completeness to theta = 28.26°	93.2 %	
Absorption correction	None	
Refinement method	Full-matrix least-squares on F^2	
Data / restraints / parameters	6183 / 0 / 404	
Goodness-of-fit on F^2	0.891	
Final R indices [I>2sigma(I)]	R1 = 0.0613, wR2 = 0.1298	
R indices (all data)	R1 = 0.1162, wR2 = 0.1511	
Extinction coefficient	0.0202(13)	
Largest diff. peak and hole	0.341 and -0.410 $e.Å^{-3}$	

Table A55. Crystal data and structure refinement for **55**.

Empirical formula	C27.65 H20 Cl N5 O6.70	
Formula weight	564.94	
Temperature	100(2) K	
Wavelength	0.71073 Å	
Crystal system	Triclinic	
Space group	P-1	
Unit cell dimensions	a = 8.2974(4) Å	α= 74.4900(10)°.
	b = 11.4200(6) Å	β= 77.9330(10)°.
	c = 14.6930(7) Å	γ = 73.8090(10)°.
Volume	1274.67(11) $Å^3$	
Z	2	
Density (calculated)	1.472 g/cm^3	
Absorption coefficient	0.208 mm^{-1}	
F(000)	583	
Crystal size	0.32 x 0.30 x 0.26 mm^3	
Theta range for data collection	2.58 to 30.00°.	
Index ranges	-11<=h<=11, -16<=k<=16, -18<=l<=20	
Reflections collected	14729	
Independent reflections	7305 [R(int) = 0.0323]	
Completeness to theta = 30.00°	98.1 %	
Absorption correction	None	
Refinement method	Full-matrix least-squares on F^2	
Data / restraints / parameters	7305 / 0 / 388	
Goodness-of-fit on F^2	1.054	
Final R indices [I>2sigma(I)]	R1 = 0.0459, wR2 = 0.1293	
R indices (all data)	R1 = 0.0560, wR2 = 0.1338	
Largest diff. peak and hole	0.643 and -0.371 e.$Å^{-3}$	

Table A56. Crystal data and structure refinement for **56**.

Empirical formula	C31 H25 N7 O8	
Formula weight	623.58	
Temperature	173(2) K	
Wavelength	0.71073 Å	
Crystal system	Triclinic	
Space group	P-1	
Unit cell dimensions	a = 9.7196(9) Å	α= 86.704(5)°.
	b = 10.7696(9) Å	β= 84.042(6)°.
	c = 13.6374(12) Å	γ = 88.924(6)°.
Volume	1417.3(2) $Å^3$	
Z	2	
Density (calculated)	1.461 g/cm^3	
Absorption coefficient	0.109 mm^{-1}	
F(000)	648	
Crystal size	0.40 x 0.20 x 0.15 mm^3	
Theta range for data collection	1.50 to 28.29°.	
Index ranges	-11<=h<=12, -14<=k<=14, -17<=l<=16	
Reflections collected	8850	
Independent reflections	5523 [R(int) = 0.0912]	
Completeness to theta = 28.29°	78.5 %	
Absorption correction	None	
Refinement method	Full-matrix least-squares on F^2	
Data / restraints / parameters	5523 / 0 / 422	
Goodness-of-fit on F^2	1.296	
Final R indices [I>2sigma(I)]	R1 = 0.0701, wR2 = 0.1898	
R indices (all data)	R1 = 0.0885, wR2 = 0.2054	
Extinction coefficient	0.007(2)	
Largest diff. peak and hole	0.475 and -0.412 $e.Å^{-3}$	